PB83-260778

REPORT NO.
UCB/EERC-82/14
SEPTEMBER 1982

EARTHQUAKE ENGINEERING RESEARCH CENTER

SEISMIC BEHAVIOR OF AN ECCENTRICALLY X-BRACED STEEL STRUCTURE

by
MING-SAN YANG

Report to the National Science Foundation

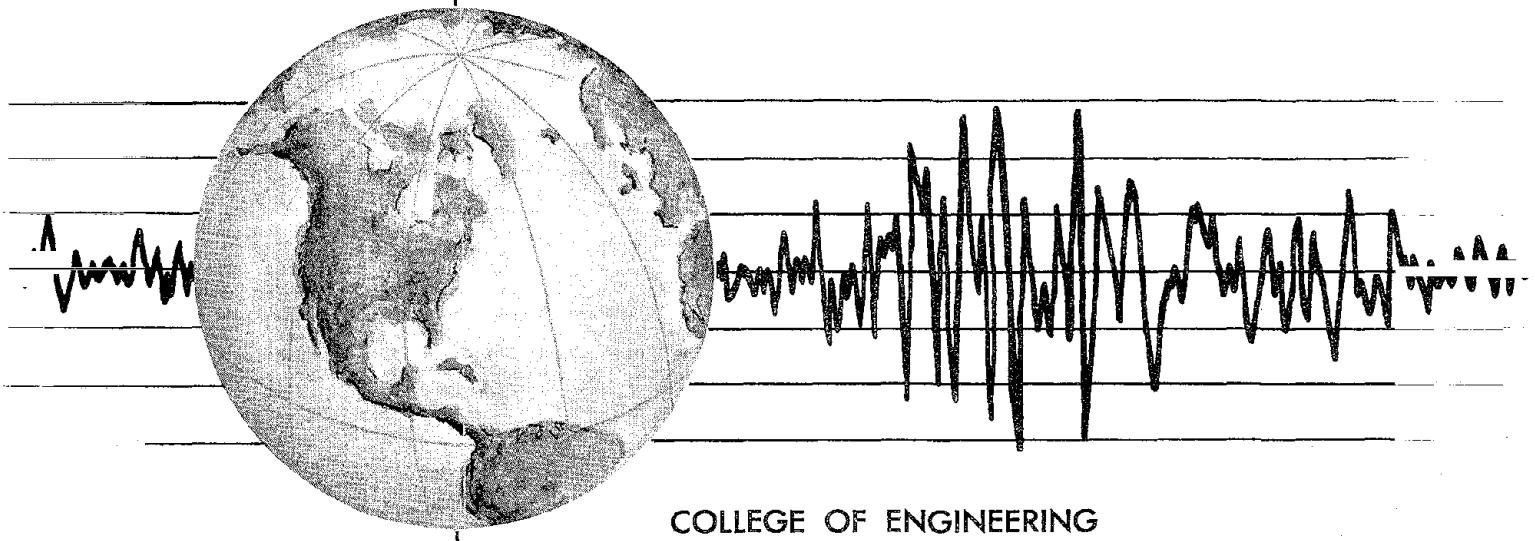

COLLEGE OF ENGINEERING

UNIVERSITY OF CALIFORNIA · Berkeley, California

REPRODUCED BY
NATIONAL TECHNICAL
INFORMATION SERVICE
U.S. DEPARTMENT OF COMMERCE
SPRINGFIELD, VA 22161

For sale by the National Technical Information Service, U.S. Department of Commerce, Springfield, Virginia 22161.

See back of report for up to date listing of EERC reports.

DISCLAIMER

Any opinions, findings, and conclusions or recommendations expressed in this publication are those of the author and do not necessarily reflect the views of the National Science Foundation or the Earthquake Engineering Research Center, University of California, Berkeley.

SEISMIC BEHAVIOR OF AN ECCENTRICALLY X-BRACED STEEL STRUCTURE

by

Ming-San Yang
Graduate Student in Civil Engineering
University of California, Berkeley

Report to the National Science Foundation

Report UCB/EERC-82/14
Earthquake Engineering Research Center
College of Engineering
University of California, Berkeley

September 1982

i.a

ABSTRACT

The earthquake resistant characteristics of an eccentrically X-braced structures were studied experimentally and analytically. A five-story one-third scale model structure of about 50 tons in weight was tested on the 20′×20′ shaking table at the Earthquake Engineering Research Center of U.C. Berkeley to observe its earthquake resistant behavior. The eccentric bracing in this study was created by a deliberate introduction of offsets into the brace-beam connections. The term 'shear links' was used to designate eccentric beams because they yielded mainly in shear. Being designed to be replaceable, three sets of shear links were sequentially installed into the structure and tested to destruction.

The experimental results indicated that the eccentrically X-braced test structure could efficiently resist an El Centro type table motion with a peak acceleration of 1.15g and a ductility factor of about 100 was recorded for shear yielding of links. It was observed that the earthquake response was strongly correlated with the strength in the links and that the weakest link was the best energy dissipator.

A simplified mathematical model was formulated in response calculation for data correlation. In this simplified model, the upper three elastic stories were replaced by an equivalent shear story to reduce the number of unknowns to obtain an economic mathematical model. The shear yielding behavior was approximately modeled by vertical truss elements with appropriate properties. With this model, a fairly good correlation between experiment and analysis was obtained for the test selected for the correlation study.

ACKNOWLEDGEMENTS

The support of the National Science Foundation in funding the research program described herein is gratefully acknowledged.

The very deep gratitude of the author is owed to Professor Ray W. Clough, the author's thesis advisor and supervisor of this research program, for his support and guidance throughout the author's study at Berkeley. The author would also like to express his thanks to Professors Stephen Mahin and Bruce Bolt for their review of the manuscript of this report. Especially, the valuable suggestions from Professor Mahin are very much appreciated.

The author is very grateful to Professor Graham H. Powell and his student, A. Kanaan, for developing the DRAIN-2D program, which was used for the analytical part of this research. He would also like to thank him for the new version of the DRAIN-2D program, DRAIN-2D2, although the new version was not utilized because of shortage of time and funding. Gratitude is also extended to Professor Egor P. Popov for providing the shear beam element, which was used in the early stage of this research.

The facilities provided by the Earthquake Engineering Research Center and the Computer Center of the University of California, Berkeley and the help from the staff associated with the Centers are given credit for the success of this research program. Special thanks are due to Donna Stanonik for her constant help during the author's stay at the EERC.

The author is very appreciative of the encouragement from his former colleague Akira Niwa and the help from Yu-Chang Chen, Yusof Ganaat, Keith Hjelmstad, Hong-Ming Lee and others in this study. Many thanks are offered to Marcial Blondet for providing his computer program DIPS which helped the author in the data reduction work.

The author cannot thank his wife, Yann, enough for her patience, understanding and help through these years.

Preceding page blank

TABLE OF CONTENTS

Preceding page blank

LIST OF TABLES

Preceding page blank

LIST OF FIGURES

Preceding page blank

CHAPTER ONE

INTRODUCTION

1.1. Objectives and Scope

The main objective of this report is to investigate the earthquake resistance efficiency of steel structures with an eccentric X-bracing system by studying the responses of a one-third scale structure (see **Figs.** 1 and 2) to simulated earthquake excitations. The investigation was carried out on the shaking table of the Earthquake Simulator Laboratory at the University of California Earthquake Engineering Research Center (EERC).

The idea of eccentric X-bracing was employed by deliberate introduction of an offset, or eccentricity, between the brace connections to the first story girders as shown in **Fig.** 3. This arrangement shifts the energy dissipating activity from the conventional tension-yielding-and-compression-buckling mechanism of braces to the shear-yielding mechanism of the eccentric beams. The terminology 'shear link' is adopted to denote these beams because they mainly yield in shear.

The secondary objectives of this research program were: (1) to establish an economical mathematical model for the eccentrically X-braced test structure, (2) to evaluate the ability of DRAIN-2D [1], a nonlinear analysis program, to predict the yielding behavior of shear links and the global behavior of structures with shear links, (3) to evaluate the feasibility of repairing earthquake damage by using replaceable links, (4) to evaluate the effect of link strength on the response to earthquake excitations. Since the excitation was parallel to a plane of symmetry of the structure, this study is basically 2-dimensional in nature. It is adequate, however, for the achievement of the objectives.

The tasks associated with this work included (1) designing the eccentric brace system, (2) installing the instrumentation to make various measurements, (3) conducting the shaking table experimentation, (4) analyzing and interpreting the acquired data, (5) correlating the

experimental results with those of theoretical analyses.

In the rest of this chapter, the following topics will be dicussed: (1) some aspects of the brace seismic resistant behavior, (2) some design variaties of eccentric bracing systems.

1.2. Some Aspects of Brace Seismic Resistant Behavior

1.2.A. Braces as Seismic Resistant Components

Many structures may be subjected to rare but severe lateral loads, such as those located in seismically active regions and offshore structures. They must have the ability to resist extreme lateral loads due to earthquakes and/or hydrodynamic actions, and wind loads as well. In the present discussion, however, attention is focused on the earthquake resistant behavior of braced steel frame buildings.

The design of building structures must comply with two conditions [2]. First, during frequent small earthquakes there should be no non-structural damage, and during occasional moderate earthquakes, the non-structural damages should be minimized. This condition usually requires that a structure remain elastic and have sufficient stiffness to prevent excessive drifts to prevent nonstructural damage.

Secondly, during rare major earthquakes, serious structural damages or catastrophic collapses should be ruled out. Other than satisfaction of the stiffness and strength requirement, the fulfillment of the second condition depends first on the capacity of a structure to absorb and dissipate energy through yielding of members, and secondly on the ability of the structure to isolate the earthquake through a softening mechanism associated with yielding of structural members to avoid response build-up.

Bracing systems provide the basis for good seismic resistant design because of the following reasons: (1) they can easily provide sufficient stiffness to minimize non-structural damages when structures are subjected to frequent minor and occasional moderate earthquakes, (2) they can dissipate energy through a yielding-and-buckling mechanism when occasional moderate and

rare severe earthquakes occur, (3) they can reduce the risk of instability caused by the $P-\Delta$ effect, and (4) they decrease bending moments and correspondingly increase axial forces in structural elements for optimal use of materials.

1.2.B. Pinching of Hysteresis Loops

In general, because of brace buckling, the hysteresis loops of a braced structure exhibit, to some extent, a 'pinched' shape depending on the displacement the structure experiences and, especially, depending very much on the slenderness ratios of braces [3]. The thiner the braces are, the more severely pinched the loops become.

However, this does not necessarily mean that pinching is so detrimental that it has to be eliminated to make an efficient energy dissipating structure. During earthquakes, slender braces can still fulfill their function of dissipating energy by larger elongations and more loop cycles. An adequate amount of hysteretic energy can be dissipated in this way, provided that the story drifts are not too excessive to be acceptable.

Nevertheless, it is apparent that the energy dissipation potential will be increased if the pinching is reduced to make the enclosed area larger. Stocky or stubby braces can be used to improve the energy dissipating ability of a structure not only because they are less likely to buckle but also because they possess higher tensile strength. Thus, for the same ductility, they can dissipate much more energy than slender braces.

1.2.C. Strong Bracing Alternative

As mentioned above a slender brace tends to buckle and thus loses most of its load resistant capacity, therefore, a strong brace may be a promising alternative. The results of the quasi-static tests conducted by Wakabayashi and Nakamura confirmed that strong braces were good energy dissipators [4].

They observed that braces with smaller slenderness ratios were able to display more corpulent loops and that the deterioration of strength and stiffness is smaller. This is not surprising since a brace with smaller slenderness ratio is stronger and thus less likely to buckle. Moreover, it was also observed that the hysteresis behavior of X-shaped braces is superior to that of single diagonal braces. The X-shaped braces generate symmetric loops, which are more favorable than the 'one-sided' loops produced by single diagonal braces. In other words, during earthquakes, the X-bracing can provide similar strength and stiffness in both directions when the structure vibrates back and forth regardless of whether brace buckling has occurred.

As stated before, yielding can change natural frequencies of a structure and thus prevent excesive response build-up. However, structures with stocky braces are stiffer and more difficult to give in than those with standard, conventionally designed braces (not to memtion moment-resisting frames). Therefore, if the structures are in resonance with one of the dominant frequencies of an earthquake, they may induce larger base shears and over-turning moments when subjected to the earthquake. This is reflected in the Uniform Building Code [5]*, which requires a larger equivalent static design lateral load for a stiffer, shorter period structure. Consequently, the employment of strong braces might not only uneconomically give a structure too much stiffness for frequent events, but also, for extreme events, introduce a large response which could make a design expensive.

1.2.D. Fracture of Braces

A potential hazard associated with the buckling of braces needs to be pointed out. Since buckling of a brace is usually accompanied by highly localized plastic deformation [4], a buckled brace is susceptible to low cycle fatigue that can crack or even rupture the brace. Moreover, when subjected to an earthquake excitation, the re-straightening of a slender buckled brace may cause shock impacts, and thus generate high strain impulses which may fracture the material.

* However, the Code generally provides inadequate seismic load estimation for major earthquakes.

Since the bracing system of a structure resists the greater part of the lateral load, in general more than 80 percent, the rupture of braces may result in serious consequences. Thus the local buckling behavior may be a topic of of great concern that needs further investigation not only because it may induce cracks and rupture, but also because structural shapes used in practical design usually have large aspect ratios which make local kinking after buckling likely.

1.3. Some Examples of Eccentric Bracing

Based on the above review, it can be concluded that the optimal seismic resistant system needs to have enough stiffness and strength to meet the first design condition (see Section 1.2.A), and to have good energy dissipating ability to meet the second. In other words, the system should be stiff for frequent moderate earthquakes but ductile for rare strong events.

The eccentrically braced frame is a system that can achieve this optimum. In the eccentric bracing system, the bracing gives the necessary stiffness and strength, whereas the ductility and energy dissipating capacity are ensured by bending or shear yielding of girders associated with eccentric connections. Of course, to achieve the ultimate merits of eccentric bracing, it is essential that yielding and buckling of the braces be prevented to avoid such inherent problems as mentioned previously and to assure that the yielding behavior occurs in the girders.

The eccentricity can be, for some examples, obtained in the following ways (see **Fig.** 4):

(1) arranging a finite distance between brace-beam and beam-column joints, such as the eccentric diagonal bracing [6], and the V-bracing [16,24],

(2) connecting the brace-brace joint and girder with a small stub, such as the Y-bracing [8,9],

(3) using a pure shear panel as the junction of two cross braces, such as the 'panel-zone' bracing [10],

(4) splitting the brace-beam joint, such as the eccentric K-bracing [7], and the eccentric X-bracing, the subject of this report.

If eccentricities are arranged at column-beam joints, such as the eccentric diagonal-bracing and the V-bracing, this eccentricity arrangement provides rotational restraint to prevent column-beam joints from rotation. Therefore, a structure with this type of eccentricity arrangement may be stiffer than its concentric counterpart because of this rotational restraint [24]. This is not the case for an eccentrically K-braced frame or an eccentrically X-braced frame; they are always softer than their corresponding concentrically braced frames [7].

All the mentioned eccentric schemes have been shown by quasistatic tests to be very promising. They all possess high strength, large stiffness, and very ductile hysteretic behavior. Especially, they demonstrated no pinching of hysteresis loops or degragation in strength and stiffness. To the knowledge of the writer, however, no genuine earthquake-resistance dynamic testing of eccentric bracing was performed prior to this shaking table experiment, which was conducted in the Earthquake Simulator Laboratory at the Earthquake Engineering Research Center, University of California, Berkeley in April 1981.

CHAPTER TWO

TEST STRUCTURE AND SPECIMENS

2.1. The Formulation of the Test Structure

To reduce the expence of the experiment, it was decided to make use of an existing one-third scale nine-story steel building frame originally designed for the study of the column uplifting behavior of buildings [11]. The skeleton of the nine-story structure is shown in **Fig.** 5, and the dimensions in **Fig.** 6, taken from Reference 11. This structure comprised two three-bay plane frames in the longitudinal direction, and four one-bay plane frames in the transverse direction. An eccentric K-bracing system was placed in each of the two exterior one-bay frames. The eccentricity of the bracing system was 12 inches. Double angles $L1\frac{1}{2}\times1\frac{1}{2}\times\frac{1}{8}$ were used for the braces of the upper seven stories. Stronger double angles $L2\times2\times\frac{3}{16}$ were used to make the braces of the lower two stories. For the floors, single angles $L3\frac{1}{2}\times3\times\frac{1}{4}$ were used to make an X-shaped brace system. As mentioned in Reference 11, the eccentric K-bracing system was intended not only for increasing the torsional rigidity of the structure, but also for future testing of that particular kind of bracing system. In planning the present reseach, however, it was found that extensive modifications of the structure were needed in order to study the eccentric bracing system. The reasons for and details of the modification will be discussed in this chapter.

Comprehensive elastic and inelastic analyses were carried out on the nine-story structure in exactly the same condition as was used in the original uplifting tests, but with the direction of the structure turned 90 degrees so that the braced plane frames were parallel to the plane of shaking table motions. Of these analyses only a few by the non-linear analysis program, DRAIN-2D, will be discussed.

The earthquake motions used in the preliminary analyses were derived from the N-S component of the El Centro, 1940, earthquake. The time scale of this component was reduced by a

factor of $\sqrt{3}$ to maintain similitude*. To create a more damaging ground motion, the acceleration amplitudes were increased to have a peak value of 1.0g, which was presumed to be the maximum table acceleration that would be generated by the table in this experiment. Assuming a fixed table condition, i.e., without considering any pitching or rolling of the table, and assuming that the braces can develop their full strengths in compression and in tension, the analysis predicted that a ductility factor of 5.6 would result in the bottom links and of 1.5 in the links of the second story.

In the nine-story structure, the braces in the bottom two stories are the double angle, $L2\times2\times\frac{3}{16}$, which have a section area twice as large as the double angles $L1\frac{1}{2}\times1\frac{1}{2}\times\frac{1}{8}$ of the remaining braces in the upper seven stories. The height of the first story is one third larger than the others. Therefore, the second story has the strongest braces in compression because they have the smallest slenderness ratio. The analytical results reflected the property of this structural geometry by indicating inelastic brace yielding and buckling in the 1st, 3rd, 4th, and 5th stories, in addition to significant shear yielding of the two first-story links.

Since brace buckling and yielding may limit link-damaging ability, it is interesting to study the difference in link damages between a frame with all elastic braces and a frame with some braces that yield and buckle. To investigate the difference, the analysis was repeated, using a brace system with a brace area of 2.72 square inches (equivalent to the section area of a double angle $L2\times2\times\frac{3}{8}$) in each story. In this repeated analysis all braces remained elastic. However, similar link nonlinearity characteristics were calculated. A ductility factor of about ten was found in the first-story links and of 1.2 in the second-story links; the rest of links remained elastic.

These results showed that the nonlinearity in the lower links did not propagate up into the links of the upper stories and significant shear yielding took place only in the first story links. This was attributed to the soft-story response characteristic of the nine-story structure because a

* Discussed later in Section 2.6.

collapse-mechanism was formed in the bottom story as the links yielded significantly.

Even though significant shear yielding was predicted in the bottom links, however, the reproduction of these results on the shaking table was doubtful because the overturning moment and base shear requirements associated with the response were far beyond the capacities of the shaking table. According to Reference 11, the maximum permissible base overturning moment is 1700 ft-kips whereas the calculated overturning moment was almost twice this amount.

Besides, because bolted connections not only reduce the gross area but introduce a notch effect, the braces of the original design were not able to develop their full strengths. Thus premature failure is bound to happen before the braces' capacities are reached. Moreover, slippage at joints would be inevitable. Bolted joints are practical only if the brace capacity is large enough to cause link damage before any joint slippage occurs. For instance, premature brace failure due to insufficient bolted joints was observed in damages of Miyagiken-Oki earthquake [12].

Consequently, it was decided that three major changes were required to make the structure suitable for this research.

The three modifications are:

(1) reducing the height of the test structure from nine stories to five stories, i.e., from 28 feet to 16 feet in height. This modification drastically reduced the base overturning moment requirement so that it would be within the range of the shaking table capability. The reduction in height was carried out by taking the upper half of the nine-story frame and resting it on column extensions to make a complete structure with a suitable first story.

(2) inverting the braces of the even-numbered stories to create an eccentric X-bracing system instead of the original eccentric K-bracing system. The resulting eccentric X-bracing system is shown in **Fig.** 7. This change causes the shear forces of two consecutive stories to be added together in damaging the link between them.

With this modification, the brace stress levels required to induce shear link damages were greatly reduced. Therefore, the use of braces that are stockier than the existing ones became unnecessary, and also the required base shear input from the shaking table was reduced.

(3) changing the brace-girder and brace-column joints from the bolted type to a welded type, so that the braces can have ductile performance without slippage and can develop their full strength should their elastic capacity be exceeded.

2.2. Allocation of Concrete Weights

Concrete weights were added to the structure to introduce the desired inertia forces. The allocation of the concrete weights is constrained by the following conditions:

(1) the shaking table payload capacity, which is about 100 kips,

(2) the practicality of managing the concrete weights into the clearances of stories, and

(3) symmetric distribution of masses.

The weight allocation chosen is shown in **Fig.** 8. Including the weight of the structure (about one kip per story), the weight of the structure after addition of concrete weights is 95 kips distributed from top to bottom in a pattern of 25-19-19-19-13 kips.

The effect on the response of putting the greater weight on top of the structure can be interpreted as equivalent to the effect of some imaginary higher stories.

2.3. A Further Modification of the Test Structure

Based on preliminary analyses of the five-story eccentrically X-braced frame shown in **Fig.** 7, the base shear requirement for the structure to develop significant nonlinearity in the shear links is about 110 kips, and the associated overturning moment is about 1300 ft-kips. It has been mentioned earlier in Section 2.1. that the shaking table has a base shear capacity of

roughly 100 kips and overturning capacity of 1700 kips; however, a review of the previous shaking table tests indicated that a base shear of 80 kips was rarely achieved.

To assure a successful experiment, it was decided to remove the lateral force resisting ability from the two interior unbraced plane frames, thereby putting nearly the entire lateral load on the two exterior braced plane frames. Not only would this bring the base shear requirement within the capacity of the table, but it would also prevent forces from redistributing between exterior and interior frames at moments of link yielding in the exterior frames. Thus, the seismic forces can be more effective in damaging the critical elements of the exterior frames.

Accordingly, the high strength bolts at girder-and-column connections of the interior frames were removed or totally loosened. The interior girders were still supported by gusset plates welded to columns. Thus, the disabled girders had little contribution in resisting the story shears. Each 'dummy' girder was expected to have no role except supporting its own dead weight. It was believed that the rigidity of the floors was not harmed by this modification, because it was guaranteed by the strong X-shaped floor bracings made of heavy angles $L3\frac{1}{2}\times3\times\frac{1}{4}$.

2.4. Links and Specimens

2.4.1. Design of the Eccentric X-Bracing System

To investigate how the strength of shear links can affect the response of a structure to earthquake excitations, replaceable shear links were designed. Links of various strengths thus could be installed into the structure successively during the testing program. Also the replaceable link design could have practical value because it may be easier to repair a structure by replacement of damaged removable links.

An over-all view of the five-story eccentric X-bracing system is shown in **Fig.** 7. The second-story brace size was chosen to be the same size as that of the upper stories, namely, the

double angle $L1\frac{1}{2}\times1\frac{1}{2}\times\frac{1}{8}$, while the first story braces were selected so as to have a similar stress level to that of the second floor braces. Welded joints stronger than the tensile strength of the braces were desined, so that the braces could develop their full strength and behave in a ductile manner even if their capacities were exceeded.

As shown in **Fig.** 9, three different kinds of links were designed and fabricated. Denoted by the section used, they are (1) M6×4.4, which has the thinnest web of all and thus the lowest shear capacity, (2) W6×9, of which the flanges were trimmed away 13/16 inch from both sides to make the bending moment capacity compatible to its shear capacity, (3) W6×9, which is the original first-story girder section. All links were ten inches in length from end to end. The eccentricity was eight inches, however, determined as the distance between the two intersection points of the center lines of braces and links.

The choice of this eccentricity was based on the shear and the moment capacities of the weakest link according to the suggestion given in Reference 13 that the shear capacitp, V_p, and the reduced moment capacity, M_{ps}, should satisfy the following inequality:

$$1.1\,V_p \leqslant \frac{2M_{ps}}{e} \leqslant 1.3\,V_p \tag{1}$$

where e is the eccentricity. The shear and the moment capacities are calculated from the following two equations:

$$V_p = \frac{\sigma_y}{\sqrt{3}}\left(d - t_f\right)t_w \tag{2}$$

$$M_{ps} = t_f\, b_f\, \sigma_y \left(d - t_f\right) \tag{3}$$

where σ_y is the uniaxial tensile yield stress of the steel, and t_w, d, t_f, b_f are the web thickness, section depth, flange thickness and flange width respectively.

The link capacities of the first two kinds satisfy this inequality, while the third has a bending capacity much higher than its shear capacity.

Annealing the Links of Specimens 1 and 2

Because of rapid cooling and cold forming, steel coupons display higher yield stresses when they are tested in as-rolled condition. The phenomenon is demonstrated by the coupon test results in **Fig.** 10. Annealing is often used to remove residual stresses. Accordingly, the M6 × 4.4 and flange-cut W6 × 9 links were annealed as a whole to remove the residual stresses due to link fabrication and steel manufacturing. It was hoped that the shear strength of the annealed links would be reduced sufficiently so that the base shear requirement would be brought further down to ensure a successful experiment.

The thermal condition under which the annealing was done is qualitatively shown in **Fig.** 11. During annealing, each link was buried in a sand box to have a gradual temperature rise. Boxes, containing the links, were left in the furnace to cool off after the furnace was turned off.

2.4.2. Definition of the Specimens

The term *Specimen* is used to denote the test structure with a particular kind of shear link installed in it. For example, Specimen 1 designates the test structure with the first kind of shear link, i.e., the weakest links, M6 × 4.4. Thus different links make different specimens, even though the test structure is the same otherwise. Consequently, there were a total of three specimens used in this test program, namely, Specimens 1, 2 and 3.

By using the DRAIN-2D program, analyses of the preliminary five-story eccentrically X-braced frame (shown in **Fig.** 7) were carried out to examine the possible performance of the structure under earthquake excitations. The earthquake motion used was the same as the one used in the preliminary analyses of the nine-story structure. As described before, the earthquake was speeded up by a factor of $\sqrt{3}$, and the intensity was scaled up to have a peak acceleration of 1.0g.

Significant shear yielding with a ductility factor of about 15 in the bottom link was predicted by the analyses. The middle link, however, showed at most a ductility factor of 1.2,

and the top link remained elastic. Therefore, to economize on expenses, it was decided that the modification of the bracing system be limited to the lower two stories only. The bracing system used in the test structure was finally chosen to be as shown in **Fig.** 12-1. This system will be referred to as the eccentric X-bracing system, or briefly as ecc-X-bracing. Accordingly, the structure will be called the ecc-X-braced structure. The detailed design layout of the lower two stories is shown in **Fig.** 12-2. Some pertinent dimensions not available in **Fig.** 12-2 are given in **Fig.** 21-1, where the deployment of elastic strain gages is shown.

To give a global idea of the integrity of the finalized test structure, the skeleton of the entire structure is sketched in **Fig.** 13. The dashed lines in the figure indicate the positions of 'dummy' girders.

As mentioned previously, the test structure was anchored to the shaking table with its braced plane frames parallel to the direction of table motion, i.e., the north-south direction, thus producing an essentially two-dimensional test. The two braced frames were at the east and west ends of the structure. The west frame was close to the shaking table control room, and much more instrumentations were installed in it than the east frame.

The preliminary analyses indicated that inelastic behavior was expected to take place mainly in the first and second stories, where the eccentric X-bracing was installed. The two disabled one-bay interior plane frames are assumed to take a negligible part in the lateral resistance and are only occasionally mentioned in the discussion that follows.

Finally, the term 'test frame' is used to denote the ecc-X-braced plane frame; if it is not specifically pointed out, the 'test frame' indicates the west frame. And the term 'test structure' is reserved for the times when the whole structure is involved. In other words, *frame* implies the 2-dimensional nature of the eccentrically braced frame while *structure* designates the whole specimen.

2.5. Collapse Mechanism of the Test Structure

Because the columns bent about their weak axes, the structure was of the weak-column-strong-girder category. The section moduli of girders are about 3 times as large as that of the columns. Concurrently with link failure, plastic hinges tended to form at the lower ends of the first-story columns and at the upper ends of the second-story columns. In **Fig.** 14, the collapse mechanism of this test structure is illustrated. As shown, the rotation of the link is nine times as large as that of the columns. This implies that a small ductility factor in the columns is accompanied by a large ductility factor in the link.

After link yielding, the test structure tends to behave like a structure with a soft story. However, unlike a conventional soft story frame, the eccentrically X-braced frame has a tendency to recover its lateral stiffness with increasing deflections since sufficient deformation can make the shear deformed link become an 'axial link' between the two tension braces. This mechanism is more likely for short links because shorter links rotate more in compliance with column rotation. The measured axial response of the west link of Specimen 3 will be discussed in Section 6.1.6.

2.6. Similitude Consideration

The test results can be extrapolated to represent those of any true-scale structure through laws of similitude. Although the tested structure is not the model of a particular prototype, a corresponding prototype can be formulated by similitude laws.

The similitude ratios, calculated when the geometric scale or the length ratio is assumed to be one third (which seems to be a reasonable scale) and the acceleration ratio is one because both the model and the prototype are in the same gravitational field, are listed in Table 1.

Similitude Ratios

Parameter	Prototype/Model
Length	3
Time	$\sqrt{3}$
Mass	9
Displacement	3
Acceleration	1
Stress	1
Strain	1
Force	9
Moment	27
Area	9
Moment of Inertia	81

Table 1. Similitude Ratios

CHAPTER THREE

TEST FACILITIES

3.1. Earthquake Simulator

The experiment was carried out at the Earthquake Simulator Laboratory. Rea and Penzien give a complete description of the laboratory in Reference 14, so only features pertinent to this experiment will be discussed here.

The main facility of the laboratory is the $20' \times 20'$ shaking table, i.e., the earthquake simulator. The shaking table is a one foot thick concrete slab heavily reinforced both with ordinary reinforcement and with post-tensioning tendons, and weighs about one hundred kips. It was designed to be stiff so that its lowest natural frequency is higher than 20 cps and therefore it behaves essentially like a rigid body when it is operated in the frequency range from 0 to 17 cps.

The table is independently driven by three 50-kip horizontal hydraulic actuators and four 25-kip vertical actuators, located in the pit below it. The actuator forces are resisted by a massive foundation, which is a reinforced concrete open box with a wall thickness of 5 feet. The inside dimensions of the box are $22' \times 22' \times 10'$. The shaking table is the lid of the box. The details of the shaking table system are shown in **Fig.** 15.

The flow rate of the servo-valves of the actuators limits the maximum velocities in the horizontal and vertical directions to 25 in/sec and 15 in/sec, respectively. The stroke of the horizontal actuators is 12 inches, i.e., 6 inches in both positive and negative directions. And, the stroke is 4 inches for the vertical actuators. However, the horizontal stroke is limited to about 10 inches.

During operation, the chamber of the box is pressurized so that the weight of the shaking table plus the payload it carries is balanced by the differential air pressure. Consequently, the vertical actuators are free from carrying any gravity load. The actuators have a capacity to

accelerate the unloaded table to a maximum of 1.0g vertically, and 1.5g horizontally. The performance limitations of the shaking table with zero payload for both horizontal and vertical motions are shown in **Fig.** 15-1.

Normally source earthquake signals are in the form of digitized acceleration time histories. Double integration of the accelerations is necessary to obtain the required displacements. Then the displacement time histories are transmitted to an analog tape recorder. When a test is to be performed, the analog tape provides the input to the MTS console, which controls the motion of the shaking table.

Because large overturning moments are generated when heavy and tall structures are tested, control of the table pitching motion is essential and a passive stablizing system has been installed to increase the pitching resistance. With additional help from the four vertical acuators (that also serve as active stablizers), the shaking table has a nominal overturning capacity of up to 1700 ft-kips.

3.2. Data Acquisition System

Associated with the shaking table are a NOVA 1200 mini-computer, operating in conjunction with a Diablo 31 magnetic disk unit, and a Neff data aquisition system, which has the ability to sample up to 128 analog channels at a rate up to 155 samples per second per channel.

By passing through an analog-to-digital converter housed in the Neff system, analog signals originated in accelerometers, DCDT's, strain gage bridges, etc., are digitized and stored on the magnetic disk before the they are transferred to the 9-track Wang digital magnetic tape recorder for permanent storage. The data was further transferred to 7-track CDC 6400 compatible magnetic tapes for processing at the campus.

Photographs of the control room and the shaking table are shown in **Fig.** 15-2*. In the background of the control room is the NOVA computer and the data aquisition devices. The MTS control console is at the right end of the same picture.

*This picture was taken before installation of the second tape drive. Currently, there are two tape drives.

CHAPTER FOUR

INSTRUMENTATION

Accelerometers, potentiometers, direct current differential transformers (DCDT), as well as strain gages of elastic and post-yield types were used to measure the behavior of the test structure subjected to simulated earthquake table motions.

For Specimens 1 and 2, 88 channels of instrumentation were installed. For Specimen 3, the two channels used to measure plastic bending of the west shear link were replaced by one channel measuring the axial strain of the same link. Therefore, the total number of instrumentation channels for Specimen 3 was 87.

Of the total channels, 7 were devoted to monitoring the shaking table motions; they measured average table displacements and accelerations in the horizontal and the vertical directions, and the pitching, rolling, and twisting angular accelerations of the table.

The sampling rate of all channels in each test was 100 Hz, i.e., 100 samples per second per channel.

A detailed description of the instrumentation and positions where they were installed, together with their purposes are presented in the following sections. A complete listing of channels used for each specimen is given in Appendix A.

4.1. Floor Acceleration Measurement

Five accelerometers were used to measure five floor accelerations. They were mounted on the north column of the west frame. The five accelerometers can be seen in the picture of the test structure in **Fig.** 1. They are located in the joint panels of the column nearest to the reader.

Of the five accelerometers, one was a Statham A39TCB-5-500 resistive bridge strain gage

type, which needed a strain gage conditioning circuit. The other four were Setra model 141A linear accelerometers that produce instantaneous DC output signals proportional to sensed accelerations. The Statham accelerometer was used at the first floor level and the Setras at the upper floor levels.

4.2. Floor Displacement Measurement

Positions of potentiometers for measuring displacements are shown in **Fig.** 16. One potentiometer was assigned to each floor to measure the horizontal displacements of the west frame. In addition, four potentiometers were assigned to the south interior columns to measure the distortions of the 4th and 5th floors. Another potentiometer was assigned to measure the horizontal displacement at the top of the east frame in order to record, if any, the torsional displacement of the structure.

The linear potentiometers used for displacement measurement were from Houston Scientific Inc. They were mounted on a reference frame off the shaking table. Hence, displacements measured by the potentiometers are absolute values, not relative to the shaking table. Therefore, to obtain relative floor displacements, the table displacement must be subtracted from the quantities measured by the potentiometers.

4.3. Local Inelastic Deformation Measurements

Preliminary analyses indicate that the most likely type of nonlinear behavior is shear yielding of the links. Buckling of the 1st floor braces of Specimen 3 is also likely to occur. In addition, as visualized from the collapse mechanism of the test structure (see Fig. 14), nonlinear bending strains are expected at the top ends of the 2nd story columns and at the bottom ends of the 1st story columns of the two ecc-X-braced frames. Plastic bending strains can also be expected at the ends of the shear links, especially for Specimens 1 and 2 because the links' bending strength is close to their corresponding shear capacity. Accordingly, it was necessary to

monitor local deformations of all these positions of possible nonlinearities.

4.3.1. DCDT Stations

Two DCDT's, Sanborn model 7DCDT-500 with ± 0.5 inch stroke, were used to measure the shear deformation of each shear link. One DCDT, Sanborn model 7DCDT-1000 with a travel range of ± 1.0 inch, was used to measure axial elongation of each of the four first floor braces. Another two DCDT's, Sanborn model 7DCDT-3000 with a stroke of ± 3.0inches, were positioned to measure lateral displacements at the middle of the two first floor braces of the west braced frame, in case brace buckling should occur.

The use of two cross DCDT's on the links to measure the diagonal length changes associated with shear deformation was adopted after Clough and Tang, who used the same setup to measure shear deformations of joint panels [15].

Positions of all DCDT's are shown in **Fig.** 17. (The links shown in the figure are the damaged links of Specimen 1 after tests*). The aluminum frame for mounting the DCDT's on the links is shown in **Fig.** 18.

4.3.2. Post-Yield Bending Gage Stations

Post-yielding foil strain gages manufactured by Tokyo Sokki Kenkyujo, Type YL-10, were chosen for the measurement of inelastic deformations at places where plastic hinging was possible. Four post-yield strain gages were installed on the four flange tips of a column section to measure the bending strain at that section, because it would bend about its weak axis. At both ends of a link, gages were placed along the center lines of both flanges to measure the link plastic bending strain. In addition, post-yield gages were also installed at the top ends of the 1st floor columns in case buckling of the 1st floor braces should lead to large strains in the columns at those positions.

*Detailed description of the link damages is in Section 6.1.2.

To minimize the volume of data, only the west frame was fully instrumented with post-yield strain gages. The locations of post-yield gage stations are shown in **Fig.** 19.

4.3.3. Post-Yield Rosette Stations

Because the links' nonlinear behavior is important for the evaluation of the efficiency of the eccentric bracing system, post-yield strain rosettes were deployed on the webs of the shear links to acquire additional imformation on local yielding strain distribution. The rosette stations used for each link of all specimens are shown in **Fig.** 20.

4.4. Force Measurements

Structural overturning moments and base shears, and link shear forces were derived from pertinent member forces. In addition, overturning moments and base shears can alternatively be derived from the inertia forces determined as the products of floor masses and their corresponding accelerations if the damping effect is neglected.

Member forces such as axial forces, bending moments, and shear forces were obtained from strains measured in the elastic portion of members. In other words, the various resultant member forces were derived by multiplying the measured elastic strains by appropriate elastic constants based on the assumptions that plane sections remain plane after straining and that strains do not exceed their elastic limits. The first assumption implies that strain distribution is linear across sections.

In the calculation of bending moments and axial forces of the structural members, nominal properties of the sections (section moduli for bending moments and section areas for axial forces) were used, and 29600 ksi was assumed to be the Young's modulus of the steel. A linear bending moment variation was assumed along the clear span of members so that shear forces and end moments could be calculated.

4.4.1. Elastic Gage Stations

Foil gages manufactured by Tokyo Sokki Kenkyujo, Type FLA-6, and foil gages manufactured by Micro-Measurement, Type EA-06-250-BG-120, were used for the measurement of elastic strains. The former gages were used to measure the elastic bending strains and the latter gages for brace strains (because of a shortage of the former type).

The locations of the gages used for elastic measurements are shown in **Fig.** 21. As mentioned above, the column bending strains were monitored by strain gages placed on the flange tips because the columns were expected to bend about their weak axes. For axial strains in columns, gages were placed along the center lines of the two flanges.

Two strain gages were used to measure the axial strain in each first or second story brace. They were placed on the neutral axis of the double-angle section with one gage on each angle; thus the axial force error due to brace bending was minimized.

CHAPTER FIVE

TEST PROGRAM

5.1. Table Motions

The two kinds of horizontal table motions used in this experiment were derived from the S00E component of the El Centro 1940 and the S74W component of the Pacoima 1971 earthquakes. No vertical excitation was applied to the structure in this experiment. The very low frequency components of the earthquakes were filtered out so that the displacements of the skaking table could remain within the favorable range of $\pm$5inches.

For some selected strong table motions, the Fourier amplitude spectra are presented in **Fig.** 22 to show their frequency content.

The El Centro motions have a more uniform spread of frequency content over the range into which most of natural frequencies of the building fall, and have a longer duration of significant shaking. The Pacoima motions have a shorter duration and include a unique long pulse, which may cause significant nonlinearity.

The intensity of the table motions was changed by adjusting the 'span setting' of the shaking table control console.

As stated in Section 2.6., because the model structure was presumed to be 1/3 of a prototype in length scale. The time scale of the table signals was divided by a factor of $\sqrt{3}$ so that the acceleration ratio is 1.

5.1.1. A Simulated Table Motion vs. Original Earthquake Record

One of the accelerations generated by the shaking table (i.e. the simulated) and the corresponding original but time-scaled El Centro earthquake record with the same peak value are shown in **Fig.** 23 for comparison. The simulated record lacks the high frequency spikes of

the original; however, the general characteristics of the original are fairly well captured by the simulated motion.

The response spectra of the two records are shown in **Fig.** 24. Since the low frequencies are filtered from the table motion to control the table displacement, the simulated earthquake is not effective in exciting soft oscillators having a period larger than 2 seconds. Additionally, the shaking table efficiency drops rapidly for frequencies greater than 15 cps, which is the actuator oil column resonant frequency. Consequently, the original motion may be more effective in exciting both low and high frequencies.

5.2. Sequence of Tests

As mentioned in Chapter 2, three kinds of links were fabricated for the experiment. Their strengths were increasing as their reference numbers, 1, 2, and 3. The test sequence adopted was mainly for safety considerations. The sequence started with the least intense table motion and the weakest specimen, Specimen 1. The strength of the table motion was increased in successive tests until significant damage was observed. Then the damaged links were replaced by a stronger pair and the procedure repeated. To evaluate the property changes because of link damage, free vibration tests were carried out at the beginning and at the end of the test series for each specimen. The structure was given an initial deformed position by tightening a cable attached to an anchorage peg in the floor away from the shaking table. The free vibrations were initiated by cutting the connecting bolt between the cable and the peg.

The cable was in the plane of symmetry, which is parallel to the two ecc-X-braced plane frames of the structure, and was attached at the fifth floor level. In some early tests it was attached at the fourth floor, but since the fourth floor is approximately a stationary node of the second mode of the structure, the second mode was not appreciably excited; hence these tests were not so satisfactory. A complete chronological listing of tests performed in this experiment is presented in Table 2.

In Table 2, every test for each specimen is identified first by the file name, which indicates the date of the test (day, month, year) and the sequence number of the test for that date. In addition, except free vibrations, each test is named by a combination of ordered symbols representing the time scaling factor, the source signal and the span setting of the control console. EC and PAC represent the El Centro and Pacoima sources, respectively. The span setting controls the intensity of a table motion. It represents the displacement directly, but the peak acceleration of a given motion (shown in column 3) is also approximately linearly proportional to the setting.

The numbers shown in the fourth column of the table are the frequencies corresponding to the spikes on the Fourier spectra of the fifth floor accelerations. The spectra were shown on the screen of the real-time FFT analyzer during free vibration tests. The frequency corresponding to the largest (also the first) spike in each free vibration test roughly represents the first-mode frequency of the test structure during a small amplitude vibration.

The interesting fact that can be generalized from the free vibration real-time results is that link damage did weaken the structure. For example, for Specimen 1, the Fourier amplitudes of the fourth floor accelerations of the 160481.01 and 170481.07 free vibration tests were plotted together in **Fig.** 25 for a typical comparison. The first natural frequencies before and after damage are 3.223 cps and 2.734 cps, respectively. The change is equivalent to about a 30% reduction of the first mode stiffness if the effective mass is assumed to be constant.

Sequential Listing of Tests Performed on Shaking Table				
No.	File Name (1)	Test Name (2)	Acc. Peak (3)	Comments (4)
		Specimen 1		
1	150481.01	free vib.(D)		
2	150481.02	free vib.(U)		3.20, ..., ...
3	150481.03	free vib.(U)		
4	160481.01	free vib.(D)		
5	160481.02	1.73*EC 50	.103g	
6	160481.03*	1.73*EC 75B	.147g	
7	170481.01	1.73*PAC 25	.098g	
8	170481.02*	1.73*EC 200	.434g	web buckled
9	170481.03	free vib.(U)		3.10, 7.75, 18.50
10	170481.04	1.73*EC 300	.738g	web cracked, data lost!
11	170481.05*	1.73*EC 75A	.167g	
12	170481.06	free vib.(U)		2.65, 7.45, 18.30
13	170481.07	free vib.(D)		2.80, 7.55, 18.35
		Specimen 2		
14	210481.01	free vib.(D)		3.25, 7.75, 18.50
15	210481.02	free vib.(U)		3.25, 7.80, ...
16	210481.03	1.73*EC 50	.107g	
17	210481.04	1.73*EC 75	.150g	
18	210481.05*	1.73*EC 200	.415g	
19	210481.06*	1.73*EC 300	.684g	
20	210481.07*	1.73*EC 400	.981g	web buckled & cracked
21	210481.08	1.73*EC 75	.158g	
22	210481.09	free vib.(U)		3.05, 7.60, 18.50
23	210481.10	free vib.(D)		3.05, 7.65, 18.70
		Specimen 3		
24	230481.01	free vib.(D)		3.30, 7.85, 18.75
25	230481.02	1.73*EC 50	.103g	
26	230481.03	1.73*EC 75	.158g	
27	230481.04*	1.73*EC 200	.434g	
28	230481.05*	1.73*EC 400	.961g	
29	230481.06*	1.73*PAC 210	.741g	
30	230481.07*	1.73*PAC 300	1.111g	slight web buckling
31	230481.08*	1.73*EC 450	1.155g	significant web buckling
32	230481.09	1.73*EC 75	.158g	
33	230481.10	free vib.(D)		3.05, 7.55, 18.50

(U): table lifted; (D): table locked; *: selected for data reduction. on.

Table 2. Tests Performed

The suffixes U and D represent up and down conditions of the table during the free vibration tests. When the table is up, the structure-table system is supported only by the differential air pressure. When the table is down, it is clamped against pitching. As seen in the 4th column of the table, the frequencies for the table-lifted condition are slightly smaller than those

for the table-locked condition resulting from structure-table interaction.

From the complete set of tests conducted on the test structure, those showing significant shear link yielding were selected for data reduction. In Specimen 1, the test before and the test after the link damage were also selected to investigate the effect of the damage on the response of the structure and also to study the post-yielding behavior. The data filenames of the tests selected for data reduction are suffixed by an asterisk in the table.

CHAPTER SIX

TEST RESULTS

Generally speaking, all specimens had similar responses to the El Centro table motions. Therefore, in the first half of this chapter, 6.1., attention is focused on the general presentation of various response quantities; emphasis is placed on a comparison of the responses of specimens with different link strengths, in order to to understand the effect of link strength on the seismic resistant behavior of a structure with shear links as damageable 'fuses'.

The second half of the chapter, 6.2., is devoted to a *complete* review of the recorded data from the selected runs.

6.1.1. Performance of the Test System

6.1.1.A. Behavior of the Test Structure

Through the experiment, the test structure behaved; there was no danger of collapse, and brace buckling was prevented successfully by the yielding of the links. In the rest of the structure other than the links the strains remained elastic in every test. However, permanent elastic strains due to distortion of shear links were observed in the column bending strains.

6.1.1.A.1. Symmetric Deformation of the ecc-X-braced Frame

When a beam is bent to its plastic moment capacity, local and/or lateral buckling may occur. Therefore, it was expected that, after the links yielded in shear or bent to their plastic capacity, the girders containing the links would exhibit lateral buckling or twisting about their longitudinal axes. This twisting was previously observed in a quasi-static test of a 3-story eccentrically K-braced frame described by Manheim [16]. Therefore, plans had been made to prevent twisting by adding extra lateral bracing should the need arise during the experiment.

Fortunately, no out-of-plane distortion of the ecc-X system and no aforementioned twisting of the girders were observed after the completion of the entire experiment. Besides, even significant non-linear link deformation had occurred, the center lines of the 'link-girders' remained straight without appreciable up and down zigzags. Thus the damaged links were easily replaced.

This favorable minimal permanent deformation is attributed not only to the intrinsic properties of the table motions used, but also to the elastic behavior of the eccentric braces and the geometry of the X-shaped brace arrangement. During earthquakes, the X-braced girders always have two braces in tension to compensate for the unstable twisting tendency induced by the two compression braces. Since all braces remained elastic without buckling, the symmetry of the test frame was effectively preserved. This type of response is preferable to that of a frame which has brace-buckling behavior which can destroy the sysmmetry of the frame. In addition, retaining symmetry is advantageous in the mathematical modeling of the structure because only half the structure need be considered.

6.1.1.B. Transverse Vibration of Girders

Because the inertia forces of the massive concrete weights acted horizonally causing bending of the floor girders about their weak axes, the lateral vibration of these girders was significant, and easily seen in most of the tests.

Explosive pounding metal noises were occasionally heard because of sudden loosening of fasteners anchoring the concrete weights to the girders. No matter how much the fasteners were tightened, some always loosened, especially during tests with significant link yielding, i.e., when the shaking was intense.

Since steel has low damping and a high Young's modulus, it is an excellent sound conducting material. Any mechanical disturbances caused by the shaking table during operation, or by sliding of concrete weights, etc., can generate high frequency vibrations in the framed steel,

to which accelerometers were attached. This explains the existence of high frequency tremors and the tremendously high and sharp spikes shown occasionally in the floor acceleration records in some tests. The spikes were caused by loose fasteners bumping into the steel girders.

Unlike the floor accelerations, the table accelerations are free from the above-mentioned high frequency effects. This is because the table accelerometers are mounted on the concrete slab which can absorb trivial high frequency noises. An examination of results from previous shaking table tests [11,17] showed that accelerometers mounted on concrete weights yield smooth data without erratic spikes, as expected.

Therefore, the high frequency tremors and wild spikes seen in the acceleration records have no significance.

6.1.1.C. Floor Distortion

As mentioned in Chapter 2, even though the interior girders were disabled, the rigidity of the floors is guaranteed by the strong X-shaped bracing in the floors.

Table 3 gives the maximum values of the fifth floor distortions calculated as the difference between the relative displacements of the east exterior and interior frames. As can be seen from the tabulated data, the floor distortion is at most 10% of the floor relative displacements. **Figure** 26 is the maximum floor distortion time history.

For the floor dimension of 72"×216", a distortion only 10% of the corresponding floor relative displacement and with a value less than a quarter of an inch is considered insignificant and will be neglected in the analytic study.

	Max. Floor Distortion	% of Floor Rel. Displ.
	Specimen 1	
1.73*EC 75b	...	...
1.73*EC 200	.0874in	7.79%
1.73*EC 75a	...	...
	Specimen 2	
1.73*EC 200	.0893in	8.75%
1.73*EC 300	.1392in	10.01%
1.73*EC 400	.1302in	7.47%
	Specimen 3	
1.73*EC 200	.1203in	7.98%
1.73*EC 400	.1930in	9.48%
1.73*PAC210	.1097in	7.77%
1.73*PAC300	.1448in	7.66%
1.73*EC 450	.2223in	9.81%

Table 3. Floor Distortion

6.1.2. Observation of Damages

General Characteristics

Web buckling and subsequent web fracture of the shear links are the only damage observed in the test structure. Before this damage occurred, the links experienced tremendous nonlinear deformation by shear yielding. For El Centro table motions, three major excursions of shear yielding were evident; the webs looked like rubber pads in shear motion. Figure 27 shows typical evidence of link damage in terms of hysteretic behavior. As illustrated in the figure, the west link of Specimen 1 lost more than 60% of its original strength. A detailed description of the damage to each of the specimens is given in the following subsections.

Heavy spalling of scale and/or paint on the surfaces of the links were also evidences of severe yielding. However, this flaking occurred mainly in the center part of the webs and was hardly observed near the end plates. This is because the warping restraint provided by the end plates prevented shear deformation in that vicinity.

The web buckling pattern may be described as symmetric or antisymmetric depending on the shape of its sideward bulging. During intense cyclic loading, the alternating diagonal compressions caused buckling along the two diagonals of the web. If the buckling in the two directions caused bulges toward the same side, a roof-like symmetric shape was formed. Otherwise, an antisymmetric buckling mode emerged, and one or two 'nodes' of negligible or small sideways displacement were created.

6.1.2.A. Damage to Specimen 1

The links of Specimen 1 were the most severely damaged elements. They buckled first when subjected to the 1.73*EC 200 excitation, and additional damage was caused by the 1.73*EC 300, which fractured the specimen's west link.

With DCDT's in position, the deformed links are shown in Fig. 17. The west link buckled in the two-node antisymmetric mode which shows out-of-plane distortion toward either side

of the web. At the nodes, the straining was so intense that one of the nodes was torn into an X-shaped open crack. Each branch of the crack slopes at 45 degrees from the horizontal axis. The length of the X-crack is about two inches (50 mm) along each branch. Also a half-inch 45-degree-slope hairline crack was found at the other node of the same link.

The deformed web of the west link can be approximately separated into six parts by its 'nodal lines', the displacement for each part being in and out alternately. The term 'nodal lines' indicates lines having a negligible sideward displacement. The permanent maximum out-of-plane deformation was 5/8 inch (15.9 mm) in the center lower part.

Similarly, the east web can be separated into four parts by ridge lines, instead of nodal lines, as shown in **Fig.** 17, which shows clearly the damaged patterns of the two links. The east link has a maximum permanent bulge of 7/8 inch (22.2mm) at the web center.

In addition to the flange bending, flange twisting was found in the west link resulting from a S-shaped web distortion of the link. The permanent displacement of the 'bowed' flanges toward the web was 5/16 inch (7.9mm) maximum, and the angle of twisting about the center-lines of the two flanges was about 30 degrees.

6.1.2.B. Damage to Specimen 2

There was no appreciable web buckling in Specimen 2 until the 1.73*EC 400 table motion was applied; this motion buckled both links and cracked the west one. A unique feature of this link damage is that both links have the same antisymmetric buckled shape with one node at the center of the web. The pictures of the two deformed links of this specimen are shown in **Fig.** 28. It should be noted that the east link was painted white.

Similar to the west link of Specimen 1, but with four parts instead of six, the 'nodal lines' separate web zones of alternately in and out displacements. The maximum out-of-plane displacements for the west and the east links are 7/16 inch (11.1mm) and 6/16 inch (9.5mm), respectively. Moreover, an X-shaped closed crack with branch lengths of 1.5 inches (38.1mm)

and 0.75 inch (19.1mm) was found in the node of the west link. The inward displacements of the bent flanges due to web distortion were about 1/16 inch (1.6mm) and 1/8 inch (3.2mm) for the west link and the east link respectively.

After the tests, one strain rosette on the west link was still secure without peeling (see **Fig**. 28). The square printed on the rosette was deformed into a rhombus and a permanent shear strain of 9% was measured from the rhombus.

6.1.2.C. Damage to Specimen 3

Links of Specimen 3 were so strong that, after the 1.73*EC 400 test, their webs remained flat without any visible permanent deformation even though significant yielding had been observed and evidenced by heavy flaking on the web surfaces. A very slight out-of-plane displacement was first observed when the 1.73*PAC 300 test was completed. Finally, significant web buckling was resulted from the 1.73*EC 450 test, which had a peak acceleration of 1.155g. The damaged links are shown in **Fig**. 29. It should be noted that the east link was painted green so that possible damage could be seen better.

The damage patterns of the two links for this specimen were different. The west link buckled into an anti-symmetric shape, whereas the east link had symmetric buckling. However, the extent of buckling was less, and the deformed shapes were not as clearly defined as those of the other specimens. For instance, the central node of the west link had appreciable sideward displacement, that was not the case for Specimen 1 or Specimen 2. This sideward displacement (relative to adjacent bulges) was about 1/2 inch (12.7mm) toward the west, whereas the maximum 'absolute' displacement (relative to the undeformed position) toward the east was 3/16 inch (4.8mm). An 11/16 inch (17.5mm) out-of-plane displacement was measured at the center of the east link, which was concaved inward to the test structure.

6.1.3. Overall Review of Link Measurements

6.1.3.A. Reliability of Link Strain Measurements

All gages recorded elastic strains and remained undamaged except those installed on the shear links. Most strain gages on the links were peeled off prematurely before the prescribed maximum gage strains were reached. However, most gages remained in good condition before web buckling occurred. The problem of strain gage peeling was immaterial since strains taken from buckled webs are difficult to interpret and have little significance.

In reality, the yielding behavior of the links was a complicated process and the strains in the webs were by no means uniform. Thus local strain measurements from a few rosettes cannot give a clear picture of the shear strain distribution. The general nature of the shear yielding phenomenon, however, was lucidly portrayed by the local strains.

Definition of the Pseudo Shear Strain

The links' shear deformations were measured in a global sense by two cross DCDT's mounted on each link. Therefore, instead of local shear strain, the DCDT's measured the global 'pseudo shear strain' of a link. The term 'pseudo shear strain' was adopted because the measurement not only included the deformation due to shear but also the contribution from bending of the link even though the bending contribution is not as significant as that of the shear deformation. Nevertheless, the bending influence on the accuracy of this measurement scheme may become substantial for long links. The pseudo shear strain is equal to the true shear strain for cases of pure shear and pure bending. For the latter, the shear strain is zero.

In this study of link deformation, it is probably not valid to assume that plane sections remain plane during bending because of (1) the presence of residual stresses resulting from steel manufacturing and link fabrication processes, (2) the boundary effect resulting from the

small length-to-depth ratio (1.e. 1.50), (3) the existence of an enormous shear force, (4) the interaction between bending and shearing deformation, and (5) the change of configuration due to web buckling. Hence, link bending strains measured on the basis of the plane-sections-remain-plane assumption is of little significance. Typical bending strains recorded in the west link in the 1.73*EC 400 test of Specimen 3 are shown in **Fig**. 30. The corresponding gage stations are shown in **Fig**. 20. Seen in **Fig**. 30, separation of the two strain histories occurs at about two seconds. However, the response symmetry is maintained.

6.1.3.B. Link Shear Strains

The pseudo shear strains of the links were measured by diagonal DCDT's, as mentioned above. A sketch showing the pertinent dimensions is presented in **Fig**. 31.

By assuming that a rectangle web panel is deformed into a pure shear state as depicted in **Fig**. 31 and that the XY coordinate system is used to denote the undeformed configuration and the xy coordinate system to denote the deformed configuration, this shear deformation can be expressed as

$$\begin{Bmatrix} x \\ y \end{Bmatrix} = \begin{bmatrix} 1 & 0 \\ \tan\gamma & 1 \end{bmatrix} \begin{Bmatrix} X \\ Y \end{Bmatrix}.$$

The matrix equation can be abbreviated as

$$\mathbf{x} = \mathbf{F}\mathbf{X},$$

where

$$\mathbf{F} = \begin{bmatrix} 1 & 0 \\ \tan\gamma & 1 \end{bmatrix}$$

is the mapping matrix. The positive slope diagonal $\mathbf{D}$ ($\mathbf{D}^T = [\,e \quad d\,]$) of the shear panel (i.e. the web of a link) is deformed into $\mathbf{d}$, i.e.,

$$\mathbf{d} = \mathbf{F}\mathbf{D}.$$

If the original and deformed lengths of the diagonal are denoted by l and l', respectively, the square of the deformed length can be expressed as

$$l'^2 = \mathbf{d}^T\mathbf{d} = \mathbf{D}^T\mathbf{C}\mathbf{D},$$

where

$$\mathbf{C} \equiv \mathbf{F}^T\mathbf{F}$$

is the *deformation matrix* of the mapping [18]. Explicitly,

$$l'^2 = [\,e \quad d\,]\begin{bmatrix} 1+\tan^2\gamma & \tan\gamma \\ \tan\gamma & 1 \end{bmatrix}\begin{Bmatrix} e \\ d \end{Bmatrix},$$

or

$$l'^2 = e^2 + e^2\tan^2\gamma + 2d\,e\tan\gamma + d^2.$$

Because $l^2 = e^2 + d^2$ and if the diagonal elongation is denoted by Δ_1 (i.e. $l' = l + \Delta_1$), for small γ and if higher order terms are neglected the shear strain γ can be given by the following equation

$$\gamma \approx \frac{l\,\Delta_1}{d\,e}.$$

Similarly, the shear strain can also be expressed in terms of the elongation, Δ_2, of the other diagonal as follows:

$$\gamma \approx -\frac{l\,\Delta_2}{d\,e}.$$

For a better measurement, the shear strain γ is obtained by averaging as follows:

$$\gamma \approx \frac{1}{2}\left(\Delta_1 - \Delta_2\right)\frac{l}{d\,e}.$$

As mentioned earlier local strains were also measured simultaneously by the strain rosettes located as shown in **Fig.** 20.

Shown in **Fig.** 32 are comparisons of the pseudo (global) shear strain measured by DCDT's and the local strain measured by rosettes for the west link of Specimen 3 in the 1.73*EC 400 and 1.73*PAC 300 tests. In these two tests, little web buckling was observed. The four curves in each plot represent one pseudo shear strain (solid line) and three local shear strains (dashed lines). The long, medium and short dashed lines represent the local measurements by the north, middle, and south rosettes, respectively. As seen in the figures, all curves

display same shear yielding behavior. The highest strains were observed at the center.

6.1.3.C. Shear Force in Links

6.1.3.C.1. From Vertical Equilibrium

From the laws of statics, by applying the equilibrium condition in the vertical direction, the shear force in the links was calculated. Brace axial strains and girder bending strains were used in the calculation. The pertinent strains were determined to be in the elastic range by comparing their values with the coupon test results shown in Table 4; hence they were easily transformed into forces or moments by a simple multiplication of the corresponding elastic constants.

The free body diagram and positive directions used are shown in **Fig.** 33. The shear force in a link was calculated by adding up the shear force in the left half of the girder and the vertical components of axial forces in the two left braces. For a check of the accuracy of the measurements, the same shear force was also calculated from the right side, using the shear force in the right half of the girder and the forces in the two right braces. A comparison for this 'two-way' calculation is shown in **Fig.** 34. Except for some minor discrepancies, the consistency is quite satisfactory. An similar comparison was made for the hysteresis curves and is also shown in **Fig.** 34. This correlation shows the reliability of the measurements for the link shear force calculations.

Coupon Test Results						
	Annealed			No Annealing		
	σ_y (ksi)	$\epsilon_y = \sigma_y/29600$ *	σ_u (ksi)	σ_y	ϵ_y	σ_u
W6×8.5						
Flange	57.8	.00195	72.0			
Web	63.1	.00213	75.8			
W4×13						
Flange	44.4	.00150	66.6			
Web	48.4	.00164	67.9			
W6×9						
Flange	28.7	.00097	47.2	45.8	.00155	60.2
Flange	33.9	.00115	49.3	45.2	.00153	61.4
Web	24.4	.00082	43.2	50.6	.00171	63.7
Web	24.7	.00083	44.7	52.0	.00174	65.0
W6×4.4						
Web	41.5	.00140	56.5	50.4	.00170	71.8
Web	39.3	.00133	55.2	50.7	.00171	71.6
L1$\frac{3}{4}$×1$\frac{3}{4}$×$\frac{1}{8}$				59.3	.00200	77.4
L1$\frac{1}{2}$×1$\frac{1}{2}$×$\frac{1}{8}$				53.4	.00180	75.4

* assumed Young's modulus of steel, i.e., $E = 29600$ *ksi*

Table 4. Coupon Test Results

6.1.3.C.2. From Moment Gradients in the Links

Since shear forces are equal to bending moment gradients, the link shear forces can be obtained from bending mesurements in the links. However as discussed in Section 6.1.3.A, the assumption that a plane section remains plane after bending may no longer be valid; so even though the measured strains are within the elastic range, the direct conversion of measured bending strains into bending moments may not be justified.

The maximum shear forces of the west link of Specimen 3 calculated by the two methods just discussed is presented in Table 5.

Calculated Max. Link Shear		
Table Motion	From Vertical Equilibrium (1)	From Moment Gradient (2)
Specimen 3		
1.73*EC 200	34.7 kips	76.1 kips
1.73*EC 400	40.8 kips	94.8 kips
1.73*PAC210	34.0 kips	38.9 kips
1.73*PAC300	35.8 kips	61.4 kips
1.73*EC 450	36.9 kips	137.7 kips

Table 5. Calculated Maximum Link Shear Forces

Only in the 1.73*PAC 210 test are the results of the two methods close to each other, because in this test the yielding excursion was not very severe. Hence, the results calculated by the second method and displayed in the third column of Table 5 are of little value.

6.1.3.D. Isotropic Strain Hardening of Shear Links

The strength of the links increased in successive tests because of isotropic strain hardening. An example of this is given in **Fig.** 35 where the hysteresis loops of the west link of Specimen 2 in the beginning six seconds in three major tests are shown. Both isotropic and kinematic hardening phenomena can be clearly observed in these hysteresis loops.

The isotropic hardening is evident in Frame 1 in **Fig.** 35, which displays a growth in the elastic zone. In addition, the strength exhibited in Frame 3 is significantly larger than that exhibited in Frame 1. Also, the loops in Frame 4 would contain the loops in Frame 2. In other words, the link during the 1.73*EC 300 test was much stronger than it was during the previous 1.73*EC 200 test because of isotropic strain-hardening induced in the latter test.

The isotropic hardening had apparently reached its limit in the 1.73*EC 300 test because the elastic zones in Frames 3 and 5. are essentially equal.

Since that the link buckled in the 1.73*EC 400 test, kinematic strain hardening was prevented by the buckling. It is worth noting that a ductility factor of more than 100 can be estimated from Frame 5 if yielding excursion is taken to be the size of the largest loop, i.e., its horizontal projection on the strain axis of the plot.

6.1.4. Base Shears and Overturning Moments

Two methods were used to calculate the base shears and overturning moments: a statics method and an inertia method.

6.1.4.A. Statics Method

In this method, the appropriate force component from every contributing member is summed. The contribution from the interior frames was also included in the calculation even though it is relatively small compared with that from the exterior frames.

Because the test structure is symmetric and the direction of table motion is parallel to the symmetry plane, it was assumed that the response symmetry was preserved. Therefore, the contribution of the west half of the structure was doubled to represent the total response. **Figure 36** shows the quantities used and the positive sense of each quantity.

6.1.4.B. Inertia Method

The second method uses the inertia forces obtained by multiplying the masses by their corresponding measured total accelerations. The base shear is the sum of the inertia forces of all stories, whereas the overturning moment is the sum of the moments of inertia forces. The moment of an inertia force was computed as the product of the inertia force and the height of the corresponding mass center above ground. This method is easier and less involved, but the results may be not as reliable as those calculated by the first method. This is because inaccuracies both in measured accelerations and in the locations of the mass centers of the stories affect the results of the calculation. Besides, ignorance of the effect of damping in the inertia method will also introduce error in the calculation. The dynamic equilibrium during an earthquake is depicted by the following equation:

$$\mathbf{f}_I + \mathbf{f}_D + \mathbf{f}_S = 0,$$

where the three f's sequentially are matrices of inertia, damping, and elastic forces. As demonstrated by the equation, the inertia forces and the stiffness forces are not equal in value except for undamped systems.

6.1.4.C. Comparison between the Statics and Inertia Methods

In **Fig.** 37, results of the two calculations are presented for both the base shear and the overturning moment from the 1.73*EC 300 and 1.73*EC 400 tests for Specimen 2. Two findings emerge from a comparison of the results from the two methods.

(a) High frequency content may be seen in the inertia method results; the statics method results are smoother in appearance. This difference arises because the inertia method uses floor accelerations which are more sensitive to high frequency vibrations; whereas the statics method uses member elastic strains or the gradients of displacements, which are results of double integration of accelerations with respective to time and thus are smoother.

(b) The inertia method results are smaller than those calculated by the statics method. This is because the accelerations are measured at the floor levels rather than at the mass centers of the floors (which are above the floor levels). Besides, negligence of rotary inertia forces would also result in underestimation of the inertia results.

6.1.4.D. Maximum Base Shears and Overturning Moments

The maximum values of the overturning moments and base shears are shown in **Fig.** 38. As is evident from this figure, the specimens with weaker links produced lower forces. For example, subjected to the 1.73*EC 200 table excitation, Specimen 3 had 47% more overturning moment than Specimen 1. These results demonstrate that link yielding and web buckling can limit the amplitudes of force response.

6.1.5. Energy Dissipation Efficiency

Energy dissipating ability can be an important parameter in the interpretation of the response of a structure to strong ground motions because to survive an earthquake a structure must have the ability to absorb the total energy imparted to it by the earthquake motion without serious damages that can threaten the integrity of the structure.

During an earthquake, although part of the energy is temporarily absorbed as strain energy or kinetic energy, all the energy provided to the structure must finally be dissipated by means of Coulomb friction, viscous damping, and inelastic behavior of both nonstructural and structural elements (if no energy is trapped in elastic permanent deformations). Of course, part of the kinetic and strain energy given to a structure by an earthquake may be taken back, through the structure-soil interaction, by the earth.

6.1.5.A. Calculation of Energy Dissipated by Links

To investigate the efficiency of the shear link as an energy dissipator, the energy dissipated by the west link of each specimen was calculated.

The area enclosed by hysteresis loops of an element represents the energy dissipated by the element. By using y to denote the force function and x to denote the corresponding displacement function, as shown in **Fig.** 39, and by applying Green's lemma [19], the surface integral can be converted to a contour integral along the hysteresis loops as shown in the following equation to calculate the area A enclosed by all the loops:

$$A = \iint_A dA = \int_{loops} y\,dx \tag{1}$$

The trapezoidal rule was used to approximate the integral and is expressed as

$$A_n = \frac{1}{2}\sum_{i=1}^{n}\left(y_i + y_{i-1}\right)\left(x_i - x_{i-1}\right) - \frac{{y_n}^2}{2k}\ , \tag{2}$$

where k is the unloading stiffness. This scheme was adopted because of its simplicity and ease of application to the data acquired in the experiment. The 2nd term on the right hand side of

equation (2) represents the elastic strain energy, which is not dissipated but stored and recoverable if the element is totally unloaded. It should be noted that for the estimation of recoverable energy, it was assumed that the stiffness of the element always equals the initial elastic value.

6.1.5.B. Calculation of Energy Input

Just as the energy dissipation is represented by the enclosed hysteresis area, the energy input by an earthquake to a structure is represented by the area enclosed by all the base shear-ground displacement loops, where the base shear was generated by the ground motion. This will be demonstrated in the following.

By defining energy input as the work done by a ground motion to a structure, the total energy input, IE, can be obtained by integrating the input power, $B\,\dot{v}$, over the elapsed time. That is

$$IE = \int_0^t B(t)\,\dot{v}(t)\,dt, \tag{3}$$

where B represents the base shear, v represents the ground displacement of an earthquake, and '$\cdot$' denotes the derivative with respect to time. However, the ground velocities, i.e., the shaking table velocities, were not recorded during the experiment and one way to determine table velocities is by actually differentiating the table displacements or integrating the table accelerations. However, numerical differentiation or integration tends to introduce errors in the results, and also a base line correction may be necessary before the integration can be done. A better procedure was found by noting that $\dot{v}dt = dv$. Therefore, the integration with respect to time can be performed by a scheme similar to that used in the contour integration around the hysteresis loops. Thus equation (3) can be rewritten as

$$IE = \int B\,dv. \tag{4}$$

The trapezoidal rule was again applied to perform the integration, as follows:

$$IE_i = IE_{i-1} + \frac{1}{2}\left(B_i + B_{i-1}\right)\left(v_i - v_{i-1}\right). \tag{5}$$

The amount of energy dissipated by the west link and the total energy input were calculated and the results are shown in Table 6 to demonstrate the energy dissipation efficiency of links of various strength. The unit of the listed values is inch-kips. All values were calculated for the beginning fifteen seconds of table motions except in the case of the Pacoima table motion for which the beginning twelve seconds were used.

Energy Input and Energy Disspation			
Table Motion	Total Energy Input (1)	Dissipated by the West Link (2)	(3) = (2)/(1)
	Specimen 1		
1.73*EC 75b	16.0	1.94	12.10%
1.73*EC 200	152.9	73.3	47.93%
1.73*EC 75a	19.1	13.2	69.39%
	Specimen 2		
1.73*EC 200	142.3	49.7	34.90%
1.73*EC 300	316.4	112.5	35.56%
1.73*EC 400	516.3	215.5	41.73%
	Specimen 3		
1.73*EC 200	151.3	22.0	14.52%
1.73*EC 400	556.9	122.3	21.95%
1.73*PAC300	390.9	51.9	13.29%
1.73*EC 450	664.8	129.9	19.53%

Table 6. Energy Input and Dissipation

It should be noted that the energy input quantities were calculated on the basis of the assumption that the response is symmetric, therefore, the total base shears, which were used in the calculation of energy inputs, were obtained by doubling the contribution from the west half of the structure.

By examining the time histories of the shear strains of the two links when the specimens were subjected to major table motions, the difference in their shear deformation may be used to judge roughly if simple doubling of the energy dissipation by the west link will underestimate or

overestimate the total energy dissipation by the two links. Based on this criterion, underestimation seems likely in the tests of Specimen 3, especially in tests 1.73*PAC 300 and 1.73*EC 450 where the east link has considerably more shear yielding deformation (see **Fig.** 40) and thus can be expected to dissipate more energy than the west link.

The marked deviation from the assumption of response symmetry is also shown in **Fig.** 41 for the test of Specimen 1 after its links were damaged. Suffering from severe fracture, the west link lost more than 60% of its strength. Thus it had much greater shear deformation and dissipated more energy than the east link. Quantitatively, the maximum pseudo shear strain of the west link is a remarkable 2.78%; whereas the maximum strain for the east link is the elastic value: 0.41%. As demonstrated in Table 6, more than 69% percent of the total input energy was dissipated by the west link. On the other hand, very little hysteretic energy dissipation of the east link can be expected because the east link had only elastic response.

Nevertheless, some significant observations can be concluded from the tabulated results:

a. When the three specimens were subjected to table motions of similar intensity, say the 1.73*EC 200 tests, the weaker links dissipated more energy. Having a maximum difference of less than 10%, the amounts of input energy were of the same order of magnitude. Yet, the maximum difference in energy dissipation was more than 230%.

b. A stronger link dissipates a smaller percentage of the total energy input. The percentages of total input energy dissipated by the west link of Specimens 1, 2, and 3 are roughly 50, 40, and 20, respectively.

c. Although the Pacoima table motion, 1.73*PAC 300, and the El Centro table motion, 1.73*EC 450, have similar peak accelerations, the latter is the greater energy source and gave almost 70% more energy to the structure. This is mainly because the El Centro motion has a longer duration. If they started simultaneously, the Pacoima input would cease approximately at the 7th second, while the El Centro motion would keep inputing energy to the system for a period longer than 15 seconds.

d. Because a strong link is less effective in dissipating energy, a larger response will result for a specimen with strong links. Therefore, for stronger specimens, a larger portion of the input energy is dissipated by means other than yielding of the links (such as Coulomb friction and viscous damping), especially when the table motion is very intense.

These observations can be presented more vividly by plotting the energy input and absorption time histories as illustrated in **Figs.** 42-44. By applying the assumption of response symmetry (i.e. assuming both the west and east links have the same energy absorption), the energy absorption shown in the figures is given as twice the amount of energy absorbed by the west link.

The time histories of energy absorption of the links together with their corresponding total energy input histories are shown in the figure rather than energy dissipation histories because the energy absorption is a more meaningful quantity in representing the link ability to regulate the input energy.

Included in the absorbed energy is the strain energy that is recoverable should the link stress be released. However, the recoverable energy is a relatively small quantity compared with the energy dissipated. Thus the time histories would not look much different if the recoverable energy were subtracted.

The strain energy recovering phases in the dynamic response are evidenced by minor dips in the energy absorption curves. Nevertheless, at the end of the absorption histories, the energy absorbed is the energy dissipated because the link stress no longer exists if no elastic permanent distortion is trapped in the link.

Illustrated in **Fig.** 42 are three sets of energy input and absorption curves determined for the three specimens subjected to table motions of similar intensity. Solid, long-dashed, short-dashed lines denote Specimens 1, 2, 3, respectively. Similarly, shown in **Fig.** 43 are the energy input and absorption time histories of Specimens 2 and 3 when they were subjected to table motions of similar intensity, i.e., 1.73*EC 400. Analogous plots of Specimen 3 subjected to the 1.73*PAC 300 and the 1.73*EC 450 table motions are also shown in **Fig.** 44.

The plots show the relative energy absorption efficiency of links with different strengths. The total energy curves may not be exact in representing the total amount of energy involved because of the response symmetry assumption mentioned previously. But a valuable observation that can be made is that the links of Specimen 1 are the best in energy dissipation and those of Specimen 3 are the worst.

6.1.6. Restraint of Responses by Link Strength

6.1.6.A. Brace Strains Limited by Link Strengths

When the test structure is subjected to a table excitation, the bracing system takes most of the lateral shear. Because of the ecc-X configuration of the bracing system, the responses to the excitation are represented by shear forces in the links and corresponding shear strains. The strength of the shear links, therefore, becomes a key to controlling the amplitudes of the responses. An important measure of a braced structure's response to an earthquake excitation is the brace forces. For the test structure, the brace forces must comply with the limit set by the strength of shear links.

As stated in Chapter 4, the brace strains of the lower two stories were measured by placing two strain gages along the neutral axes of the two angles of each brace and the total elongations of the four first-story braces were also measured by DCDT's. As shown in **Fig.** 45, both types of brace instrumentation yielded reliable data. The nominal brace length of 58.5 inches ($[49\times49+32\times32]^{1/2}$) used for the conversion of DCDT-measured elongations to strains. However, the DCDT results are slightly smaller than the foil gage results because the effective axial length of the first-story braces is smaller than the nominal value, which is the distance between two intersections of centerlines.

The maximum brace strains measured from all tests plotted against the corresponding peak table accelerations are shown in **Fig.** 46. The unit of brace strains is milli-inch per inch, which is abbreviated as mil/in. The three lines in the figure separately represent the results for the three specimens when they were subjected to El Centro type table excitations. Since all strains are within the elastic limit of the brace material, the strains can be converted directly into forces by simple multiplication by their respective elastic constants.

Figure 46 shows that all specimens had the same maximum elastic response when they were excited by small motions of similar intensity, 1.73*EC 50's. As the intensity of table motion increased, the link yielding prevented the increase of forces in the braces, thus the

brace strains did not grow proportionally.

6.1.6.A.1. Brace Strains for Specimen 3

The brace strains of the west frame recorded in major tests of Specimen 3, and shown in **Fig.** 47, are chosen to demonstrate the efficiency of the shear link in limiting the responses. Since the braces remained elastic throughout the tests, the strain amplitudes can be viewed as the corresponding forces. Also since the base shear, the overturning moment and the member forces are related to the brace forces, the brace forces (in terms of strains) can be representative of the response of the structure to table excitations.

To understand the relation of link strength to the response, the time when significant link shear yielding occurs need to be observed. By examining the hysteresis plots, the occurrence of link yieldings can be briefed as follows:

(1) In the 1.73*EC 200 test, only one significant yielding excursion is observed (at about 2 seconds), and thereafter the links remain essentially elastic with only very minor hysteresis recorded for the links (see **Fig.** 96).

(2) For the other El Centro motions, namely, 1.73*EC 400 and 1.73*EC 450, the three significant link yielding excursions occur at about 2 seconds, 4 seconds and 8 seconds (see **Figs.** 101 and 111). An important fact that deserves special mention is that the two links buckle at about 2 seconds in the 1.73*EC 450 test.

(3) In the 1.73*PAC 300 test, the shear yielding is not as significant as those observed in tests of El Centro table motions. Nevertheless, a lot of yielding occurs between 2 seconds and 5 seconds. In particular, significant yielding is observed at about 4 seconds (see **Fig.** 106).

As shown in the time histories (see **Figs.** 97, 102, and 107), the brace strain drops when significant link yielding occurs.

The intensity of the 1.73*EC 400 table motion is more than double that of the 1.73*EC 200 table motion. However, the response increase from 1.73*EC 200 to 1.73*EC 400 is only

slight. Although the table motion of the 1.73*EC 450 test is even stronger than that of the 1.73*EC 400 test, less response is observed. This is because the links of Specimen 3 significantly buckled in the 1.73*EC 450 test, resulting in a strength drop.

As a conclusion to the observations, it can be said that link strength is a key factor in limiting the brace forces and thus the base shear and the overturning moment because they are related to the forces in the braces. So are the other member forces. It may also be concluded that web buckling in links is a good fuse mechanism for protecting the structure. Therefore, it may not be necessary to install stiffeners to prevent buckling.

The relation of brace forces (examined in terms of brace strains) to the link shear forces is further exhibited in **Fig.** 48. These results show an approximately linear relationship, as they should if the geometry change due to link distortion remains small. In both **Fig.** 46 and **Fig.** 48, the data bear witness to the fact that the stronger the links are, the larger the response will be.

6.1.6.B. Plastic Bending of Links

The possibility for links of each specimen to reach the plastic moment is discussed in the following:

(1) For specimen 1, the plastic moment capacity of the link was reached because its bending capacity was lower than the shear yield capacity.

(2) For specimen 2, the two capacities were made compatible by cutting the flange width to reduce the bending capacity; thus the plastic moment was expected just after shear yielding had occurred.

(3) For specimen 3, the strongest specimen, the bending strength was much larger than the shear strength, thus the possibility of bending plasticity was very low.

Based on the yielding stresses from the coupon test results (see Table 4 in Section 6.1.3.), the link shear force requirement for each specimen to achieve the corresponding plastic

moment was calculated. The calculated requirements together with the recorded maximum link shear forces are shown in Table 7.

Shear Forces in Links (Kips)			
	Specimen 1	Specimen 2	Specimen 3
Full Requirement	28	32	71
Reduced Requirement	19	22	55
Predicted Maximum	17	14	29
Recorded Maximum	22	28	41

Table 7. Shear Force Requirements for Plastic Bending in Links

The calculation and implication of the entries in the table are discussed below.

(1) The first row lists the shear forces required to achieve full plastic moments. These were calculated by assuming that the elementary beam theory holds, and

$$V = \frac{2 M_p}{e} \tag{1}$$

where

$$M_p = Z_x \, \sigma_y$$

Z_x is the plastic section modulus, σ_y is the uniaxial yielding strength, and e is the eccentricity. These full plastic moments, however, are not realistic because of the existence of very high shear forces in the webs. The shear forces are so large that the effect on bending capacity should be considered.

(2) The second row of the above table was calculated by taking the shear effect into account. Based on the distortion energy theory [25], there is no normal stress present in the web that yielded in shear, and the modified plastic moment is given by

$$M_{ps} = t_f \, b_f \left(d - t_f \right) \sigma_y \; ; \tag{2}$$

hence the shear requirement is

$$V_s = \frac{2 M_{ps}}{e} \tag{3}$$

(3) The third row, representing the predicted maximum shear force capacity of the link webs, was calculated by

$$V_p = t_w \left(d - t_f \right) \tau_y \tag{4}$$

where τ_y is the shear yielding stress. Based also on the distortion energy theory,

$$\tau_y = \frac{\sigma_y}{\sqrt{3}} \tag{5}$$

(4) The recorded maximum link shear forces are listed in the fourth row of the table.

From Table 7, it can be concluded that the link plastic moment was not reached for Specimen 3. Because the recorded maxima are larger than the reduced requirements for Specimens 1 and 2, plastic hinges were possibly formed at ends of their links. As also found from the table, estimation of link shear capacity by Equation 4 is conservative and underestimation can be 100%.

6.1.6.C. Axial Force-Bending Moment Interaction (P-M Interaction)

In reality, the yielding of links is a very complicated process. In addition to the shear force-bending moment interaction, the axial force will become important when the link shear deformation is large. Originally, by considering the symmetric property of both the structure and the response, it was assumed that there was no appreciable axial force in the links to trigger the axial force-bending moment interaction. Nevertheless, if the links have large deformation, as discussed in Chapter 2, an axial force would develop in them. For example, a maximum axial strain of 270 micro strains was recorded in the 1.73*EC 400 test of Specimen 3 (see **Fig.** 49). If the assumption that plane sections remain plane holds, the strain is equivalent to an

axial force of 21 kips, which is about 17% of the link axial yield force. The link's bending capacity is reduced about 5% because of the P-M interaction. However, the reduction is not enough to cause plastic bending in the links of Specimen 3 because the reduced shear force requirement is still about 30% more than the recorded maximum.

6.1.7. Links as Tension Elements

In cases of small deflections, due to symmetry of the ecc-X-braced frame there will be no appreciable axial force in the shear links, and the lateral strength of the ecc-X-braced frame is mostly determined by the shear strength of the links. If there were no shear strain hardening in the links and geometry changes were neglected, the frame would lose most of its lateral stiffness when the links yield. As mentioned in Section 2.5., however, the ecc-X-bracing system tends to develop additional lateral stiffness from axial forces in links after it forms a collapse mechanism and sufficient lateral sway has occurred. The loss of lateral stiffness is partially compensated by the links' tying together the two braces which are in tension at moments of large link shear deformation. This tension mechanism should be more apparent in frames with weaker and shorter links where larger shear deformations would develop.

The axial connection behavior of the links can be observed from the axial strain measurements of the west link of Specimen 3. This was the only link that had axial strain measuring gages. Shown in **Fig.** 49 are the axial and pseudo shear strains measured during the 1.73*EC 400 test.

After the completion of 1.73*EC400 test, the links showed no permanent deformation, i.e., the flanges were straight and the webs flat. Therefore, the axial strain can be considered as a qualitatively reliable measurement. The axial strain shown in the figure was magnified 100 times to demonstrate the significant features of the response. In spite of the signal noises, which also were enlarged 100 times, the sizable pulses of the axial tensile response of the link are essentially in concurrence with the events of major shear deformation, no matter what the sense of the shear deformation is. The 'all tension' response is the distinctive character of the axial connection function of the shear links.

The axial strain and the pseudo shear strain of the same link measured in the 1.73*EC 450 test are shown in **Fig.** 50. The data was essentially negative and relatively large. This is because the web was buckled in this test. To interpret this data, the definition of the link axial strain should be recalled: by assuming a linear strain variation across the depth of the link

section (i.e. plane sections reamin plane), the link axial strain is determined by the average of the two strains measured by two gages on the two flanges of the link. In this test, web buckling caused the flanges to bend considerably toward the web. Because the two gages were on the compression sides of the bent flanges, they recorded large negative (compression) strains of flange bending, which make the recorded axial strain negative. Obviously, this did not indicate that a compression link axial force was induced in this test. The axial strain corresponding to tensile link force was wiped out by the much larger negative strain of flange bending. Consequently, the link axial strain measurement in the 1.73*EC 450 test is false and is of no significance. But, the data do reveal the phenomenon of flange bending.

The strength recovery of the ecc-X-braced structure may be seen in the hysteresis plots of base shear and first floor relative displacement shown in Figs. 51 and 52; the resistance of the structure tends to increase after a certain amount of lateral displacement of the first level.

6.1.8. Relative Displacement Envelopes

To obtain the relative displacements, the table displacement was subtracted from the floor displacements. Also the difference between two consecutive floor displacements was defined as the story drift. With this definition, the first story drift and the first story relative displacement are identical.

The relative displacement envelopes recorded during the experiment are tabulated in Table 8 and are also displayed in **Figs.** 53, 54 and 55. The maximum relative displacements are concurrent in most of the tests. In some tests the maximum displacements did not occur simultaneously, but the differences between them and their corresponding concurrent displacements are small. In the table, the maximum displacements that are not concurrent with those of most of other floors in the same test are marked by an asterisk.

As shown in **Figs.** 53 and 54, the global yield mechanism is clearly demonstrated in the tests of Specimens 1 and 2. The columns of the first and second stories remain aligned because they form trusses with braces. Significant bending is expected at the top end of the second story columns and the bottom end of the first story columns because an abrupt slope change in the column lines was noted at these locations, and large shear displacements are also expected in the shear link between the first and the second stories. Of course these are the positions of the plastic hinges and the yielded shear link of the theoretical collapse mechanism discussed in Section 2.5.

Test Name	Peak Accel. (g)	Maximal Relative Displacements				
		1st Floor (inch)	2nd Floor (inch)	3rd Floor (inch)	4th Floor (inch)	5th Floor (inch)
Specimen 1						
1.73*EC 75B	.147	.168	.274	.373	.430	.552
1.73*EC 200	.434	.476	.799	.915	1.012	1.122
1.73*EC 75A	.167	.148*	.325*	.364	.392	.384
Specimen 2						
1.73*EC 200	.415	.382	.620	.744	.845	1.021
1.73*EC 300	.684	.557	.934	1.086	1.176	1.391*
1.73*EC 400	.980	.731	1.233	1.402	1.508	1.742
Specimen 3						
1.73*EC 200	.434	.526	.834	1.041	1.183	1.507
1.73*EC 400	.961	.668*	1.126	1.488	1.715	2.035
1.73*PAC210	.741	.351	.583	.876	1.058	1.412
1.73*PAC300	1.111	.474	.819*	1.142	1.332	1.890
1.73*EC 450	1.155	.804*	1.288	1.654	1.901	2.266

*: non-concurrent values

Table 8. Relative Displacement Envelopes

By examining the deflected shapes, the damage patterns of the structure due to an earthquake can be qualitatively identified. An observation that can be noted from the tabulated numbers is that the deformations of the upper three stories are relatively small because of the formation of the collapse mechanism in the bottom two stories; therefore, it can be said that nonstructural damage of these stories has been significantly reduced at the expense of increased damage in the bottom two stories.

After the links were severely damaged, in order to study the effect of the damage, Specimen 1 was again subjected to a minor table motion, 1.73*EC 75A, the intensity of which is slightly larger than that of the similar test, 1.73*EC 75B, done before the links were damaged. However, less response was observed in this 1.73*EC 75A test; in fact the maximum displacement of the top is actually reduced. Because of the isolation effect provided by the two damaged bottom stories, the earthquake motion can not do much to damage the superstructure. In the 1.73*EC 75B test, no mechanism can be identified from the displacement envelope, which happened to be concurrent. Therefore, the response characteristic is similar to that observed

for Specimen 3 for which the yield mechanism is also not very visible. The 'whip-lash' response of the top floor of Specimen 1 in the 1.73*EC 75B test is significant, and even larger than that for the 1.73*EC 200 table motion.

Different displacement response patterns were observed for the Pacoima and the El Centro table motions. For Pacoima excitations, the responses of the lower four stories are small even though the input motions have high peak accelerations; also a zigzag profile may be seen in the 1.73*PAC 210 envelope, which comprises concurrent maximum relative displacements. Moreover, both of the Pacoima responses showed large story drift at the top story of the structure. Both the zigzag profile and the larger top story drift imply that higher mode response was more important when Specimen 3 was subjected to the Pacoima type table motions. Especially for the 1.73*PAC 300 test, the top story distortion was so large that some nonlinearity probably occurred in the top story. However, no instrumentation was deployed there to acquire information about such behavior.

The responses of Specimen 3 to the El Centro table motions have a gracefully curved profile, except for the top story which has larger displacements mainly due to its larger mass and the whip-lash effect. Unlike the response profiles of Specimens 1 and 2, the characteristic yield mechanism formation is not clear for Specimen 3.

To give an idea of the relative advantages between links of different strength, the relative displacement envelopes of different specimens recorded in a similar test (1.73*EC 200) are shown in **Fig.** 56. This clearly shows that Specimen 3, which had the strongest links and the least link damage, has the greatest displacement response to this input. **Figure** 57 shows that a similar conclusion may be drawn for the response to the more severe test, 1.73*EC 400, where the top displacement of Specimen 3 is significantly greater than that of Specimen 2. In this case, however, it is clear that the deformation and drift in the lower two stories is greater for Specimen 2, reflecting the severe damage suffered in the ecc-X-braced panels of this specimen.

6.1.9. Maximum Bending Moments in Columns

Characters in the designation CBWN2U used in **Fig.** 58 sequentially stand for column, bending, west, north, 2nd story, and upper. In other words, CBWN2U designates the bending moment at the upper end of the north 2nd story column of the west frame. Similarly, CBWN1L designates the bending moment at the lower end of the north first story column of the west frame. The two positions of interest are the locations where the largest column bending moments reside.

Because of the response symmetry, only moments in the north columns are discussed. Maximum values of the two bending moments recorded in the three specimens are shown in **Fig.** 58. All recorded maxima of column bending moments are less than the plastic bending moment of columns even though the axial load effect has been considered. In other words, a plastic hinge is not formed; yet, the bending moments are strongly correlated to the deformation of the shear link. There is a striking resemblance between the time histories of a column bending moment and its coexistent link deformation as shown in **Fig.** 59.

As can be seen from **Fig.** 58, the second story moment, CBWN2U, is always larger than the first story moment, CBWN1L. This is because the 1st story is 36% taller than the 2nd, and consequently, the 2nd story columns are relatively stiffer against end rotation. Furthermore, the lower (ground) ends of the first-story columns are not rigid against rotation, because the four bolts anchoring a column base plate are too far away from the column section (see Fig. 1). This situation may reduce the column moments at these positions.

Because the stronger links of Specimen 3 prevent any significant collapse-mechanism deformation in the lower two stories, the second story moments assume smaller values. Consequently, CBWN2U and CBWN1L of Specimen 3 are closer to each other than those of the other specimens. Especially when Specimen 3 is subjected to the 1.73*PAC 300 table motion, CBWN2U and CBWM1L have almost the same maximum values.

It is generally true that a larger CBWN2U is accompanied by a larger collapse-mechanism deformation. Shown in **Fig.** 60 are the maximum CBWN2U's versus table peak accelerations.

The observation stated above is clearly demonstrated in the figure; that is, when subjected to table motions of similar intensity, a specimen with weaker links always has a larger CBWN2U.

The fact that a weaker link induces larger column moments can also be inferred from the relative displacement envelopes (shown in **Figs.** 53, 56 and 57). A larger slope change in the envelopes at the upper end of the 2nd story column implies a larger column bending moment at that position. For instance, when Specimens 2 and 3 are subjected to 1.73*EC 400 table motion, larger CBWN2U is observed in **Fig.** 60 for Specimen 2. This is due to the larger collapse-mechanism displacement (see **Fig.** 57) in Specimen 2, which has weaker links that yield and even buckle in the test.

It is also interesting to note that an even larger CBWN2U is induced in Specimen 1 after its links are damaged and fractured. This observation, once again, verifies that a larger collapse mechanism deformation (see **Fig.** 53) is accompanied by larger bending moments in columns (see **Fig.** 58, which shows that Δ_A is greater than Δ_B; the subscripts, A and B, stand for 'after' and 'before' respectively).

6.2. Data Observation

In the second part of this chapter, attention is directed to a detailed discussion of various response quantities for selected tests. Greater attention will be paid to the responses of Specimens 1 and 2, because Specimen 3 has generally similar response to that observed for Specimens 1 and 2. Only a brief discussion is given for the results of Specimen 3.

Because more damage was observed in the tests of Specimens 1 and 2, the results of Specimens 1 and 2 are more interesting. However, from a practical point of view the test results for Specimen 3 are of greater interest because the specimen has shear links made of the original girder section. It is much more practical for a designer to use the same structural section to fabricate both girders and links. In this case links can be created as simple offsets between brace-girder connections.

6.2.0. Sign Conventions

The positive sign convention adopted for data presentation is as shown in **Fig.** 61. Accelerations and displacements are positive to the right. A positive brace strain is tension. Bending moments are positive counter-clockwise at member ends or clockwise at joints. The shear force in a link is positive upward at the left end and downward at the right end. The pseudo-shear strain in a link is positive if it results in an upward displacement of the left end relative to the right end.

6.2.1. Experimental Results for Specimen 1

The links of Specimen 1 were annealed as a whole before they were installed into the structure. Three tests were selected to study the response characteristics of this specimen having the weakest links, namely, 1.73EC 75B (before damaage), 1.73*EC 200, and 1.73*EC 75A (after damage). 'Before damage' denotes that the test was done before the link was damaged. 'After damage' denotes that the test was conducted after the links had been damaged. Damage

is observed in the 1.73*EC 200 test. The last test was performed to understand the post-damage behavior of the test structure.

The response in each of the three tests is characterized by the strain histories of the south first story brace shown in **Fig.** 62. An outstanding feature of the first test is the 'beat' appearance. In test 1.73*EC 200 the reponse is spread more evenly throughout the elapsed time. The response to 1.73*EC 75A (after damage) is typical for a structure with a very soft first story.

A detailed review of these three tests follows.

6.2.1.A. Specimen 1 Subjected to 1.73*EC 75B Excitation

The table motion for this test is depicted in **Fig.** 63 in terms of time histories of displacements and accelerations, and response spectra for damping ratios of 1%, 3%, 5%, and 10%. The response to this motion is essentially elastic. However, since the strength of these links was relatively low, a minor nonlinearity was recorded (see **Fig.** 27). The 'beat' phenomenon is found in all of the histories as the unique feature of this elastic test.

The brace strains together with the pseudo shear strains of the two links are displayed in **Fig.** 64. The value identified in each frame of the figure gives the peak value of the west braced frame data. The figure shows that the response symmetry is very well preserved in this test except at about 2.2 seconds when the west link has slightly more yielding and stays permanently distorted.

The high frequency tremors in the floor accelerations shown in **Fig.** 65 are mechanical noises from the operation of the shaking table. The relative displacements of all floors are plotted together and shown in **Fig.** 66 with the base shear and overturning moment. They all show a first-mode-dominant characteristic.

By plotting five floor displacements together, the story drifts can be easily visualized as the difference between the displacements of two consecutive stories. The solid curve in the relative displacement histories represents the top floor and others, in dashed lines, represent the

lower four stories. Starting with the shortest dash for the first floor, the length of the dashes increases with the floor numbers. The relative displacements shows that the stories are fairly evenly deformed with the largest story drift in the first story which has the largest story shear and height.

Of the first two stories of the west braced frame, the bending moment histories at the ends of the north columns are shown in **Fig.** 67. From top to bottom, they are designated as CBWN2U, CBWN2L, CBWN1U and CBWN1L, representing moments generated at faces of column-beam joints. The data show that the location of maximum column moment is at the top end of the second story column, and the second largest moment is found at the lower end of the first story column.

6.2.1.B. Specimen 1 Subjected to 1.73*EC 200

The spectra of the table excitation employed in this test were calculated for damping ratios of 1, 5, 10, 25 percent and are shown in **Fig.** 68 with the table displacement and the table acceleration. Since a greater number of points were calculated, the spectra of this test show better resolution than those of other tests. The peak acceleration value of 0.43g indicates that the input intensity is about three times larger than that of the elastic test, 1.73*EC 75B. In this test, significant shear link yielding and buckling were observed.

Local and Global Hysteresis Behavior

The most vivid demonstration of the response nonlinearity is given by the hysteresis plots of **Figs.** 69 and 70. **Figure** 69 shows the hysteresis of the west link, while in **Fig.** 70, the base shear is plotted against the first floor displacement. The three major excursions of shear yielding are clearly shown in **Fig.** 69, which represents the response history in three second increments. Exhibited in the upper right quarter of the first frame, the initial link buckling is indicated by a negative slope or shear force drop that occurred at about 2 seconds. When the first

very strong thrust from the shaking table hit, the link yielded tremendously and suddenly buckled with a snap. As can be seen from the same frame, the stiffness was smaller after the web had buckled. In addition, after buckling, the link had different strengths in the two senses of shear deformation. This can be attributed to asymmetry in its web buckling shape.

As may be seen in the upper right quarter of the second and third frames, the buckled link had a tendency of strength recovery. This phenomenon may be associated with the 'truss' effect of the diagonal tension which is developed after a certain deformation has been achieved. It is also evident that the strength of the link continued to decline as the buckling distortion was intensified because of cyclic deformation.

The base shear hysteresis shown in **Fig.** 70 is generally in phase with that of the link except the senses are opposite; i.e., a positive floor displacement produces negative shear deformation (see **Fig.** 61). It is interesting to note that the strength reduction exhibited by the link is not apparent in the global hysteresis.

Histories of brace strains together with link deformation are demonstrated in **Fig.** 71. It is worth noting that each incident of link yielding is accompanied by a decrease in the brace strains. Taking a close look at the brace strain histories, one can find that the brace strains are 'rounded off' or 'truncated' when the link yields. In other words, link yielding prevents the build-up of force responses.

In this test, in addition to showing significant shear yielding, the west link buckled into an antisymmetric shape while the east link buckled symmetrically. Accordingly, different amounts of link deformation are demonstrated by the two links. After buckling, the west link is apparently softer and thus has more significant yielding. The discrepancy between the east and west brace strains observed in **Fig.** 71 is a consequence of the difference in link deformations. After the links have buckled, the east link retains more strength, therefore it induces larger east frame brace strains.

The acceleration of each floor is shown in **Fig.** 72, and the peak value is indicated in each

frame. It should be noted that the very high frequency spikes at 4 seconds and 8 seconds are caused by concrete weight anchors hitting the structure frame, because of slippage occurred at some fasteners.

The floor relative displacements, together with the base shear and overturning moment, are shown in **Fig.** 73. The displacements show a significantly different character from those of the elastic test (see **Fig.** 66). The beats are greatly diminished by the link yielding. Frequency change is apparent after each incident of link yielding at about 1.75 seconds, 3.75 seconds and 7.95 seconds. Moreover, the relative displacements are reduced after each occurrence of link yielding. A permanent shift of 0.02 in/in was observed in the link shear deformation (see **Fig.** 71) between 2.25 and 3.50 seconds. According to the equation given in **Fig.** 14, a permanent shift of about 0.2 inch is expected in the floor displacements within the same interval of time. An examination of the relative displacements in **Fig.** 73 confirms that they do shift as predicted by the equation.

In this test, the soft story effect, associated with the collapse-mechanism deformation resulting from link nonlinearity in the lower two stories, prevents the base excitation from propagating effectively upward into the upper stories. As can be seen from the relative displacements of **Fig.** 73, the story drifts of the upper three stories are relatively small if they are compared with those of the first two stories.

The column bending moments of the first two stories are depicted in **Fig.** 74. As can be seen from the figure, these quantities, especially CBWN2U and CBWN1L, are very strongly correlated to the link deformation. This is a result of the 'collapse-mechanism' deformation because bending is much more concentrated at positions of potential plastic hinges (refer Fig. 14).

Data Lost

Before reviewing the next data package, one lost test needs to be mentioned. After

the 1.73*EC 200 table motion had buckled the links, the test structure was subjected to a even stronger excitation, 1.73*EC 300. The link damage was intensified in this test; for instance, the west link was fractured (as described in detail in 6.1.2.A). Unfortunately, the entire test data were lost by accident. The only quantitative information remaining for this test is the printout of the maximum-minimum search by the NOVA computer.

6.2.1.C. Specimen 1 Subjected to 1.73*EC 75A Excitation

The purpose of this test was to understand the post-damage behavior of the test structure. A table motion of similar intensity to that of the original elastic test was employed so that the two tests could be compared.

The peak value of the table acceleration for this test was about 0.17g. The acceleration is shown in **Fig.** 75 with the table displacement and its response spectra.

It is interesting to note that the responses to this table motion are much smaller than to the 1.73*EC 75B (before damage) test, even though the table motion actually is a little stronger in this test.

The link hysteresis of this test are shown in **Fig.** 27. Because the west link was seriously damaged in the two previous tests (namely 1.73*EC 200 and 1.73*EC 300), it had only about 30% of its original stiffness left. Thus, as hown in **Fig.** 76, the fractured west link has much greater deformation than the east link. However, the strains in the braces maintain a symmetric pattern. This implies that similar force levels are developed in the two links even though they have drastically different deformations.

As may be seen in **Fig.** 77, the upper four floor levels have acceleration responses that are very similar in size. This is due to the fact that the very soft lower two stories provide a cushioning effect which effectively isolates the upper part of the structure from the excitation. Compared with their elastic response counterparts (see **Fig.** 66), the relative displacements,

shown in **Fig**. 78 with the base shear and the overturning moment, definitely demonstrate a significant softening effect on the structure provided by the damaged links.

The column bending moments are shown in **Fig**. 79. Since the west link was seriously damaged in the previous two tests, the west frame underwent significant collapse-mechanism deformation in the lower two stories. Accordingly, much larger column moments were attained. This fact can be clearly visualizeed by comparing **Fig**. 79 with **Fig**. 67; the same scale was used for easy comparison. The values for the after-damage test are significantly larger, demonstrating the direct relationship between the column bending moments and the link deformation (see **Fig**. 76).

6.2.2. Experimental Results for Specimen 2

After the completion of tests for Specimen 1, the damaged links were replaced by a stronger set to create Specimen 2. The new links were made of the same structural section as that used for girders: wide flange W6×9. However, to make its bending strength compatible with the shear capacity, the flanges of the links were trimmed as described in Section 2.4. In addition, the links were annealed as a whole after they were fabricated.

Both two tests selected for study showed significant yielding. In the first of these, 1.73*EC 300, the links yielded significantly in shear, yet the web remained flat without visible permanent deformation. In the following test, 1.73*EC 400, both links buckled seriously and one of them cracked.

To give a general idea of the quantitative results of the Specimen 2 tests, strains in one of the first story braces are shown in **Fig.** 80. Because the brace strains are elastic, they can be interpreted as forces developed in the braces. Four immediate observations can be drawn from this figure:

(1) Intense nonlinearity generates 'evenly distributed' strain histories. In other words, the beat phenomenon observed in elastic response time histories is not seen in tests having severe link damage.

(2) Because a ceiling on strain is imposed by the link strength, the strains do not grow proportionally with the intensity of table excitations.

(3) As a consequence of link buckling, the brace strains induced by 1.73*EC 400 are smaller than those induced by 1.73*EC 300 even though the former test has a stronger intensity.

(4) The damaged links still perform their function reliably for minor quakes.

6.2.2.A. Specimen 2 Subjected to 1.73*EC 300

The peak acceleration applied by the table in this test was 0.68g. The response spectra for damping ratios of 1, 3, 5, and 10 percent of critical damping are shown in **Fig.** 81 with the

input acceleration and displacement histories.

Local and Global Hysteresis Behavior

Hysteresis loops of the west link are shown in **Fig.** 82. When the first yielding commences, instead of a horizontal plateau, significant strain hardening is evident. Since the link remained flat after the test, no appreciable stiffness change was found. The force recovering characteristics of the structure are shown in **Fig.** 83, in which the base shear is plotted against the first floor displacement.

The brace strains of the lower two stories and the pseudo shear strains of the two links are depicted in **Fig.** 84. The link yielding occurrence can be detected in the brace strain histories by round-offs or truncations of the brace strain cycles. The response symmetry is perfectly maintained in brace strains, demonstrating the deformation symmetry of the two links. The importance of the links in controlling the brace response pattern is evident.

Figure 85 shows the acceleration response at each level. The resonant behavior indicated in the elastic response curve (see the top frame in Fig. 80) is modified by the link yielding. The histories of base shear and overturning moment shown in **Fig.** 86 were calculated by the statics method.

Also shown in **Fig.** 86 is the plot of the relative displacements of all floor levels. The frequency change and the shifting of the equilibrium position resulting from plastic deformations in the links are evident in this plot. In addition, the relative displacements diminish significantly each time the links have yielded. The story drifts in the upper three stories also drop at link yielding.

The strong correlation between column bending moments, shown in **Fig.** 87, and the link strains may be seen by comparing **Figs.** 87 and 84 (also see **Fig.** 59).

6.2.2.B. Specimen 2 Subjected to 1.73*EC 400

The table motion characterized by **Fig**. 88 is the strongest shaking Specimen 2 was ever subjected to. The spectra of the motion have been calculated for damping ratios of 1, 3, 5, and 10 percent of critical damping. This table motion had a peak acceleration of about 1g; thus it is not surprising that the links were seriously damaged in this test.

Local Hysteresis Behavior

Figure 89 presents the hysteresis behavior of the west link. As can be seen from the figure, the link experienced tremendous yielding. The commencement of web buckling is demonstrated clearly by the diminishing shear force seen in the upper right quarter of the first frame. The decrease of stiffness is obvious after buckling. The diagonal tension contribution to strength recovery is seen in the third frame, which shows that the shear force drops and then climbs, near the axis of zero strain. At the end of the test, both the stiffness and the strength of the link are shown to be smaller.

Global Hysteresis Behavior

To give an idea of the structural behavior as a whole, the structural hysteresis behavior in terms of the base shear and the first floor displacement is presented in **Fig**. 90. It is interesting to note that the shear force reductions associated with web buckling, as observed in the link hysteresis loops, do not exist in the structural hysteresis. This may be because the structure softening, in consequence of link yielding or buckling, is compensated by the development of axial force in the links. The strength of the structure is generally increasing rather than constant or declining as observed in the link hysteresis.

After the links have undergone a certain amount of distortion, axial forces would develop in them. Since the shear deformation tends to bring the two end plates closer, if the shear deformation is large, the shortening of distance between the two end plates will induce

significant positive (tension) axial force in the links. These positive axial forces tend to align with tension braces. Consequently, there is an increase in structural lateral stiffness.

In the brace strains of the east frame shown in **Fig.** 91, no 'beats' are identifiable. The responses demonstrate the isolation effect of a soft story; similar soft-story characteristics were also observed in the response of Specimen 1 to the 1.73*EC 75A motion.

As was described in detail in Section 6.1.2., the links buckled into the same pattern with one node at the center. The pseudo shear strains shown in **Fig.** 91 are also quite close to each other, yet, the west link, which is cracked at its node, obviously has more yielding.

The acceleration response at each story is shown in **Fig.** 92. As before, the frequency spikes are noises resulting from collision of anchorage bolts with girders because of bolt slippage.

By comparing the relative displacement histories shown in **Fig.** 93 with those of the previous test, it is apparent that the frequency change and response decrease due to link nonlinearity are significant. The collapse-mechanism deformation can be clearly observed from the relative displacements shown in the figure. As shown, the lower two stories constribute most of the lateral displacements, while the upper three stories have very small story drifts. The histories of the base shear and overturning moment also are depicted in **Fig.** 93. Once again, because the overturning moment and base shear are strongly related to the brace forces, they generally possess the same features as the brace strains.

The column moments are shown in **Fig.** 94. The resemblance of these to the link strains has already been discussed for previous tests. One thing to note here is that the bending moments of this test are the largest in the whole ensemble of tests. Even though the moment histories show drastic shifting from the zero axis, they are actually elastic; the shift is due to the plastic distortion of the link.

6.2.3. Experimental results for Specimen 3

The links of Specimen 3 were the strongest of the three kinds; they were made of the same structural section used for girder components, so when they were assembled together with the girder segments, they formed a uniform first level girder. The links of Specimen 3 were not annealed.

Because the behavior of this specimen bears considerable similarity to that of the other specimens, the data will be presented in a slightly abbreviated format. Of a total of eight tests, four tests are selected for presentation. Displayed in five plots, the data presented for each test are

(1) the table motion in terms of its displacement and acceleration, and response spectra for damping ratios of 1, 3, 5, and 10 percent of the critical damping,

(2) the hysteresis loops of the west link,

(3) the strains in all braces of the lower two stories and the pseudo shear strains in the links,

(4) the accelerations, and

(5) the relative displacements of all floor levels.

The sign conventions are positive as shown in **Fig.** 61 except for the floor accelerations. For this specimen only, an acceleration is positive when the floor is accelerated to the left, i.e., the north direction.

Another point to be noted is that frequencies higher than 20 cps have been filtered from the recorded floor accelerations in order to reveal the important frequency content.

6.2.3.A. Specimen 3 Subjected to 1.73*EC 200

The table motion used for this test has a peak acceleration of 0.434g, as shown in **Fig.** 95. Because the links have high strength, only slight yielding is induced in this test. After the yielding shown in the first frame of **Fig.** 96, the structure responds to the motion essentially elastically.

The brace strains together with the pseudo shear strains are shown in **Fig.** 97. The response symmetry is well preserved. As seen in the hysteresis loops, the west link remains elastic after 2.5 seconds. Therefore, even though the first resonant build-up of response is interrupted by link yielding, the second beat appears at about eight seconds indicating restoration of the elastic response characteristic (cf. **Fig.** 64).

The floor accelerations shown in **Fig.** 98 demonstrate the first mode dominance, but a rather unimportant 2nd mode response is also visible in the records. The very high spikes shown at about 2 seconds are again resulted from impacts between loosed concrete weights and the structure.

Because the links experience only trivial deformations, the story drifts are quite evenly distributed along the height. This can be seen in **Fig.** 99 in which the five floor relative displacements are plotted together. As can be seen from the figure, the equilibrium position shifts due to the permanent distortion observed in the links.

6.2.3.B. Specimen 3 Subjected to 1.73*EC 400

By comparing the spectra of this table motion, shown in **Fig.** 100, with that of the similar motion applied to Specimen 2 (see Fig. 88), a striking similarity is shown, demonstrating repeating capability of the shaking table.

The nonlinear behavior of the west link is depicted by the hysteresis loops shown in **Fig.** 101. The large strength of this link inhibits buckling even though the applied motion is of high intensity and severe shear yielding has occurred. In the previous 1.73*EC 200 test, when the link was fresh without yielding experience, a fairly flat yielding plateau was observed. However, an appreciable secondary stiffness resulting from the Bauschinger effect and strain hardening is demonstrated in **Fig.** 101. As was observed in the previous test, a permanent shear deformation remains at the end of this test.

Again, the effect of link nonlinearity can be seen in the brace strains of **Fig.** 102. It may

be seen that each significant yielding incident is associated with a strain reduction.

Owing to significant link yielding, the resonant build-up of the first mode response is not as much in this test as was observed in the previous one. This fact can also be witnessed by comparing the floor accelerations given in **Fig.** 103 with those of the previous test (see **Fig.** 98); the first mode response is not as evident in the accelerations of the lower two stories because of significant link yielding. Because of the high intensity of the table motion, the second mode response is visible in this test, but still is not significant.

Generally speaking, the features of the relative displacements shown in **Fig.** 104 resemble those of the similar test for Specimen 2 (see **Fig.** 93). For Specimen 3, similar but larger responses are induced because of the higher link strength and thus less link yielding. However, the pattern of the story drifts is different from that of Specimen 2. The drifts of the first two stories of Specimen 2 were much larger than the upper three. This is not the case for Specimen 3, because the collapse-mechanism deformation in the lower two stories is not as significant resulting from the higher link strength. Therefore, as can be seen from **Fig.** 104, the story drift of the third story is of the same order of magnitude as that of the second story. This is never the case in any of the tests for Specimens 1 and 2.

6.2.3.C. Specimen 3 Subjected to 1.73*PAC 300

The source record for this test, the N76W component of the San Fernando Earthquake recorded at Pacoima Dam, has a different character from that of the El Centro. The Pacoima is a near focus impulsive motion and of shorter duration. The spectra of the simulated Pacoima record together with the acceleration and displacement histories are shown in **Fig.** 105. The large intensity of the motion is indicated by its peak acceleration of 1.11g.

The nonlinear response generated by this motion is displayed in **Fig.** 106. Significant yielding is shown in the figure, yet it is not as much as that observed in the previous El Centro test. Even though some asymmetry exists in the shear deformation between the west and east

links, little difference is found between the brace strains of the two braced frames shown in **Fig.** 107.

This motion is relatively efficient for the higher modes. As indicated by the floor accelerations shown in **Fig.** 108, the higher mode responses are more effectively excited in this test.

The relative story displacements for this test are shown in **Fig.** 109. A unique feature of this response is that the third floor story drift is even larger than the second story drift. Moreover, the top story drift is extraordinarily large compared with its counterpart in any other test. This is due to the higher mode contribution to the structure response to this impulsive table acceleration.

6.2.3.D. Specimen 3 Subjected to 1.73*EC 450

Shown in **Fig.** 110 is the strongest table motion ever applied to the test structure. As indicated by its peak acceleration which is 16% greater than gravity (1.0g), it has an intensity comparable with that of the Pacoima excitation shown previously. The motion is also more effective in exciting the first mode than the Pacoima. In addition, the longer duration of this motion is able to supply more energy to produce more damage. As can be seen from **Fig.** 111, a greater amount of nonlinearity is achieved by this motion. In addition to severe yielding in the two links, both of them buckled in this test. The figure shows that the strength of the west link apparently decreased after buckling. Since the excitation is strong, the floor accelerations of **Fig.** 113 show a relatively greater second-mode response than was observed in the other El Centro tests. A detailed description of the link damage has been presented in 6.1.2.C; the effects of the link yielding and buckling on the responses are shown in **Figs.** 112, 113 and 114.

CHAPTER SEVEN

THEORETICAL CORRELATION

As stated in the beginning chapter, one of the objectives of this study was to evaluate the use of the existing computer program, DRAIN-2D. To establish an economical mathematical model was, of course, another objective. With data in hand, the capability of the program to calculate nonlinear responses of the eccentrically braced frame to earthquake ground motions can be evaluated. Especially, it was of interest to study how to model the nonlinearities of a link by using available elements.

DRAIN-2D was selected as the tool for data correlation because (1) it is relatively simple and inexpensive to employ as compared with other nonlinear analysis softwares such as NON-SAP [20], ANSR's [21,22], etc., which need large core memories, (2) the DRAIN-2D program has a fairly complete library of building related elements that can be used to model commonly encountered structural members, (3) the two-dimensional nature of the experiment also led to the selection of this program which is specifically designed for 2-dimensional problems.

7.1. DRAIN-2D, A Nonlinear Structural Analysis Program

The program, fully documented by Kanaan and Powell [1], is designed for the determination of the inelastic dynamic response of two-dimensional structures of arbitrary configuration to earthquake type ground motions. Independent vertical and horizontal ground excitations can be specified in terms of acceleration time histories. However, no out-of-phase multiple support excitation can be considered.

The program has an element library including six elements of five different types. The library is adequate for modeling the nonlinear behavior of structural members commonly encountered in structural analysis. The program handles plane structures made up of arbitrary combinations of 1-D elements and 2-D infill panels. Semi-rigid connections and beam stiffness

degradation can also be modeled. To date, two multilinear post-buckling brace elements have been separately developed and can be incorporated into the program [23]. Therefore, there is a total of eight elements available to the public. The program may be obtained from the National Information Service for Earthquake Engineering (NISEE), University of California, Berkeley.

One of the merits of the program is its simple scheme to model nonlinear behavior. The bilinear strain hardening scheme is used for all elements except the stiffness degrading beam element and the post-buckling truss elements. The bilinear characteristic alone is sufficient to model steel members, which have well defined stress-strain relationship. By deploying more than one element between two nodes and assigning them appropriate properties, a multilinear or curvilinear yielding mechanism can be created for more sophisticated behavior.

The program uses a constant average acceleration step-by-step integration algorithm to calculate the dynamic response. Within each time step, the structure is assumed linear and has a stiffness equal to the tangent value at the beginning of the step. Unbalanced loads due to error in the assumptions are calculated at the end of the step. Correction is done in the next step by adding the sign-changed unbalanced loads to the external dynamic loads. At moments of yielding or stiffness change, a small step size is required to prevent large overshoots to ensure the accuracy of the calculation. Because of the constant step-size algorithm used in DRAIN-2D, a small step size is required throughout the computation. Therefore, the cost of calculation may be excessive. A variable time step algorithm is now an available option in the new version of the DRAIN-2D program, DRAIN-2D2, but it was not ready in time for use in this study.

7.2. Mathematical Idealization of the Test Structure

To minimize the computation costs, the main objective of the mathematical modeling is to reduce an infinite degrees of freedom system to one with minimum degrees of freedom, which retains the significant properties of the system and, still, is able to characterize its behavior within tolerable error.

The nature of the structural response in this study is two-dimensional. The lateral loads due to spurious table excitations were resisted mainly by the braced frames. As mentioned in Chapter Two, the lateral stiffness of the interior frames is negligible because girders of the interior frames were deprived of their ability to take bending moments.

Nevertheless, since the disabled girders were held in position by gusset plates, the interaction between the disabled girders and the rest of the structure can be very complicated. Moreover, the columns of the exterior and the interior frames were interlocked by girders in the E-W direction, i.e., the direction perpendicular to the plane of table motions. This interlocking tends to reduce axial forces in the exterior columns and to increase them in the interior. On the basis of the experimental data, axial forces in the interior columns are about one third of those in the exterior columns.

With regard to resistance to the base shear, the contribution from the interior frames is relatively small compared with that from the braced frames. It was estimated, from the shear forces calculated from column bending moments, that the four interior columns together share about 10% of the total base shear.

To economize the computing cost, the analysis was done without including the relatively unimportant interior frames, but their contribution was taken into account by manipulation of the properties of the external frames.

7.2.1. The Global Mathematical Model

The plane frame shown in **Fig.** 115 is a mathematical model for the test structure. Two vertical springs were added to the model under the first story columns to simulate the shaking table compliance, giving a pitching degree of freedom to the structure-shaking table system.

The center of the shaking table is assumed to be a stationary node. The fixity of the node is assured by a rigid horizontal truss element (not shown) and a roller (not shown). The force in the horizontal rigid truss element thus is the base shear, while the roller holds the structure

in position without possibility of vertical displacement. The mass of each story is lumped at the two girder-column connections. The inertia property of the shaking table, including both linear and rotational masses, is preserved by providing equivalent lumped masses at the two ends of the rigid beam representing the shaking table.

The base shear and masses mentioned in the last paragraph represent only one half of the total values for the entire structure because the plane frame is modeled to have only one half of the stiffness of the entire structure, assuming that response symmetry holds.

In this mathematical model, there is no interaction between the interior and exterior frames. To take the interior frame contribution into account, two modifications are made to the mechanical properties of the columns:

First, the cross-section area is increased by one-third to account for the axial rigidity of the interior columns.

Secondly, the bending rigidity is increased by one tenth to take into account the contribution of the interior columns in resisting the base shear.

A short vertical truss element is used to model the link behavior. By assigning appropriate properties to the vertical truss element, it will yield when the link shear capacity is reached. Another horizontal truss element is used to hold the ends of the link as shown in **Fig**. 115. If the 'shear element', i.e., the vertical truss element, is taken to be very short, say 0.01 inch, the error due to geometric deviation, i.e., the slope in the two link segments shown in **Fig**. 115, becomes small. With this idealization, a hinge is automatically introduced at the middle of the link. This is acceptible because of the expected antisymmetric deformation.

The modeling of the shear link behavior will be discussed further in Section 7.2.3.

7.2.2. Simplification of the Global Mathematical Model

To reduce the cost of computation, advantage was taken of the very localized nonlinearity expected in this structure. Accordingly the upper three braced stories are replaced by a simple

shear story. Note that a stiffness matrix can not be fed directly into the DRAIN-2D program as input.

This simplification is justified by the following: (1) the upper three stories are expected to remain elastic; (2) the response of the test structure is dominated by the first mode. Because of (2), little error is associated with neglecting the contribution from modes higher than the first.

The requirement imposed on the equivalent shear frame is that its first mode frequency as well as responses in terms of base shear and overturning moment must not be changed. If the stiffness properties and height of the columns of the simplified frame, and the size of the simplified lumped masses are chosen as shown in **Fig.** 116, this requirement is satisfied. The two systems in the figure have the same effective modal mass and frequency. The height of the equivalent shear frame is determined so as to preserve the first mode overturning moment.

The equivalent shear frame cannot directly replace the upper three stories of the test frame, because its continuity will be seriously affected by this simple replacement. To minimize the discontinuity, an additional artificial story of very short height was created above the second story before the equivalent shear story was superposed on top. The design of the artificial story is to be discussed in Section 7.2.2.A. below.

Shown in **Fig.** 117 is the final mathematical model of the test structure. The model has only 14 nodes. Because the three rigid elements, numbered 1, 3 and 15, have no axial distortion and element number 6 has no axial force in it because of anti-symmetry, the mathematical model has only 17 displacement unknowns provided that the rotational degrees of freedom at the hinged ends of girders 6 and 10 are deleted after giving the girders proper stiffness factors. Great simplicity is achieved for the 3-D five-story test structure by this mathematical model used for the correlation study.

As mentioned in Section 6.1.9., the lower end of the first story column was not sufficiently rigid against rotation. For example, if the lower ends of the columns were assumed rigid, the trial analysis of the 1.73*EC 300 test of Specimen 2 gave a CBWN2U/CBWN1L (see

Section 6.1.9. to interpret this notation) ratio of 1.12 while the recorded CBWN2U/CBWN1L ratio is 1.76. The error in CBWN2U is about 1% and the error in CBWN1L is about 55%. Therefore, a semi-rigid connector was deployed at the position to relax the joint. By an interpolation scheme, the stiffness of the semi-rigid element was determined to be about 15,000 in-kips per radian.

Mathematical modeling for link nonlinearity and table pitching are discussed in Sections 7.2.3. and 7.2.4., respectively.

The First Mode Period

The first mode period is a parameter used to check the fidelity of this simplification process. For the original structure and the simplified model, the first mode periods are 0.249 seconds and 0.243 seconds, respectively, if a rigid foundation is assumed. In other words, an error of about 2.4% in the first mode period resulted from this simplification. The reduction in the period may be due to neglecting the effect of the higher modes in the simplification process.

7.2.2.A. The Artificial Story

The artificial story of the mathematical model was only one tenth of an inch in height (see Fig. 117). The property of the column of this story, designated as Element 4 in **Fig.** 117, is determined by the condition that the rotational stiffness K must be the same as that of the upper three stories of the test frame. The equality of the rotational stiffnesses is shown in **Fig.** 118. A simply supported beam was arbitrarily chosen for the model. Therefore, a hinge should be placed at the upper end of the artificial column as shown in **Fig.** 117. In addition, the column is rigid in axial deformation. With this manipulation, the rotational stiffness of Joint A (see Fig. 117) is more or less preserved.

The girder of the artificial story, Element 3, is rigid in both axial and bending deformation. This assumption was adopted to assure the equivalence of the simplfied shear story to the original upper three stories. A rigid truss element, Element 5, was added to form a rigid trian-

gle which serves to transfer the lateral shear force to the lower stories.

7.2.3. Modeling of the Link Nonlinear Behavior

The beam elements of the DRAIN-2D program have no shear yielding mechanism. However, there are ways to model the shear yielding by utilizing the available elements in the program element library.

In cases of shear yielding, a threshold is set for the bending moment, i.e., the bending moment cannot increase after the element has yielded in shear except for the increase due to strain hardening in shear. Similarly, if plastic hinges have formed at both ends of a link, the shear force in the link can no longer increase except for some minor growth due to strain hardening in bending. In other words, the interdependence between bending moment and shear force furnishes a base on which the modeling of shear yielding can be achieved. Instead of physical yielding in shear, the bending capacity of a link is assigned according to the shear capacity of the link. Therefore, yielding in bending is equivalent to yielding in shear.

However, this idea can only be applied to a structure (such as the ecc-X-braced test structure) where the position of zero moment in a link during horizontal excitation is known. For an eccentrically diagonal-braced frame, it is not feasible to use the above idea to model the shear yielding behavior because the position of contra-flexure is not known in advance.

Another way to model the shear yielding is shown in Fig. 119. It is essentially the same idea as described above. At the center of the link, zero moment condition is assumed. Two truss bars perpendicular to the link are given appropriate properties so that the bars will yield when the shear capacity of the link is reached. In the model, the nodes at the ends of the bars should be prescribed to have the same horizontal displacement.

More than one truss bar or 'shear truss element' can be deployed between two nodes to model curvilinear shear yielding behavior.

7.2.4. Model of the Table Pitching

The sixteenth element in Fig. 117 is a truss element or 'pitching spring' provided to give the mathematical model the pitching degree of freedom. This element is very important because the first mode frequency depends very much on its stiffness. The dependence of the first mode period of the test structure-shaking table system on the pitching spring stiffness is demonstrated in **Fig.** 120 by the curved line with triangles.

It should be noted that the abscissa of the figure is the linear stiffness of a single pitching spring. Rigorously, the pitching stiffness of the whole system equals the product of the linear stiffness of a pitching spring and the bay width of the structure, i.e., 72 inches. The solid line in the figure represents the rocking period of the system if the structure were rigid. On the other hand, the dashed line represents the lower limit for the period of the system, i.e. 0.249 sec, which is the period of the test structure on a rigid base, where no pitching is allowed. As shown, the period curve of the system is asymptotic to these two lines: for very soft springs, the system becomes like a rigid block; for very stiff springs, the system becomes like one on a fixed base.

A difficulty arising with the model is that the stiffness of the pitching spring is indeterminate and also its force-displacement relationship is unknown. Generally, it is assumed to be linearly elastic and the stiffness is determined according to the experience of the analyst and the nature of a test. According to past experience [17], the stiffness varies from test to test and a smaller value is usually associated with larger pitching. This approach to determine the pitching stiffness is of a trial-and-error nature. Many analyses may be needed to have good estimation, and thus the cost to reach a good correlation may become high.

7.3. Correlation with the Test of 1.73*EC 300, Specimen 2

In this section, three correlation studies are presented using the simplified mathematical model. In each calculation, different properties were assigned to the two important elements, namely, the shear link and the pitching spring.

The 1.73*EC 300 test of Specimen 2 was selected for data correlation. This test was chosen because significant shear yielding in the links was generated without web buckling. Those tests which had web buckling were not chosen for study because the DRAIN-2D program has no capability to model this type of nonlinearity.

Viscous damping was assumed proportional to the initial stiffness and 0.01 second was the step size in all calculations. A constant stiffness-proportional coefficient β_0 of 0.003 was used to give a first mode damping ratio in the range of 2 to 4 percent depending upon the fundamental period of the structure-shaking table system.

7.3.1. The First Correlation

In the first calculation, a single shear truss element was used to model the link shear yielding behavior. The yield stress, the strain hardening ratio and the elastic modulus of the shear truss element were measured from the recorded shear hysteresis loops of the west link to be 21 ksi, 0.01667, and 7200 ksi, respectively. The pitching spring stiffness is assumed to be 500 kips/in to give a first mode frequency of 2.62cps. The damping ratio associated with this choice of pitching stiffness is 2.47%.

The calculated results with the above parameters are shown together with their corresponding experimental data in **Figs.** 121-123. From five to eight seconds, the calculated results have a slow but steady growth. This indicates that the analytical model has not enough damping. Quantitatively, except for the last excursion, the yielding was not very precisely calculated. However, the timing of the three major yielding excursions in the link was accurately calculated. Implied by a slightly larger period, the analytical model is slightly softer than the

test structure. As shown in **Fig.** 121, at moments of significant link yielding, large overshoots will occur in the calculated brace forces. Therefore, the peak values at moments of significant yielding are not reliable. This phenomenon is due to equilibrium unbalance associated with the assumption of linear behavior within the time step. The unbalance will eventually be corrected after a short period. However, the overshooting phenomenon will appear in the calculated time histories. To reduce the overshooting, a small step size may be needed for integration.

Beside overshooting and false steady growth, the force quantities have good correlation. The permanent set in the link deformation observed in the experimental data during the period from 2 to 4 seconds is not reproduced in the analysis. Therefore, the experimental and analytical floor displacements do not correlate well.

7.3.2. The Second Correlation

To improve the correlation, the calculation was repeated with the following modifications:

(1) The shear link strain hardening ratio was changed to 0.01 from 0.01667.

(2) The link yield stress in shear was changed to 22 ksi.

(3) To make the structure-table system stiffer, the stiffness of the shaking-table pitching spring was changed to 800 *kips/in* from 500 *kips/in*. Then, the damping ratio became 2.80%.

The calculated results are shown in **Figs.** 124-126. Correlation is improved within the period from five to eight seconds. The sizes of overshoots during link yielding are proportional to the extent of shear yielding. If compared with the previous calculation, the link has larger first and second yielding excursion but a smaller third excursion in this second analysis. The sizes of overshoots were found to follow this trend. After 8 seconds, rather than keeping constant amplitudes in the experimental data, the responses decrease gradually because of overestimated damping resulting from the increased pitching stiffness. Although the correlation is not quite satisfactory, the maximum relative displacements calculated are accurate.

7.3.3. The Third Correlation

It was believed that the shaking table compliance was not adequately represented by a linear elastic force-displacement relationship. Furthermore, a curvilinear shear stress-strain relationship for the link might be needed for a good correlation.

In this third trial, a nonlinear shaking table compliance was employed. The pitching spring was required to yield at a 40-kip axial force and a strain hardening ratio of 0.25 was chosen. The two quantities were decided by assuming that the north and south edges of the shaking table have a vertical displacement of about half an inch at the maximum overturning moment. In addition, a curvilinear stress-strain relationship was given by three parallel shear truss elements.

The calculated results are shown in **Figs.** 127-129. Generally speaking, this correlation is better than before except for the shear strain in the link. Good correlation was obtained for the base shear and the first-story brace force for the beginning four seconds. The nonlinearity in the link was reduced because yielding in the pitching spring reduced the deformation in the structure. Part of the energy imposed on the system by the shaking table was dissipated through the assumed nonlinearity in the pitching spring.

It should be noted that the shaking table has a tendency to return to its original position. Therefore, a yielding pitching spring may be not realistic because a permanent set due to yielding would be implied by this model. However, it is believed that some of the input energy was dissipated through pitching of the structure-shaking table system.

7.3.4. More Correlations

It is very difficult to fathom how good calculated results are in calculating the seismic behavior of a system unless dynamic experimental data is available for comparison. When some unknown parameters are involved in the calculation, the comparison becomes even more difficult.

The data correlation in this study is of a trial-and-error nature. If there were a reliable isotropic hardening model in the DRAIN-2D program to characterize the link behavior, and if the trial-and-error procedure of adjusting the various parameters, such as pitching compliance, link stiffness and strength, damping, integration step size, etc., were continued it is believed that a good match would be reached between calculated and experimental data. However, it was decided that further trial-and-error efforts were not worthwhile in this study.

CHAPTER EIGHT

CONCLUSIONS

8.1. Merits of Eccentrically Braced Frames

During a major earthquake, a conventionally designed concentric braced structure has the defects of excessive lateral displacements and poor energy dissipation because of pinched hysteresis behavior and strength deterioration associated with brace yielding and buckling. On the other hand, although a moment resisting frame has stable hysteretic behavior and good energy dissipation capacity, it may become unstable resulting from the P-Δ effect induced by excessive lateral displacements.

An eccentric bracing system possesses not only the merits of conventional concentric bracing system, such as large stiffness and high strength for frequent earthquakes, but also large ductility capacity of a moment resisting frame to absorb the energy imposed by an extreme earthquake. Moreover, for similar lateral displacements, the ductility factors in eccentric beams are much greater than those in girders or columns of a moment resisting frame. In other words, for the same amount of energy dissipation, an eccentrically braced frame has less lateral displacements and thus less nonstructural damage, and less stability hazards than a moment resisting frame.

8.2. Experimental Observations

The structure tested in this experiment demonstrated that allowing damage in girders is effective in seismic resistance. The test structure resisted the table motion mainly in two ways:

(1) absorbing the energy input to the structure from the shaking table by shear hysteretic yielding in the girders and by viscous damping and Coulomb friction of the structure,

(2) isolating the structure through the soft-story effect at the expense of a large mechanism deformation in the bottom two stories.

In the prototype structure, floor damage due to large up-and-down shear displacement in the eccentric girders is expected. Also expected is damage in partitions and infill panels due to large story drifts associated with the collapse-mechanism deformation in the lower two stories. To prevent floor distortion, it may be feasible to design a floor system isolated from the girders containing eccentric elements.

8.2.1. The Weakest Link is the Best

The earthquake response of the test structure is limited by the shear strength of the eccentric beams. For the eccentric beam, the terminology, shear link, is adopted because the eccentric beam yields mainly in shear.

Links of three different strengths were tested. It was observed that the weakest link was the best energy absorber and least response was induced when the test structure had the weakest links. The base shear and the overturning moment as well as the member forces were strongly related to the strength of the links. In fact, a linear relationship was observed. The floor relative displacements also depended strongly on the link shear deformation.

8.2.2. Web Buckling of Links

The mechanism of web buckling in the shear links was found effective in controlling the earthquake response. The earthquake resistance stages of the shear links can be summarized as follows:

(1) The shear links remained elastic for minor earthquakes.

(2) The shear links yielded in shear for moderately large earthquakes.

(3) The shear links both yielded in shear and buckled in webs during extreme earthquakes.

8.2.3. Stiffness Recovery

It was observed that the test structure had a tendency to recover its lateral stiffness. This took place after the links had yielded in shear and significant lateral relative displacements at the first two stories had occurred. It is because the two braces in tension were aligned with the shear-yielded link to function as a single diagonal brace across the first story girder.

8.2.4. Replaceable Links

In the test structure, the links were designed to be replaceable. In practice, permanent deformation in the shear links may be so severe that replacement becomes difficult. However, the feasibility of repair implied by replaceable links is good, because after an earthquake, deformed links are very likely to be able to be jacked back to a position so that repair by replacement becomes possible.

8.3. Correlation Studies

A simple mathematical model was formulated for the calculation of the dynamic response, and a fairly good correlation between experimental and calculated results was achieved for the selected case.

To improve the correlation, more study is needed regarding the determination of the shaking table compliance. A more accurate shear yielding model that includes both kinematic and isotropic hardening phenomena observed in the experimental results is also required. The choice of damping is another important factor that will affect the quality of correlation. A better correlation may be expected if a more rigorous system identification algorithm were employed, however, this is not pursued in this investigation.

Since the program DRAIN-2D cannot model web buckling behavior, no correlation was done for web-buckling cases. Besides, the effect of large deformation is not considered by the program, either. Therefore, stiffness recovery of the structure because of axial force

development associated with large deformation in the links can not be calculated by the program.

8.4. Strong Girder-Weak Column Test Structure

The test structure was of a strong girder-weak column category. Potential plastic hinge locations were in columns. The earthquake force cannot be transmitted upward to the higher stories because of a collapse-mechanism induced in the lower two.

For a strong column-weak girder structure, plastic hinges form in the girders. Therefore, plastic bending or shear hinging in girders and links would be distributed upward into upper stories. Thus, better earthquake resistant capacity would be expected for a strong column-weak girder structure, because there are more energy dissipation sources. However, more dynamic study is required to understand the behavior of an eccentrically braced structure with strong columns.

REFERENCES

[1] Kanaan, A. E. and Powell, G. H., "A General Purpose Computer Program for Dynamic Analysis of Inelastic Plane Structures," University of California, Berkeley, *EERC Reports*, No. EERC 73-6 and EERC 73-22, April 1973, Revised September 1973 and August 1975.

[2] *Recommended Lateral Force Requirements and Commentary,* Seismology Committee, Structural Engineers Association of California, San Francisco, California, 1976.

[3] Wakabayashi, M. Matsui, C., Minami, K. and Mitani, I., "Inelastic Behavior of Full Scale Steel Frames with and without Bracings," *Bulletin*, Disaster Prevention Research Institute, Kyoto University, Vol. 24, Part 1, No. 216, March 1974.

[4] Wakabayashi, M., Nakamura, T. and Yoshida, N., "Experimental Studies on the Elastic-Plastic Behavior of Braced Frames under Repeated Horizontal Loading," *Bulletin*, Disaster Prevention Research Institute, Kyoto University, Vol. 27, Part 3, No. 251, September, 1977.

[5] *Uniform Building Code,* International Conference of Building Officials, Whittier, California, 1979.

[6] Roeder, C. W. and Popov, E. P., "Inelastic Behavior of Eccentrically Braced Steel Frames under Cyclic Loadings," University of California, Berkeley, *EERC Report*, No. EERC-77/18, August 1977.

[7] Fujimoto, M., Aoyagi, T., Ukai, K., Wada, A. and Saito, K., "Structural Properties of Eccentrically K-Braced Frames," (in Japanese), *Trans.*, Architectural Institute of Japan (AIJ), No. 195, May 1972.

[8] Hisatoku, T., Segawa, T. and Mukai, H., "Experimental Study on the Static Behavior of the Y-Typed Bracings," (in Japanese), *Report*, Takenaka Technical Institute, No. 12, August 1974.

[9] Tanabashi, R., Kaneta, K. and Ishida, T., "On the Rigidity and Ductility of Steel Bracing Assemblage," *Proceedings*, Fifth World Conference on Earthquake Engineering, Vol. 1, Rome, Italy, 1974.

[10] Matsumoto, Y., et al, "Experimental Investigations for Bracing Members and the Braced Frames," Second Paper in the Recomposed Theme Report, "On the Elastic-Plastic Behaviors of the Braced Frames," *Transactions*, Architectural Institute of Japan (AIJ), No. 243, May 1976.

[11] Huckelbridge, A. A., "Earthquake Simulation Tests of a Nine-Story Steel Frame with Columns Allowed to Uplift," University of California, Berkeley, *EERC Report*, No. EERC-77/23, August, 1977.

[12] Tanaka, A., Morita, K. and Yamanouchi, H., "Damage of Braced Steel Frames due to the 1978 Miyagiken-Oki Earthquake," *Proceedings*, Sixth World Conference on Earthquake Engineering, Vol. 4, Istanbul, Turkey, 1980.

[13] Popov, E. P. and Roeder, C. W., "Design of an Eccentrically Braced Steel Frame," *AISC Engineering Journal*, 3rd Quarter, Vol. 15, No. 3, 1978.

[14] Rea, D. and Penzien, J., "Dynamic Response of a 20ft × 20ft Shaking Table," *Proceedings*, Fifth World Conference on Earthquake Engineering, Vol. 2, Rome, Italy, 1974.

[15] Clough, R. W. and Tang, D. T., "Earthquake Simulator Study of a Steel Frame Structure," Vol. I (Experimental Results), University of California, Berkeley, *EERC Report*, No. EERC-75/6, April, 1975.

[16] Manheim, D. N., "On the Design of Eccentrically Braced Frames," Ph.D. Thesis, Department of Civil Engineering, University of California, Berkeley, 1982.

[17] Ghanaat, Y., "Study of X-Braced Steel Structures under Earthquake Simulation," University of California, Berkeley, *EERC Report*, No. EERC-80/08, April 1980.

[18] Pister, K. S., *Advanced Mechanics of Materials,* Notes for Course CE 230A, Department of Civil Engineering, U.C. Berkeley, 1976, Revised 1978.

[19] Wylie, C. R., *Advanced Engineering Mathematics,* Fourth Edition, McGraw-Hill Book Company, 1975.

[20] Bathe, K. J., Wilson, E. L. and Iding, R. H., "NONSAP, A Structural Analysis Program for Static and Dynamic Response of Nonlinear Systems," Structural Engineering Laboratory, *SEL Report*, No. UC-SESM 74-3, Department of Civil Engineering, University of California, Berkeley, February 1974.

[21] Mondkar, D. P. and Powell, G. H., "ANSR-I, General Purpose Program for Analysis of Nonlinear Structural Response," University of California, Berkeley, *EERC Report*, No. EERC-75/37, December 1975.

[22] Mondkar, D. P. and Powell, G. H., "ANSR-II, Analysis of Nonlinear Structural Response, User's Manual," University of California, Berkeley, *EERC Report*, No. EERC-79/17, July, 1979.

[23] Jain, A. K. and Goel, S. C., "Hysteresis Models for Steel Members Subjected to Cyclic Buckling or Cyclic End Moments and Buckling," Department of Civil Engineering, University of Michigan, *Report*, No. UMEE-78R6, December 1978.

[24] Kasai, K., Private Communication.

[25] Timoshenko, S., "Strength of Materials," Part II, Third Edition, McGraw Hill Book Company, 1956.

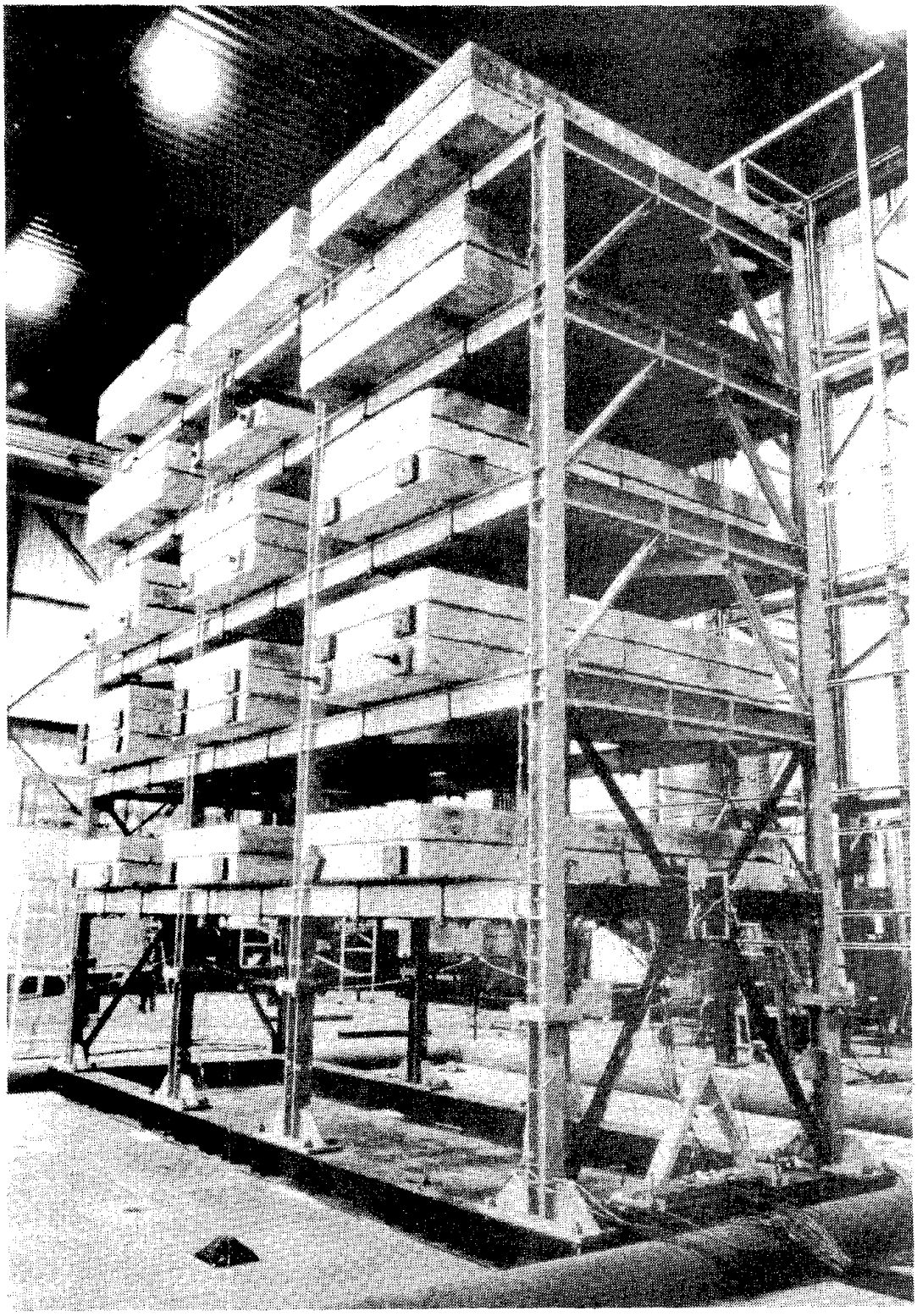

Fig. 1 The Fifty-Ton Test Structure

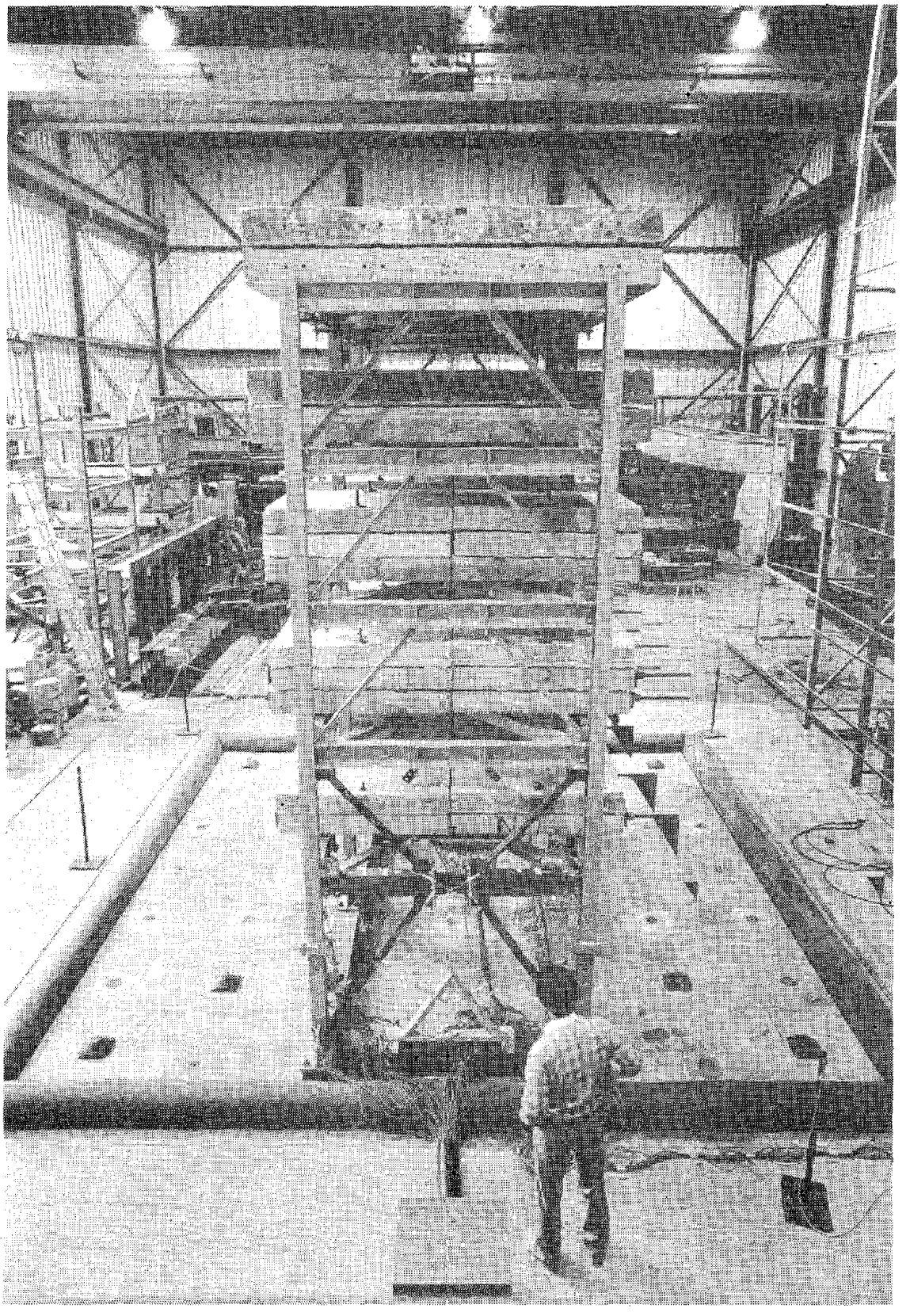

Fig. 2 The West Frame of the Test Structure
(Courtesy of *the San Francisco Examiner*)

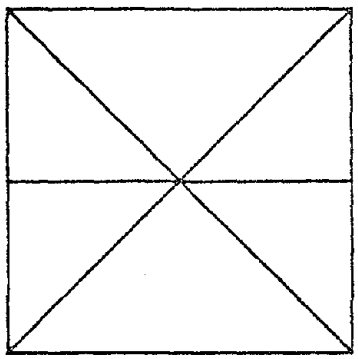

CONCENTRIC-X

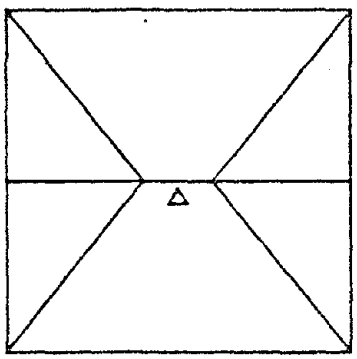

ECCENTRIC-X

Δ ECCENTRICITY

Fig. 3 Concentric Bracing and Eccentric Bracing

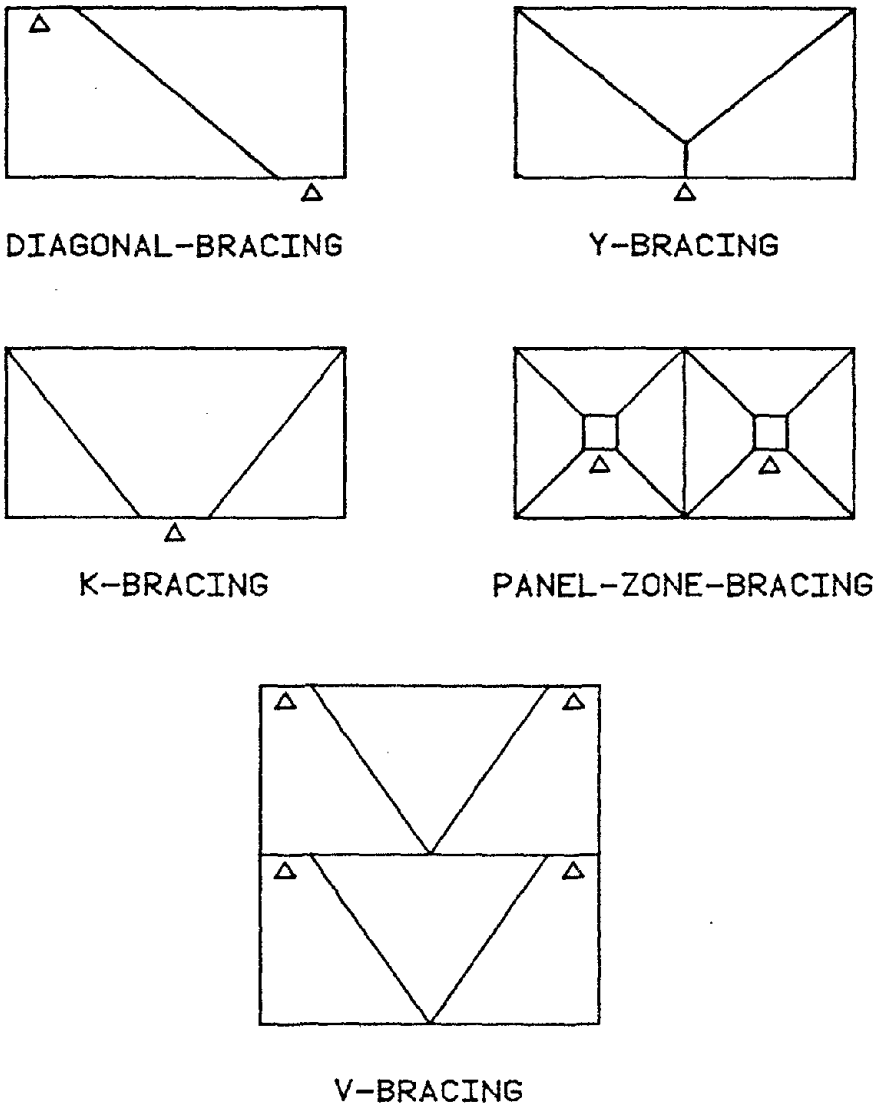

FIG. 4 SOME EXAMPLES OF ECCENTRIC BRACING

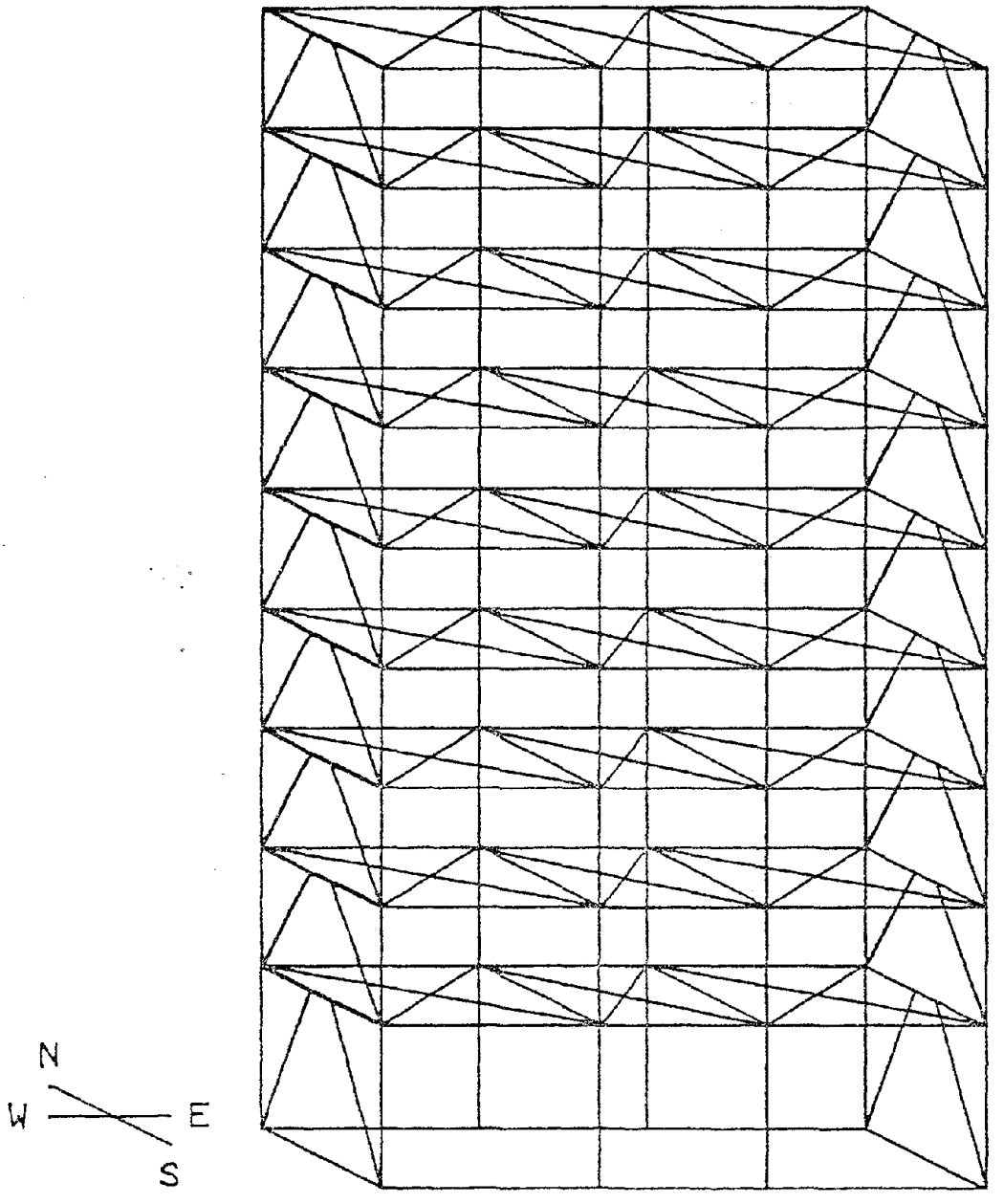

Fig. 5 Skeleton of the Nine-story Structure

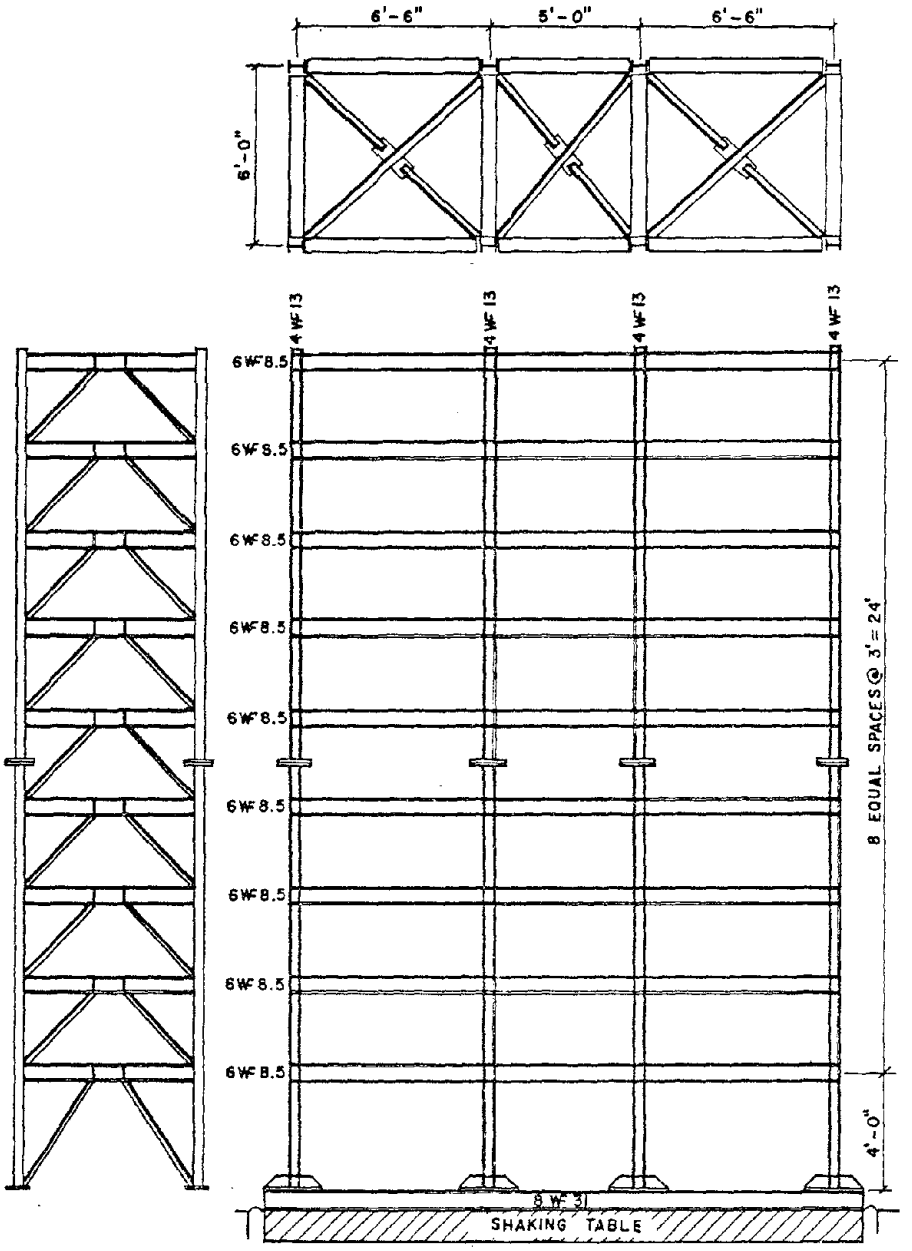

Fig. 6 General Design Layout of the Nine-Story Structure
(After Huckelbridge, EERC report *EERC-77/23*)

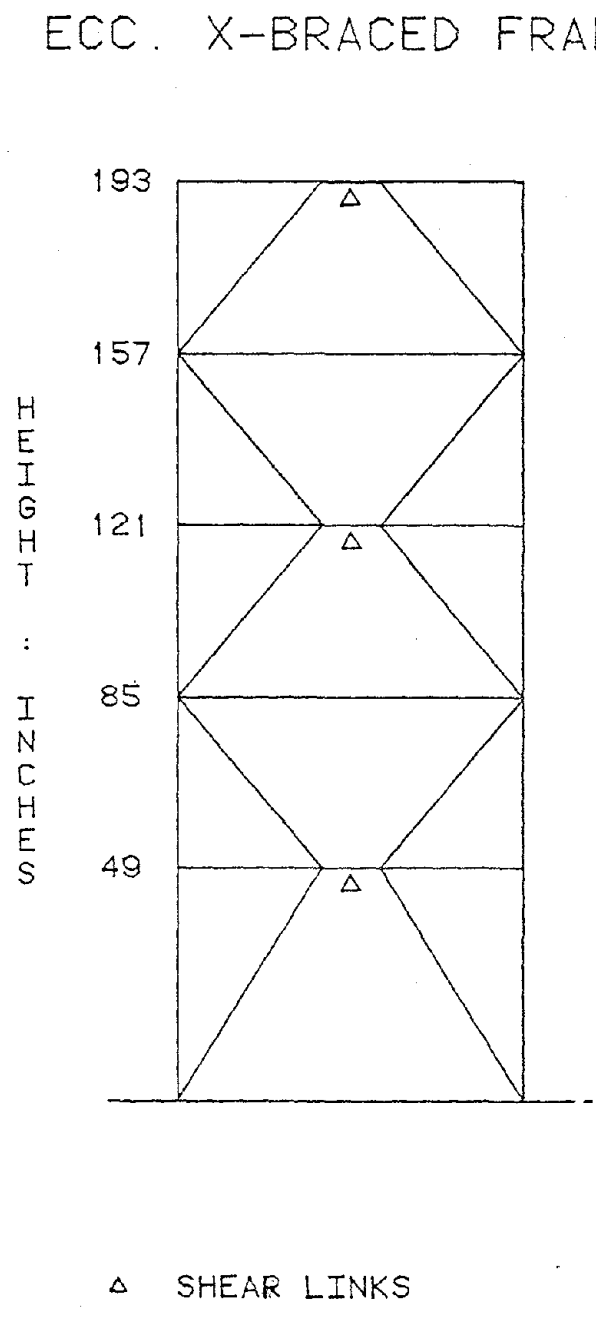

Fig. 7 Preliminary Eccentrically X-braced Frame

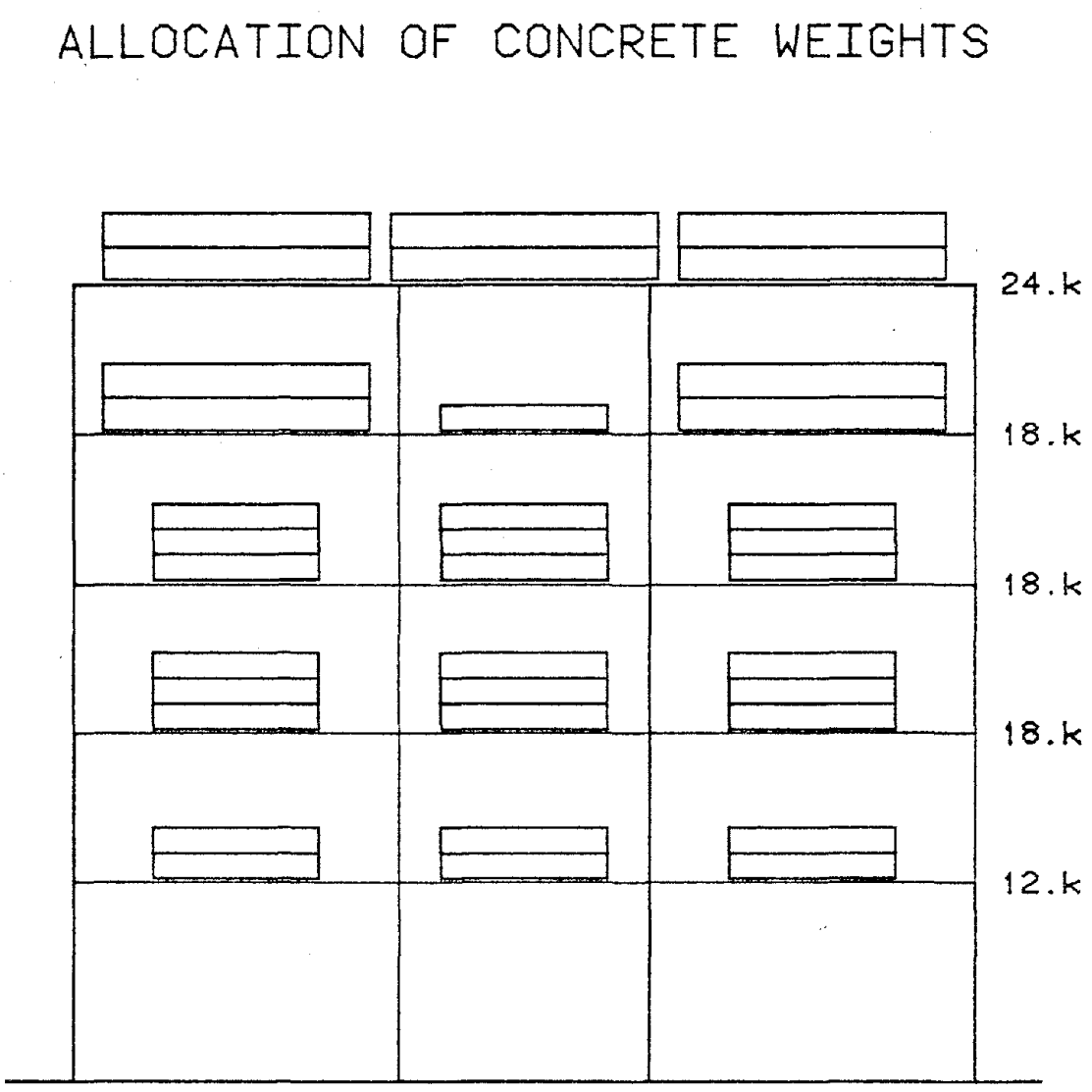

Fig. 8 Allocation of Concrete Weights

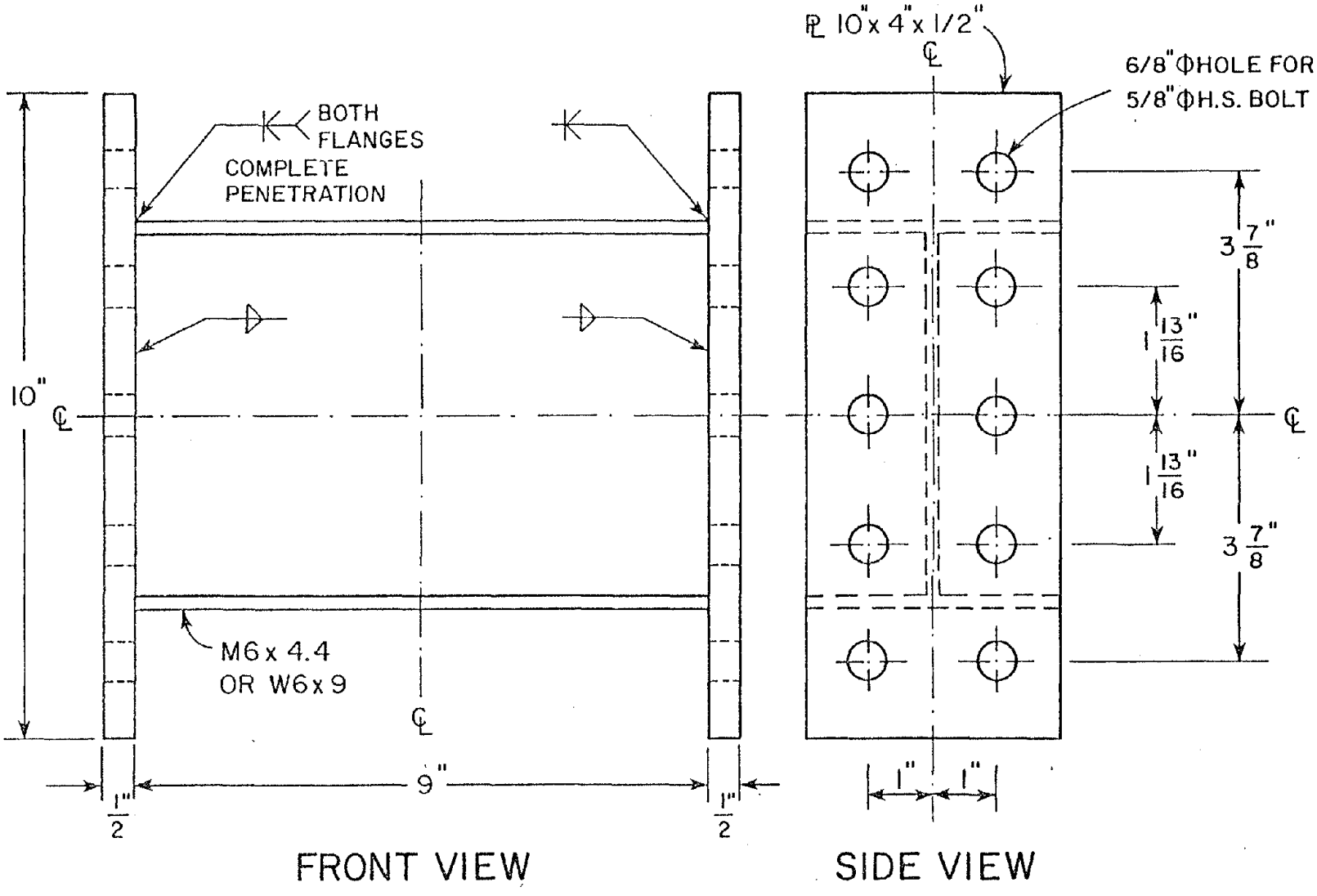

Fig. 9 Details of the Shear Link

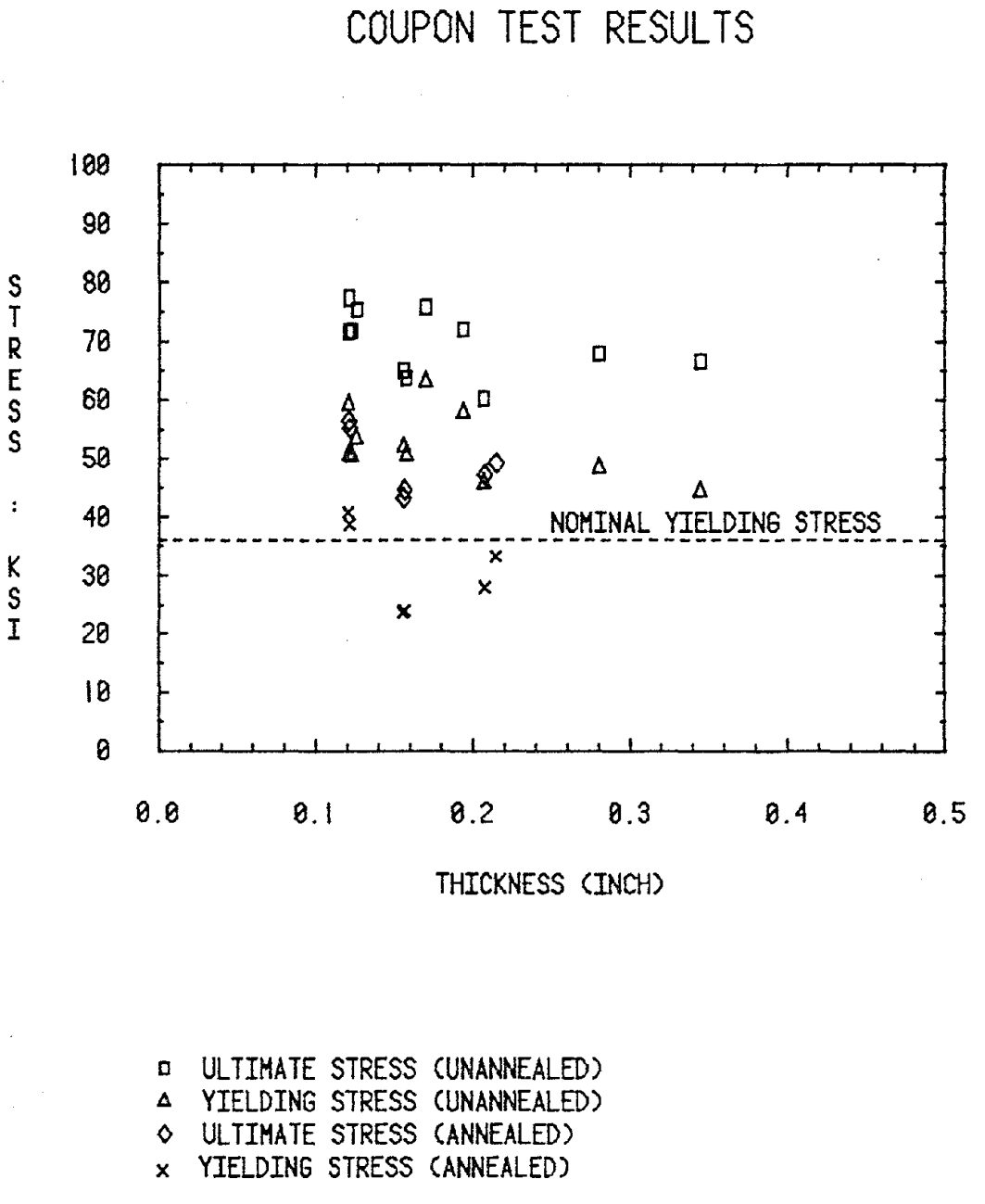

Fig. 10 Coupon Test Results

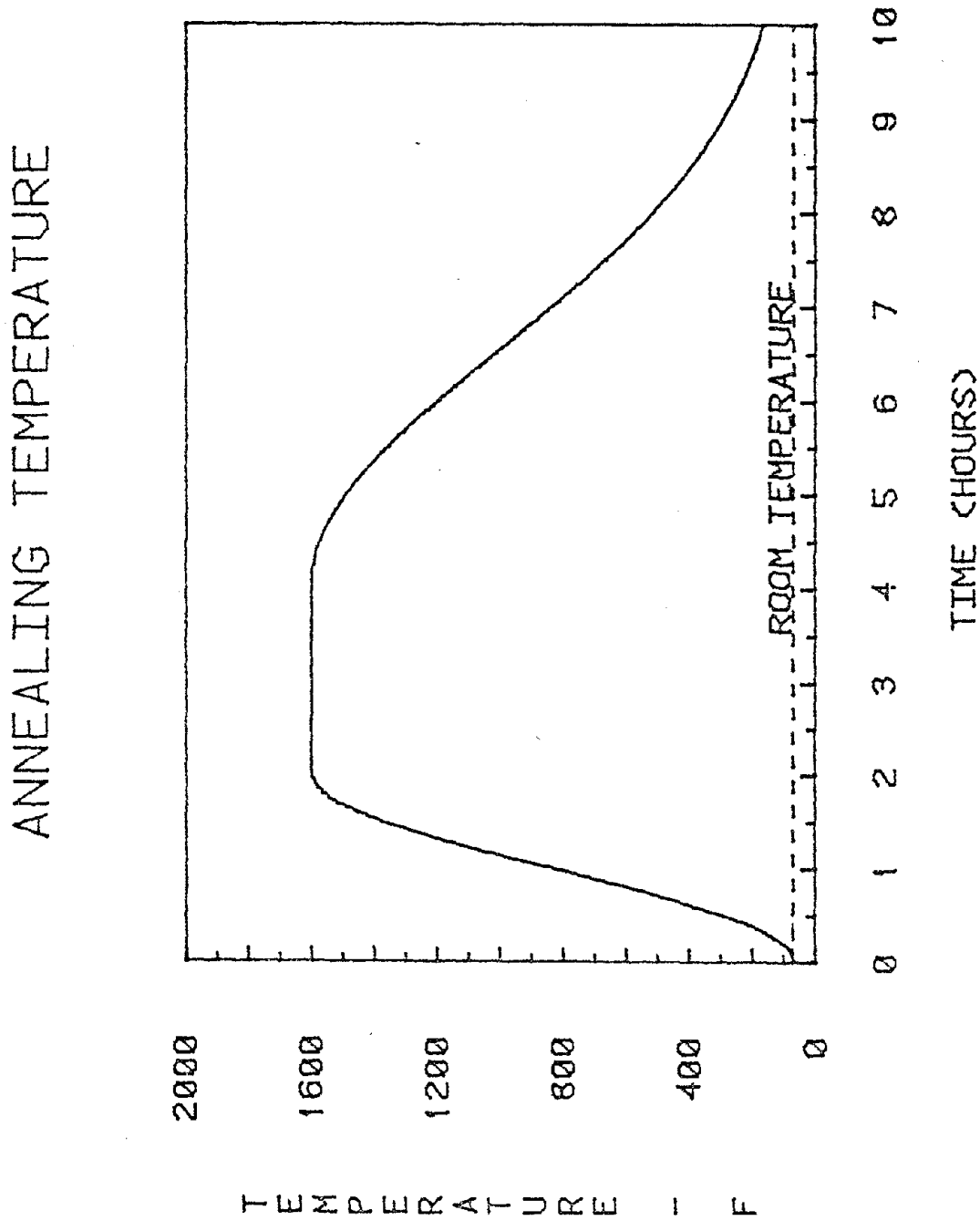

Fig. 11 The Annealing Temperature

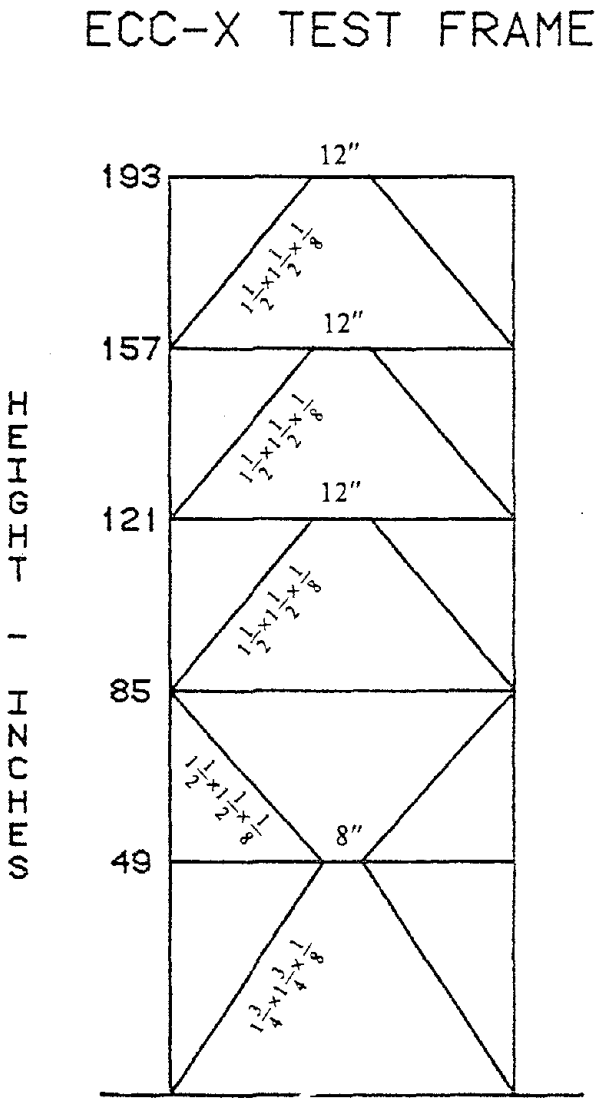

Fig. 12-1 The Eccentrically X-braced Test Frame

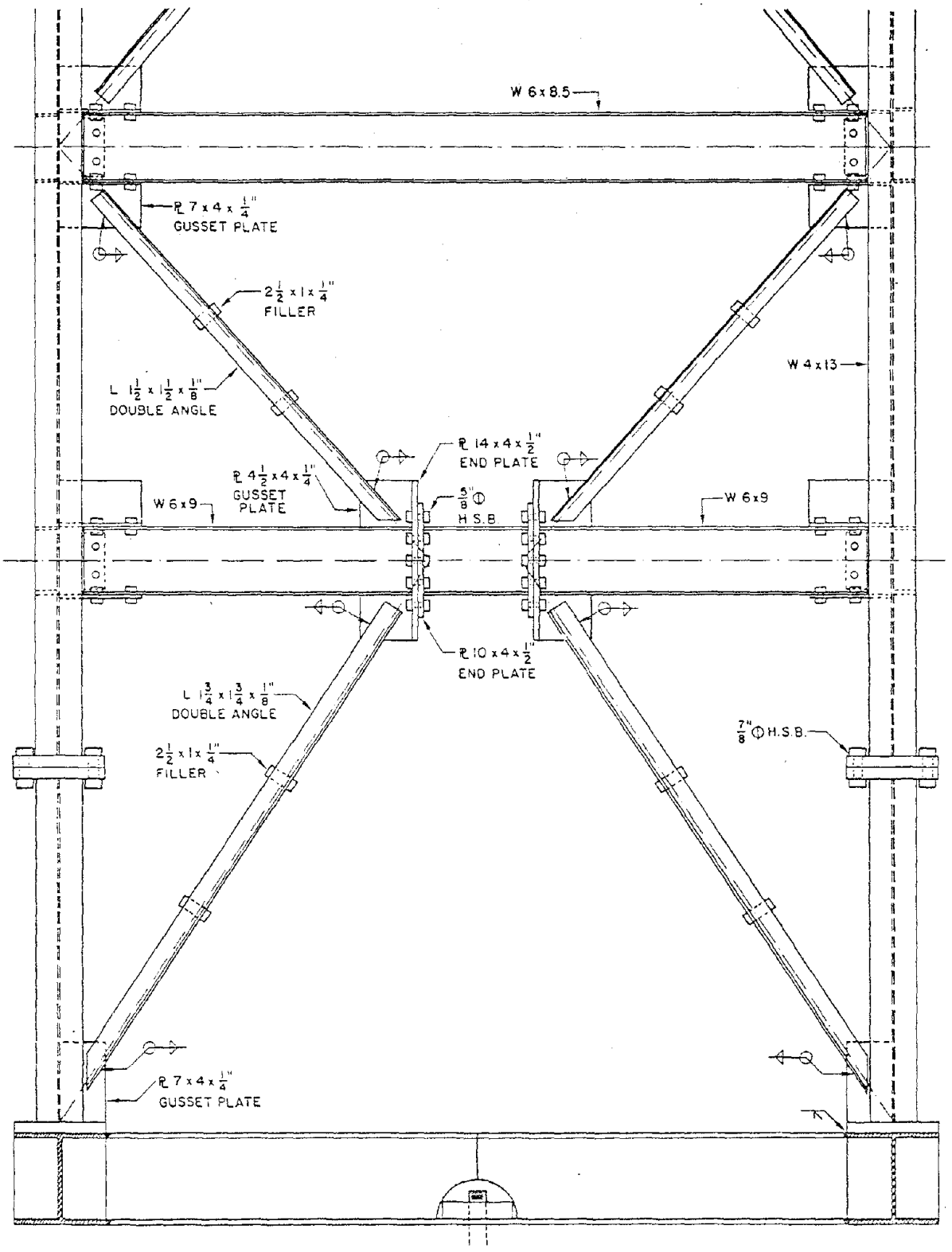

Fig. 12-2 Design Details of the Lower Two Stories of the Exterior Frames of the Test Structure

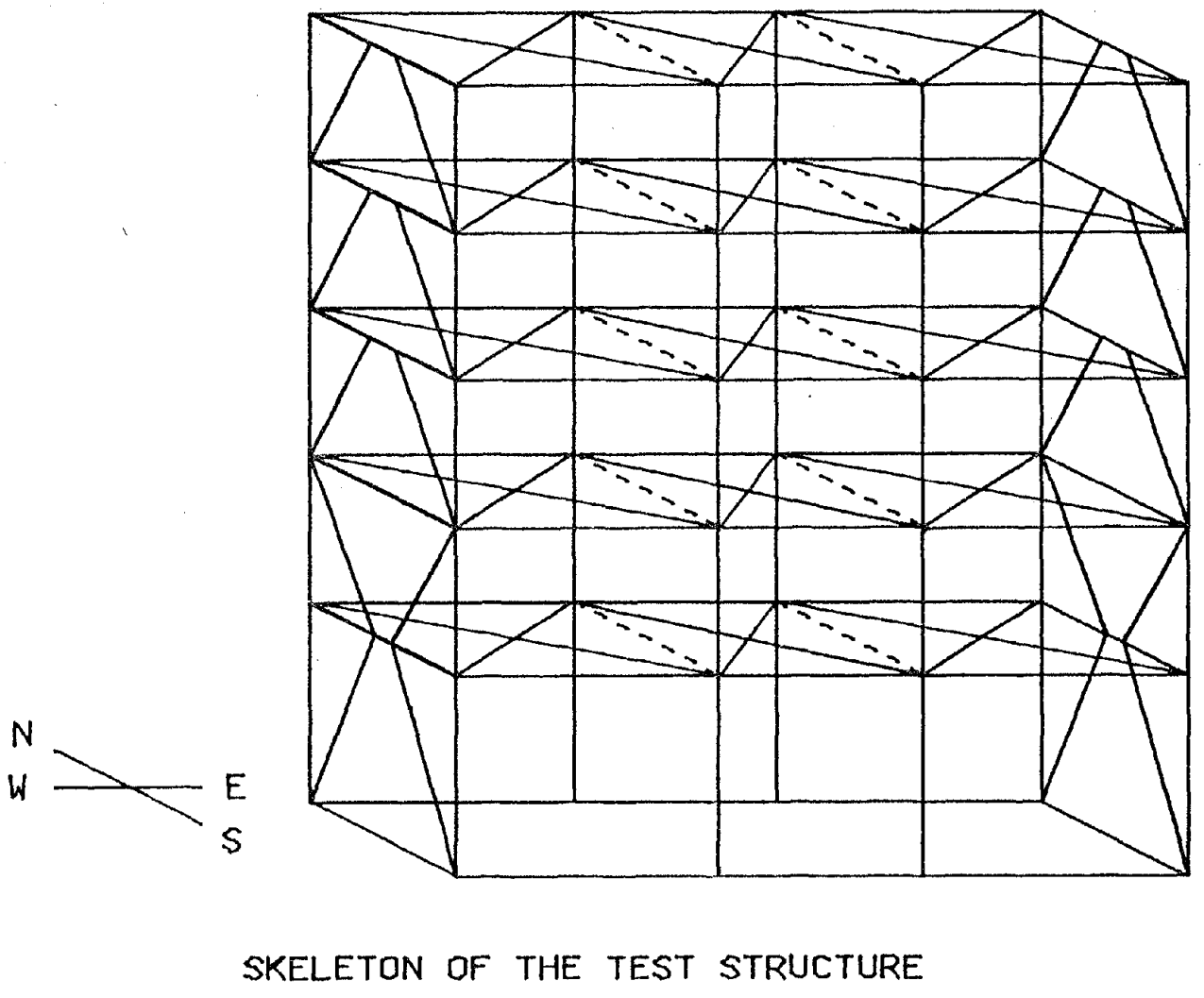

Fig. 13 Skeleton of the Five-Story Test Structure
(Members designated by dash lines are the dummy girders.)

COLLAPSE MECHANISM

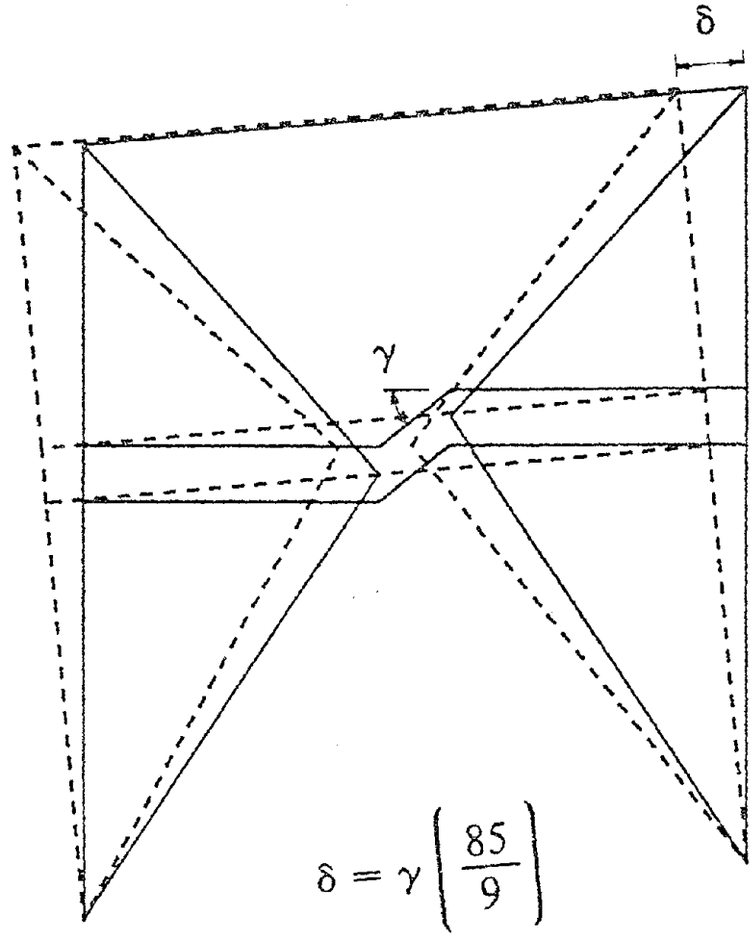

Fig. 14 Collapse Mechanism of the Test Structure

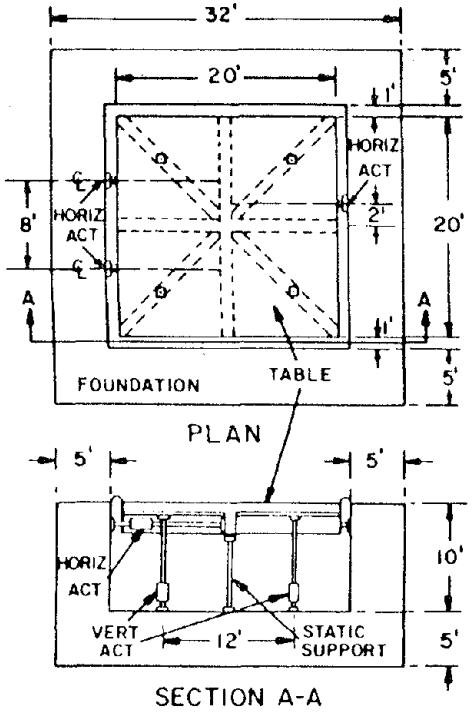

ACTUATOR LOCATIONS

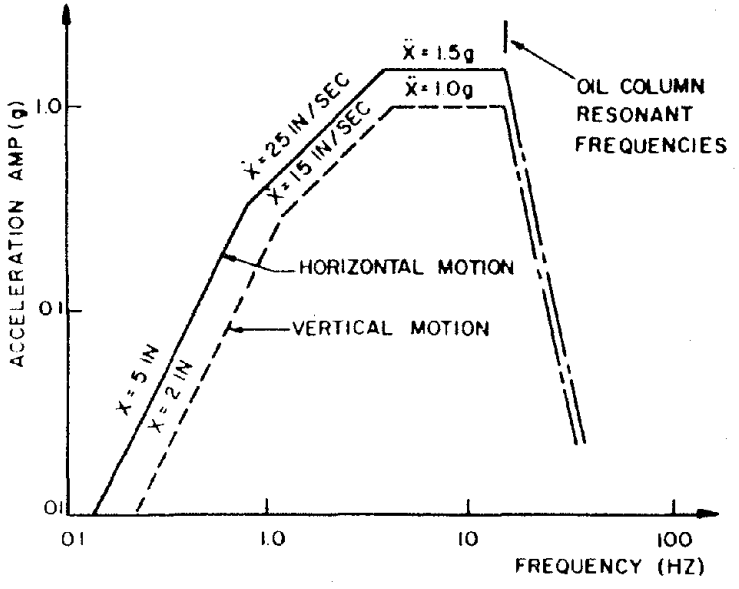

LIMITATIONS OF DYNAMIC PERFORMANCE

Fig. 15-1 . Details and Performance Limitations of the Shaking Table (After Rea & Penzien)

Reproduced from best available copy.

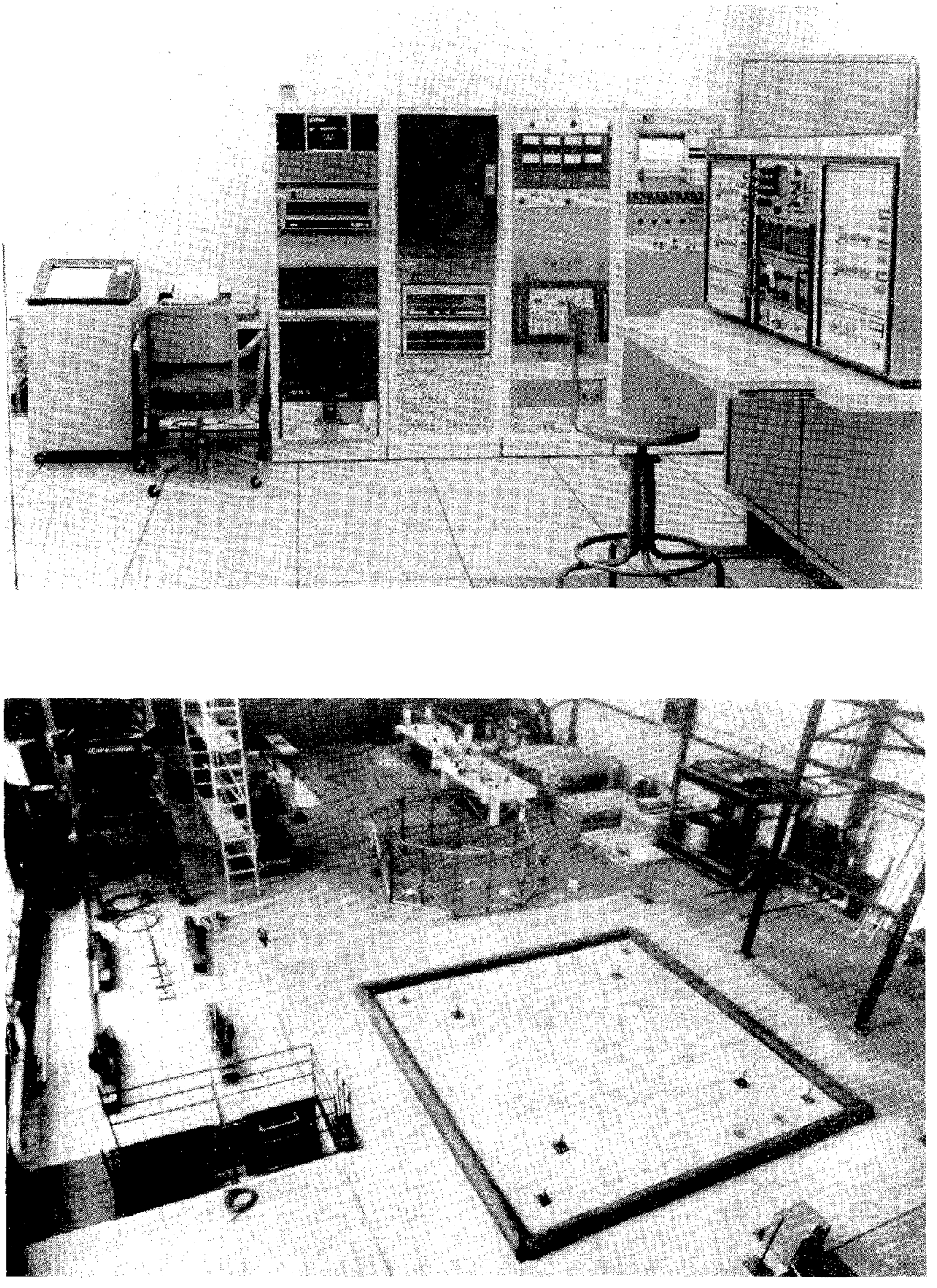

Fig. 15-2 The Control Room and The Shaking Table

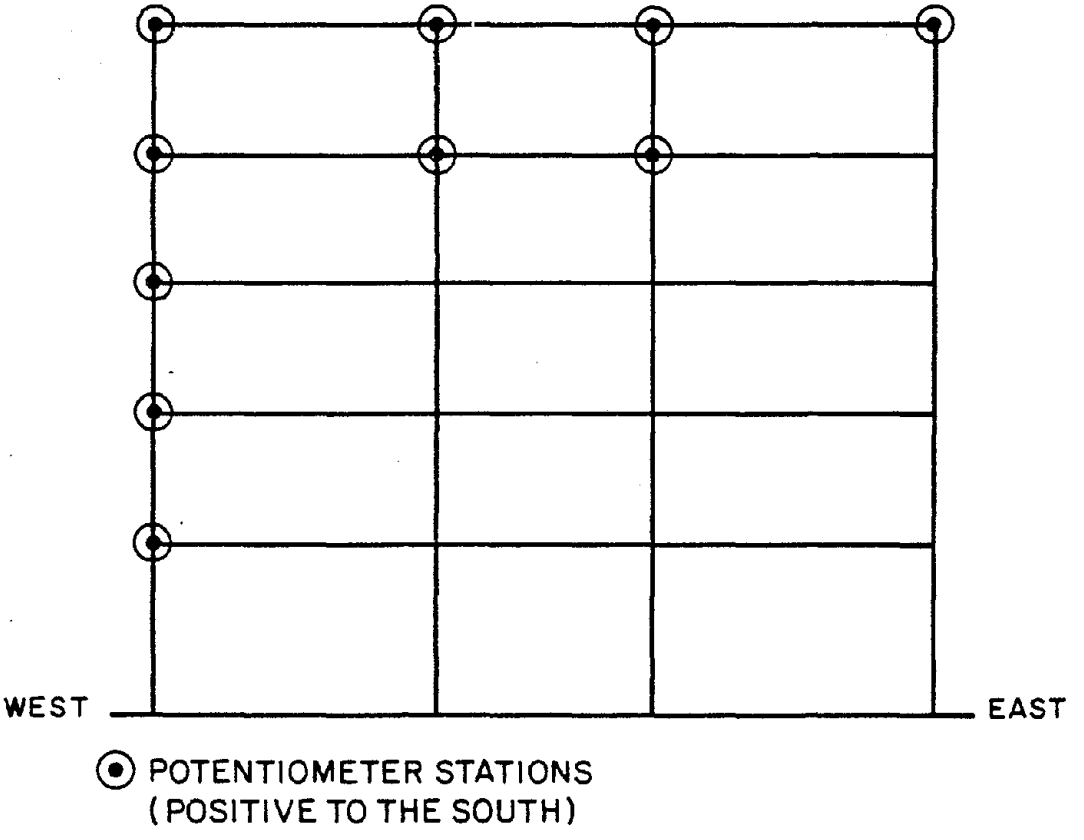

SOUTH-SIDE VIEW OF THE TEST STRUCTURE

Fig. 16 Potentiometer Stations

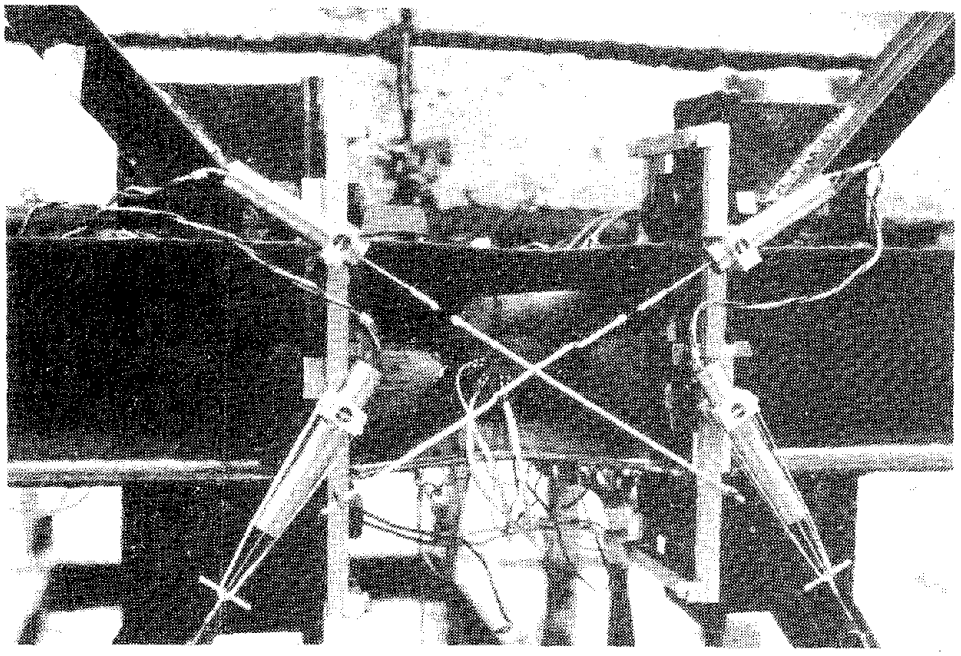

West Frame

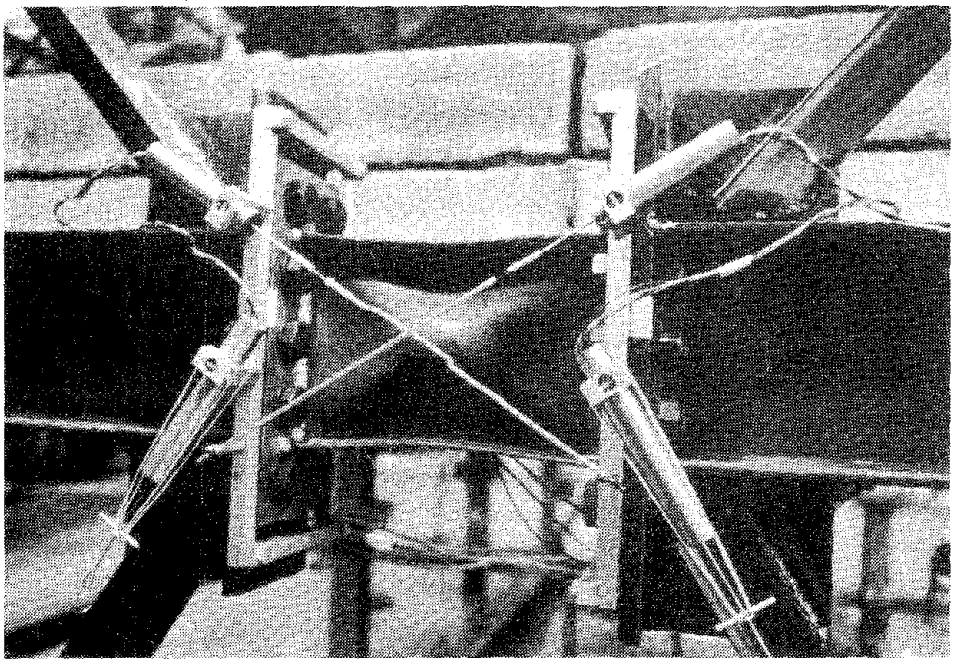

East Frame

Fig. 17-1 DCDT Stations: For Pseudo Shear Strains & Brace Axial Strains
(The Links Shown are the Damaged Links of Specimen 1.)

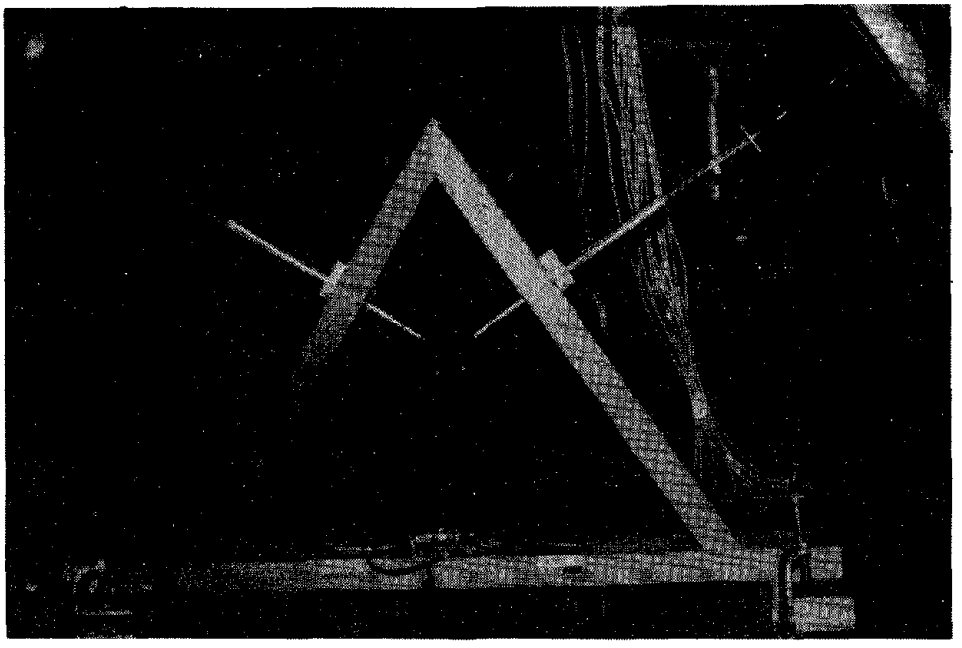

Fig. 17-2 DCDT Stations (Continued): For Lateral Brace-Buckling Displacements

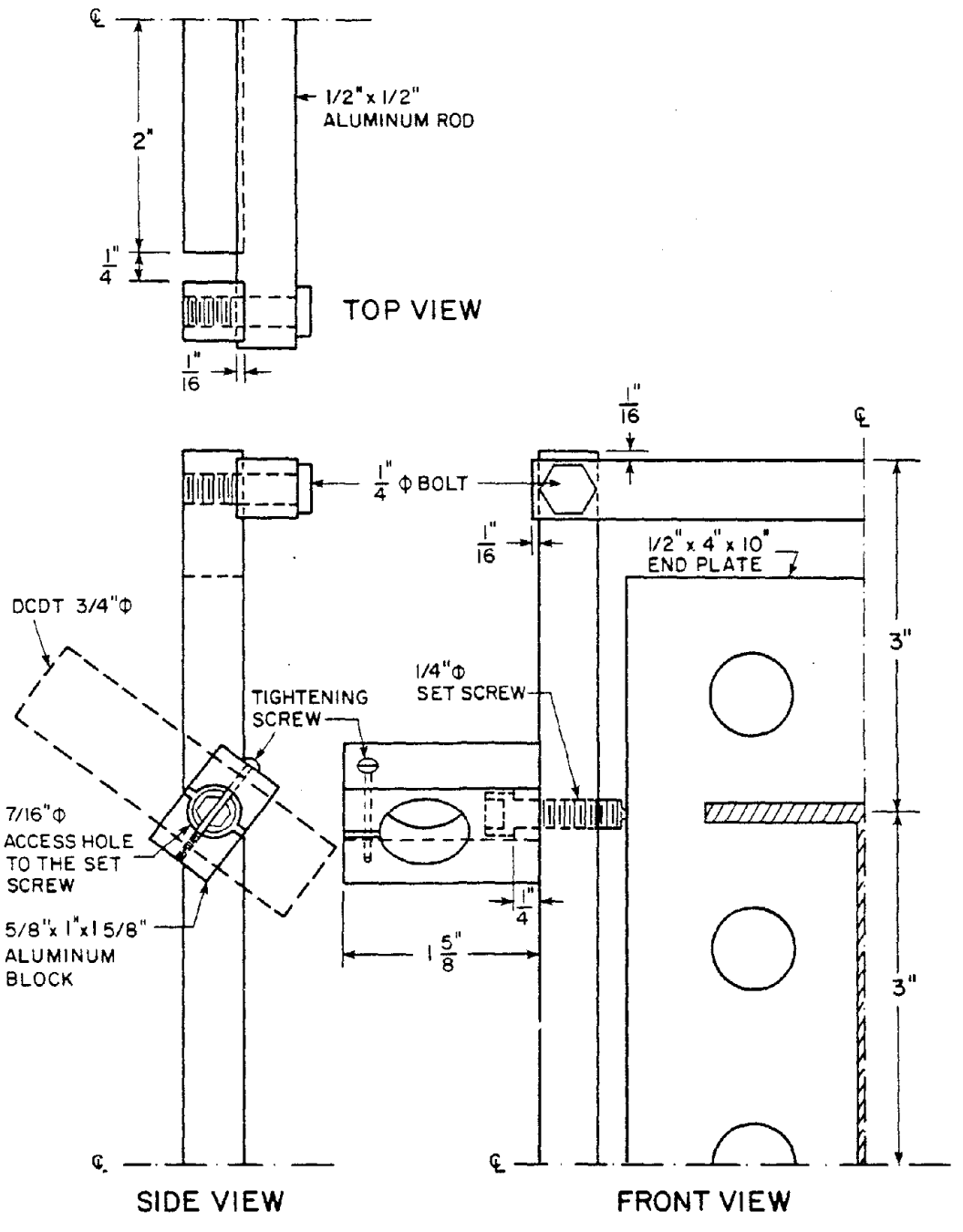

Fig. 18-1 Details of A Quarter of A DCDT Aluminum Mount

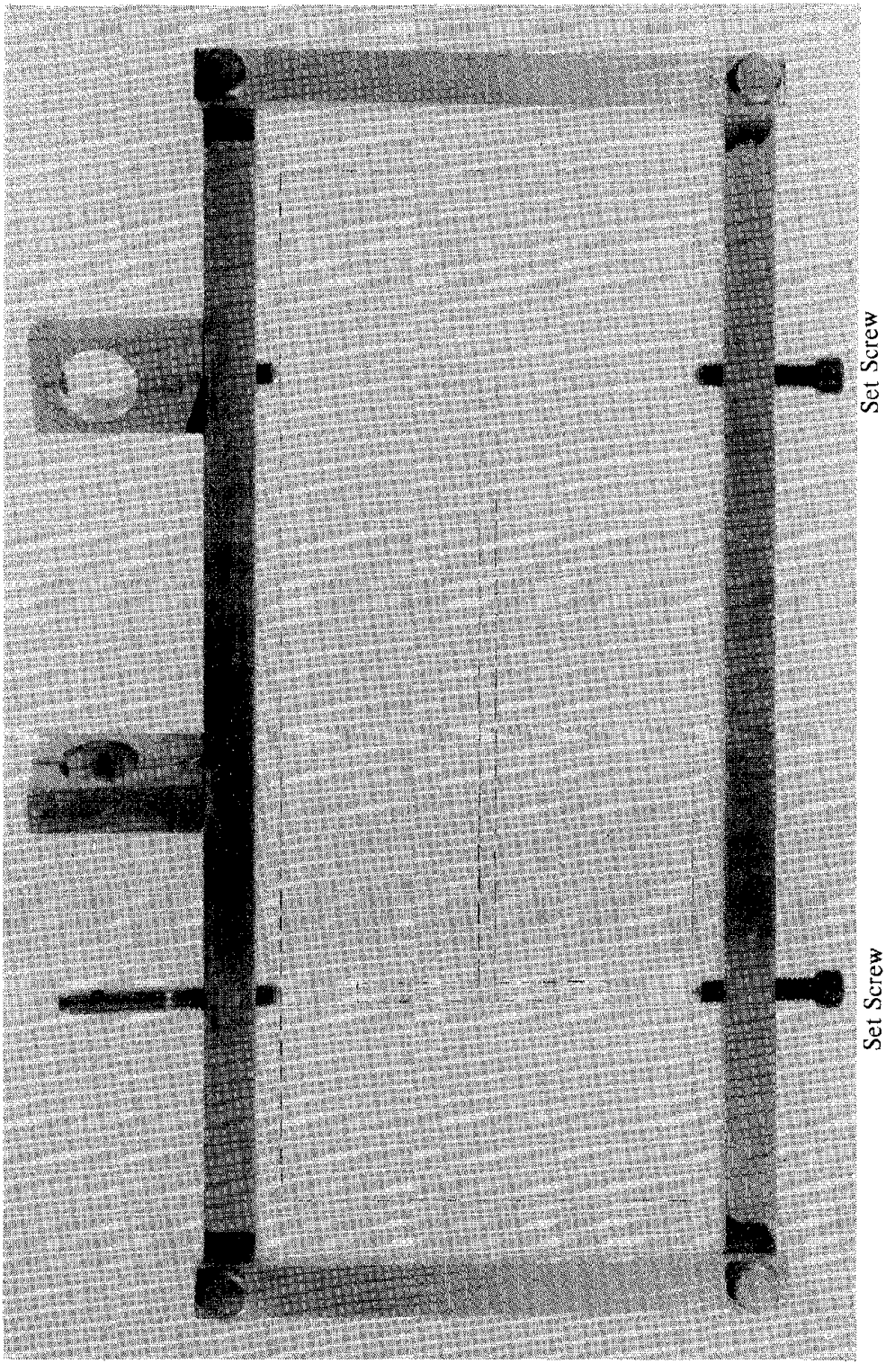

Fig. 18-2 Photograph of A DCDT Aluminum Mount

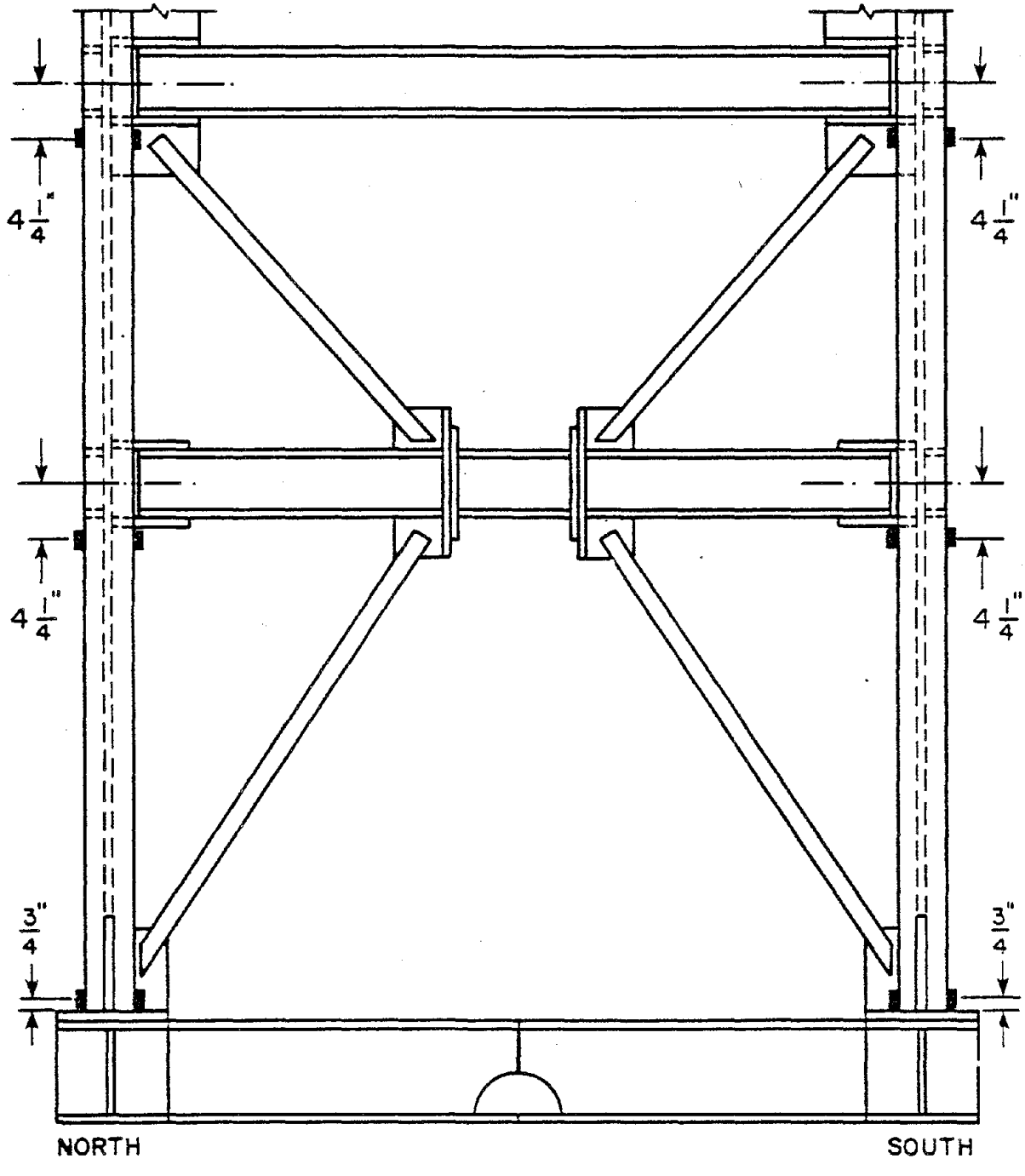

Fig. 19 Post-Yield Flexural Strain Gage Stations

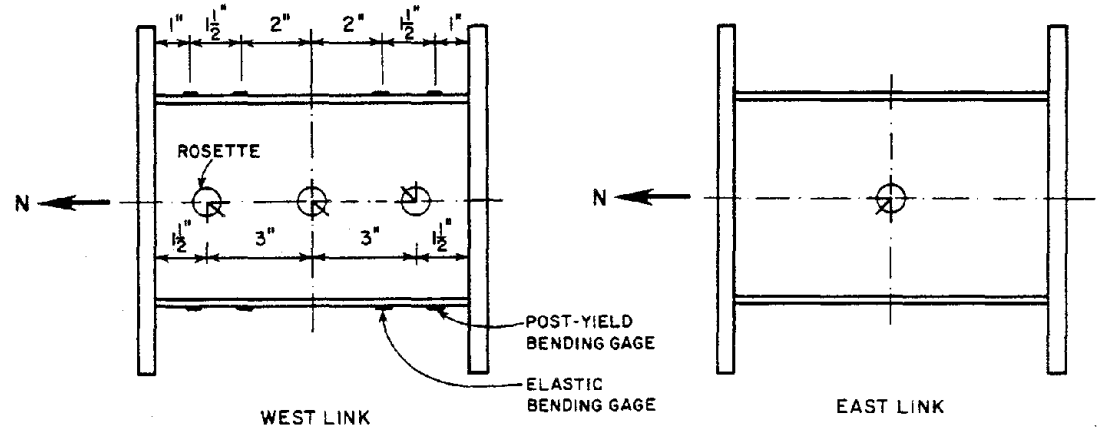

STRAIN GAGE STATIONS (LINKS OF SPECIMEN 1)

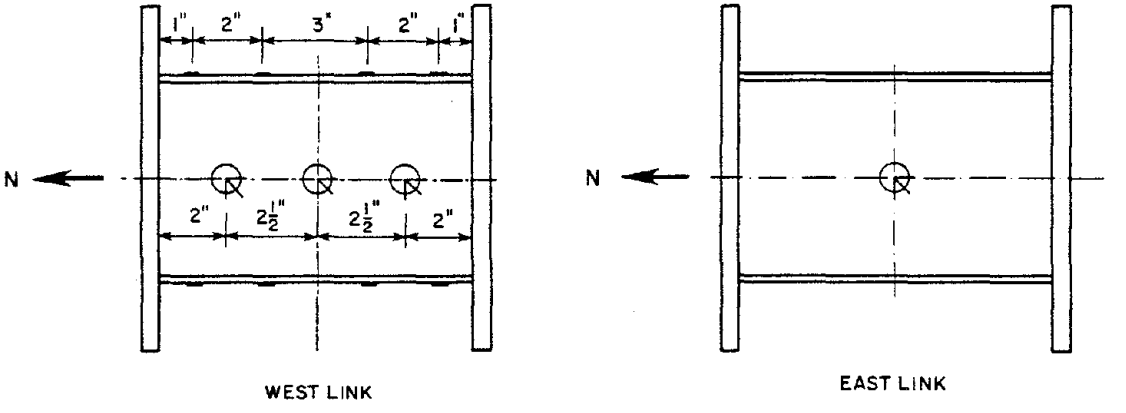

STRAIN GAGE STATIONS (LINKS OF SPECIMEN 2)

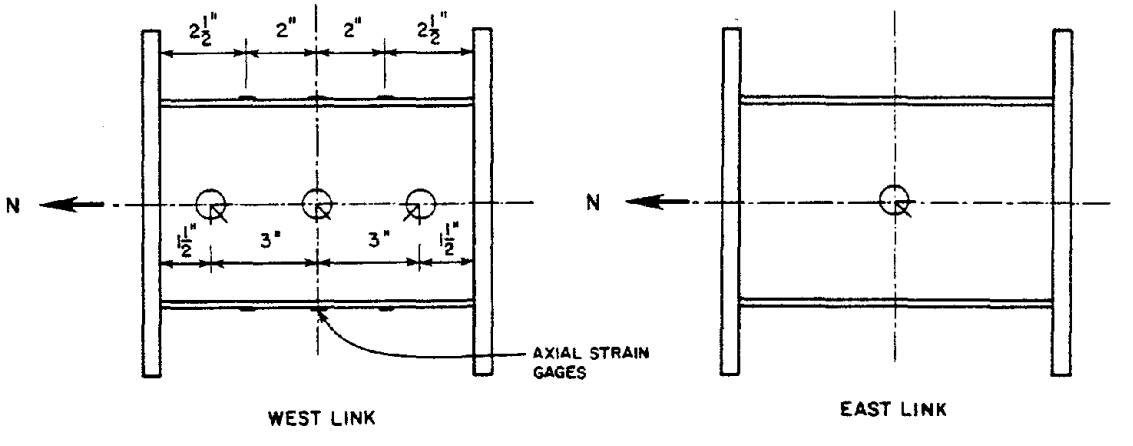

STRAIN GAGE STATIONS (LINKS OF SPECIMEN 3)

Fig. 20 Link Strain Gage Stations

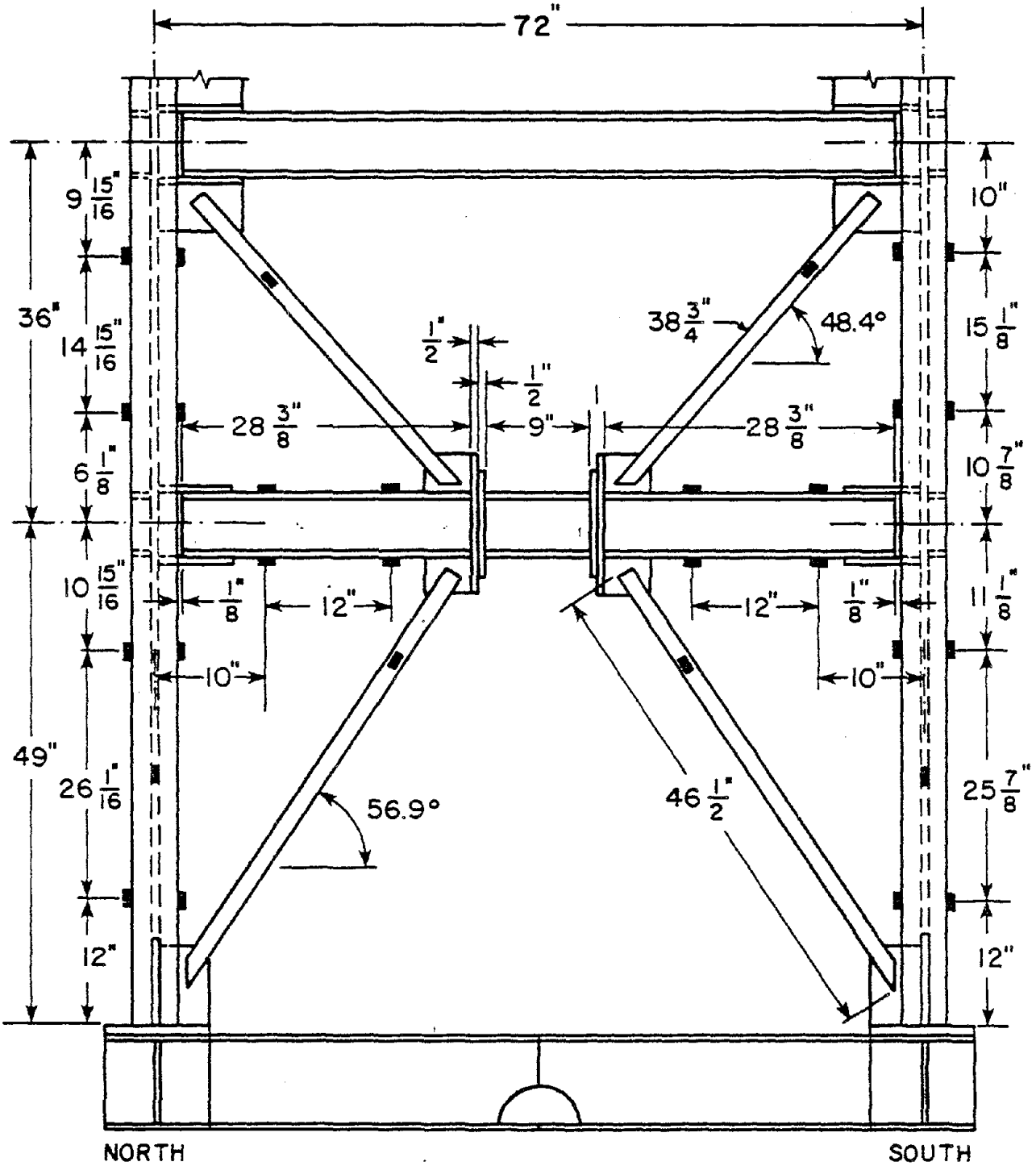

WEST FRAME

Fig. 21-1 Elastic Strain Gage Stations

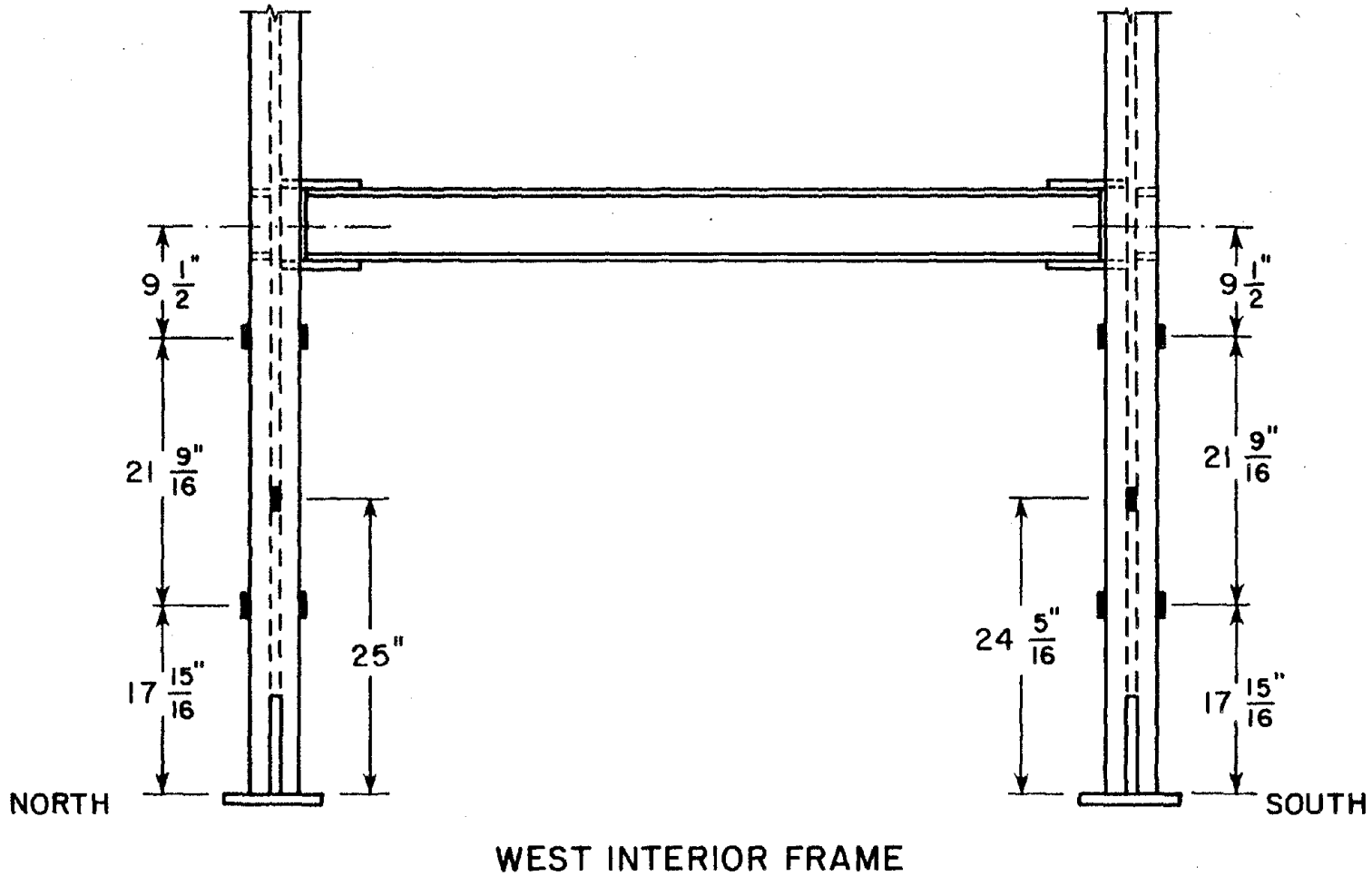

Fig. 21-2 Elastic Strain Gage Stations (Continued)

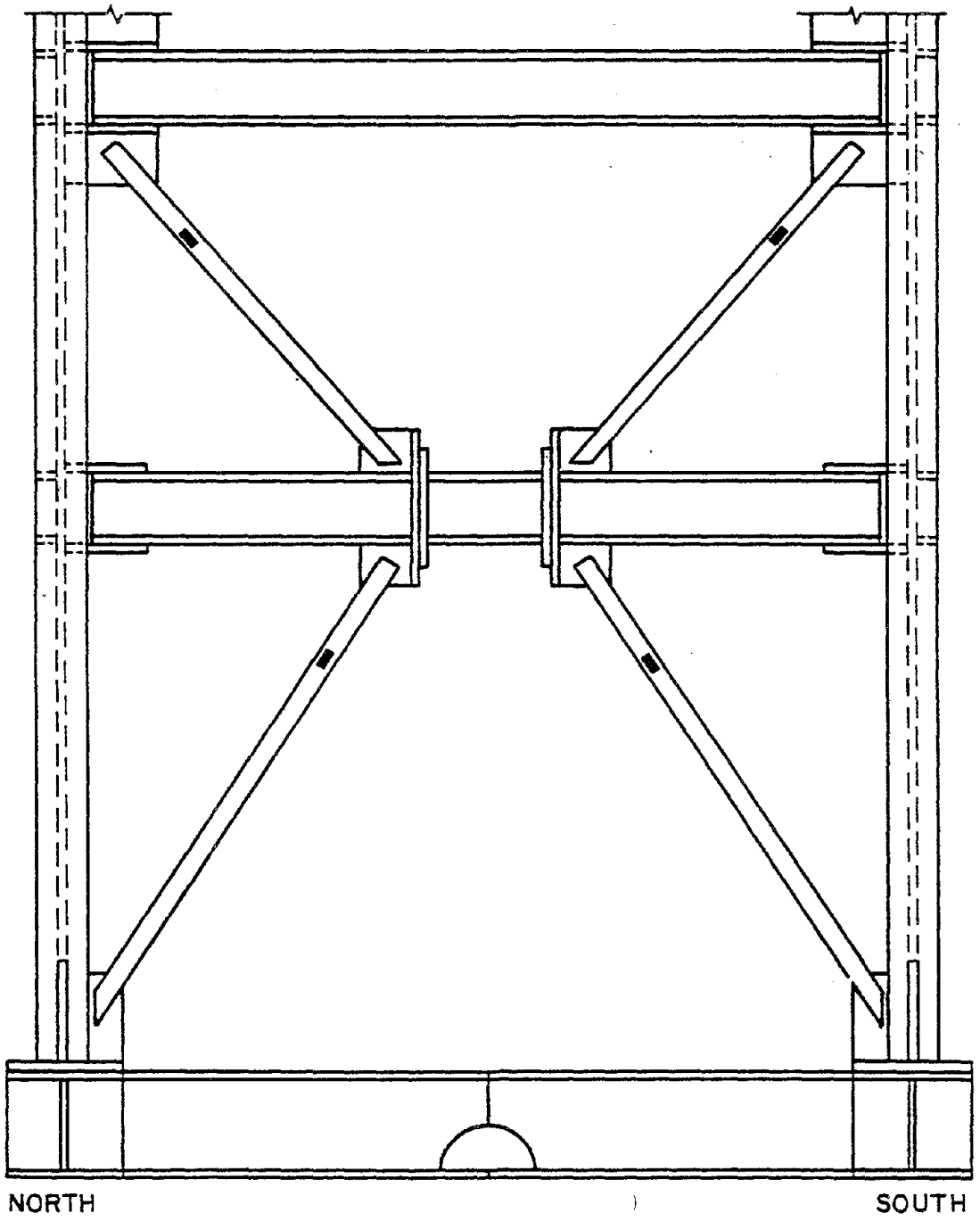

Fig. 21-3 Elastic Strain Gage Stations (Continued)

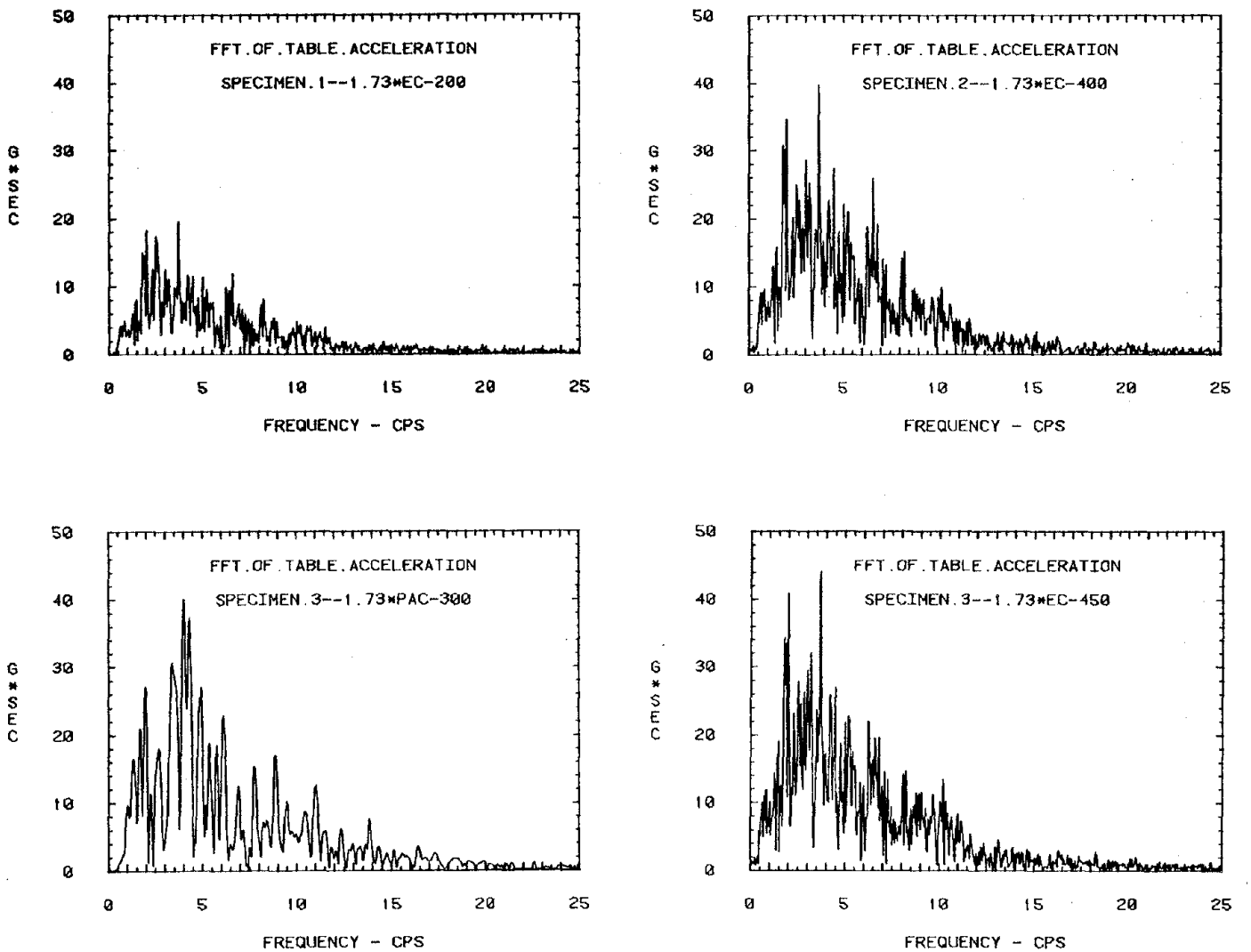

Fig. 22 Fourier Amplitudes of Some Selected Table Motions

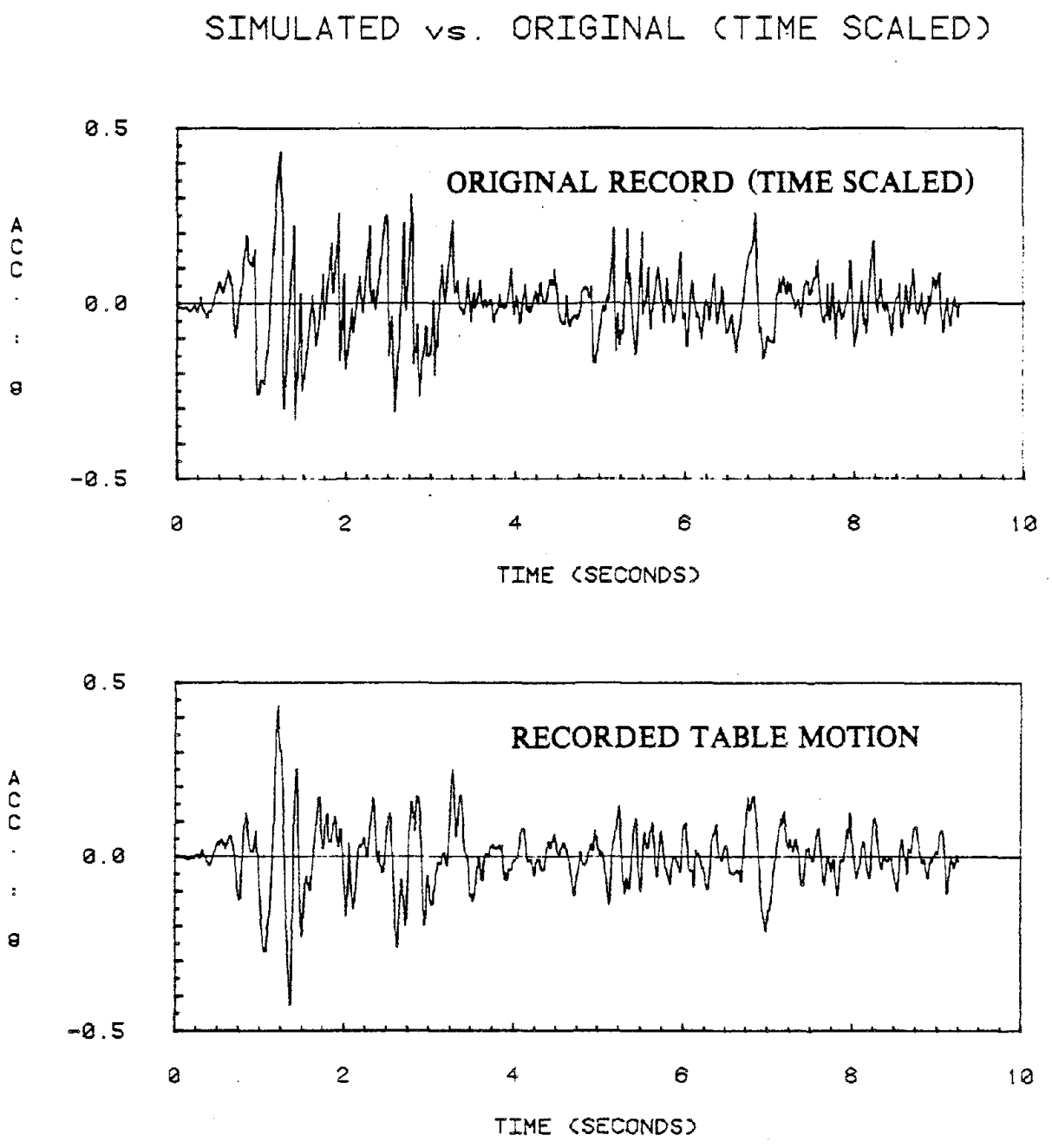

Fig. 23 Simulated and Original Source Ground Motions

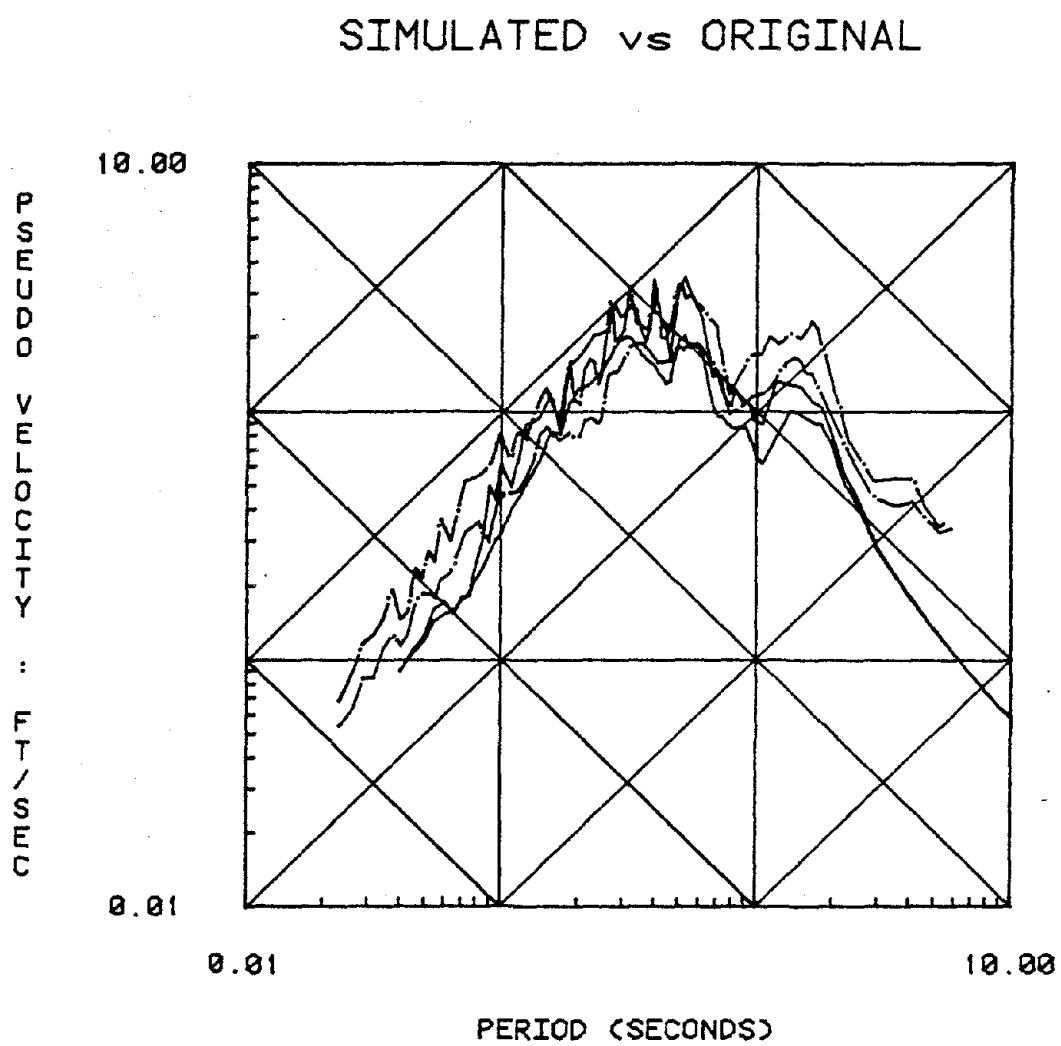

Fig. 24 Response Spectra of the Simulated and the Original Ground Motions

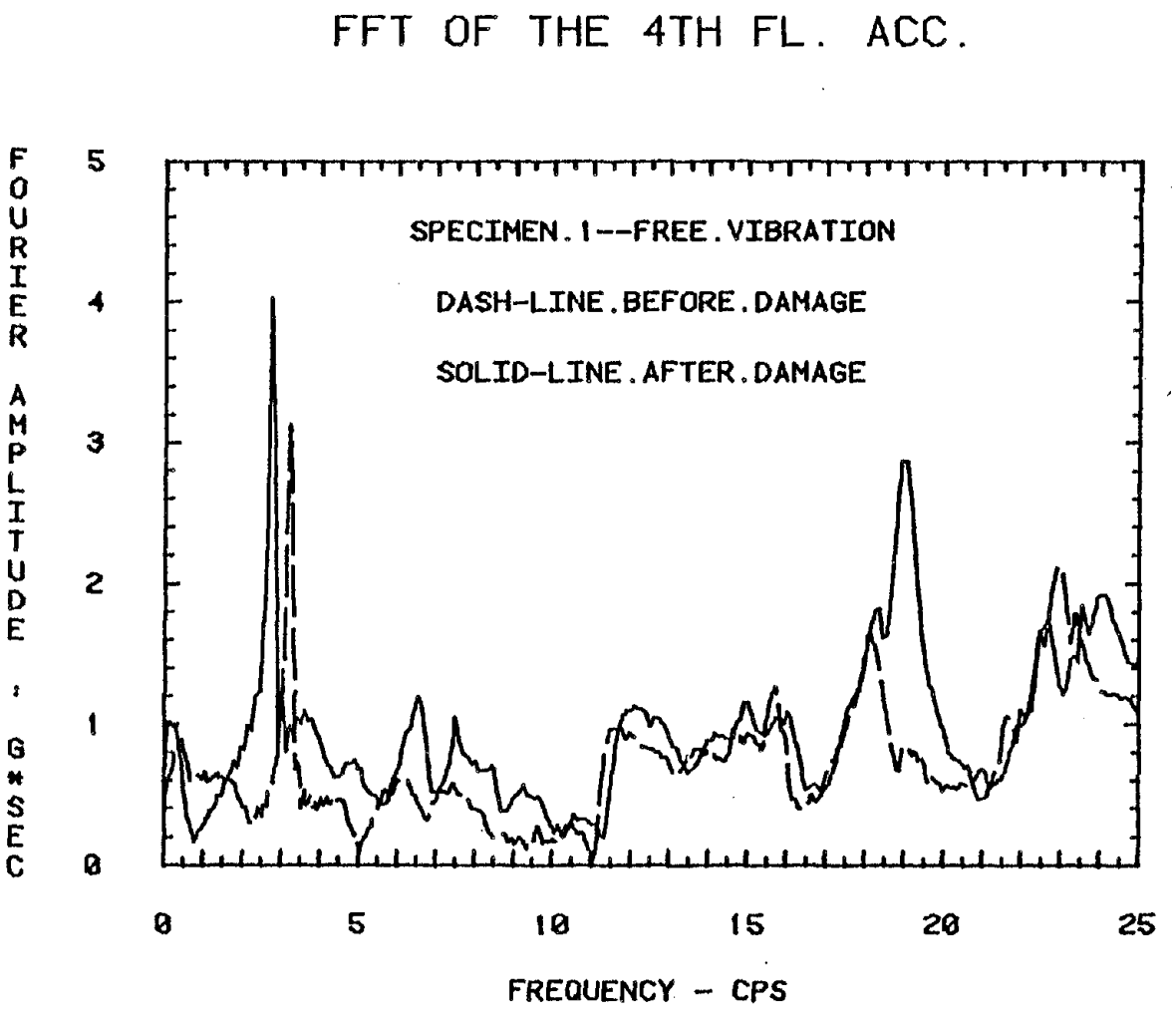

Fig. 25 Fourier Amplitudes of the 4th Floor Acceleration before (Dash Line) and after (Solid line) Being Damaged

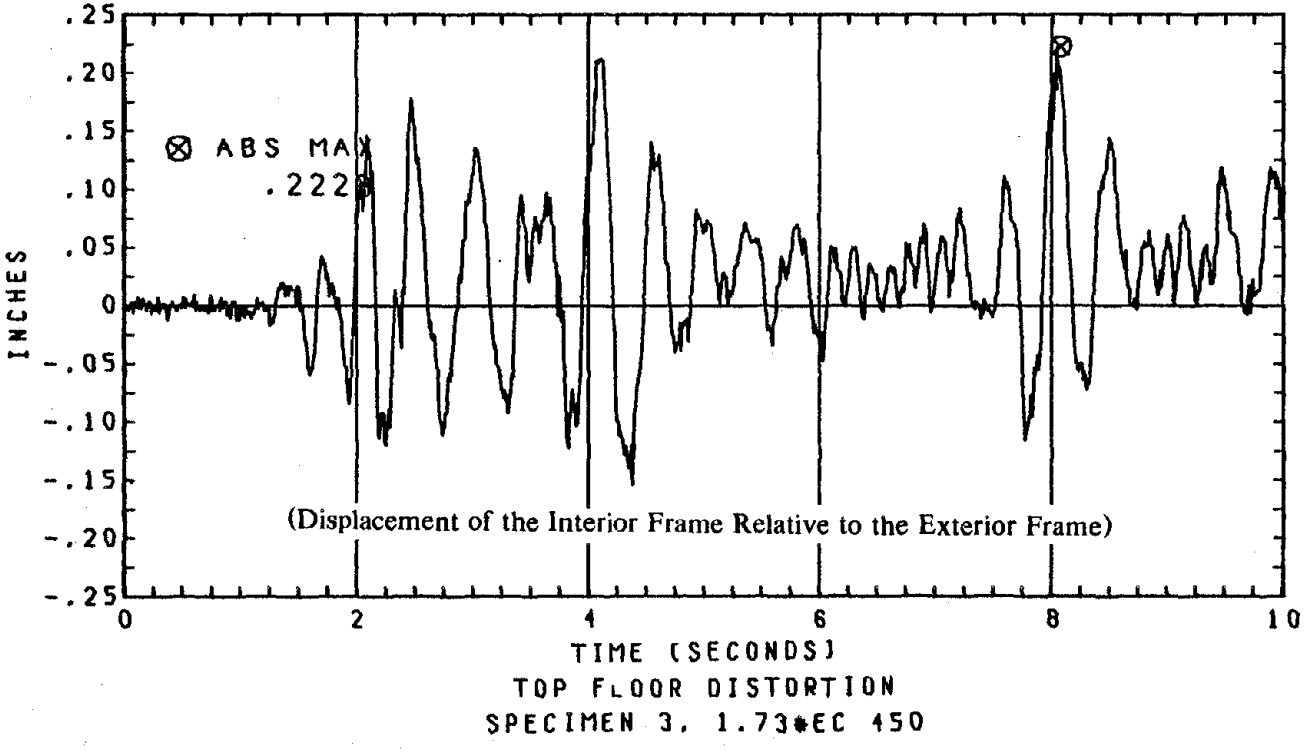

Fig. 26 Distortion of the Top Floor

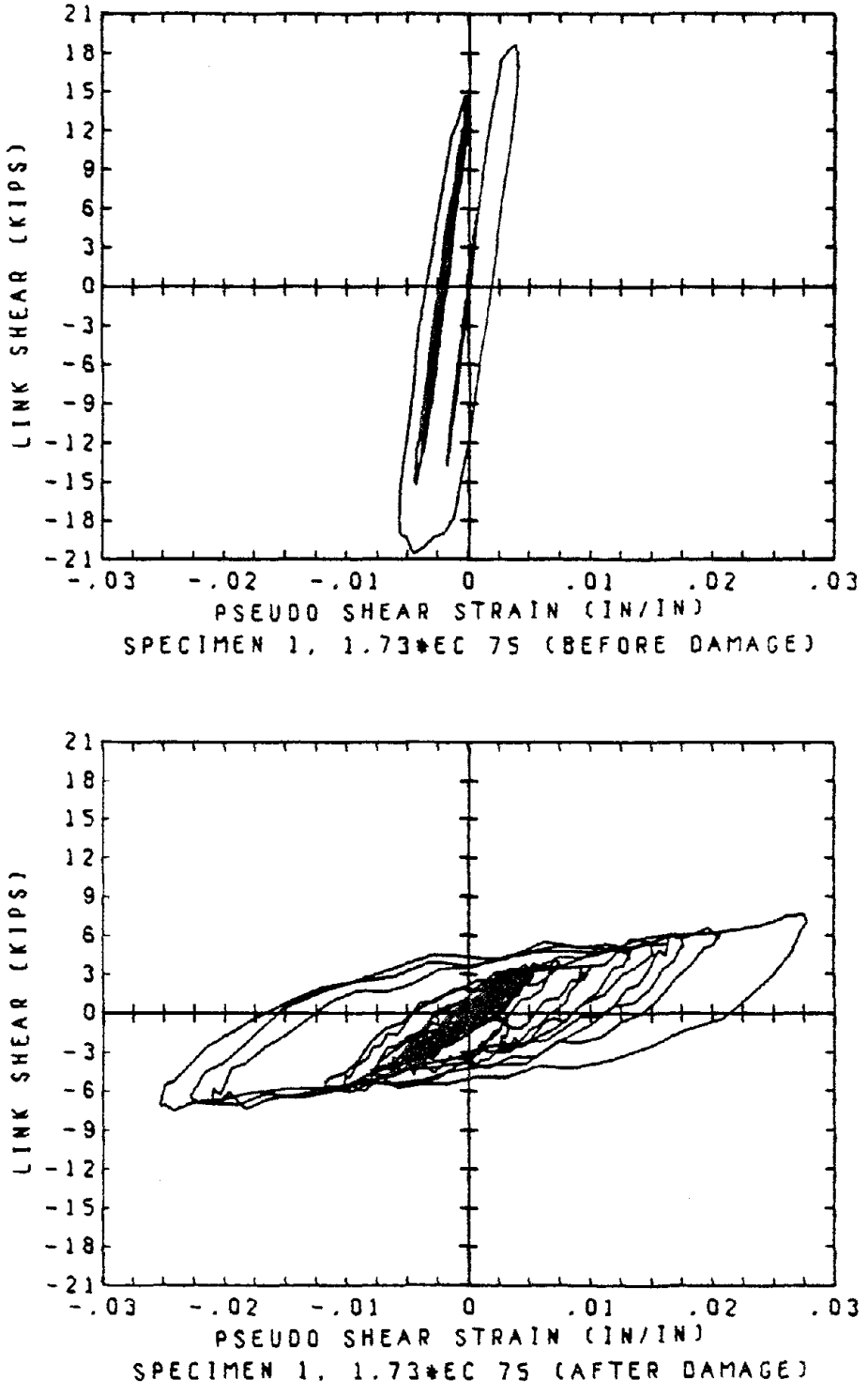

Fig. 27 Hysteresis Behavior of the West Link of Specimen 1 before and after Being Damaged

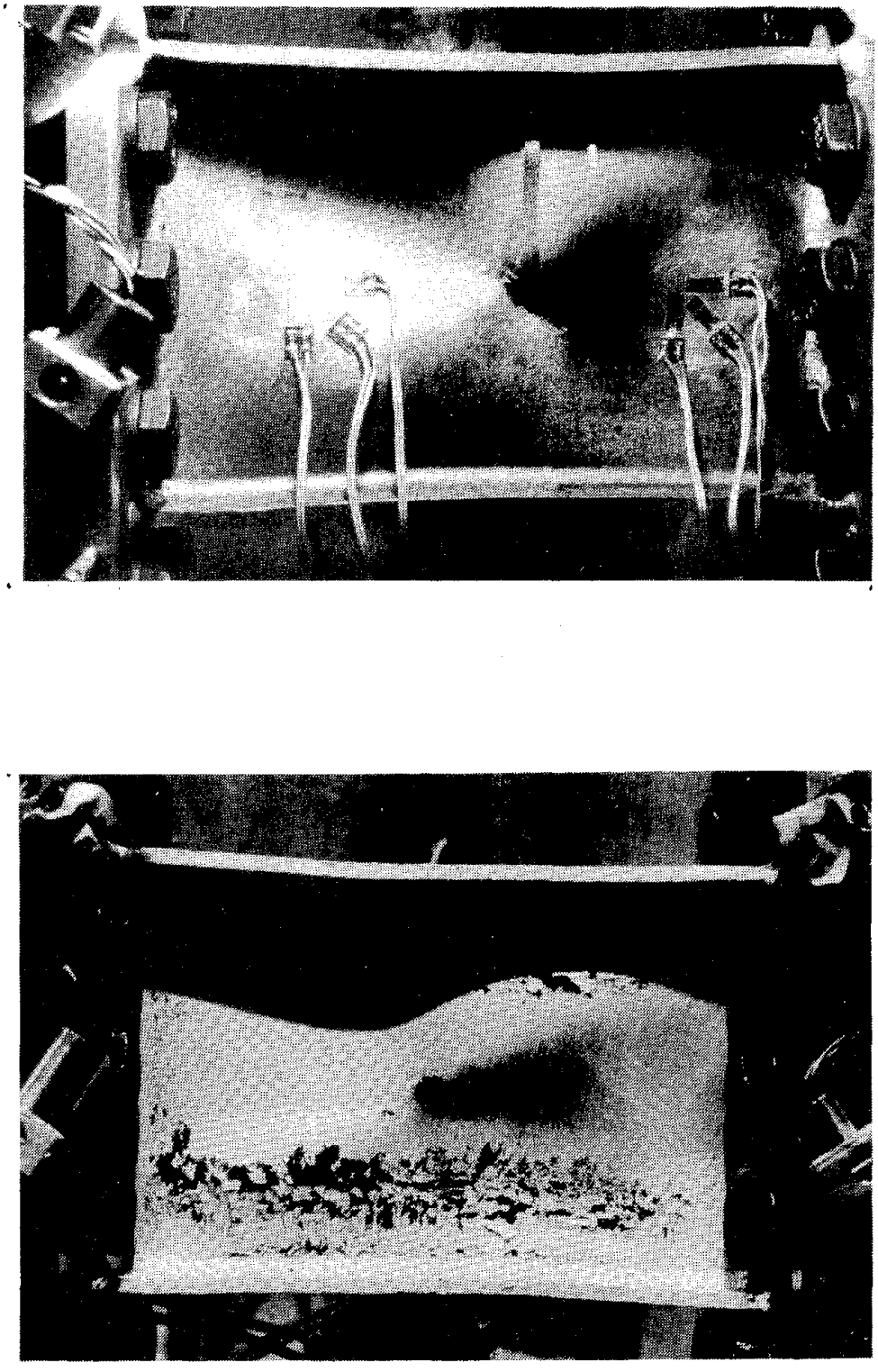

Fig. 28 Damaged Links of Specimen 2 (Upper One = the West Link)

Reproduced from
best available copy.

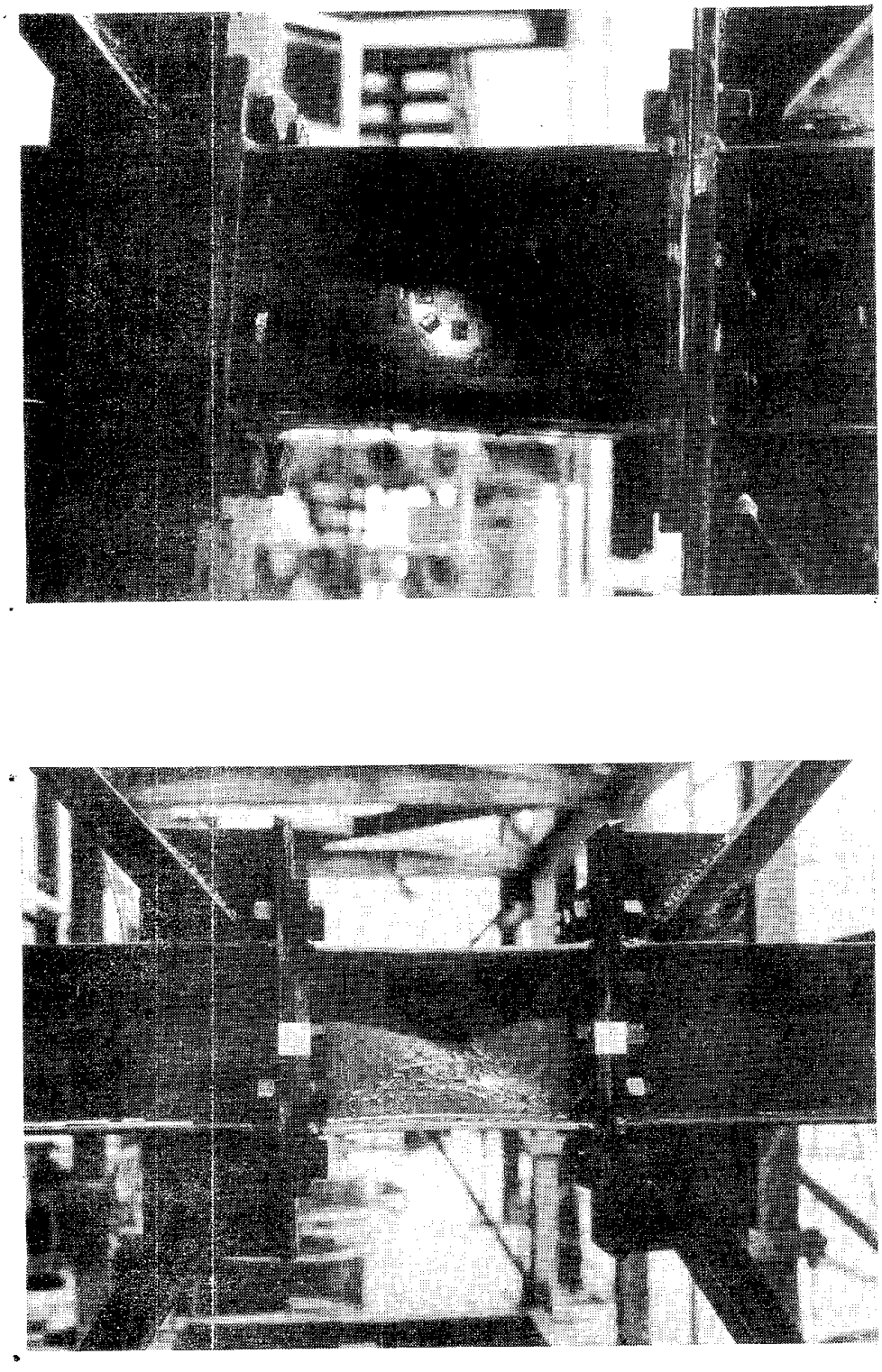

Fig. 29 Damaged Links of Specimen 3 (Upper one = the West Link)

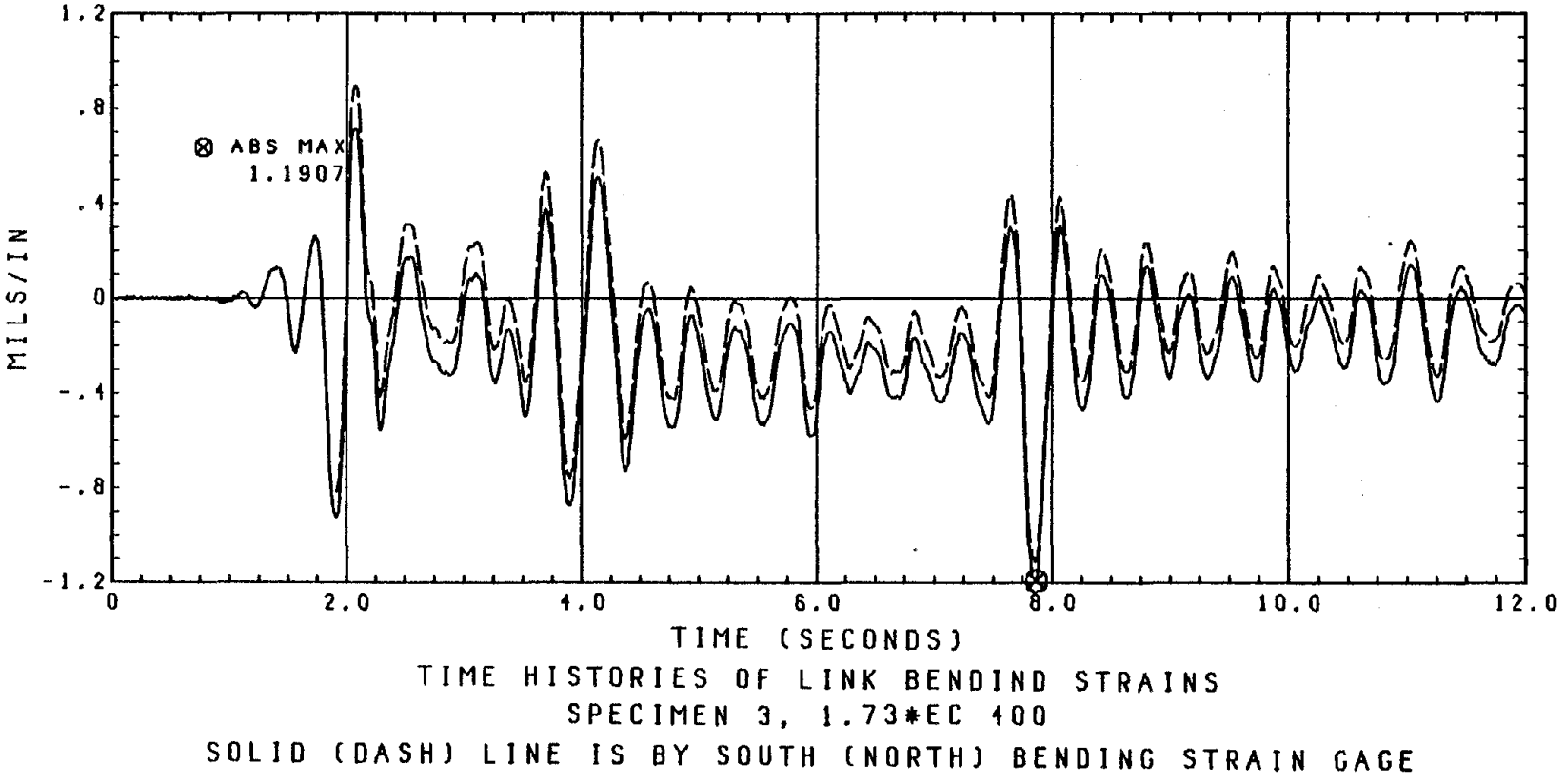

Fig. 30 Typical Time Histories of Measured Link Flexural Strains

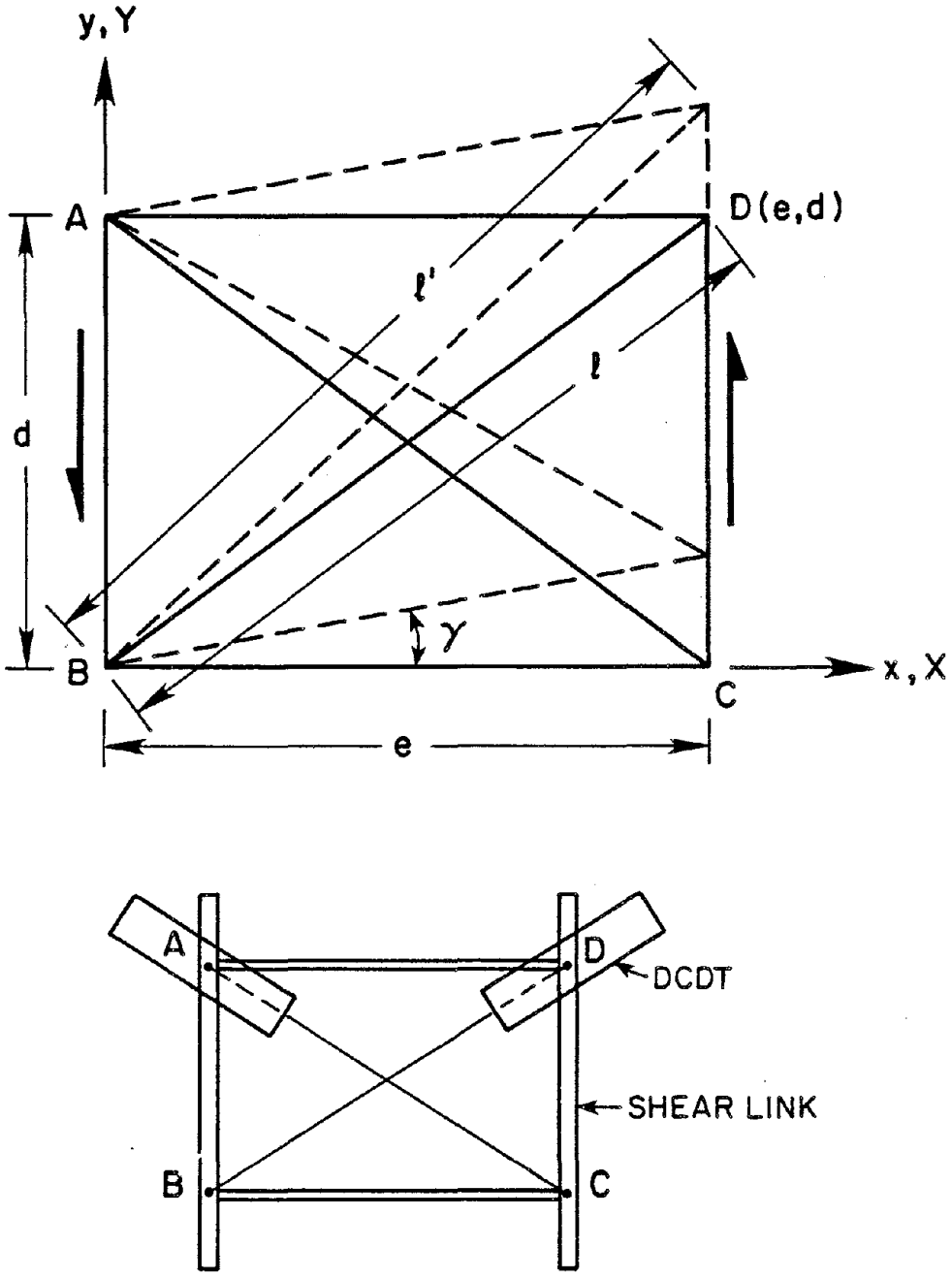

Fig. 31 Link Shear Deformation Measurement

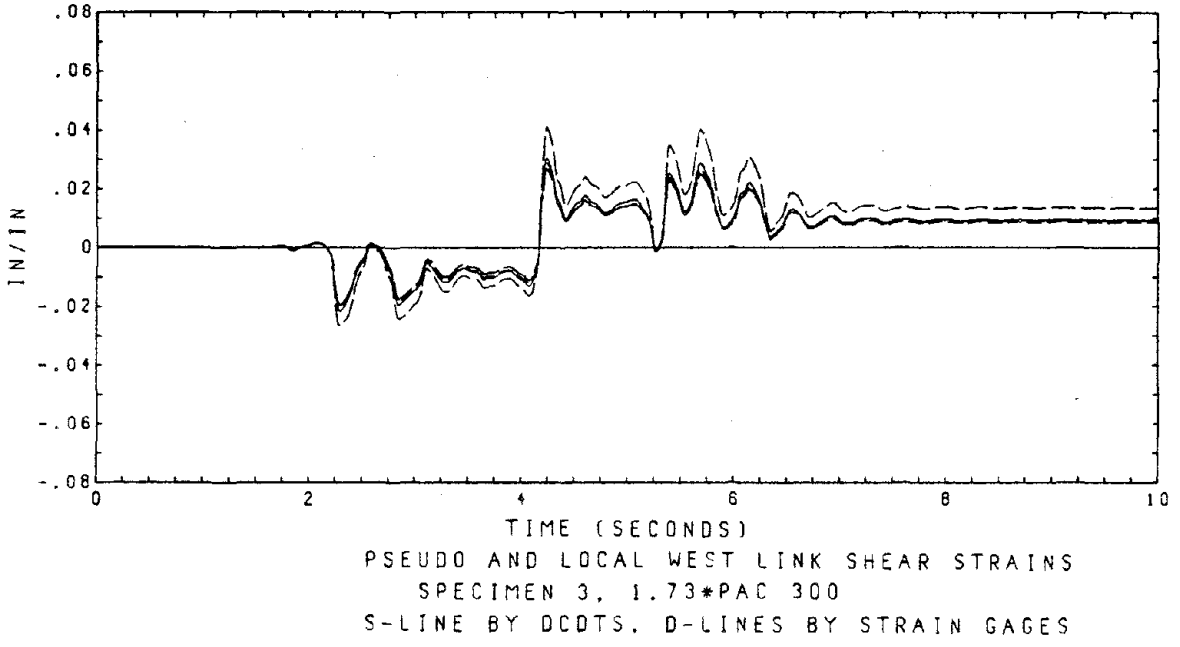

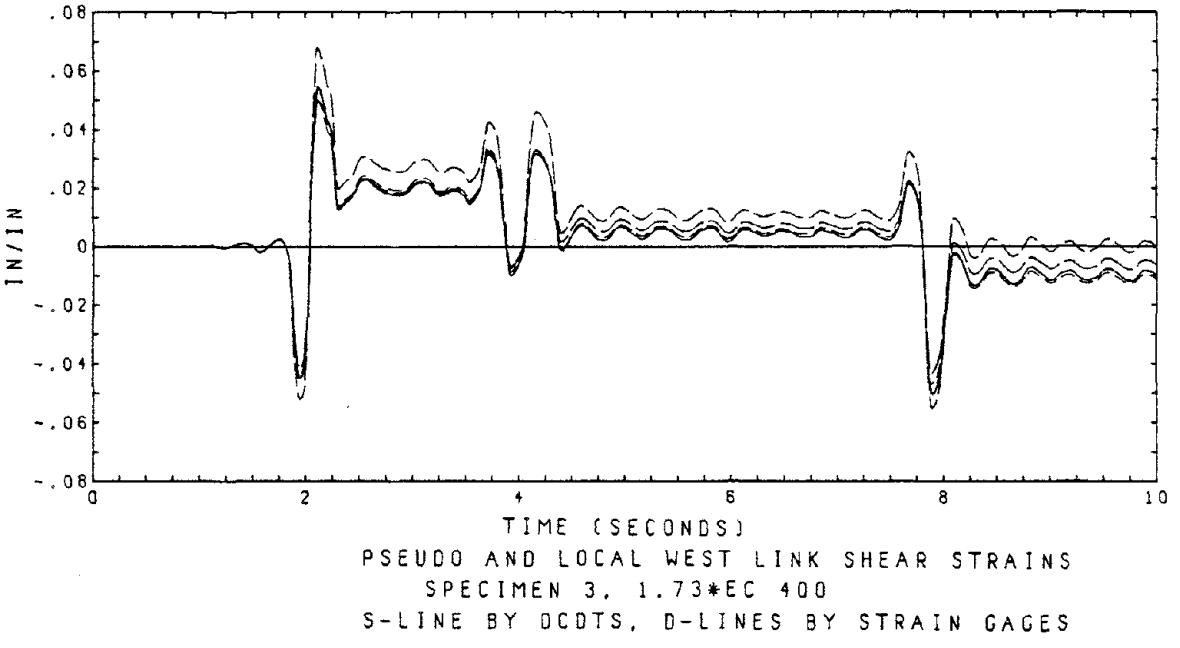

Fig. 32 Global (Pseudo) and Local Shear Strains of the West Link of Specimen 3

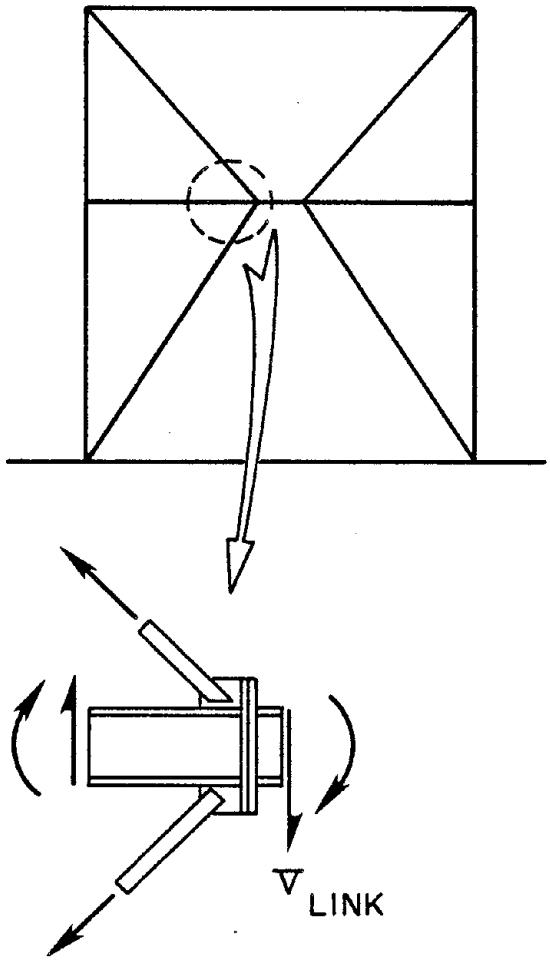

Fig. 33 Freebody Diagram for Link Shear Force Calculation

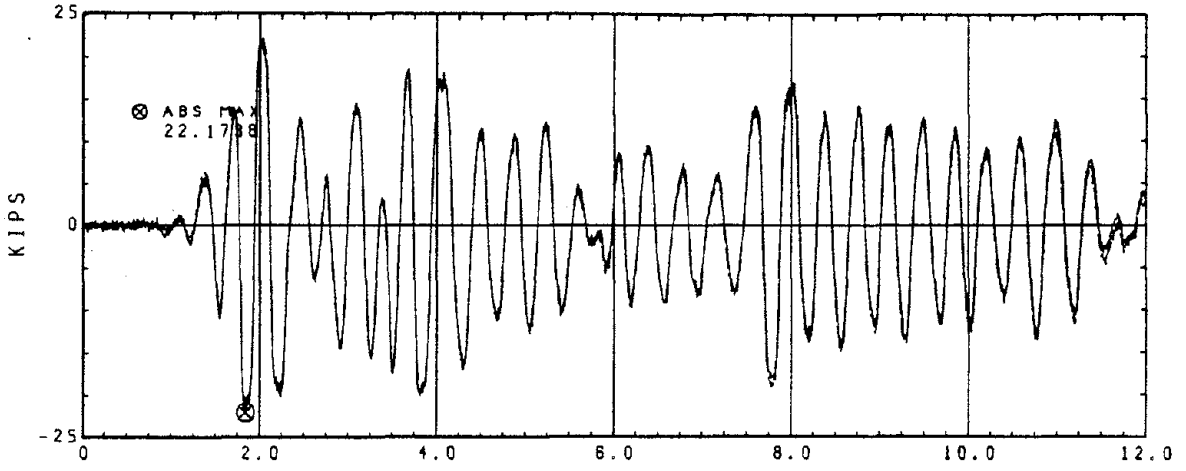

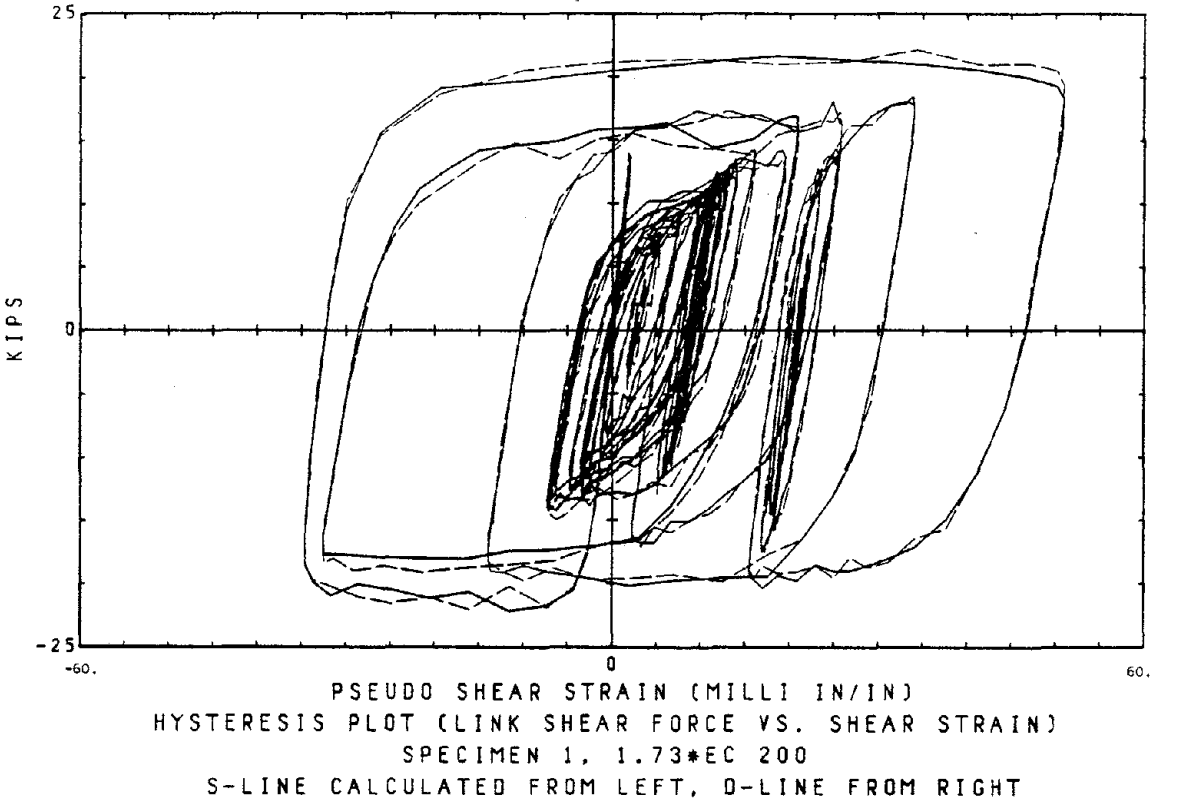

Fig. 34 Consistency of the 'Two-Way' Calculation

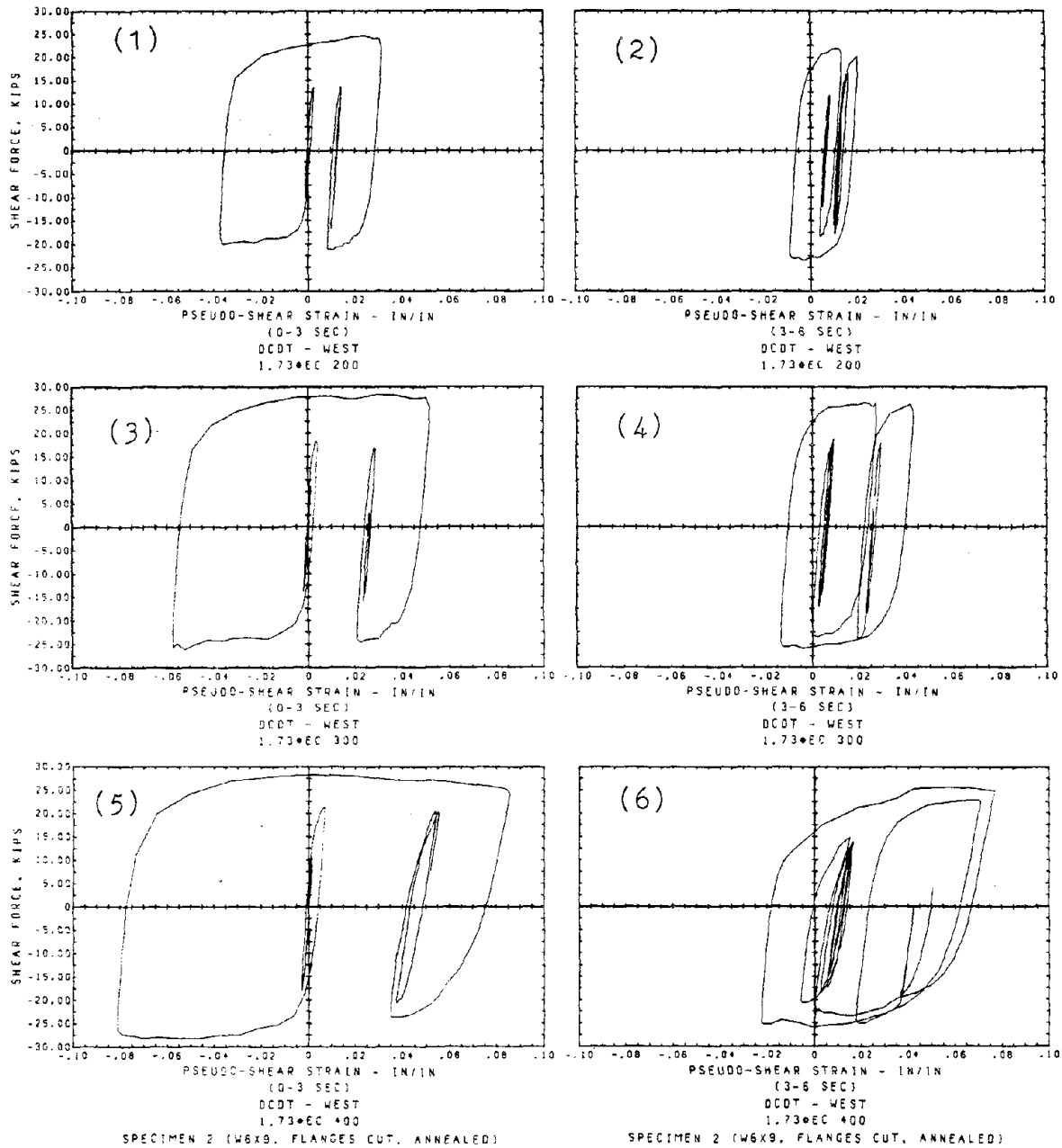

Fig. 35 Isotropic Hardening in the West Link of Specimen 2

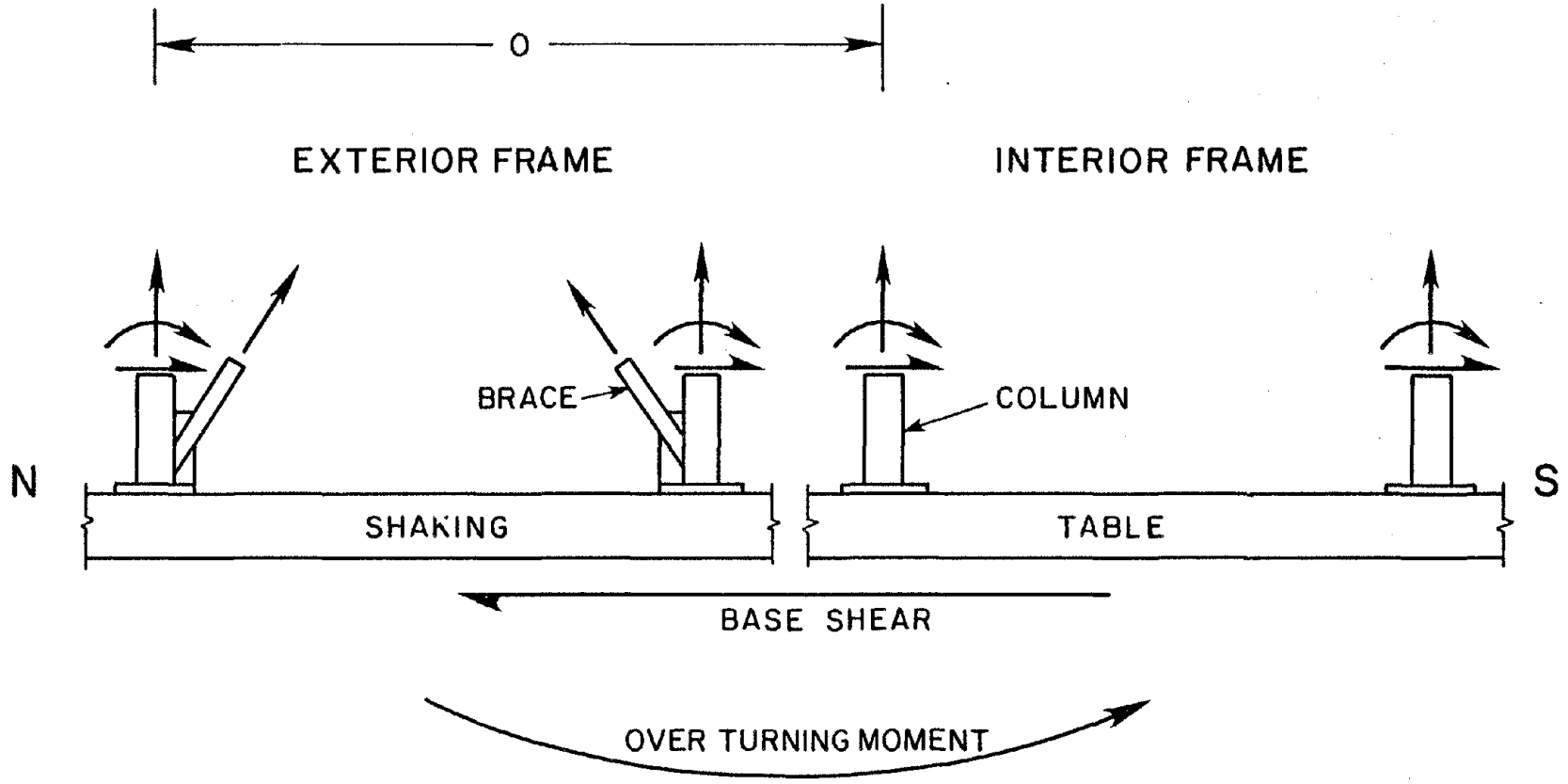

Fig. 36 Freebody Diagram for Base Shear and Overturning Moment Calculation
(The Statics Method)

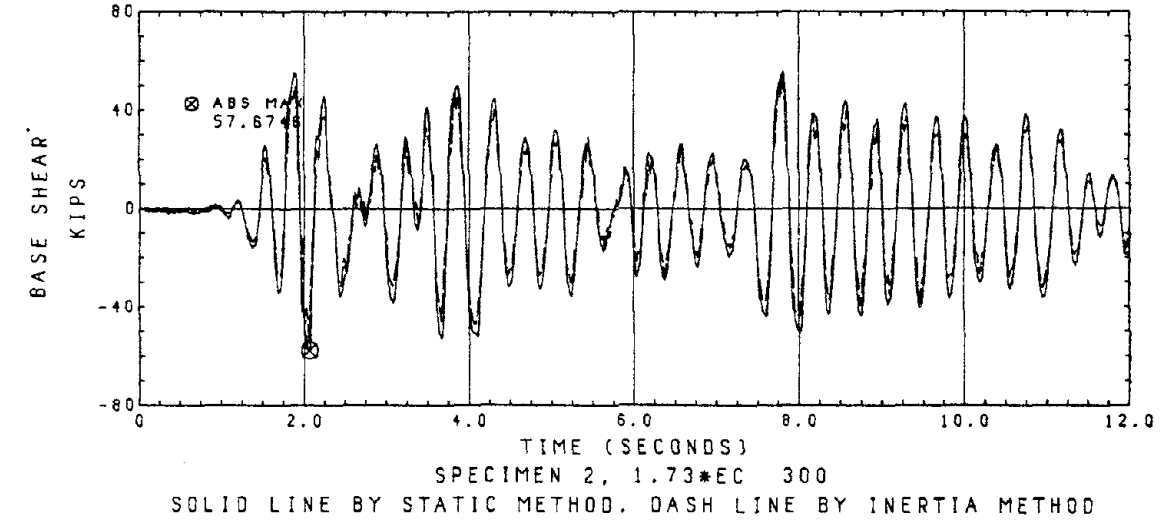

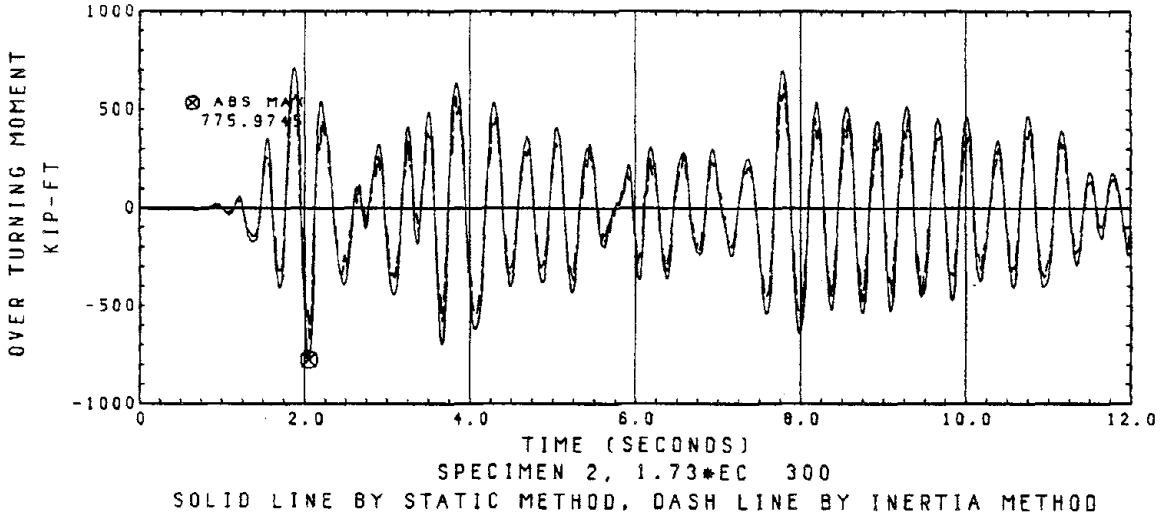

Fig. 37-1 Statics Method vs. Inertia Method

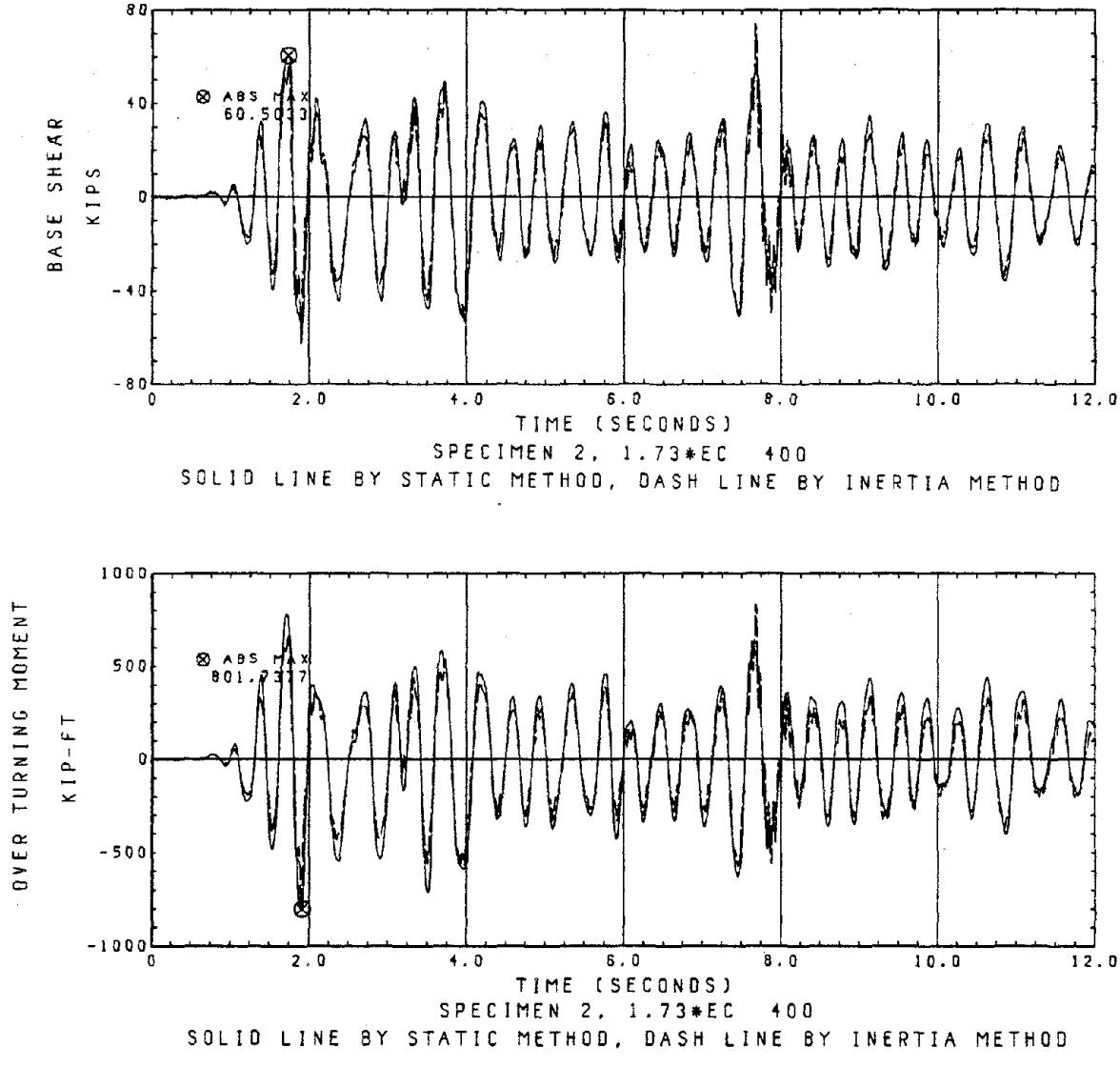

Fig. 37-2 Statics Method vs. Inertia Method (Continued)

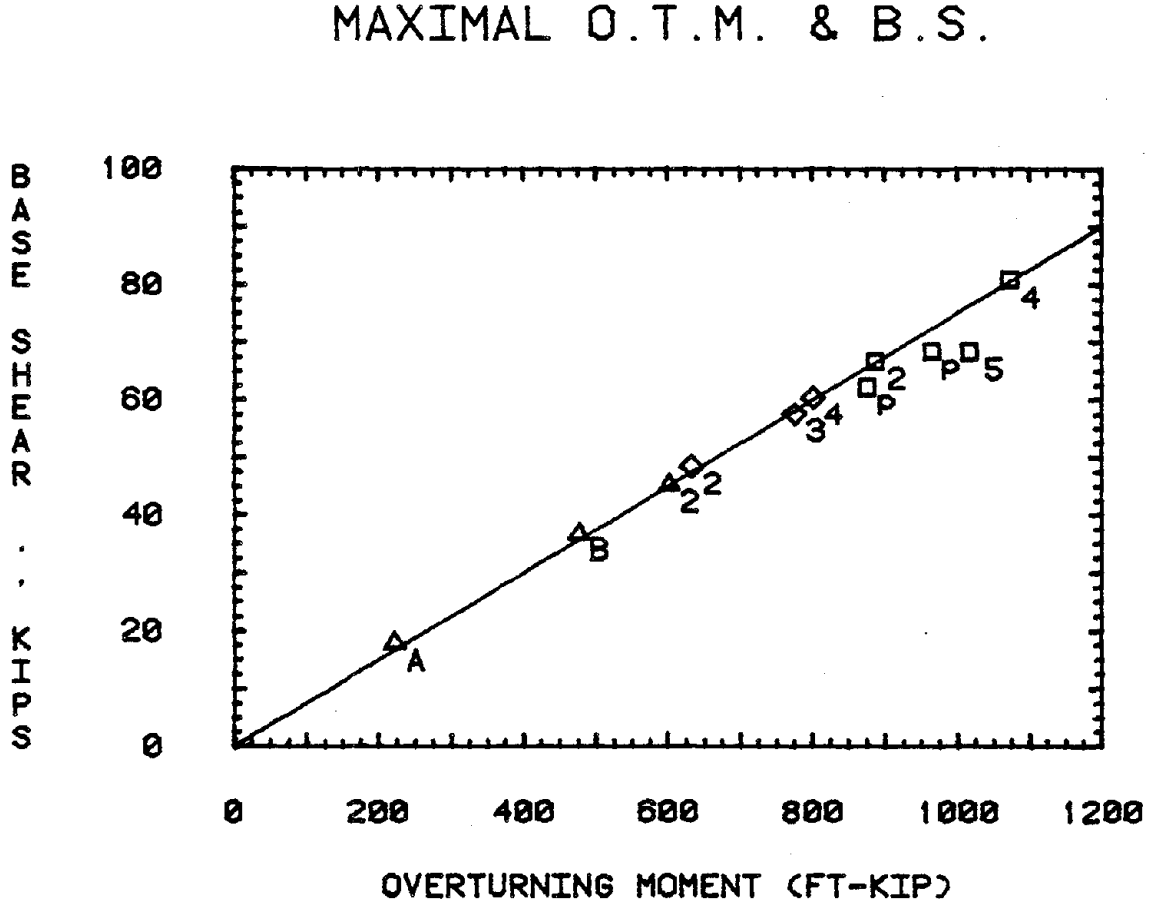

Fig. 38 Measured Maximum Overturning Moments and Base Shears

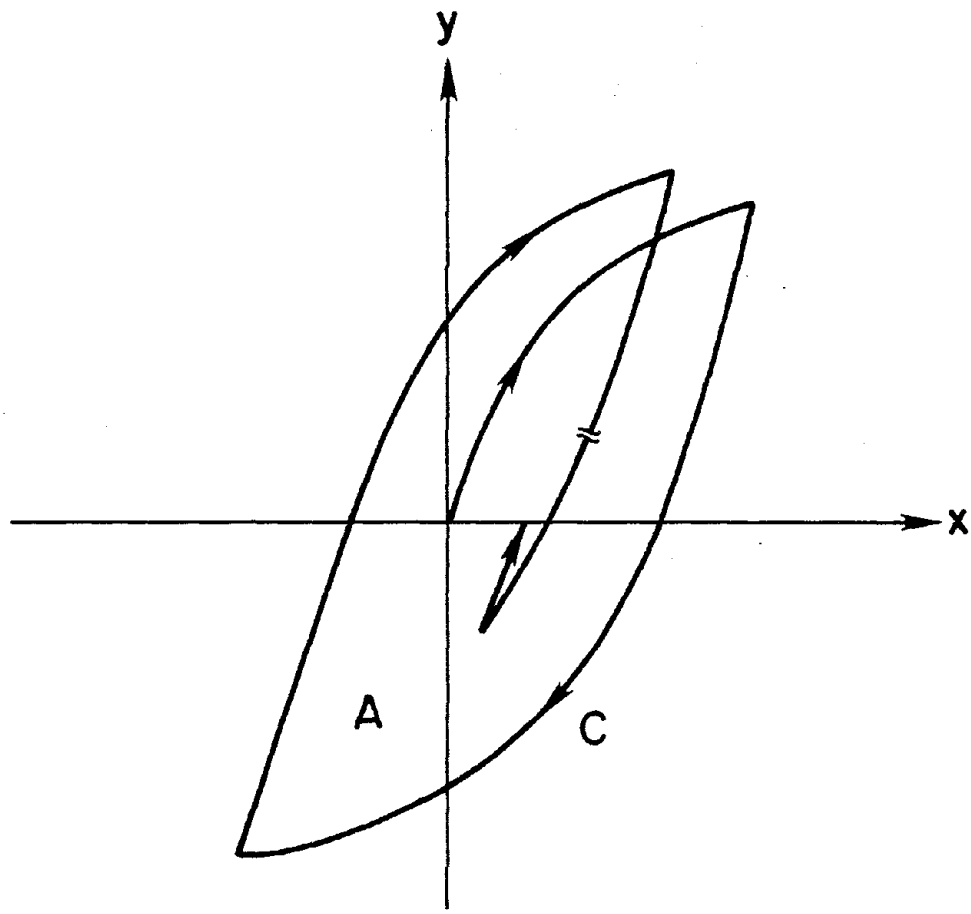

$$A = \int_C y \, dx$$

Fig. 39 Coordinate System for Energy Absorption Calculation

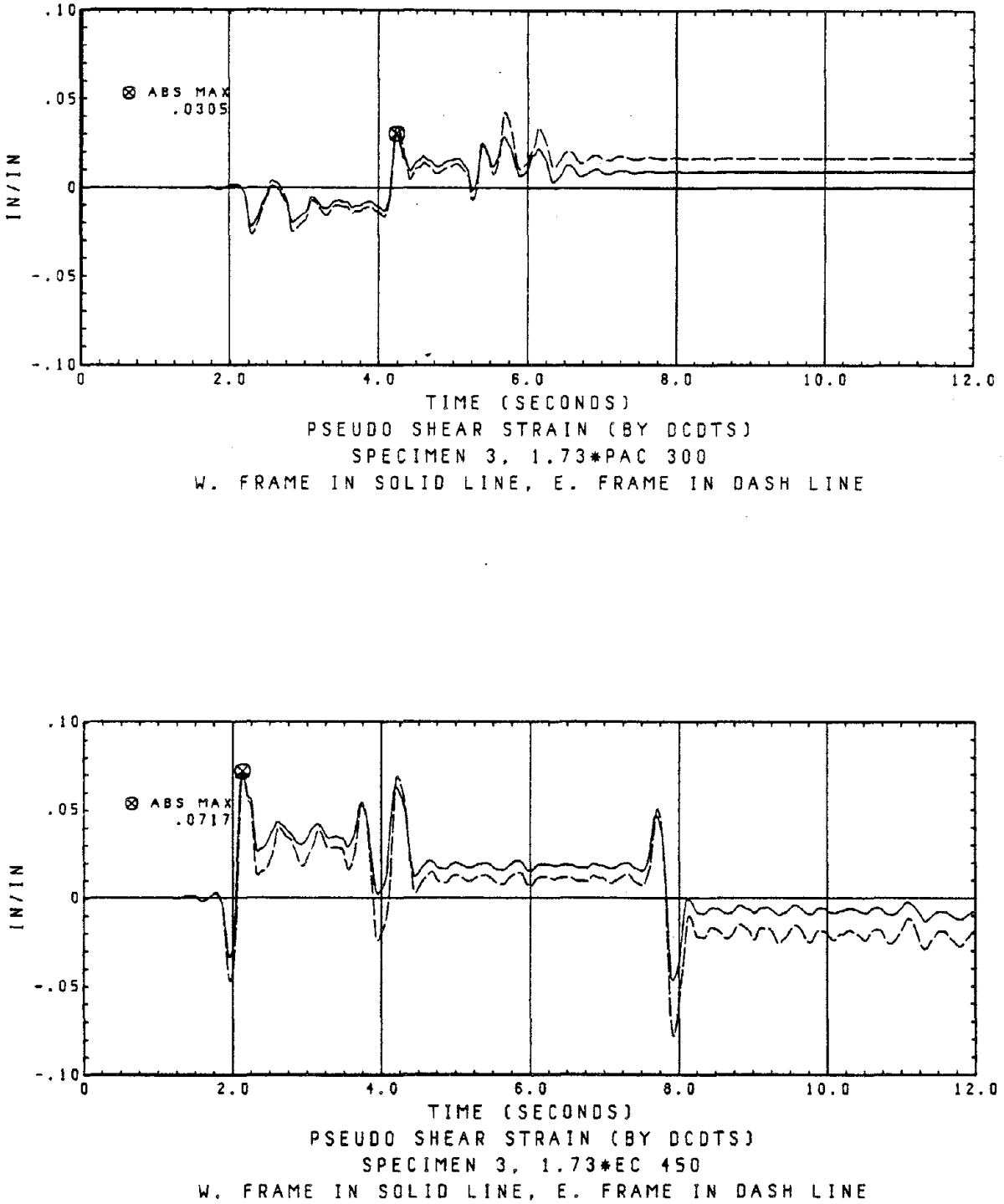

Fig. 40 Comparison for the Measured Pseudo-Shear Strains between the West and East Frames
(1.73*PAC 300 and 1.73*EC 450, Specimen 3)

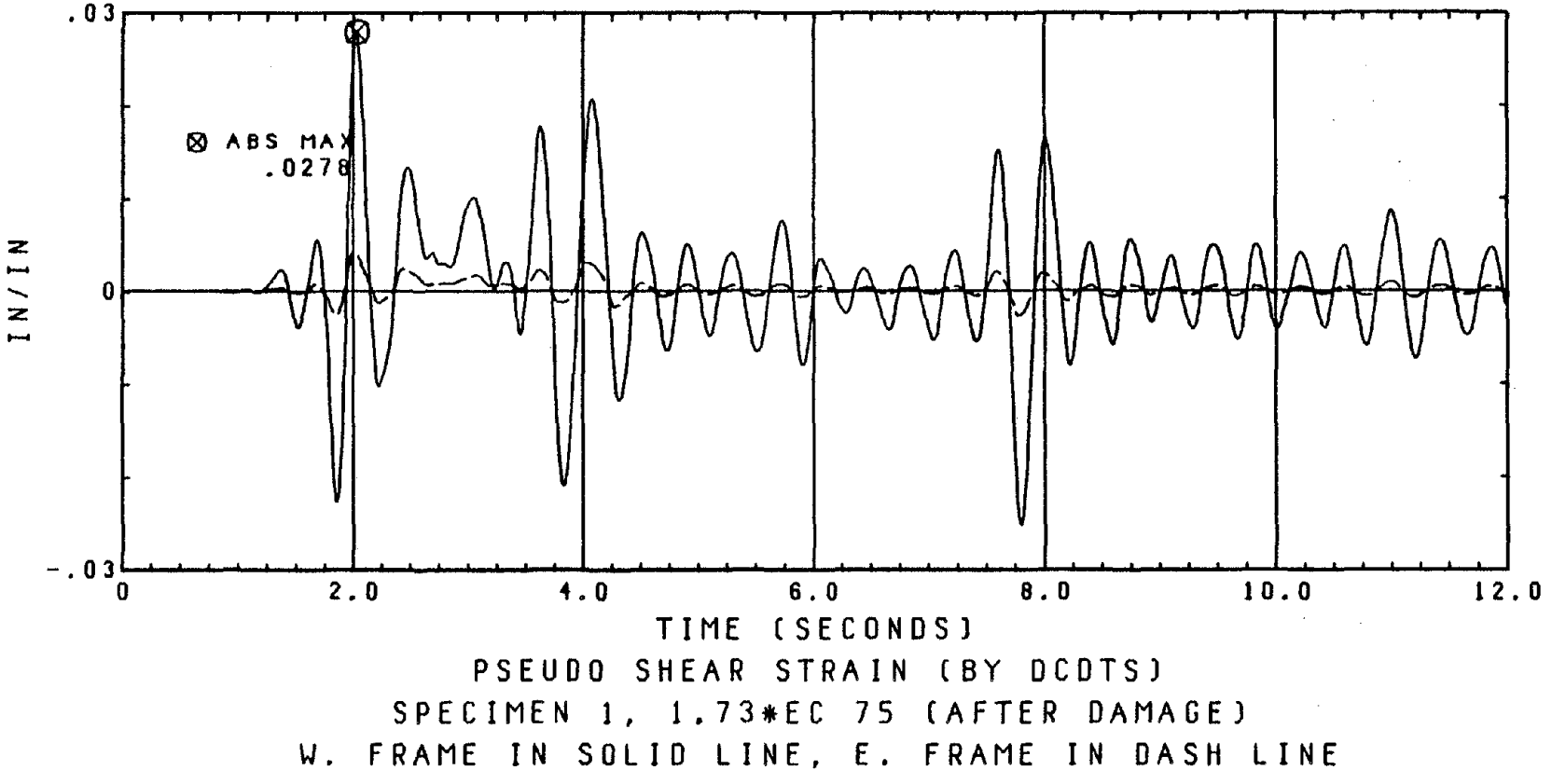

Fig. 41 Comparison for the Measured Pseudo-Shear Strains between the West and East Frames
(1.73*EC 200, Specimen 1) Measured Shear Strains in the Links of Specimen 1

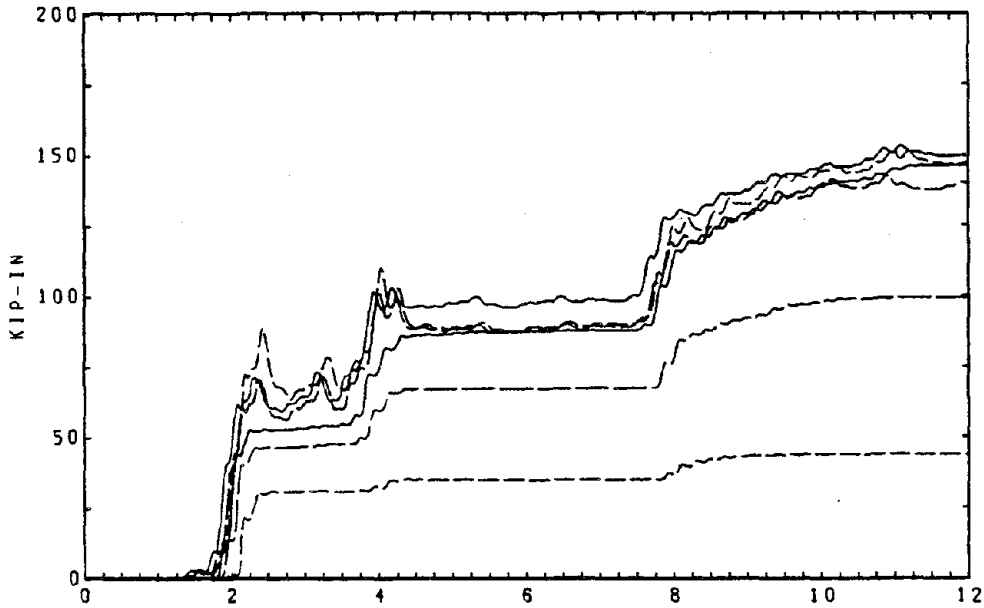

ENERGY ABSORPTION BY THE SHEAR LINKS
1.73*EC 200, ALL SPECIMENS
UPPER 3 LINES = INPUT, LOWER 3 LINES = ABSORPTION
S-, LONG D-, SHORT D-LINE ARE SPECIMEN 1, 2, 3 RESPECTIVELY

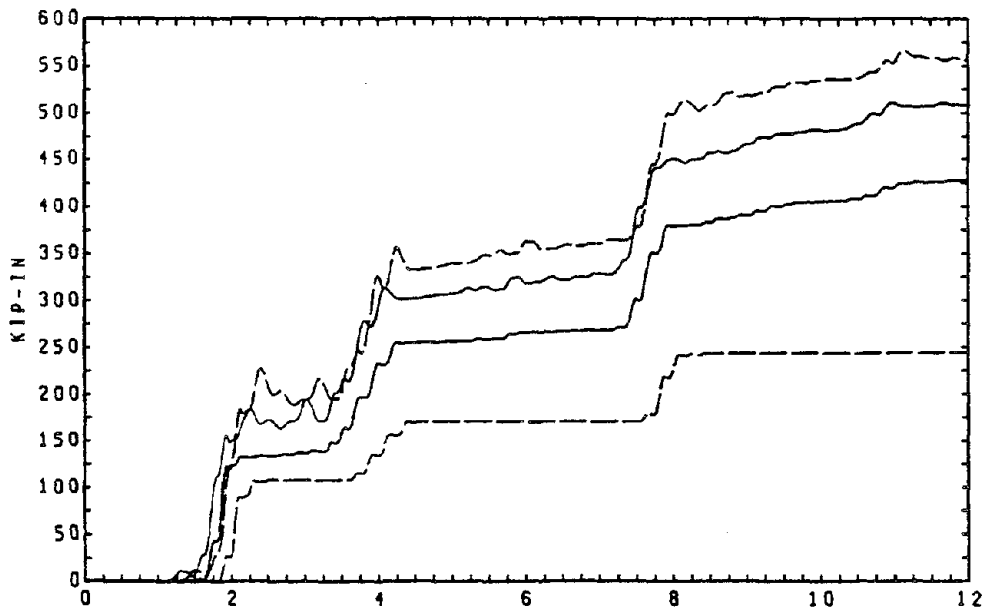

ENERGY ABSORPTION BY THE SHEAR LINKS
1.73*EC 400, SPECIMEN 2 AND 3
UPPER 2 LINES = INPUT, LOWER 2 LINES = ABSORPTION
S-LINE, D-LINE = SPECIMEN 2, SPECIMEN 3 RESPECTIVELY

Figs. 42 & 43 Earthquake Energy Input and Link Energy Absorption
(Comparison between Different Specimens Demonstrated)

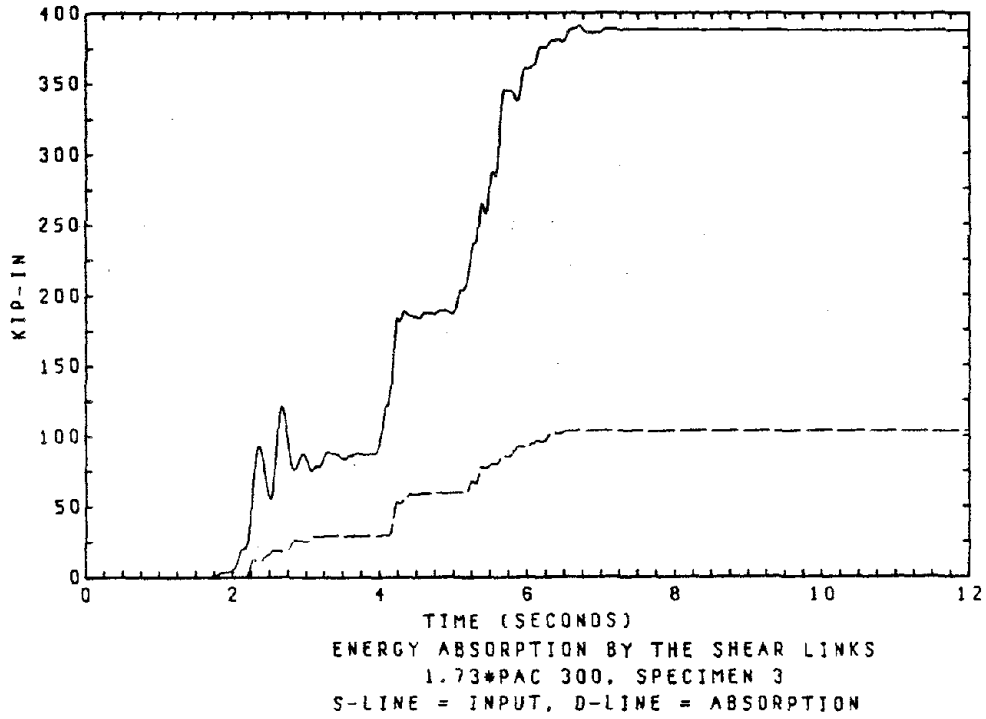

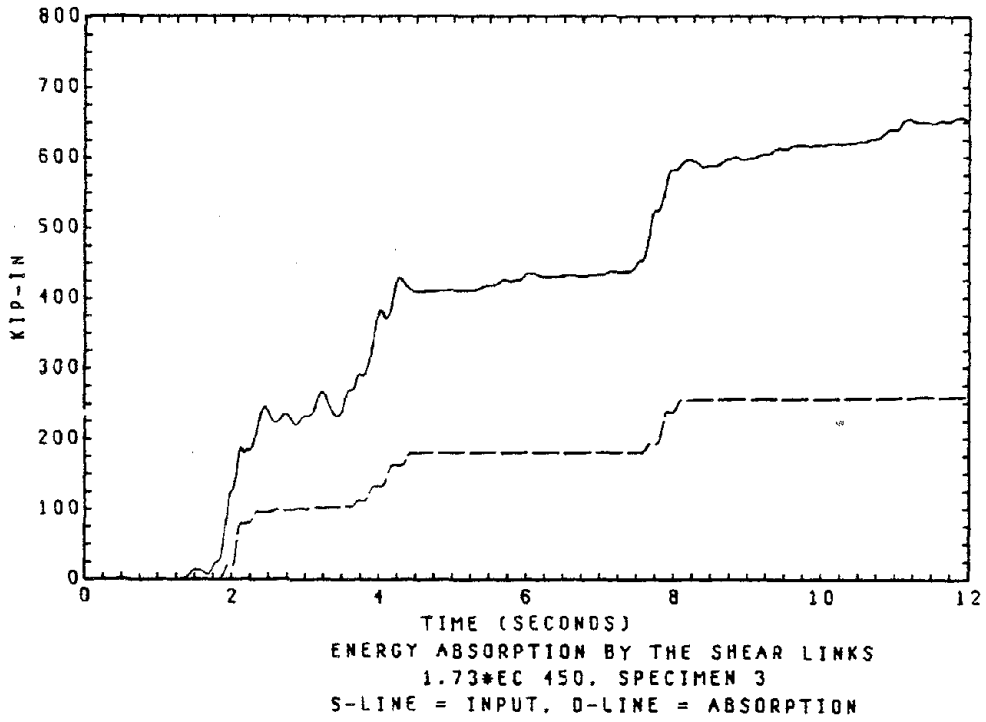

Fig. 44 Earthquake Energy Input and Link Energy Absorption

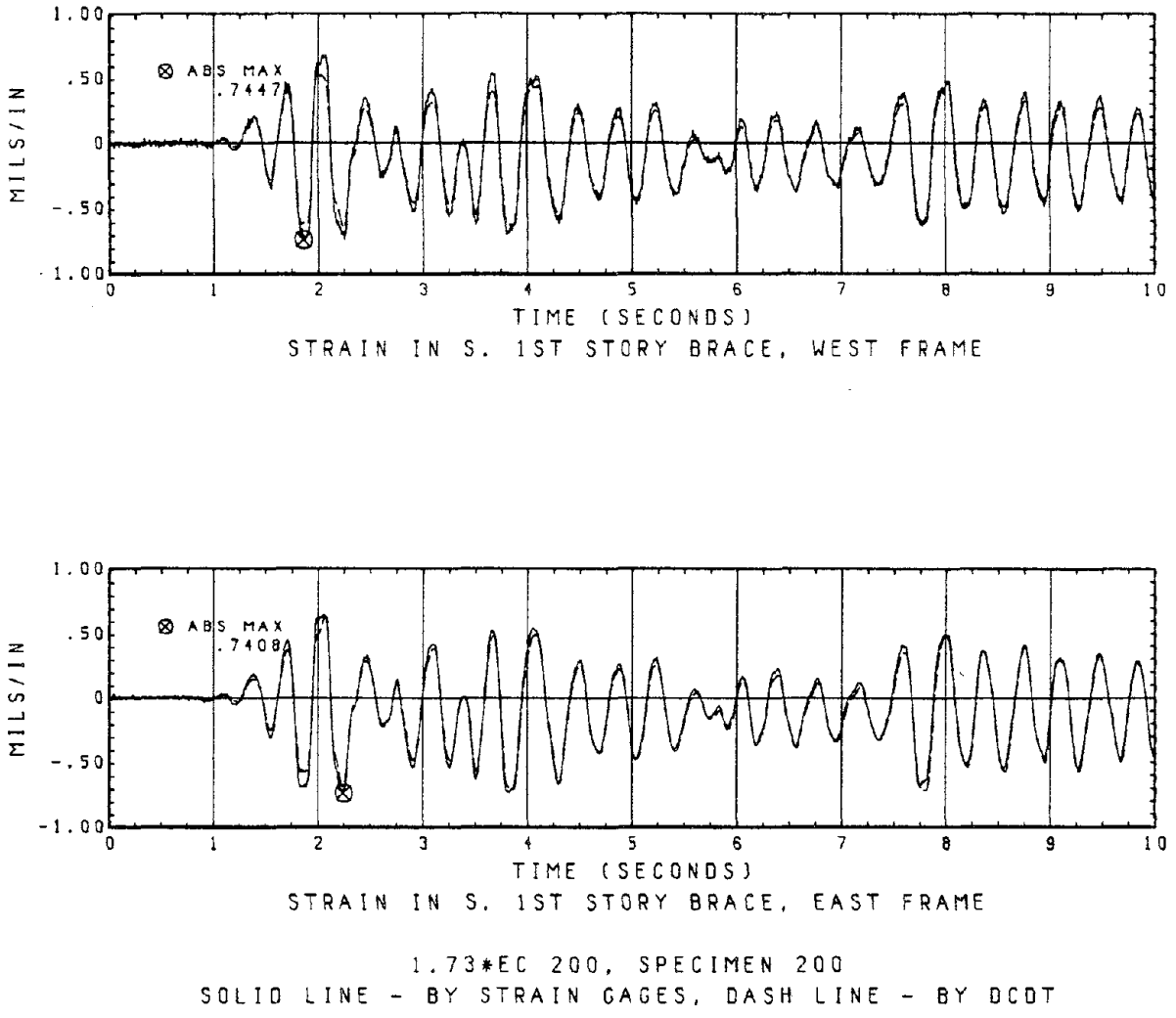

Fig. 45 Strain Gages vs. DCDT in Measuring Brace Strains

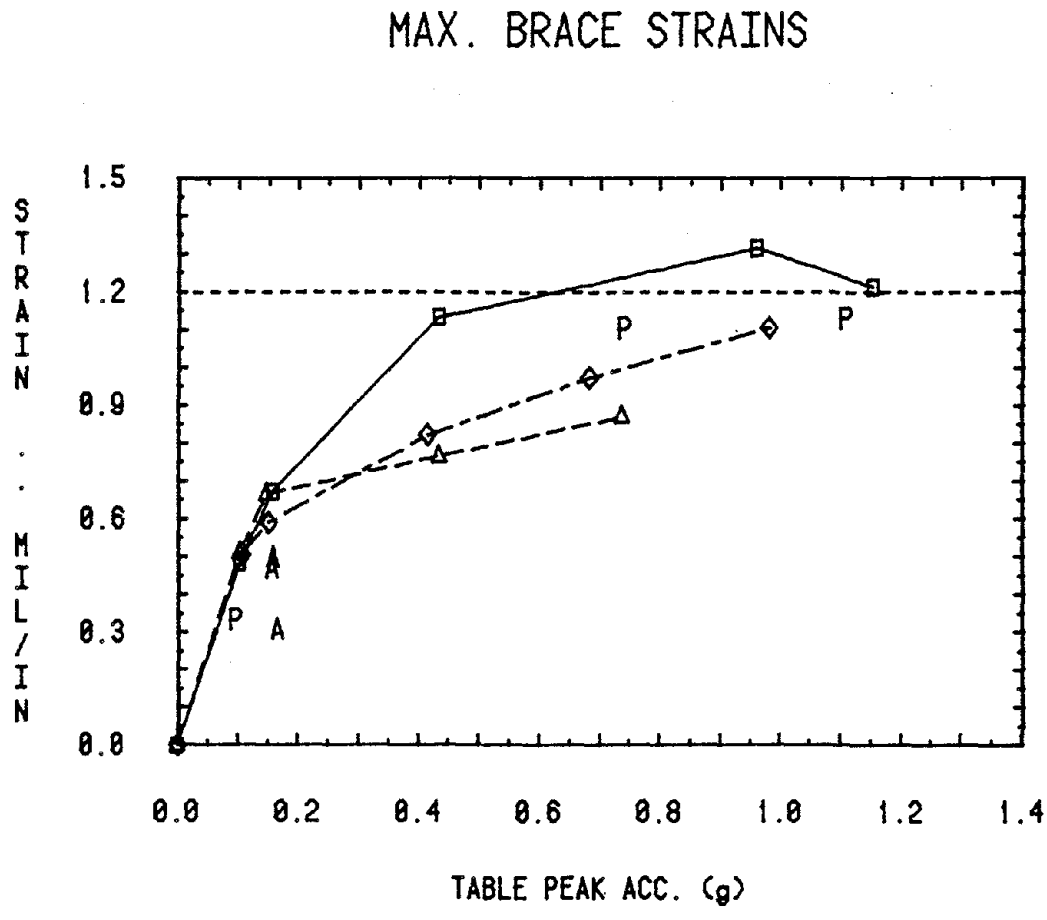

Fig. 46 Maximum Brace Strains in All Tests

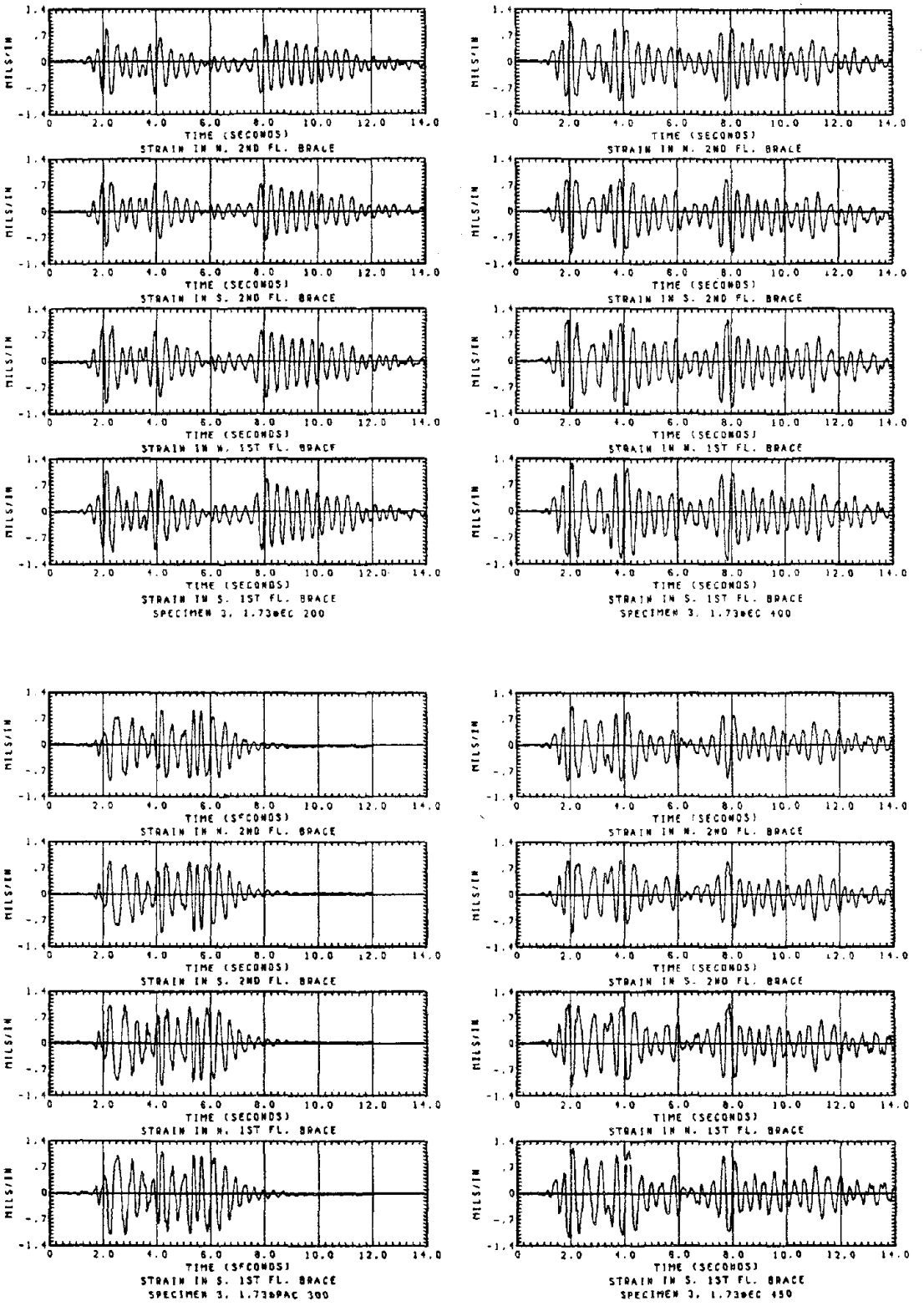

Fig. 47 Brace Strains Measured in Major Tests of Specimen 3

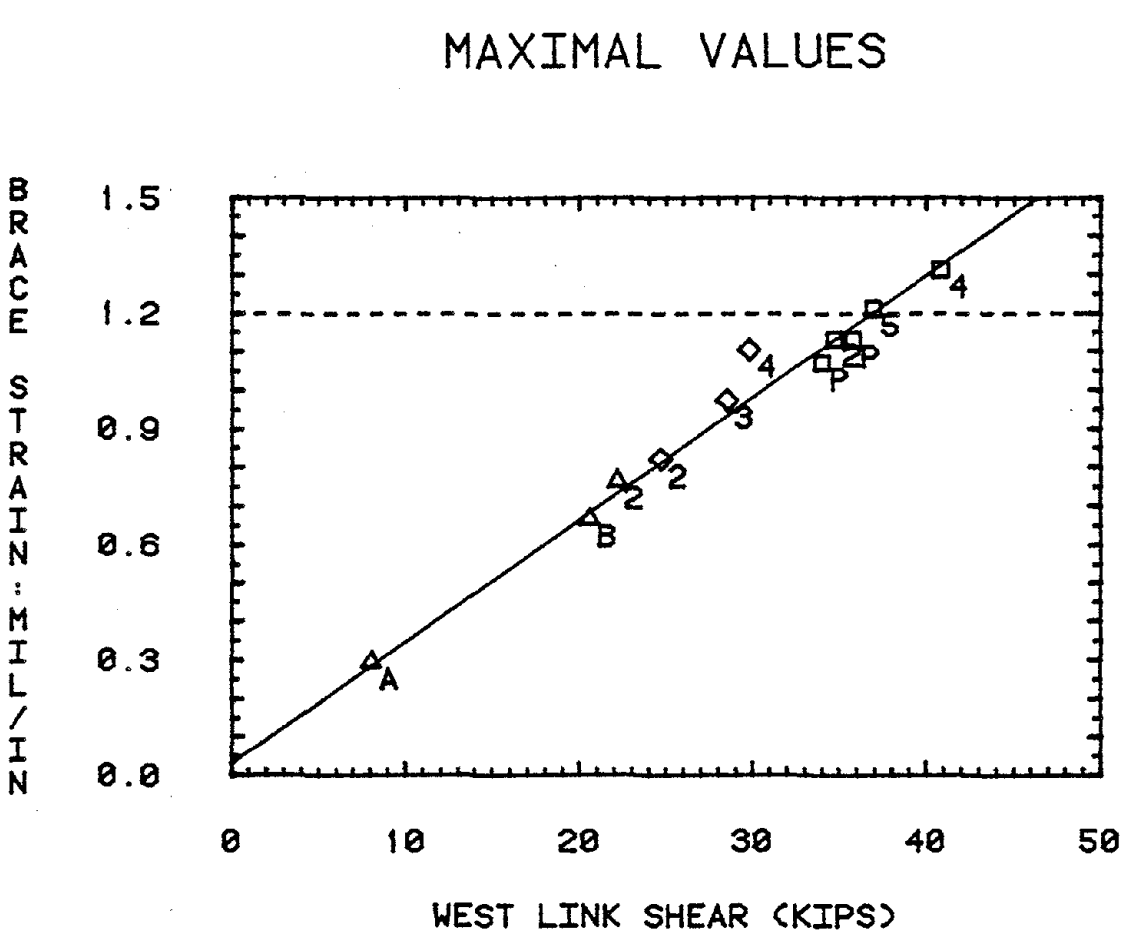

Fig. 48 Maximum Brace Strains and Maximum West Link Shear Forces

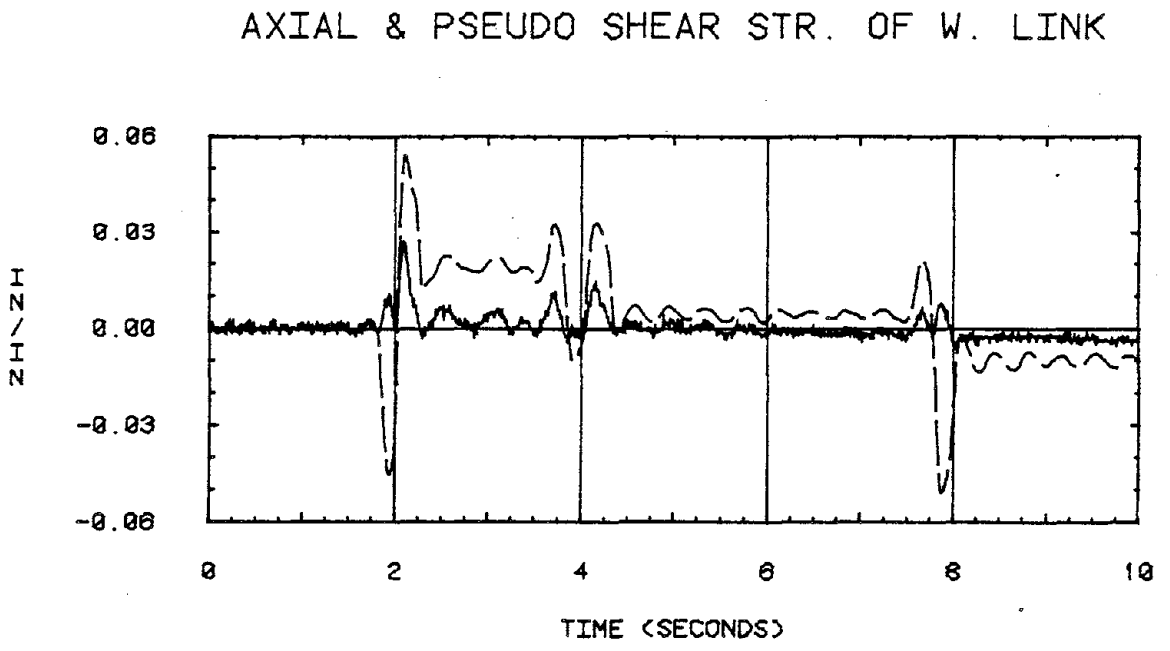

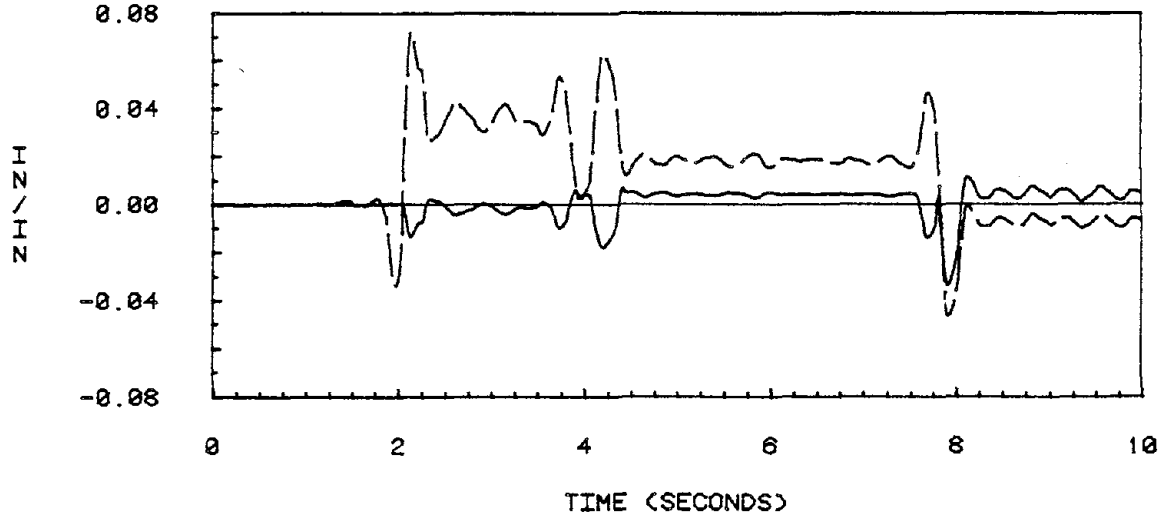

Figs. 49 & 50 Link Axial Strains and Pseudo-Shear Strains

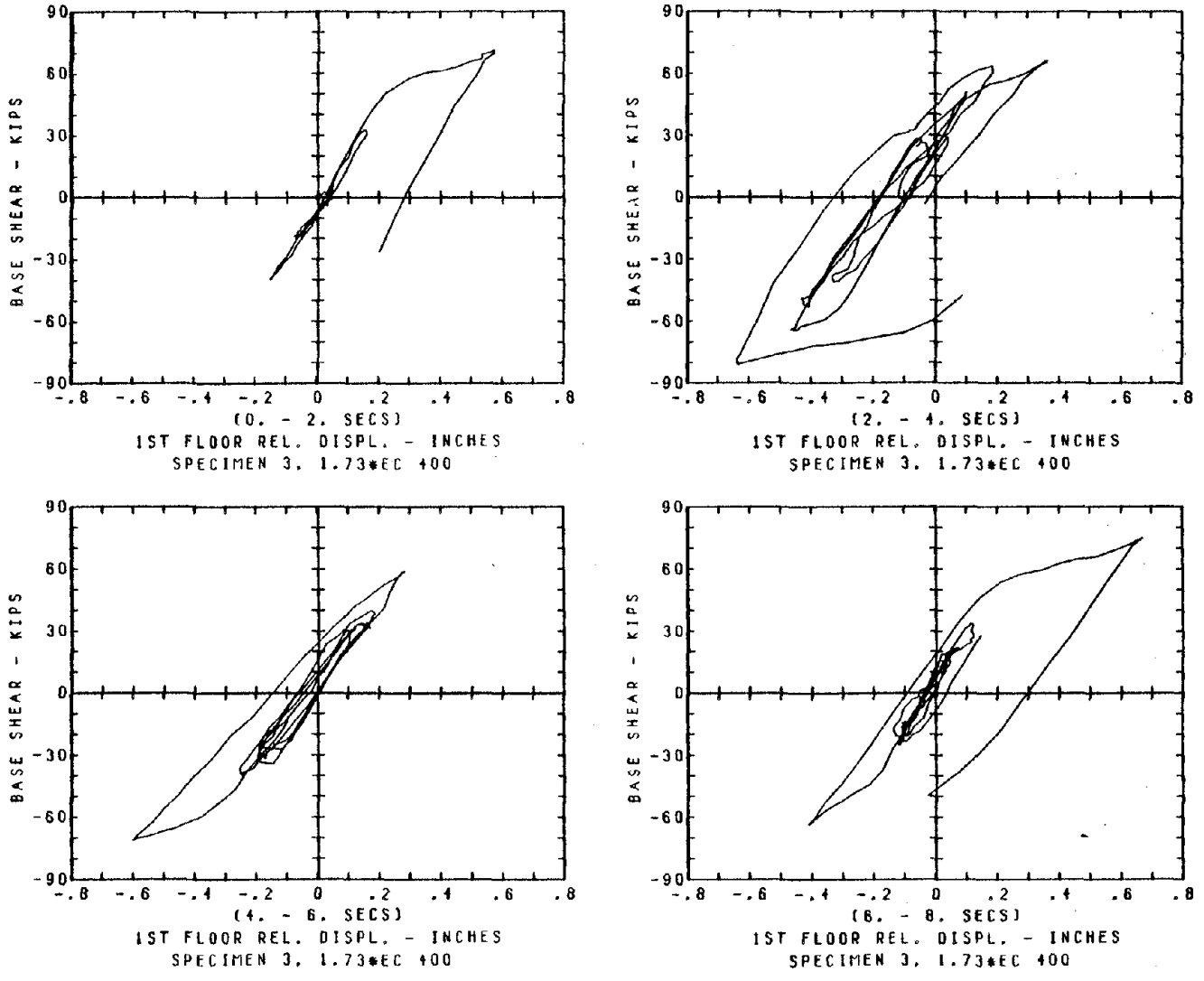

Fig. 51 Structural Hysteresis Behavior (Specimen 3 in 1.73*EC 400)

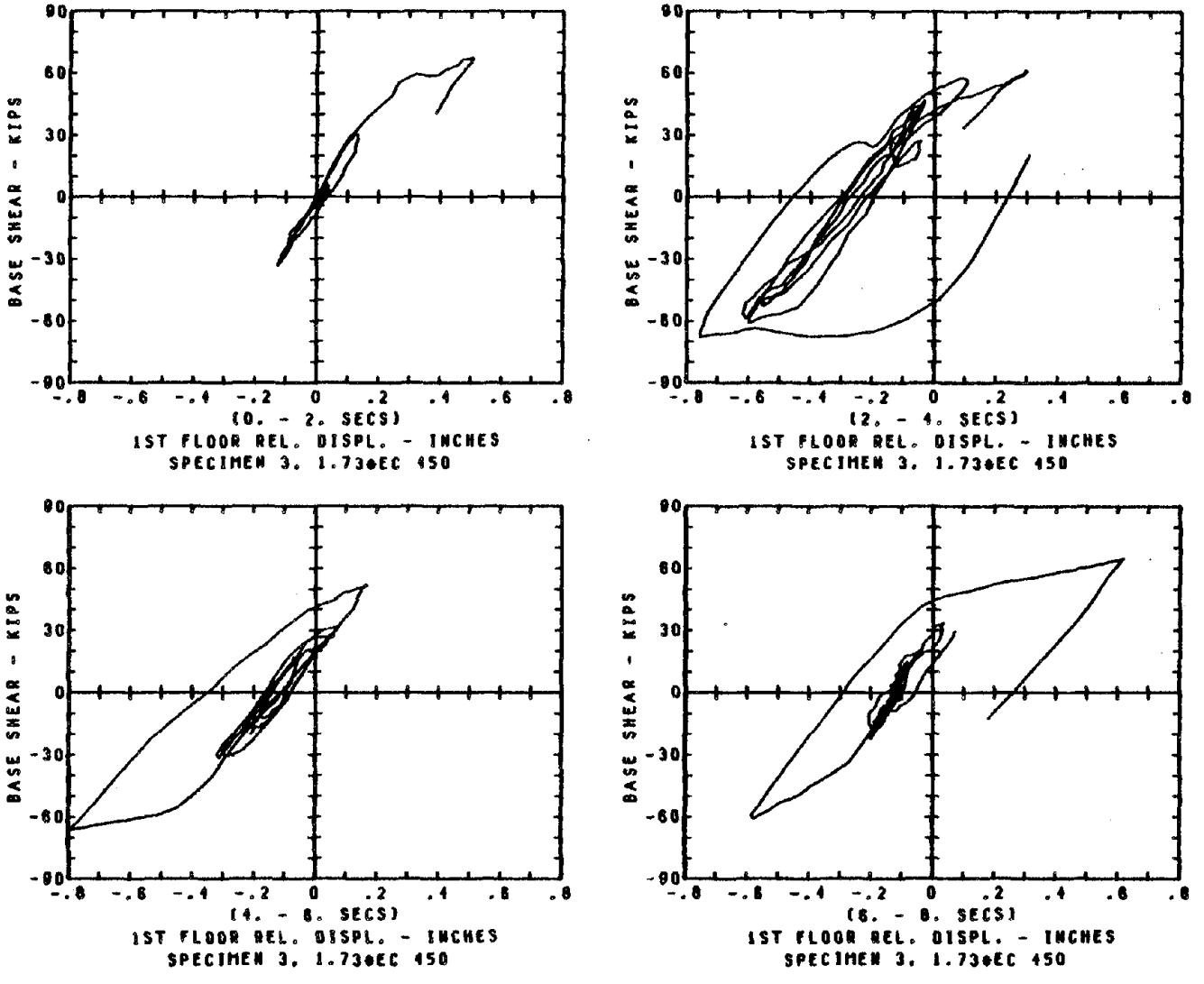

Fig. 52 Structural Hysteresis Behavior (Specimen 3 in 1.73*EC 450)

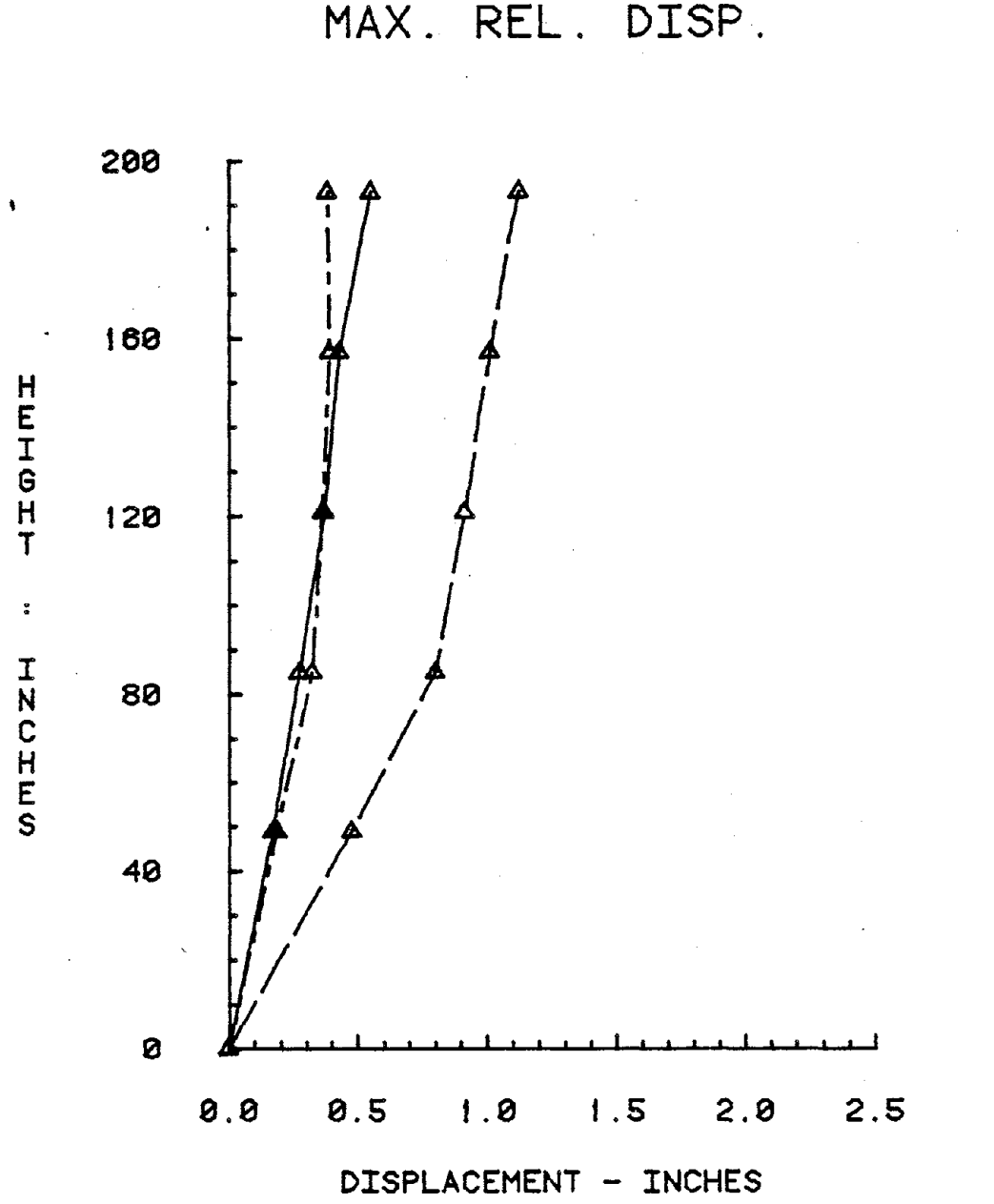

Fig. 53 Displacement Envelopes of Specimen 1

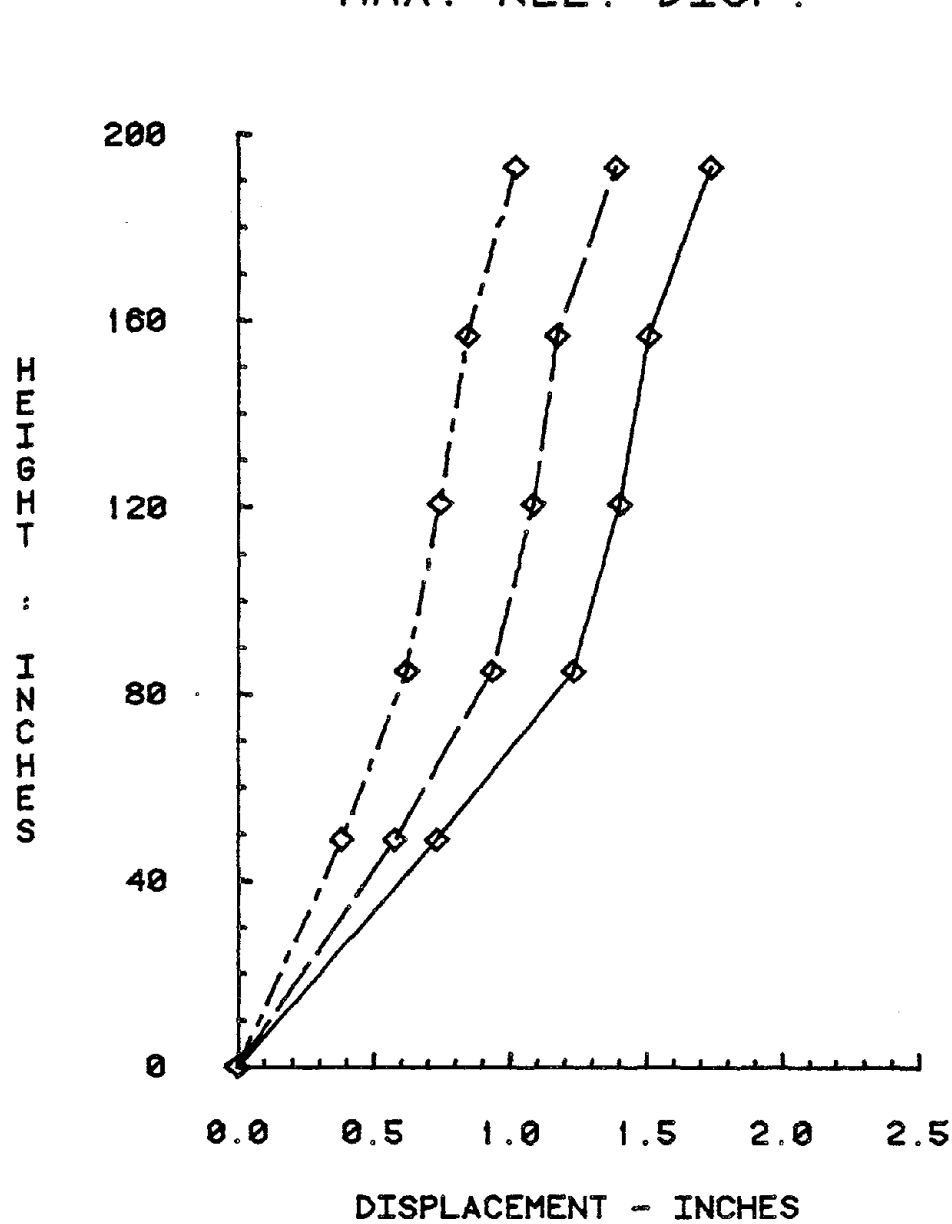

Fig. 54 Displacement Envelopes of Specimen 2

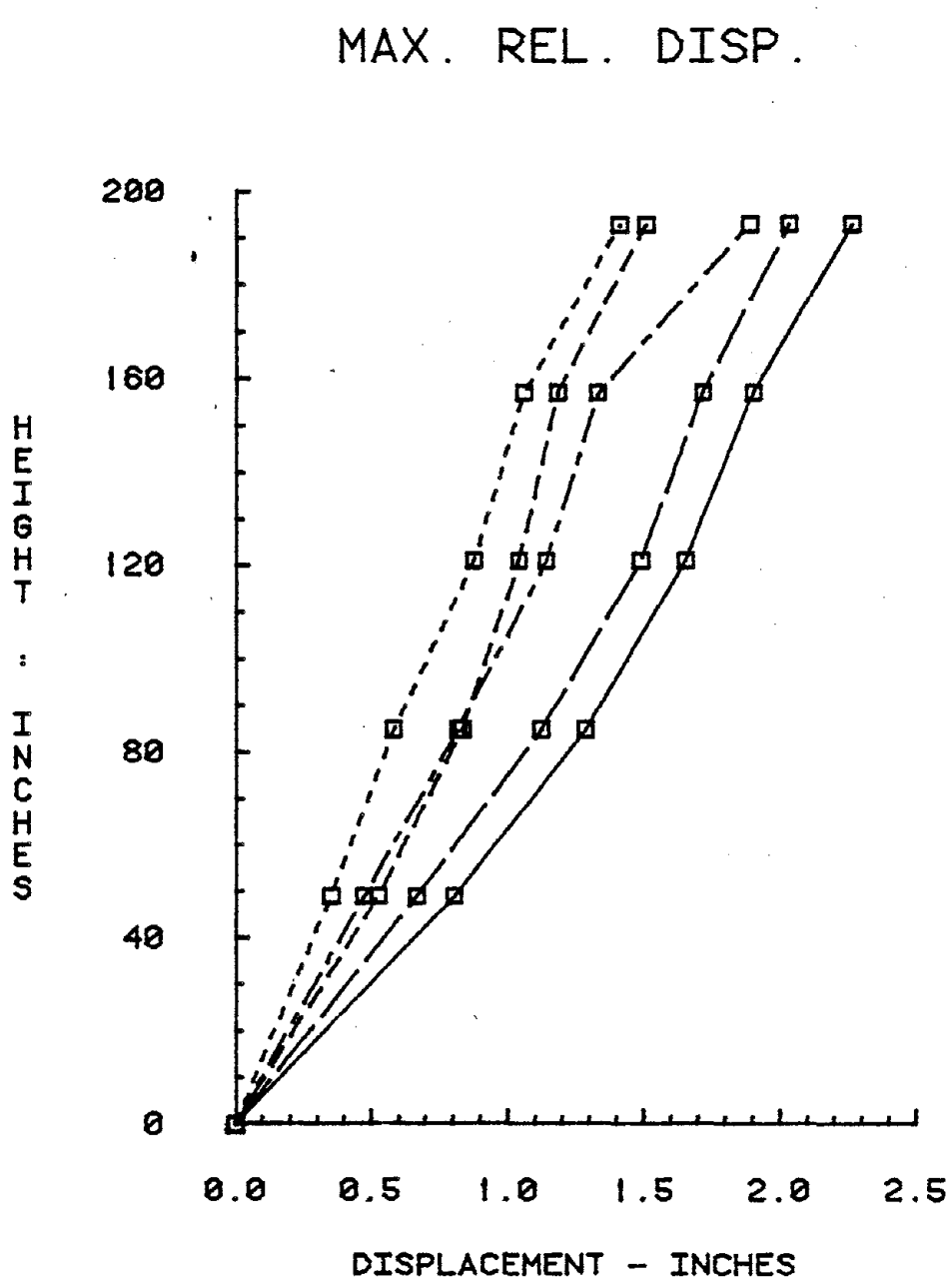

Fig. 55 Displacement Envelopes of Specimen 3

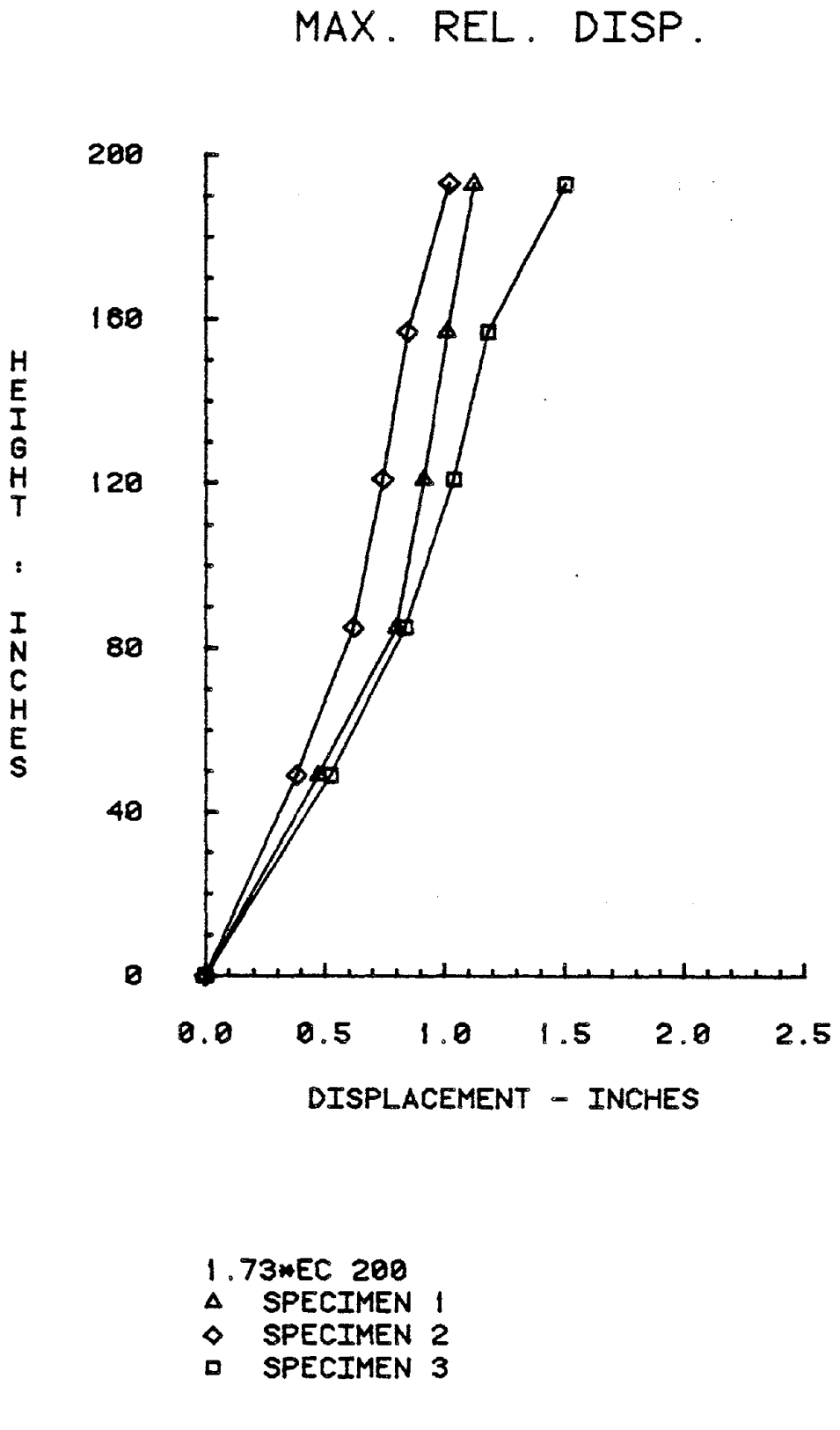

Fig. 56 Displacement Envelopes of 1.73*EC 200

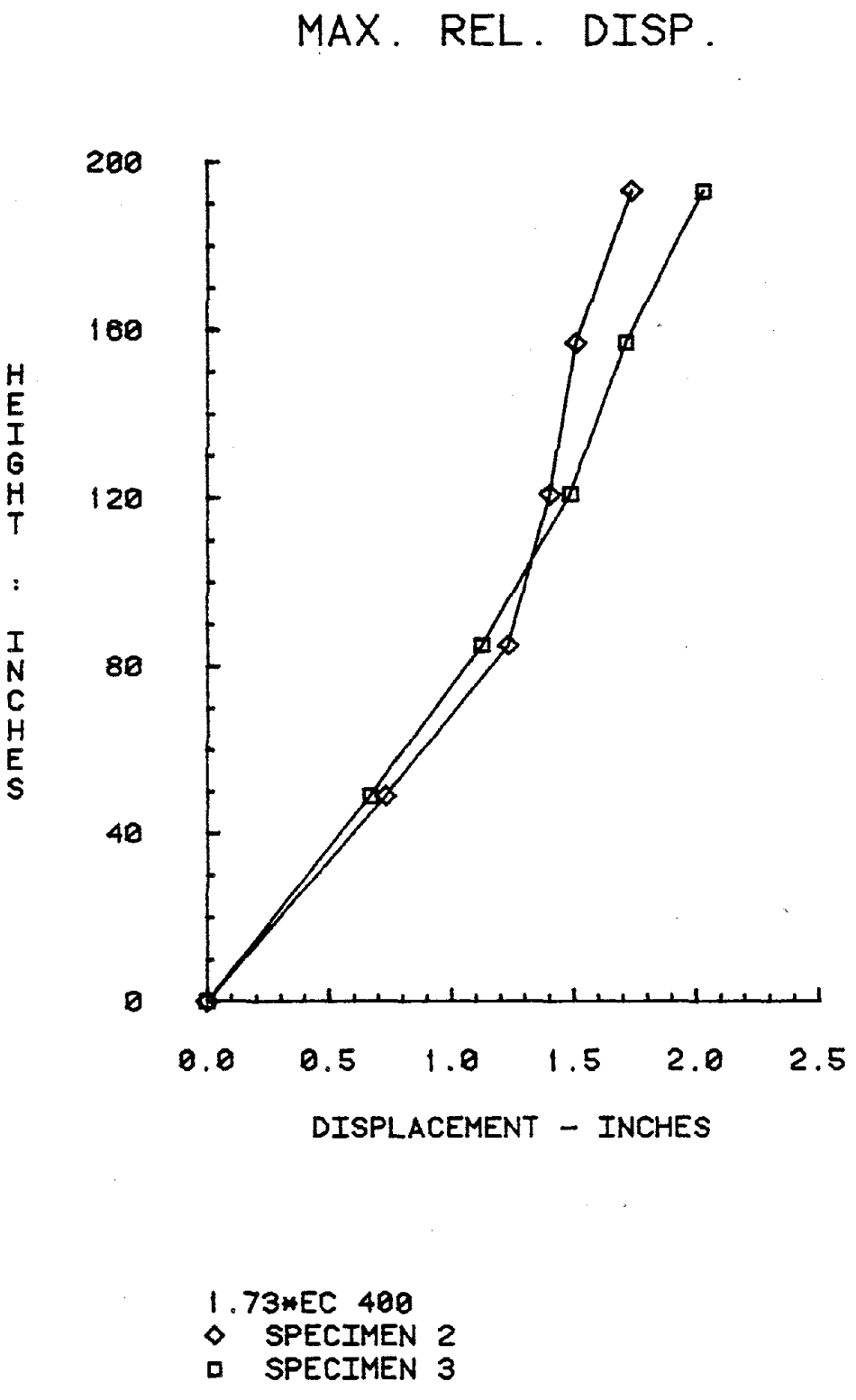

Fig. 57 Displacement Envelopes of 1.73*EC 400

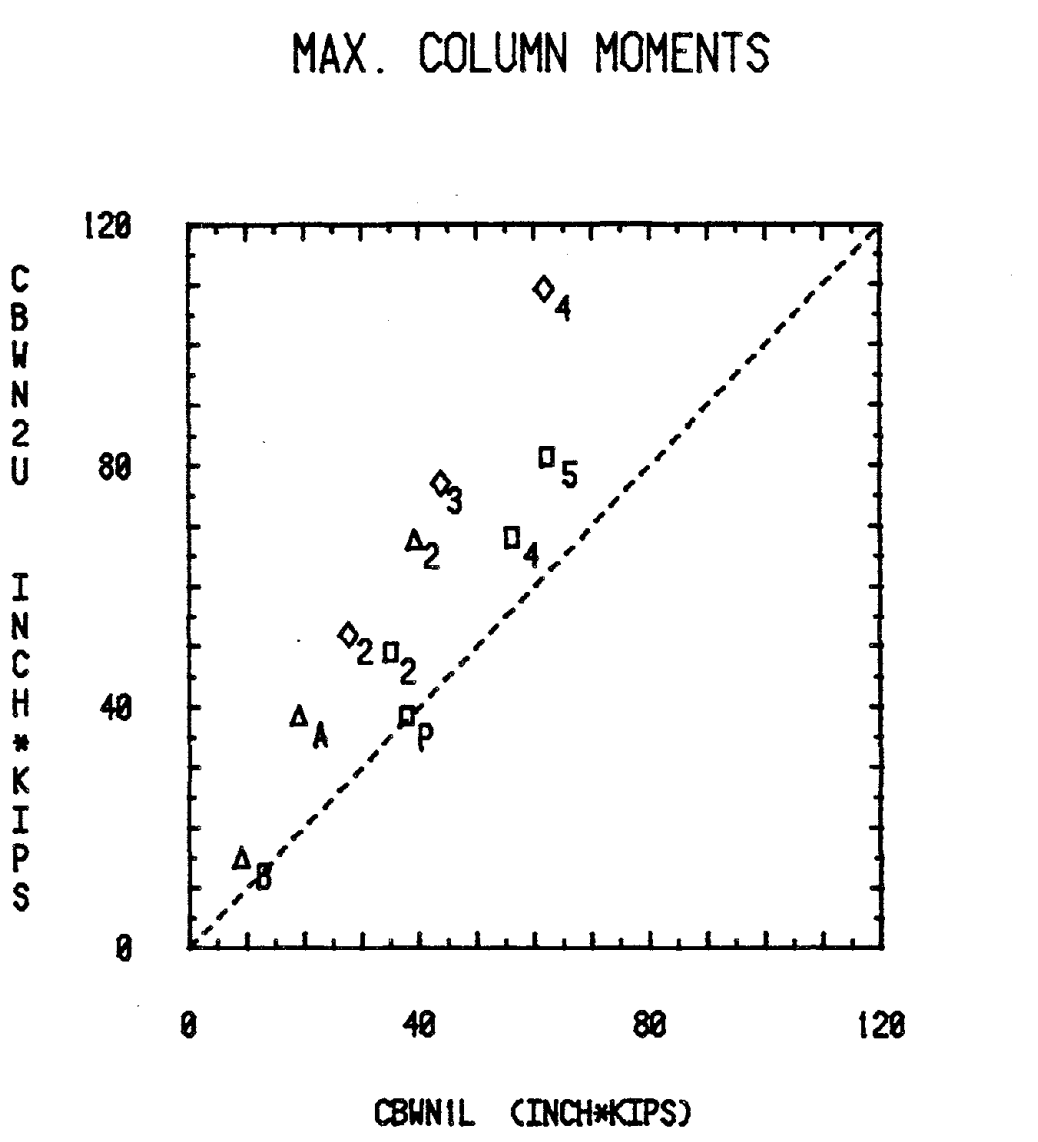

Fig. 58 Maximum Column Bending Moments (CBWN2U & CBWN1L)

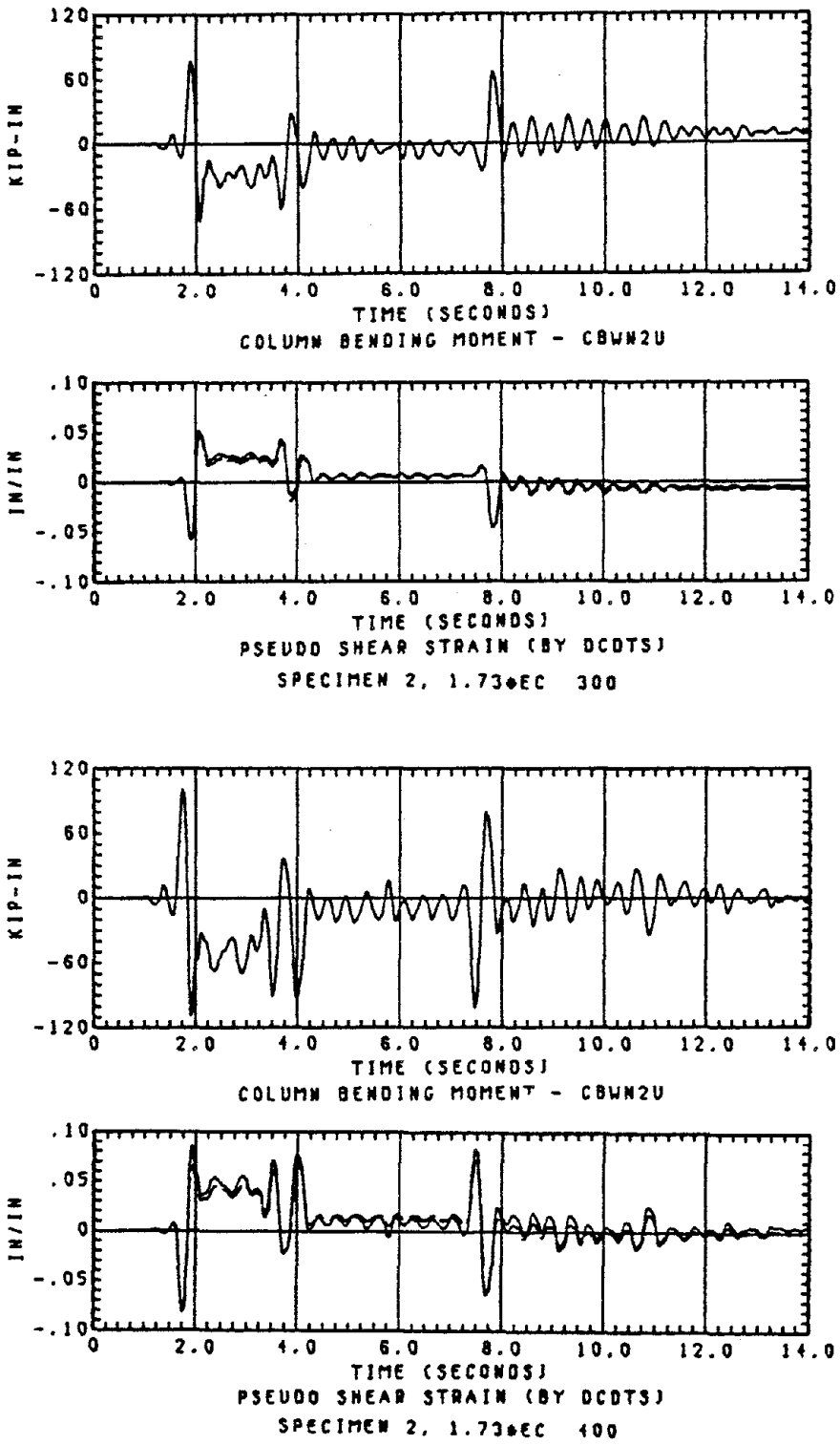

Fig. 59 Correlation between Column Bending Moments and Their Correponding Pseudo Shear Strains

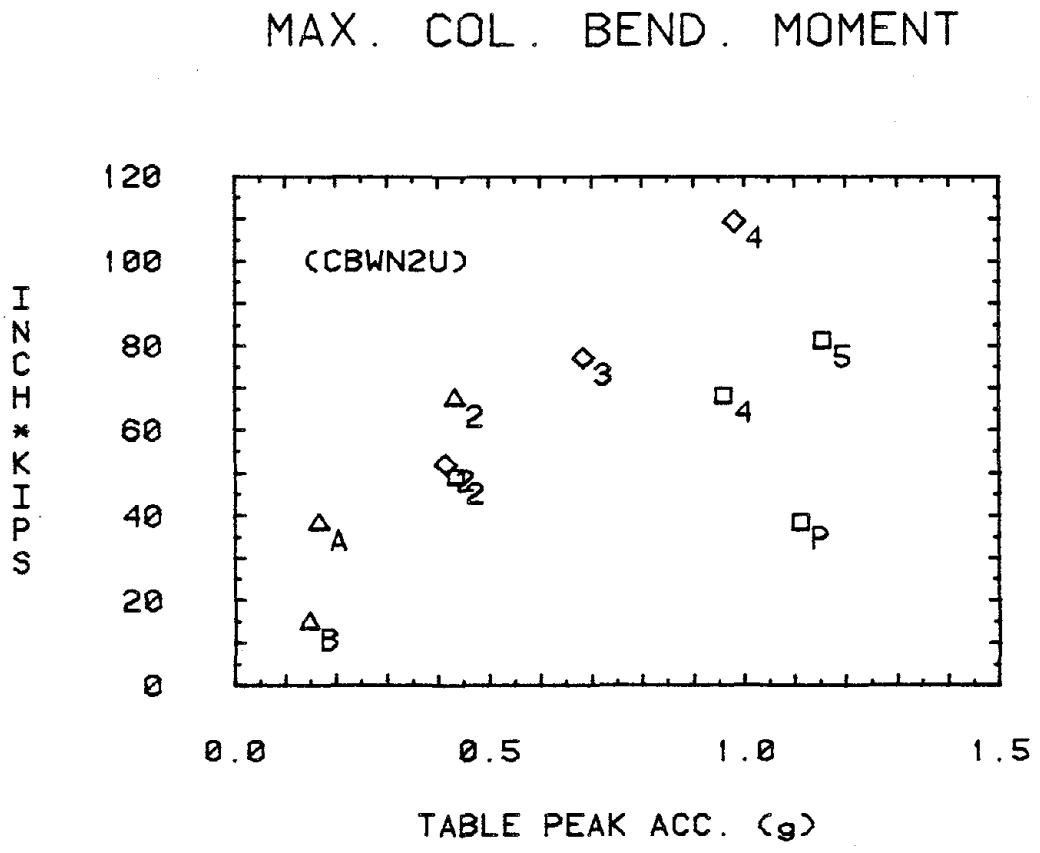

Fig. 60 Maximum Column Bending Moments vs. Table Acceleration Peaks

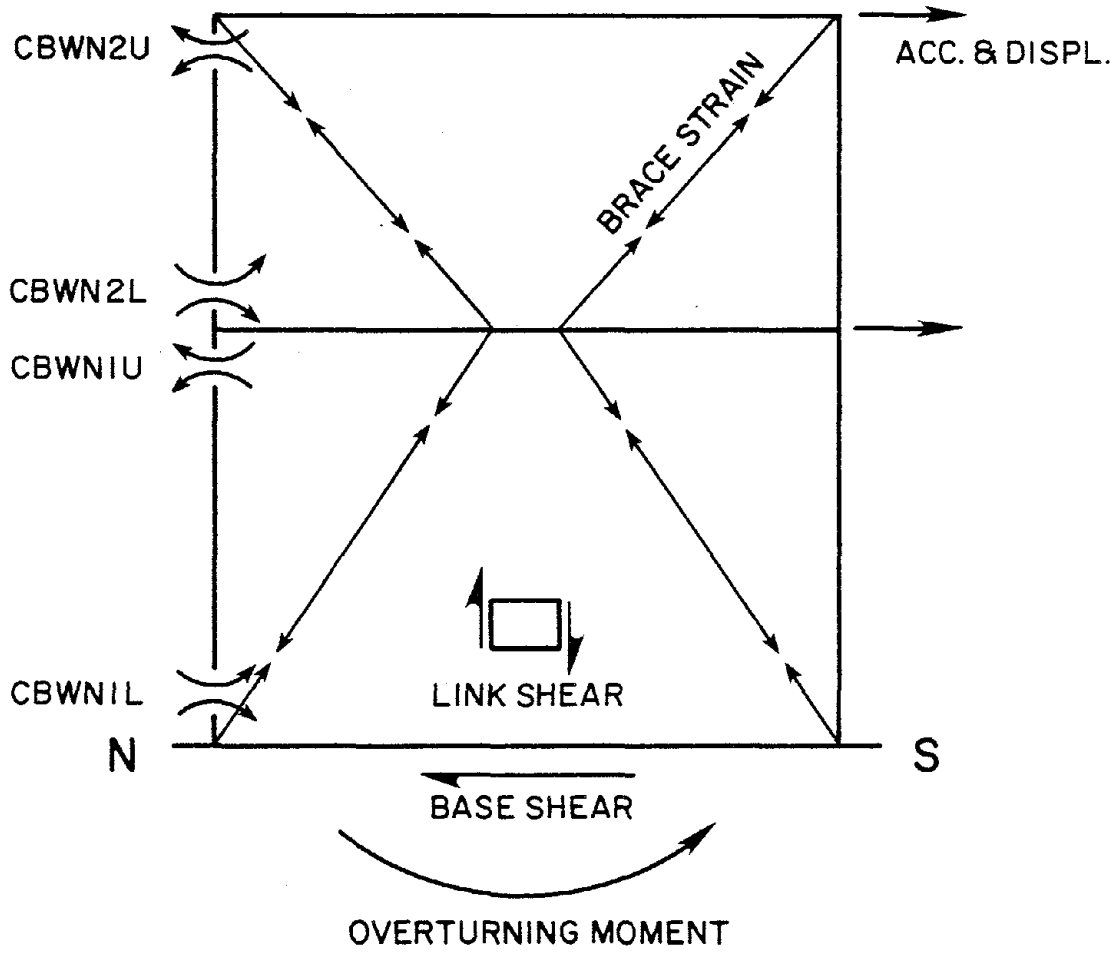

POSITIVE SIGN CONVENTIONS

Fig. 61 Positive Sign Conventions for Data Presentation

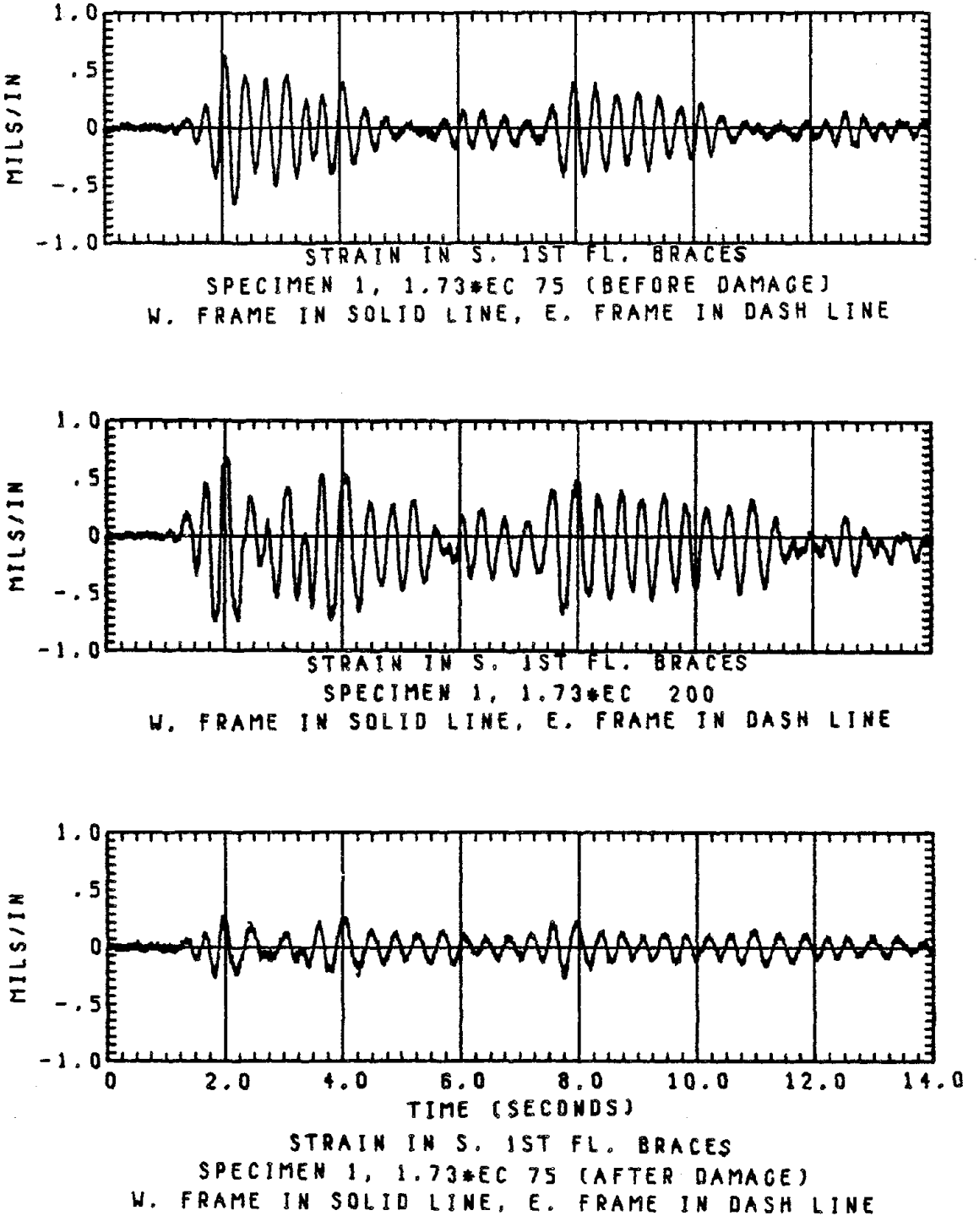

Fig. 62 Strains in the South First-Story Braces in Selected Tests of Specimen 1

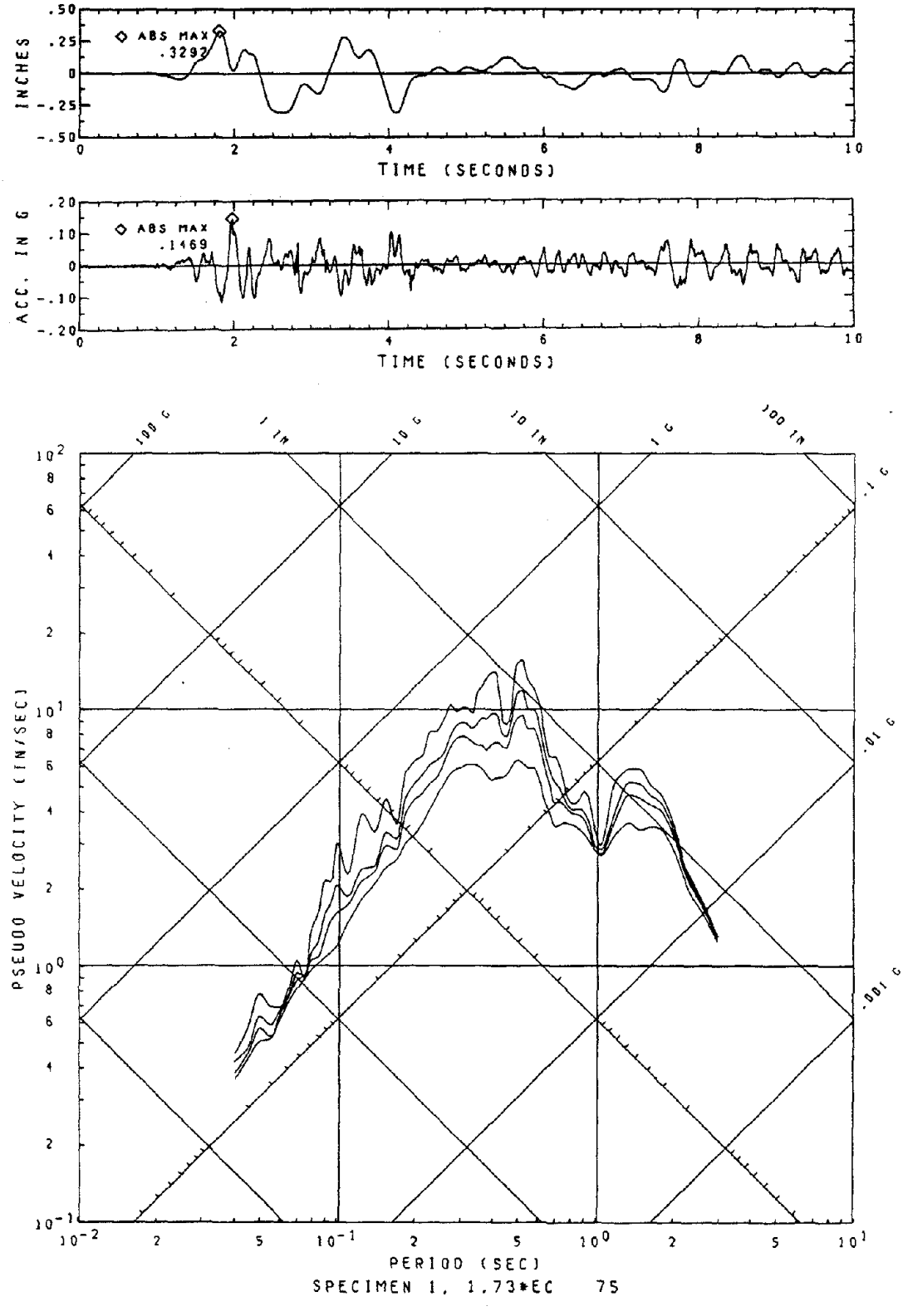

Fig. 63 Displacement, Acceleration of Table Motion 1.73*EC 75B and Its Response Spectra (Damping Ratios = 0.01, 0.03, 0.05, 0.10)

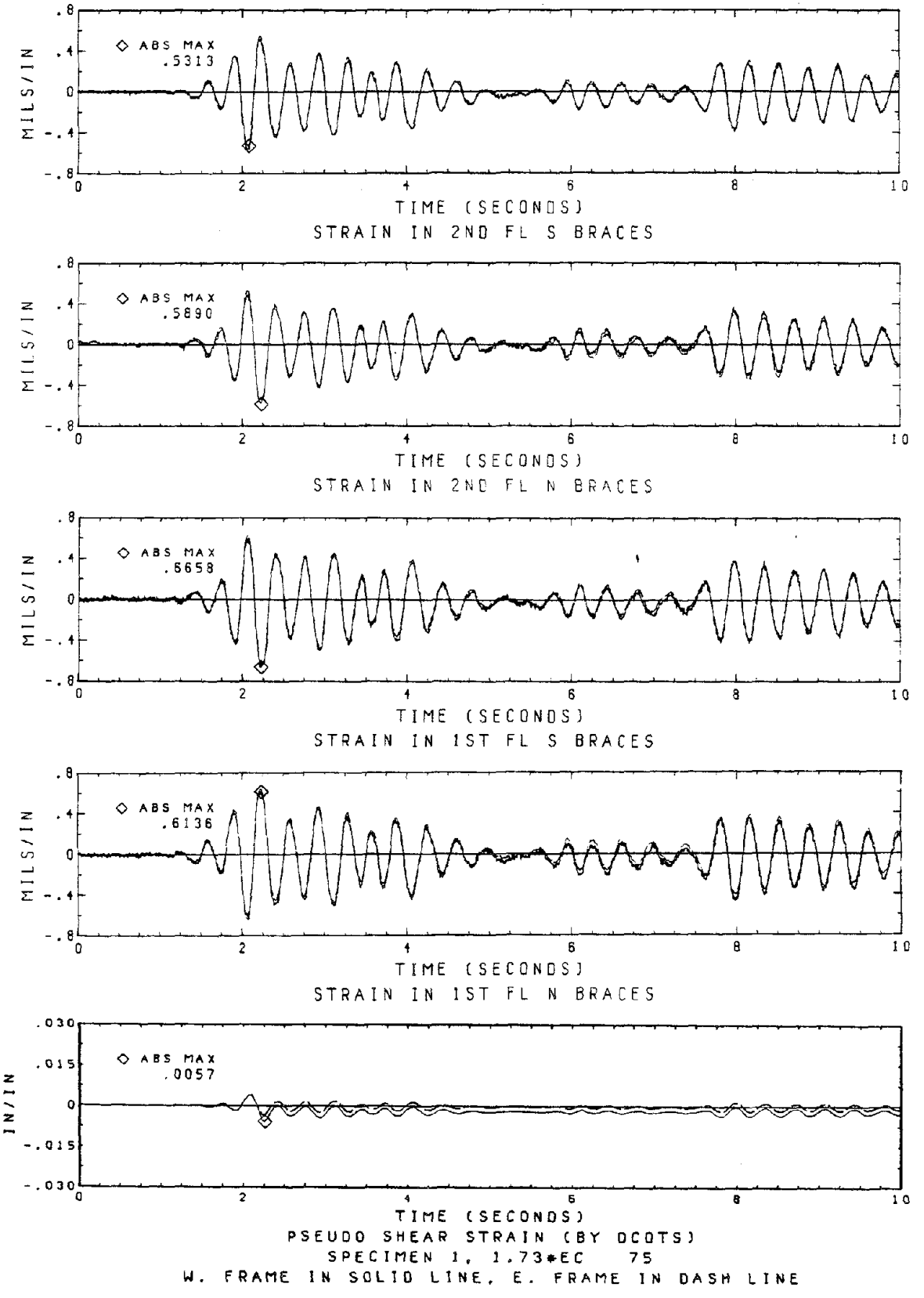

Fig. 64 Brace Strains and Pseudo Shear Strain

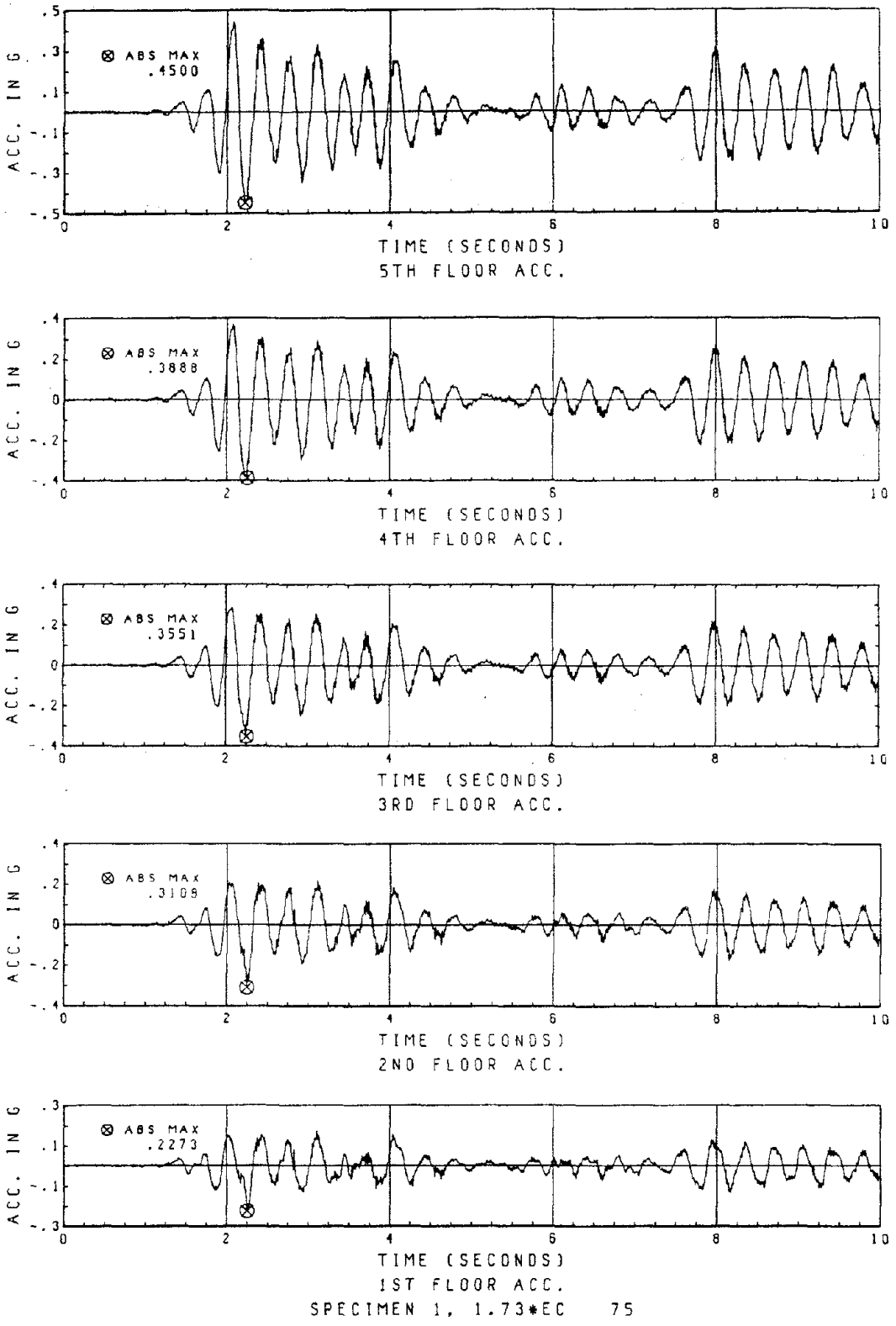

Fig. 65 Floor Accelerations

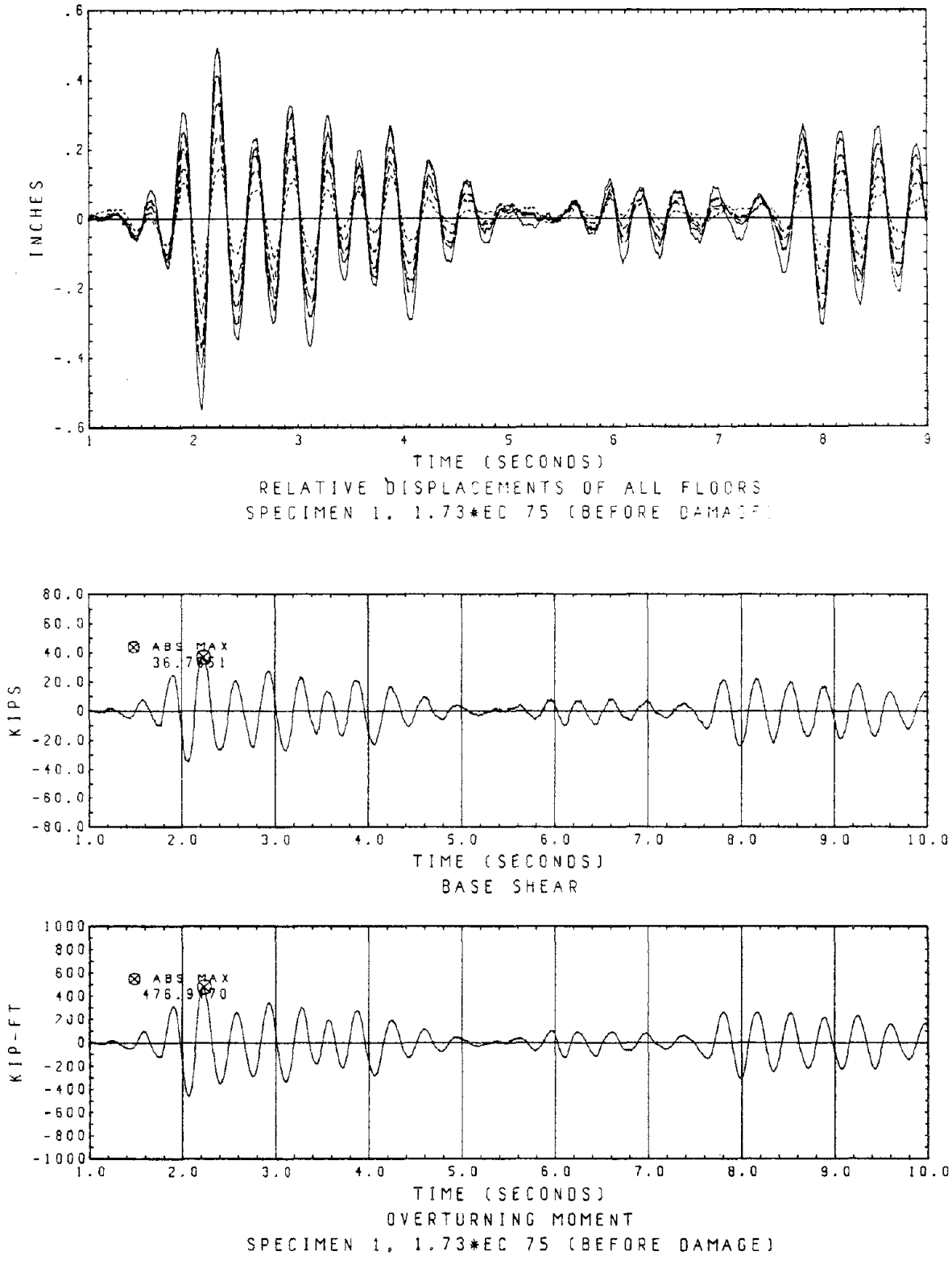

Fig. 66 Floor Displacements, Base Shear and Overturning Moment

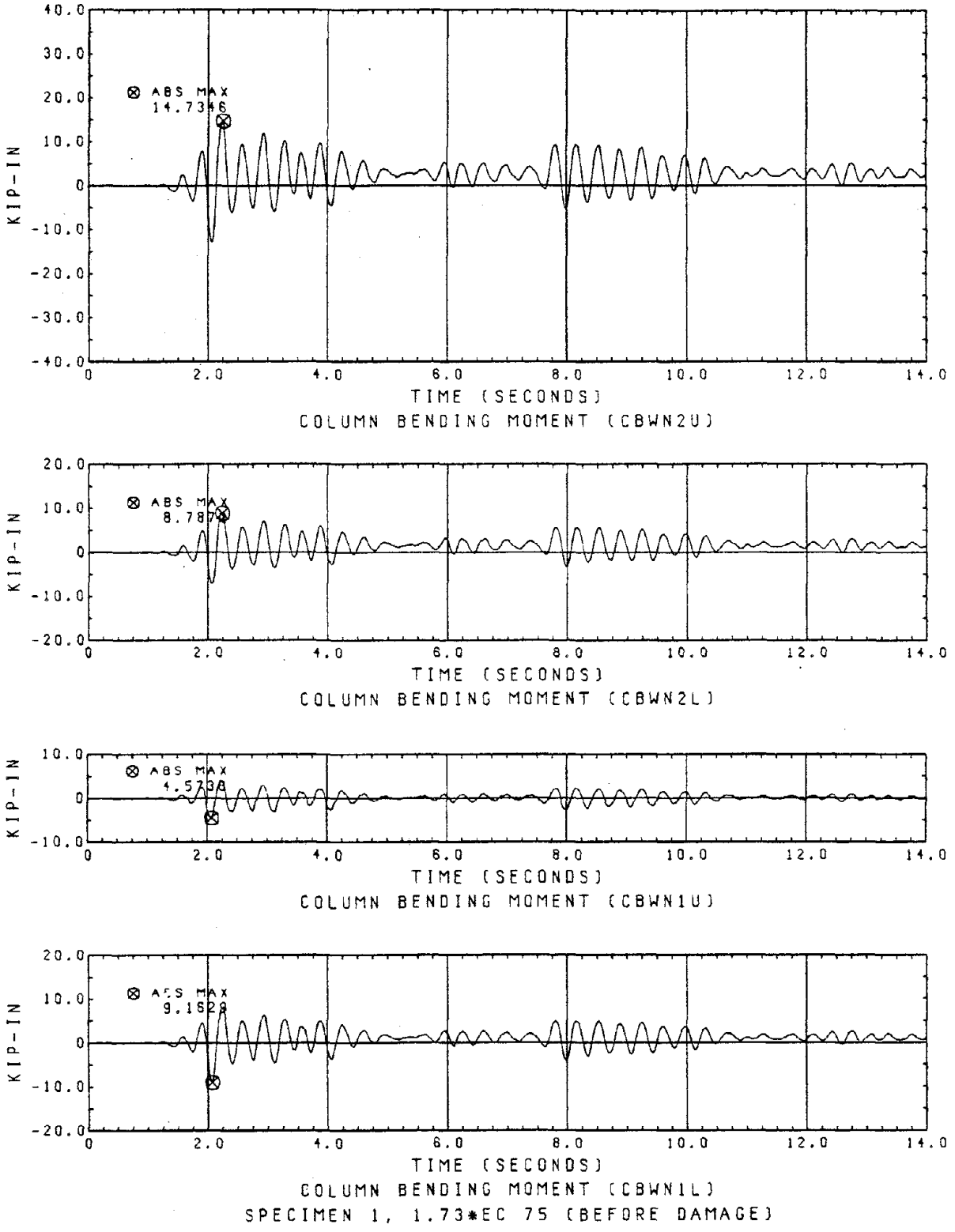

Fig. 67 Column Bending Moments

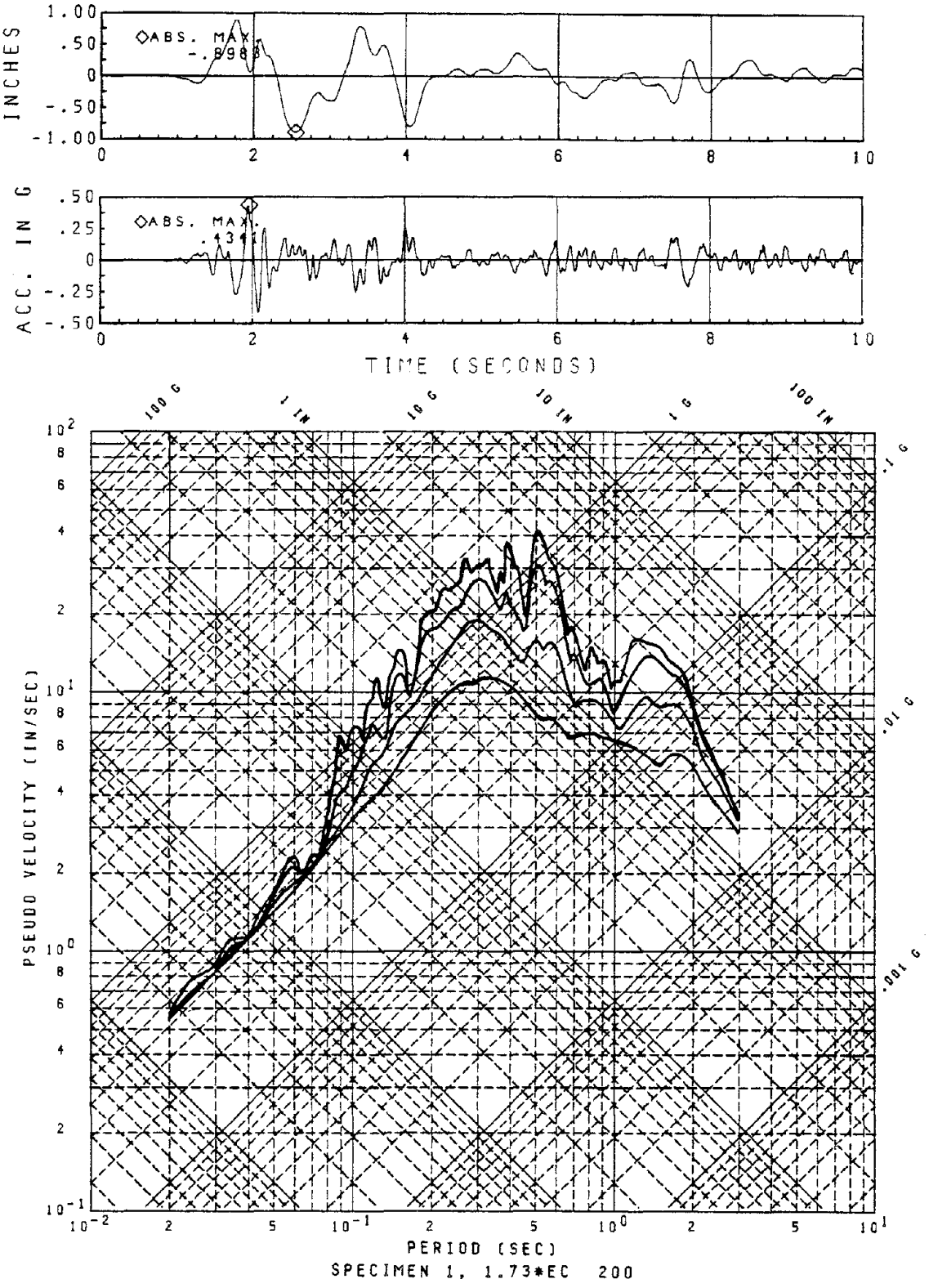

Fig. 68 Displacement, Acceleration of Table Motion 1.73*EC 200 and Its Response Spectra (Damping Ratios = 0.01, 0.03, 0.10, 0.25)

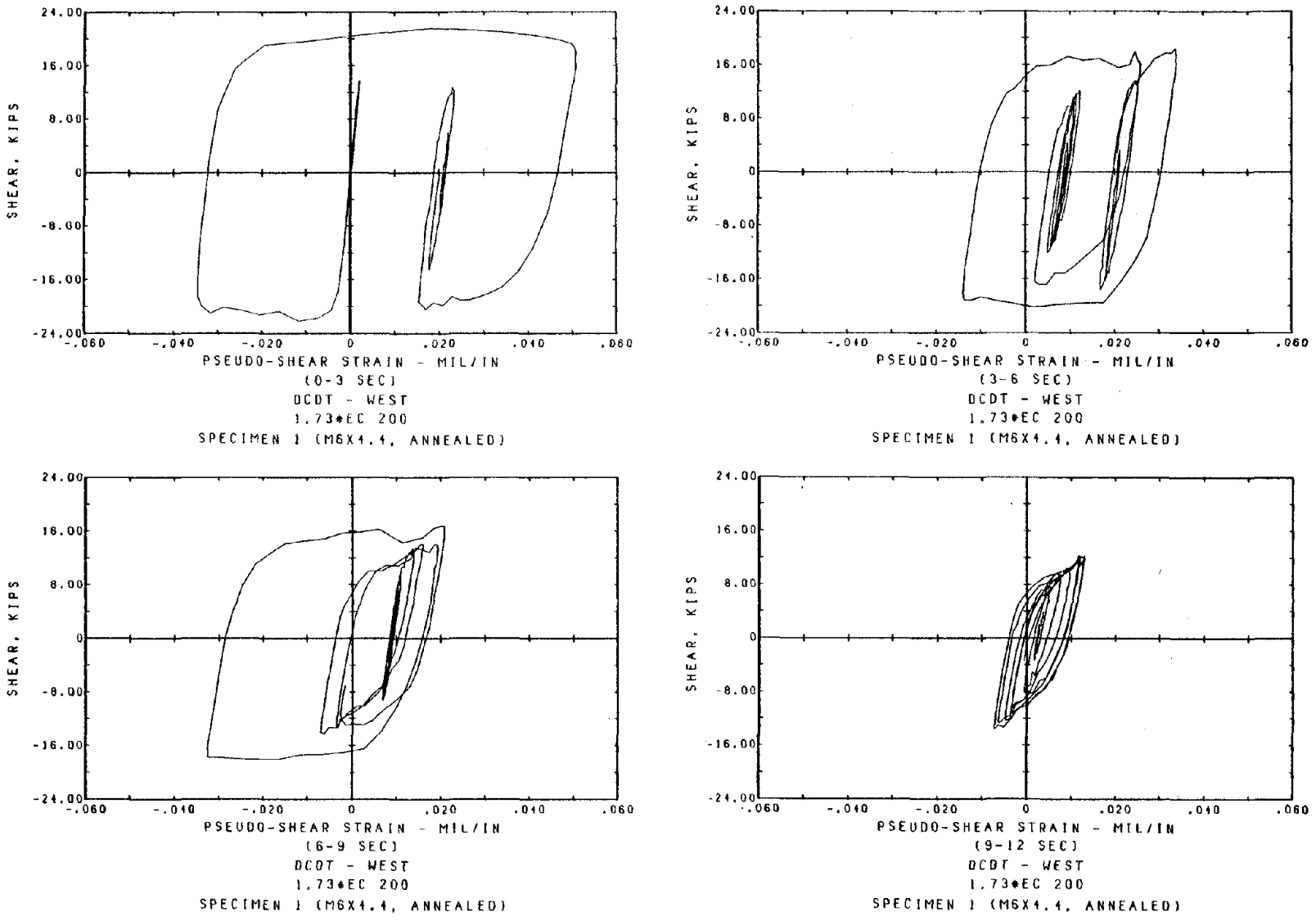

Fig. 69 Shear Link Hysteresis: Link Shear Force vs. Pseudo-Shear Strain

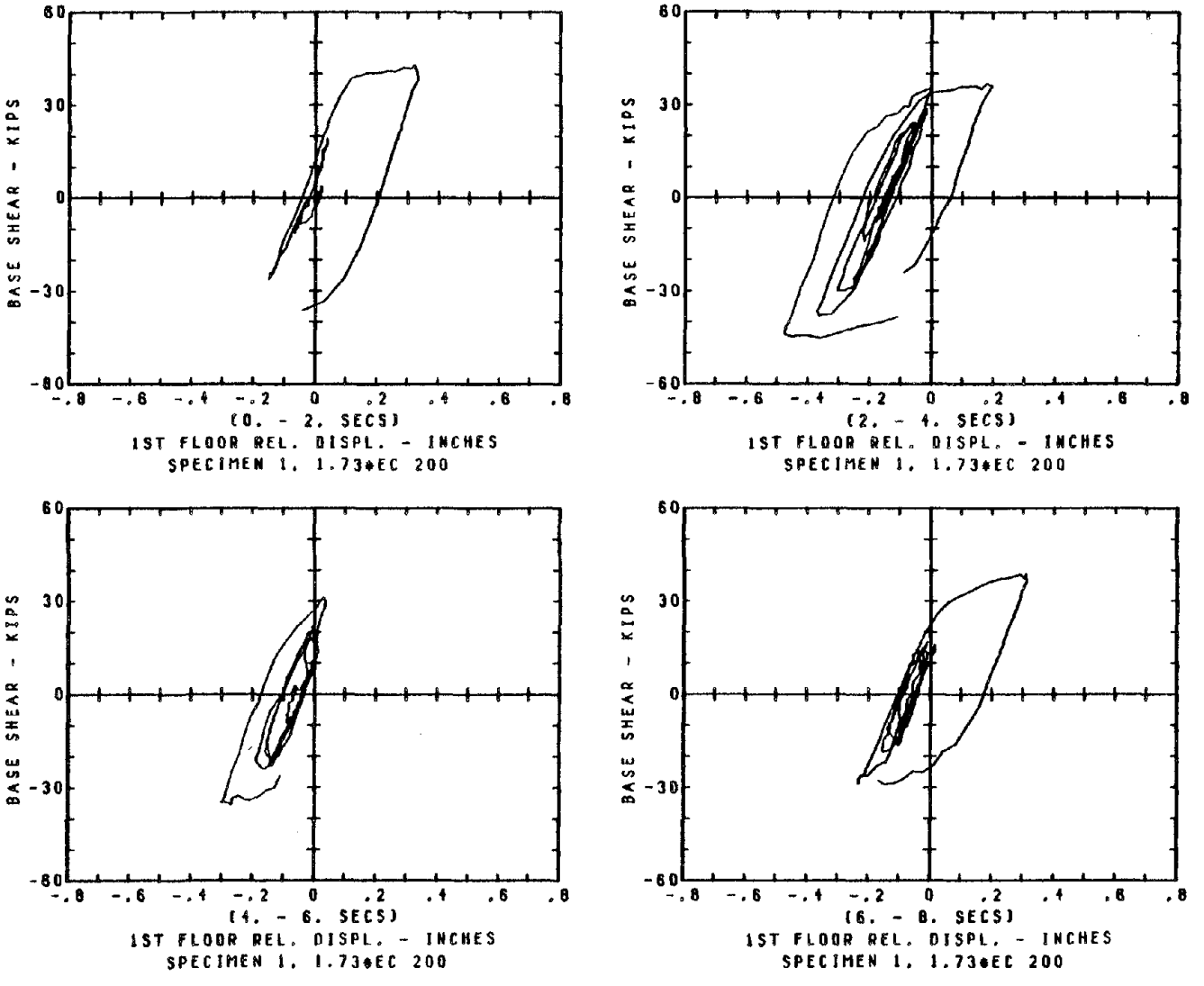

Fig. 70 Structural Hysteresis: Base Shear vs. First Story Drift

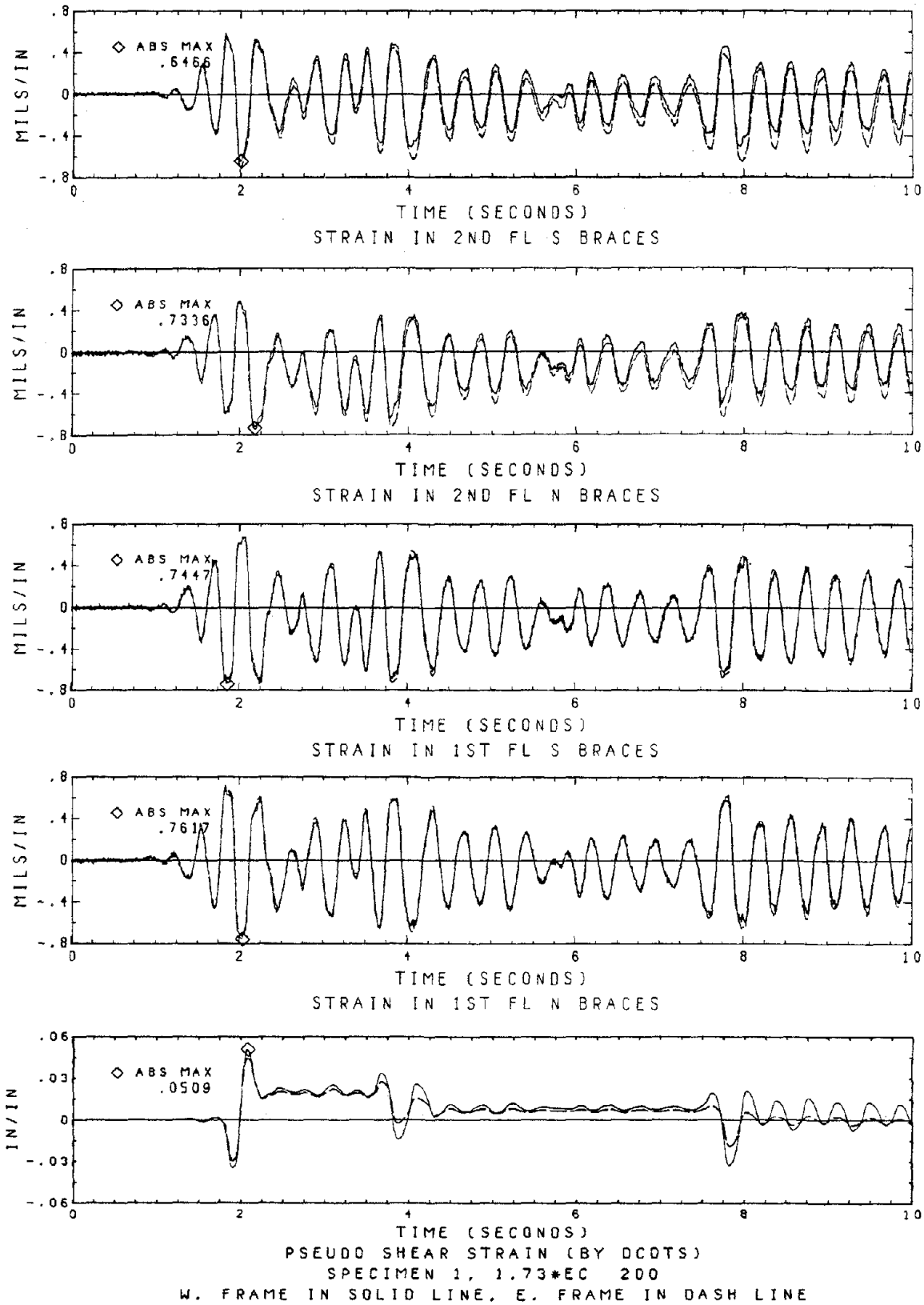

Fig. 71 Brace Strains and Pseudo Shear Strain

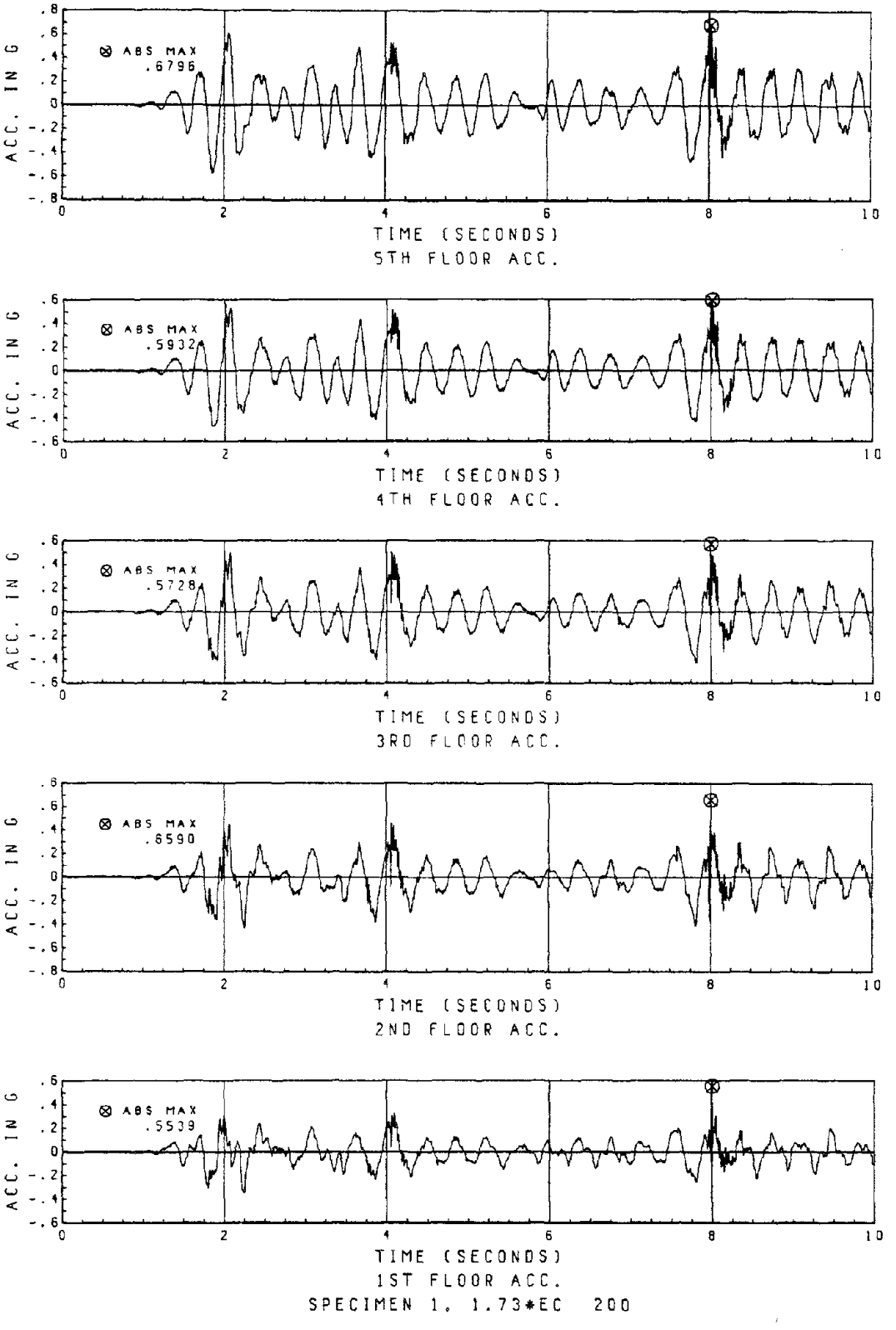

Fig. 72 Floor Accelerations

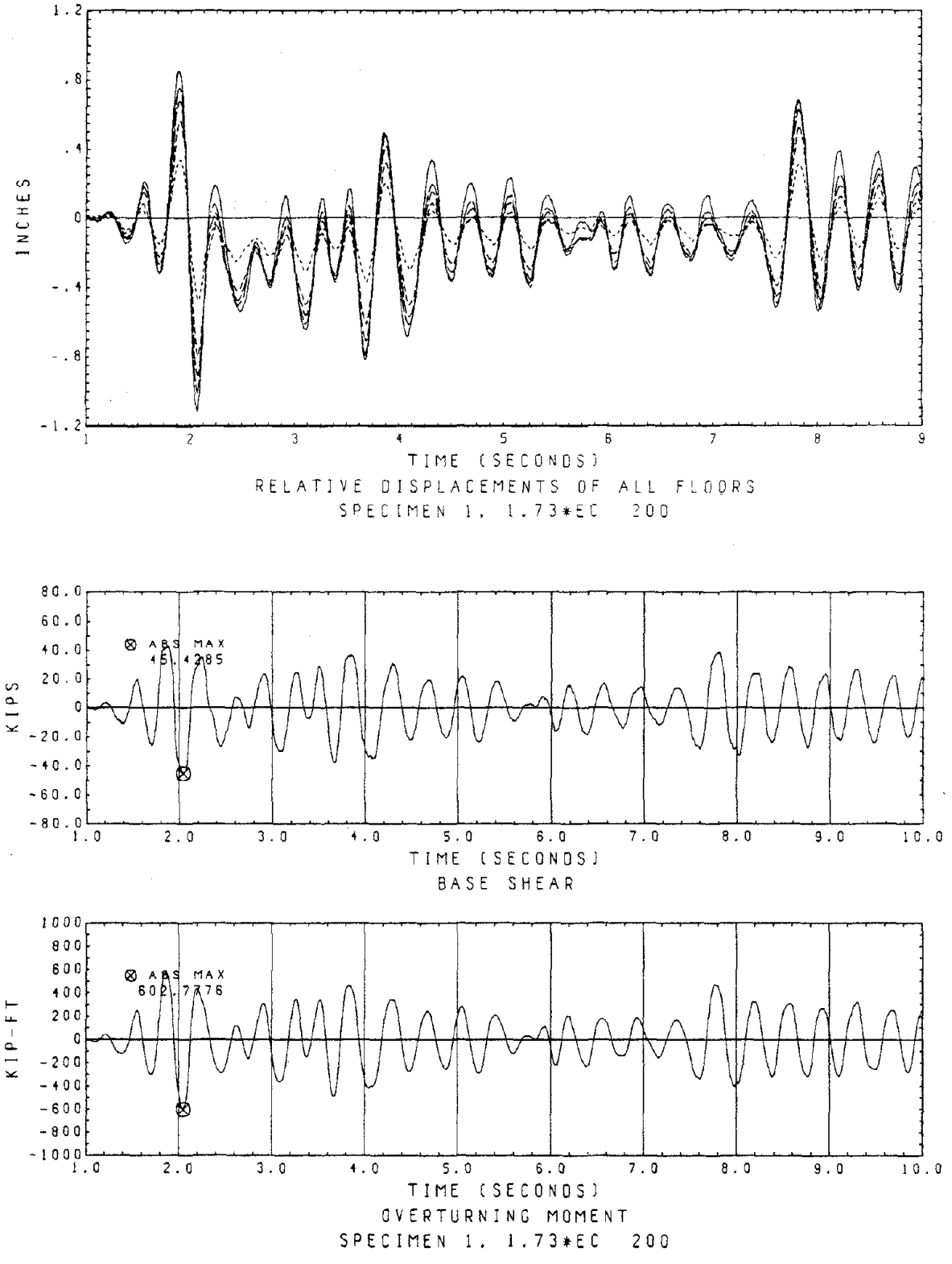

Fig. 73 Floor Displacements, Base Shear and Overturning Moment

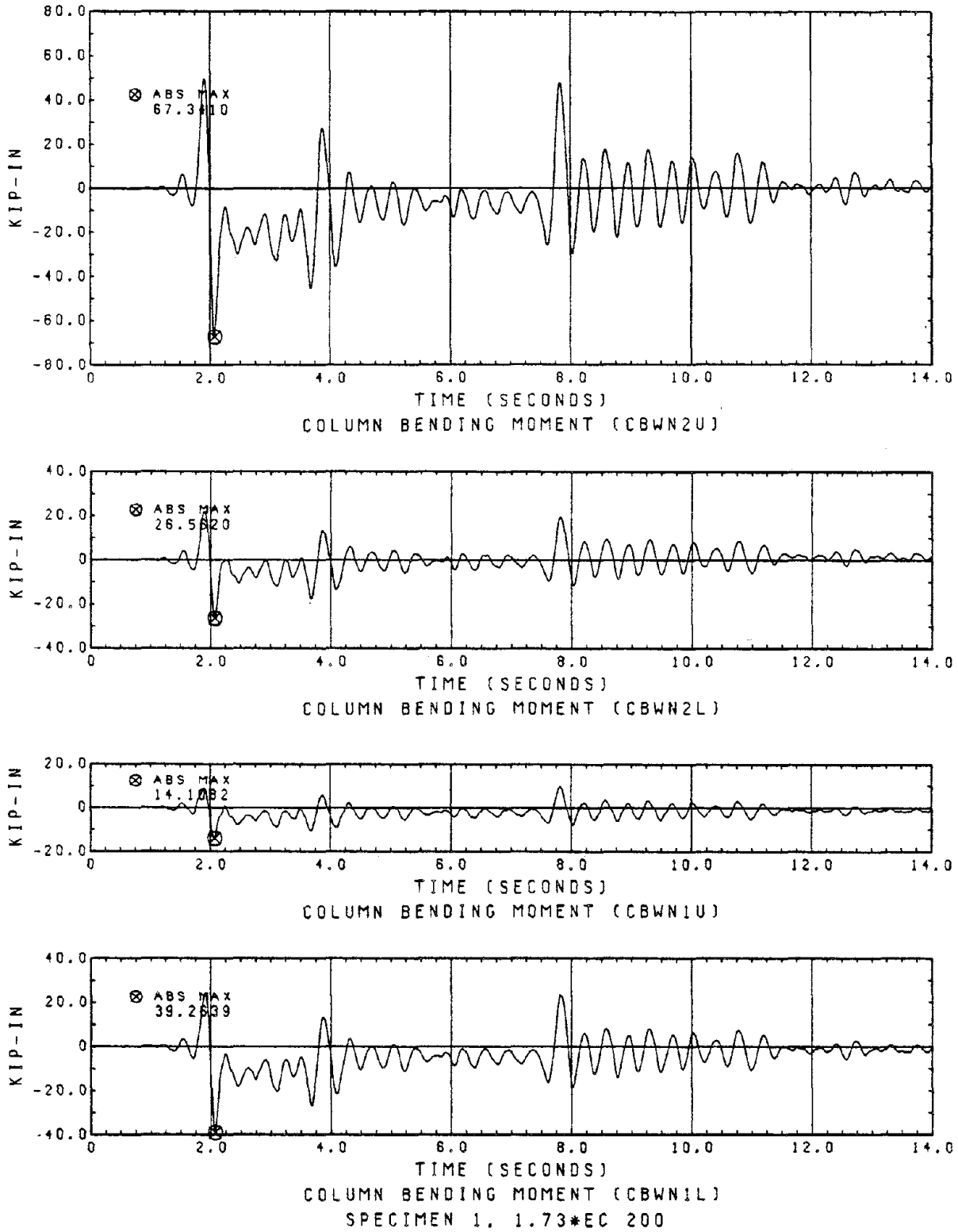

Fig. 74 Column Bending Moments

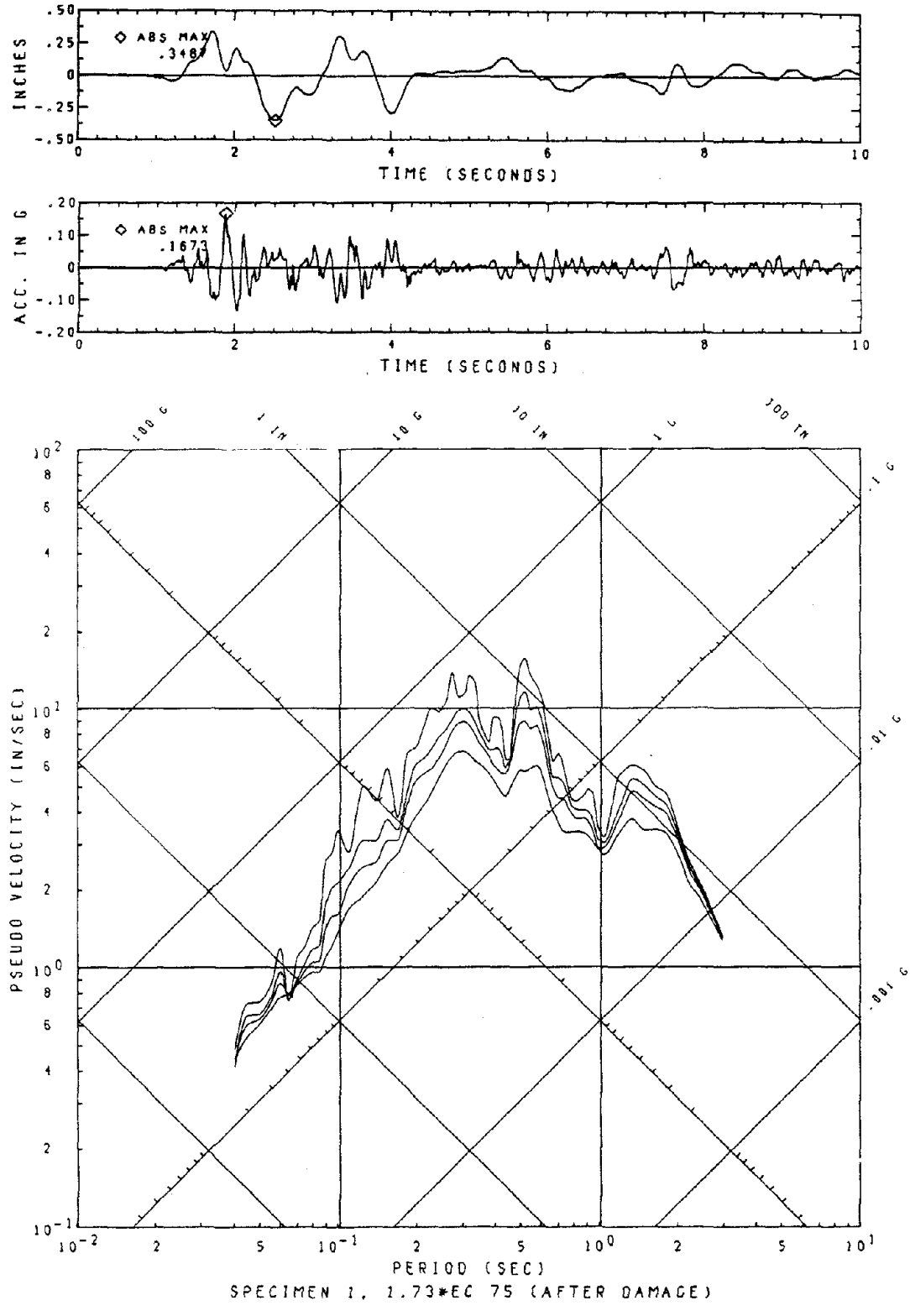

Fig. 75 Displacement, Acceleration of Table Motion 1.73*EC 75 and Its Response Spectra (Damping Ratios = 0.01, 0.03, 0.05, 0.10)

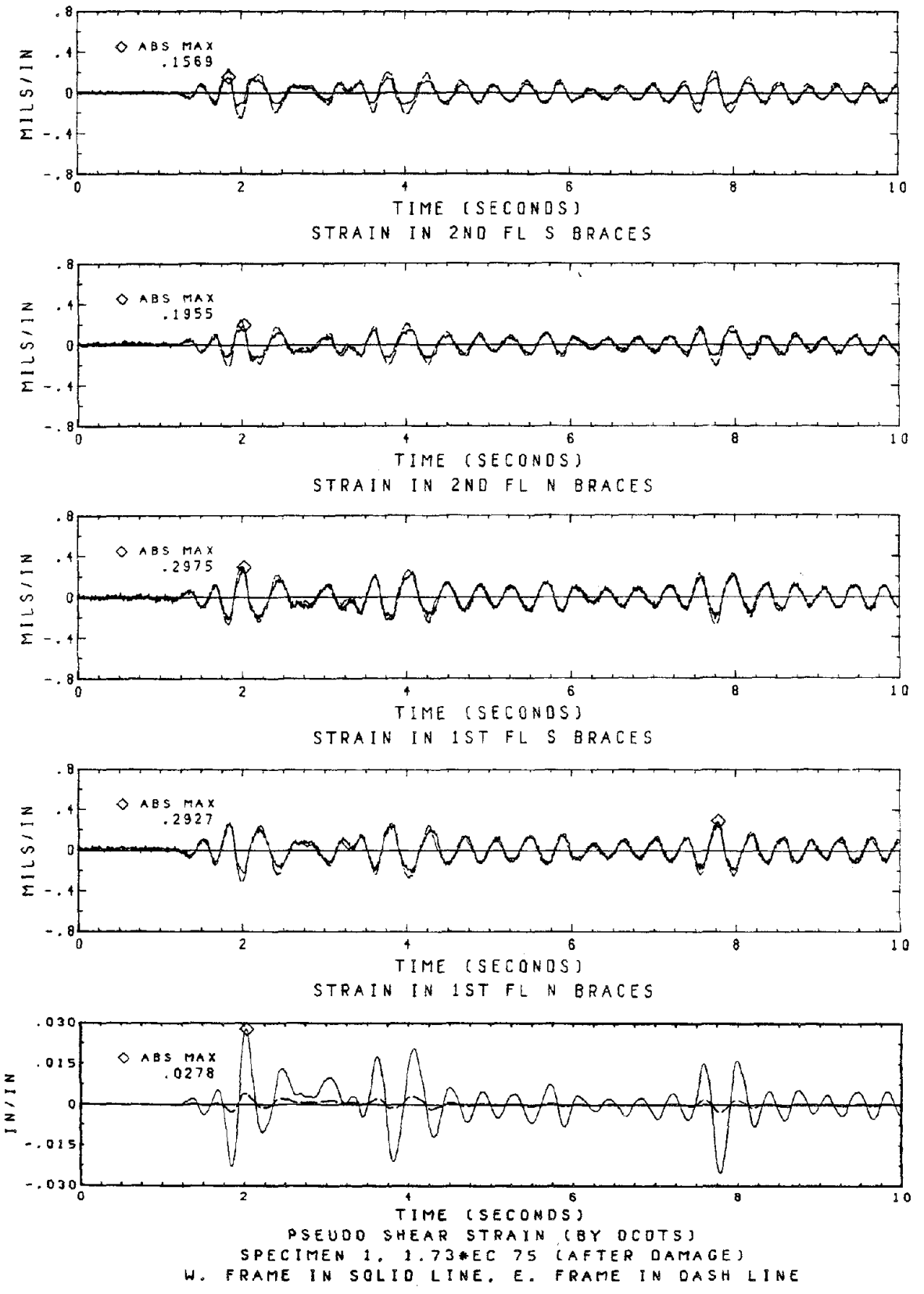

Fig. 76 Brace Strains and Pseudo Shear Strain

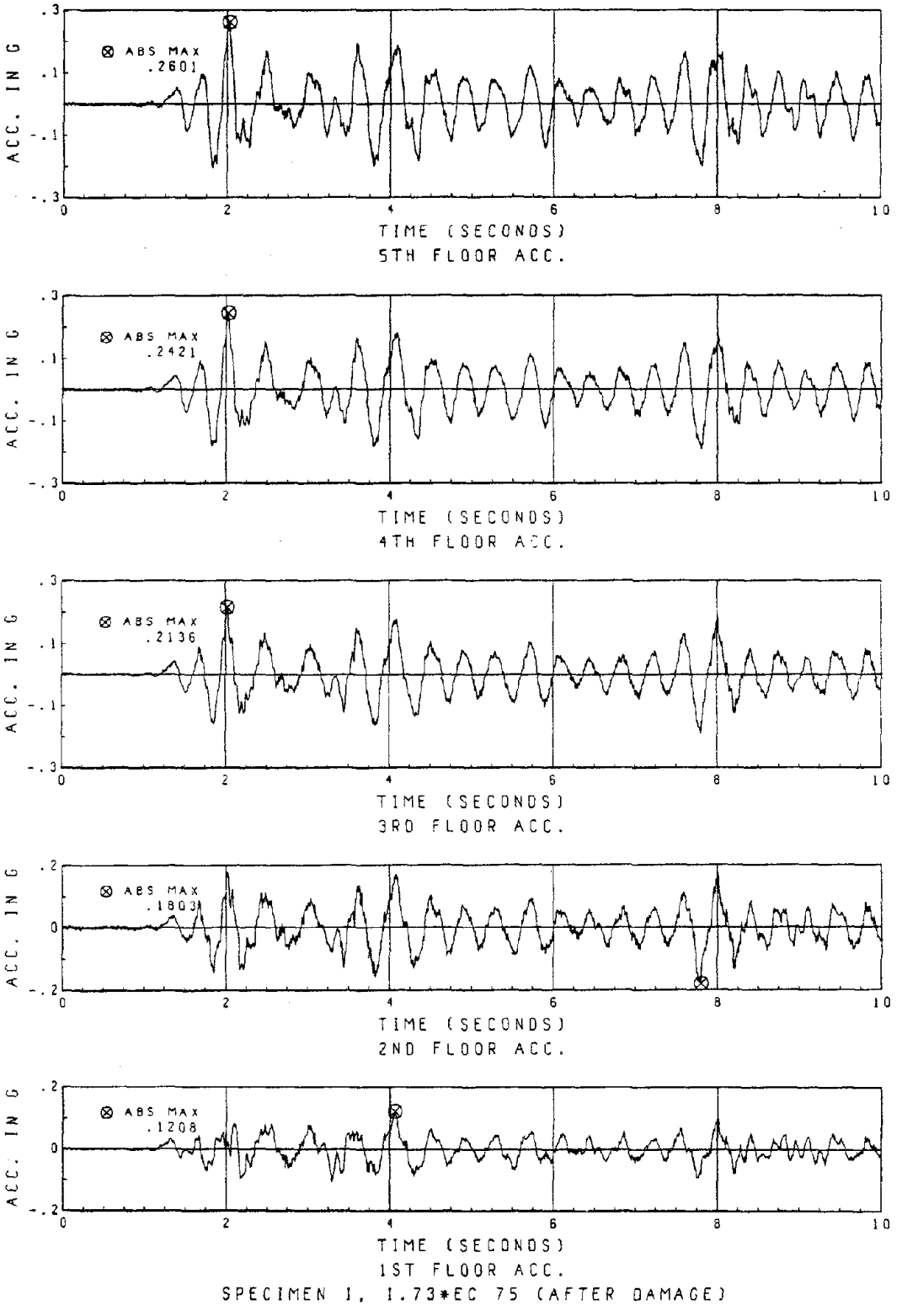

Fig. 77 Floor Accelerations

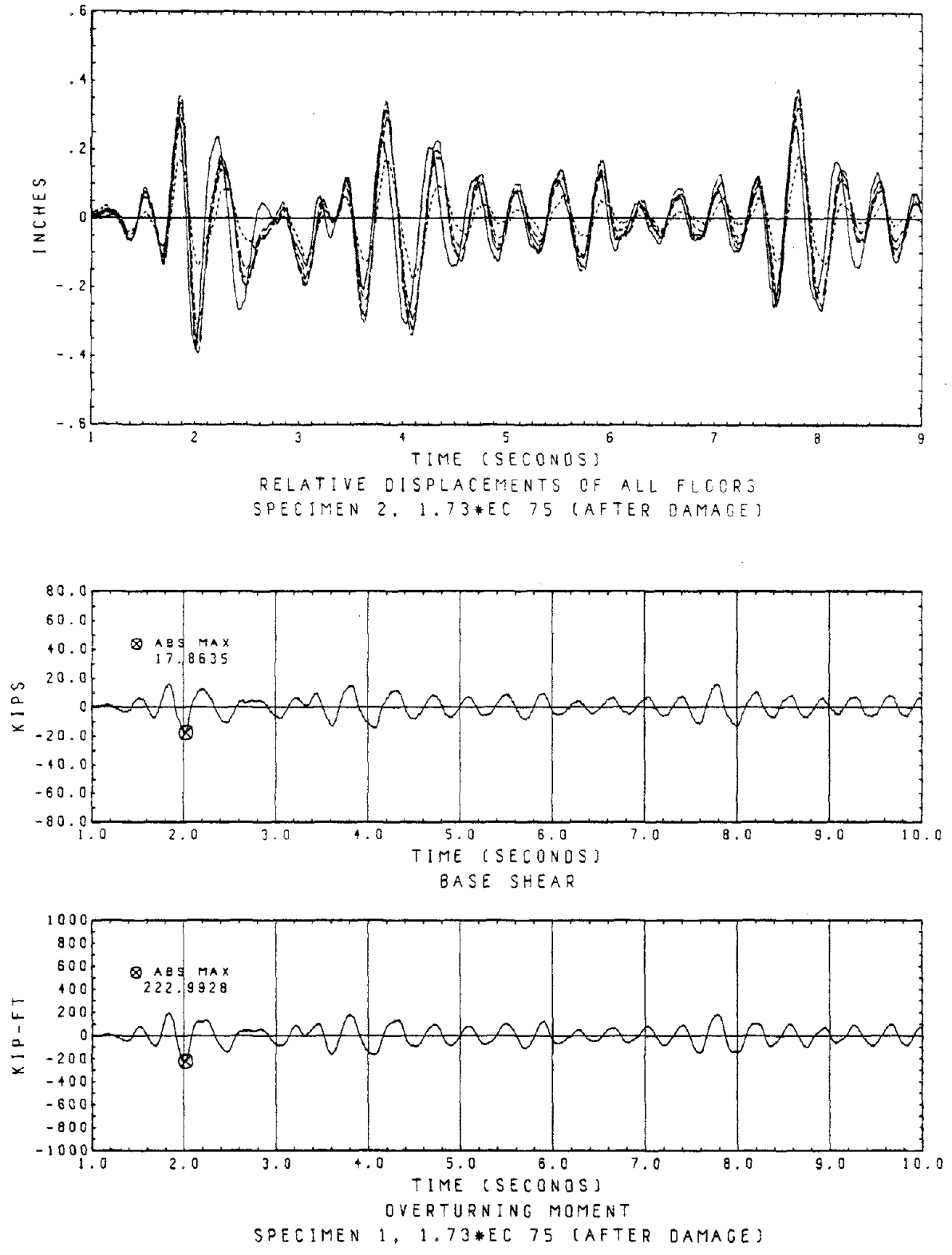

Fig. 78 Floor Displacements, Base Shear and Overturning Moment

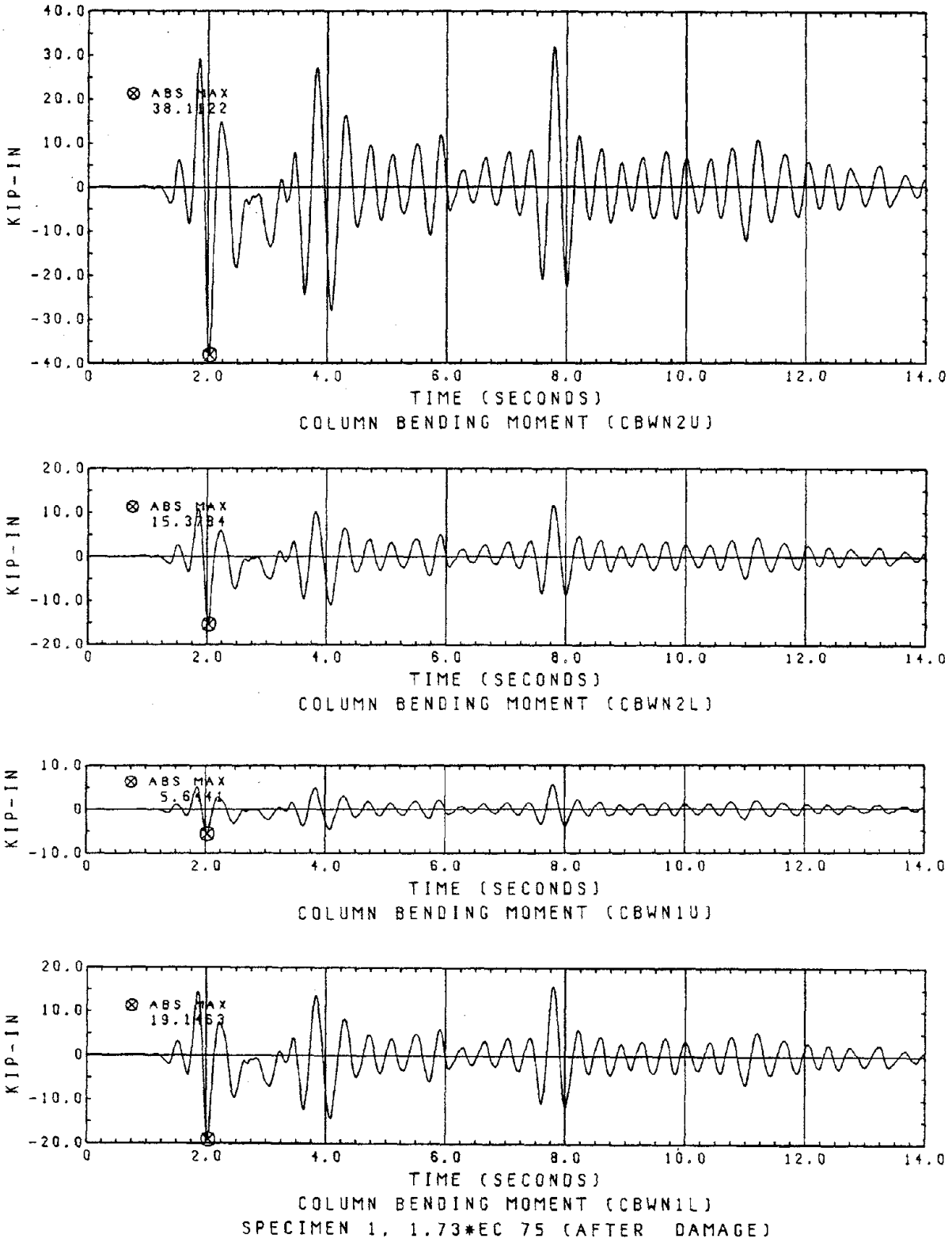

Fig. 79 Column Bending Moments

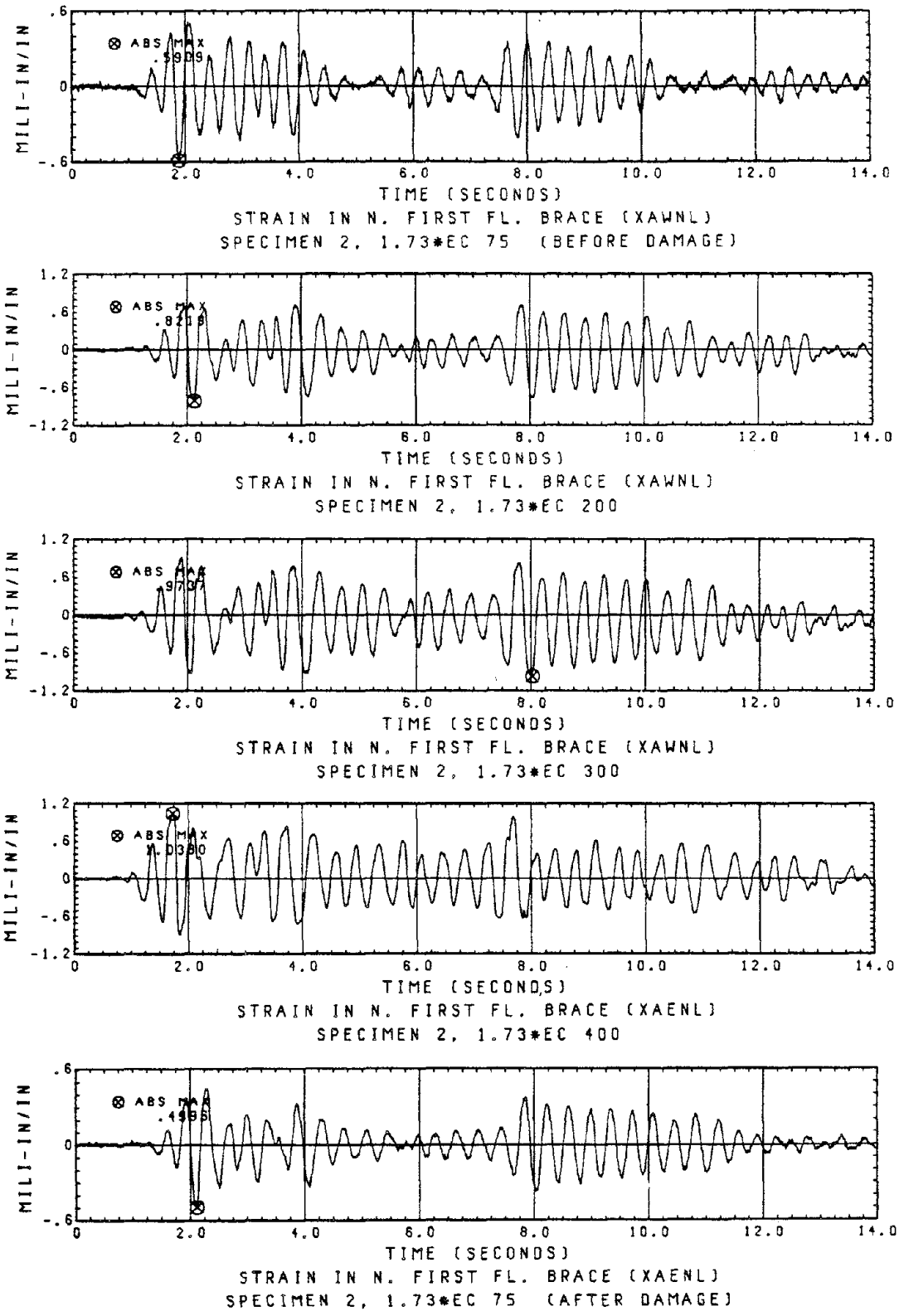

Fig. 80 Strains in the North First-Story Brace in Selected Tests of Specimen 2

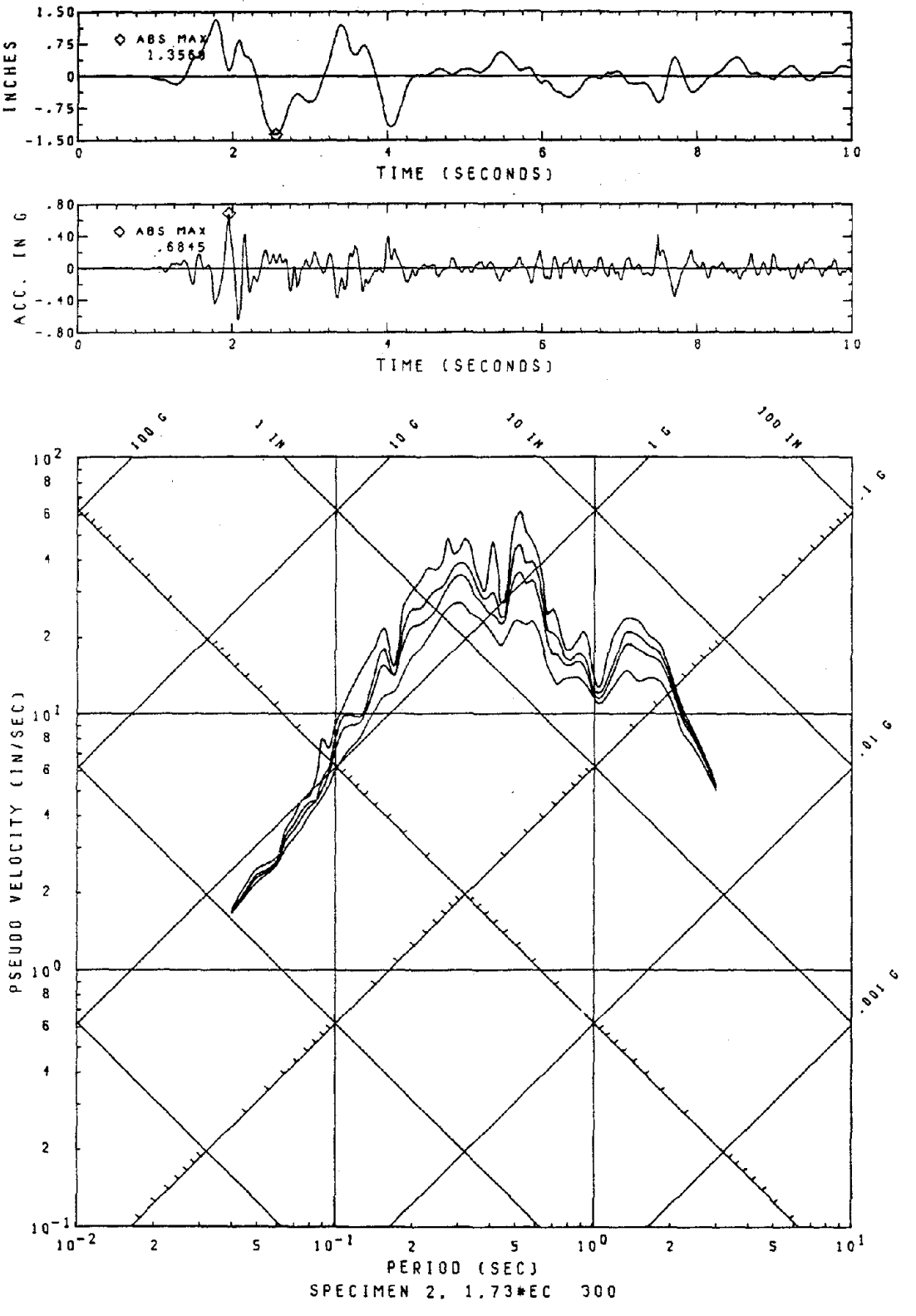

Fig. 81 Displacement, Acceleration of Table Motion 1.73*EC 300 and Its Response Spectra (Damping Ratios = 0.01, 0.03, 0.05, 0.10)

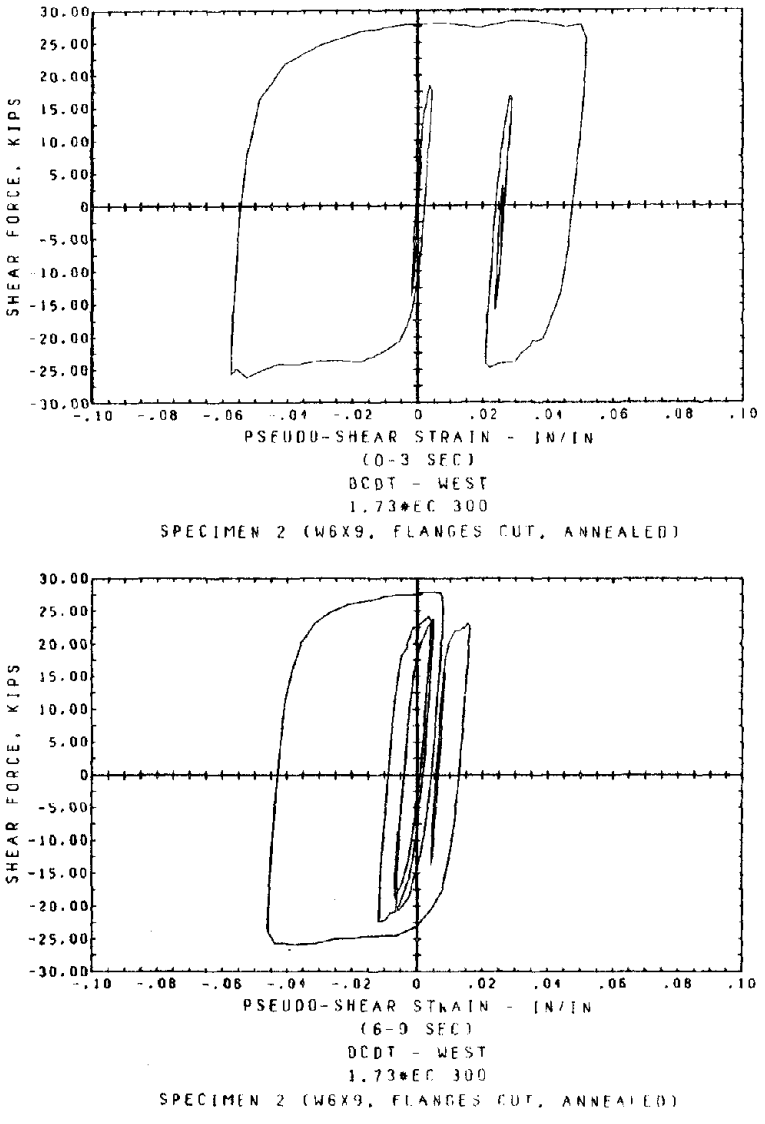

Fig. 82 Shear Link Hysteresis: Link Shear Force vs. Pseudo-Shear Strain

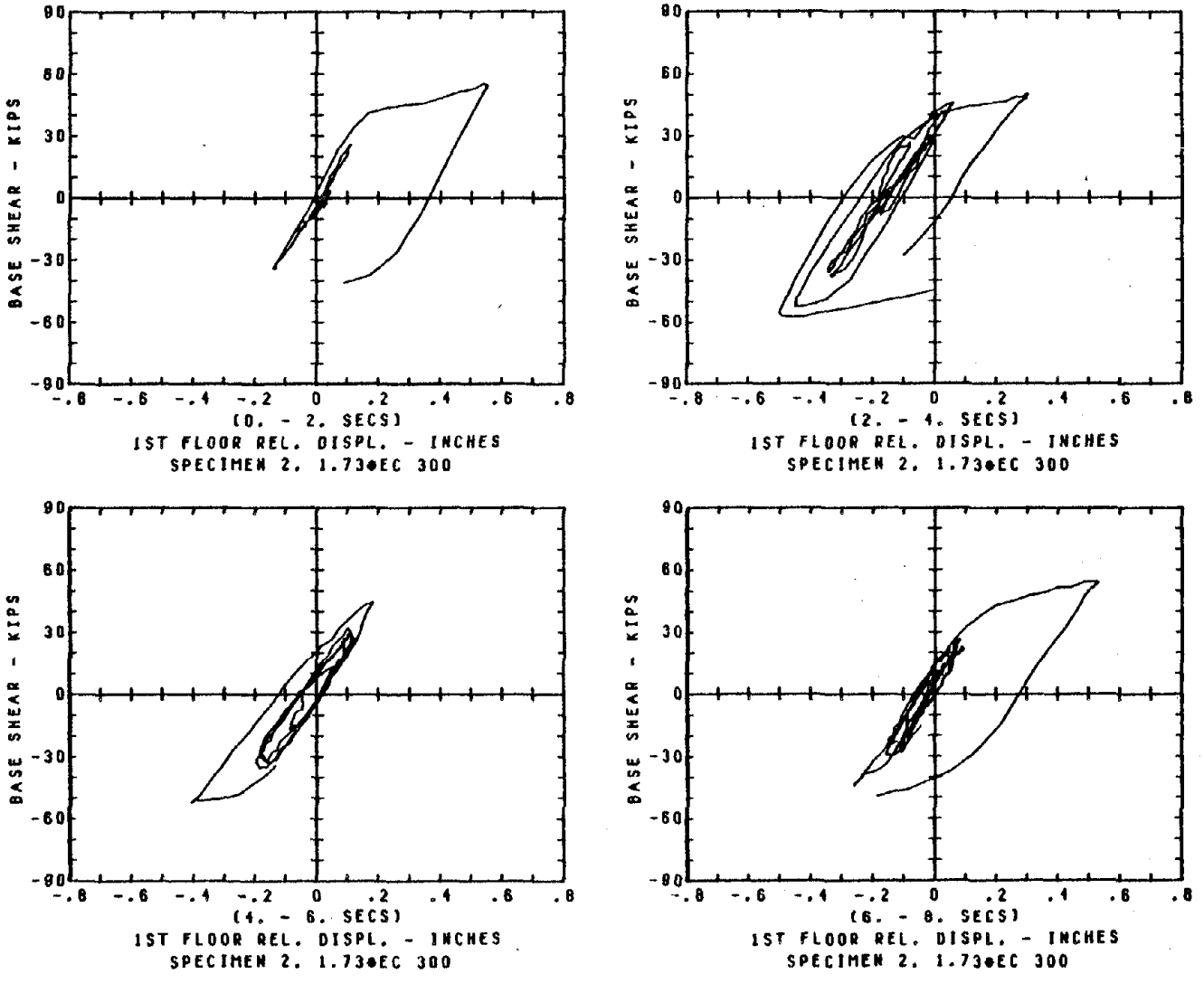

Fig. 83 Structural Hysteresis: Base Shear vs. First Story Drift

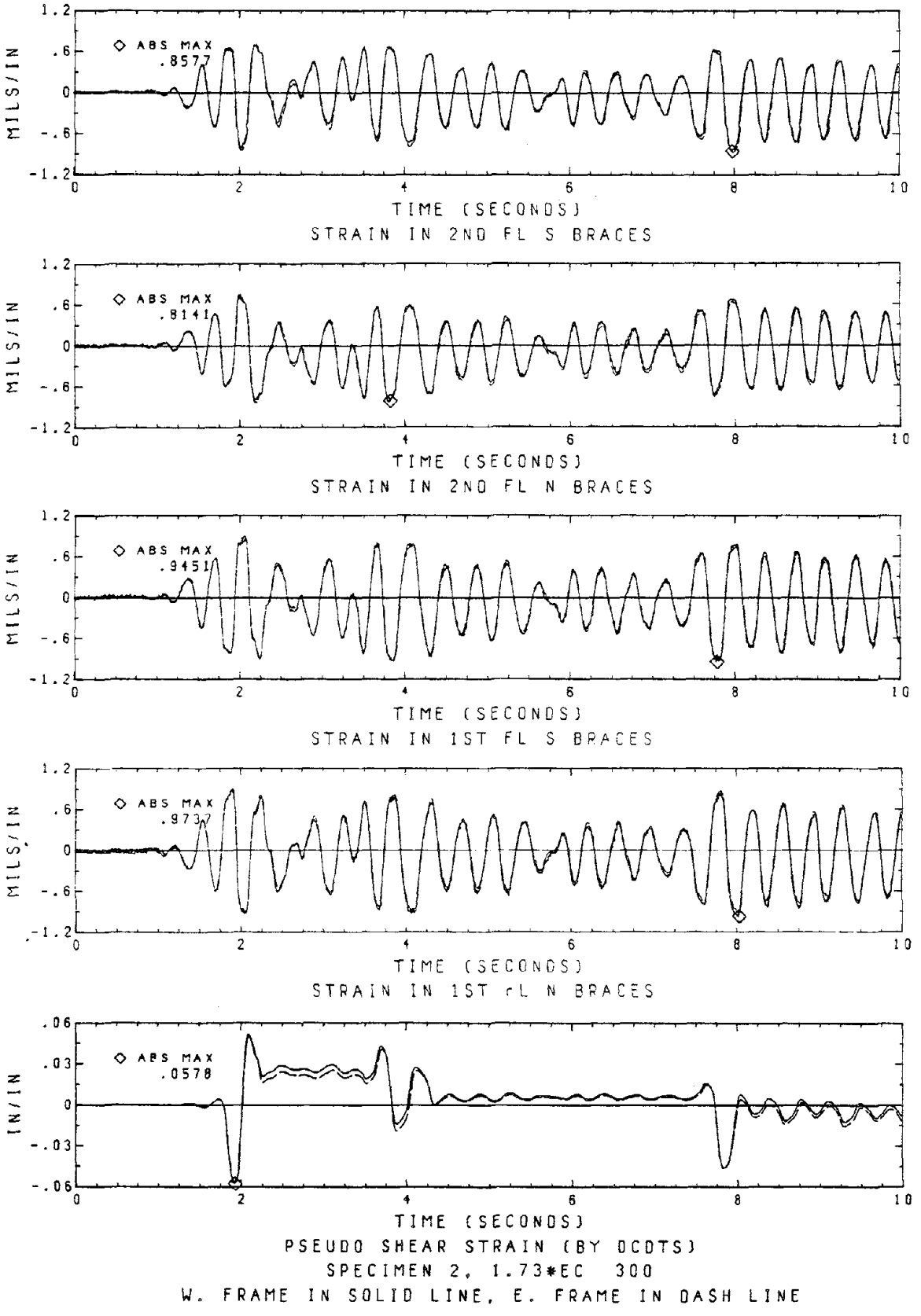

Fig. 84 Brace Strains and Pseudo Shear Strain

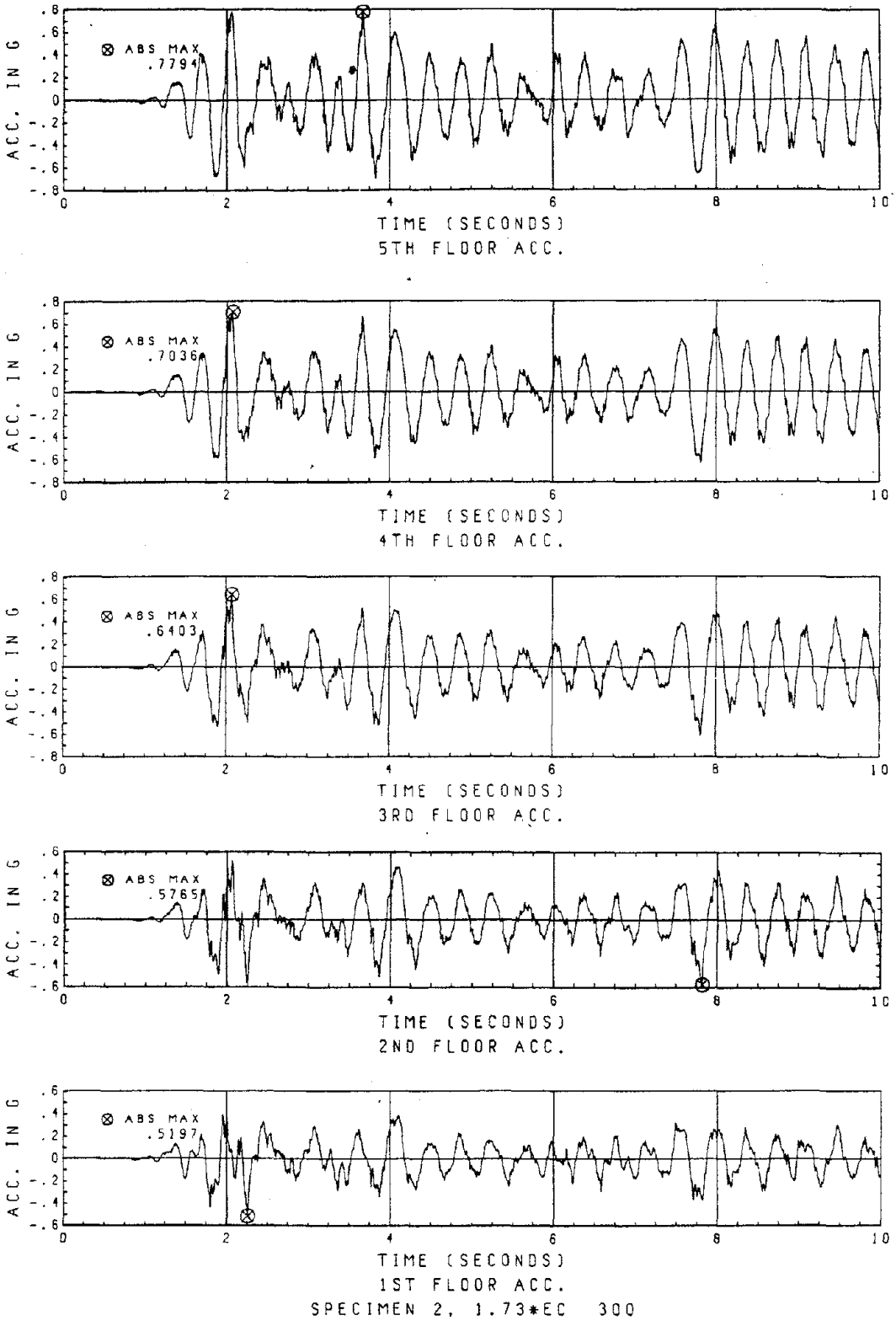

Fig. 85 Floor Accelerations

Reproduced from best available copy.

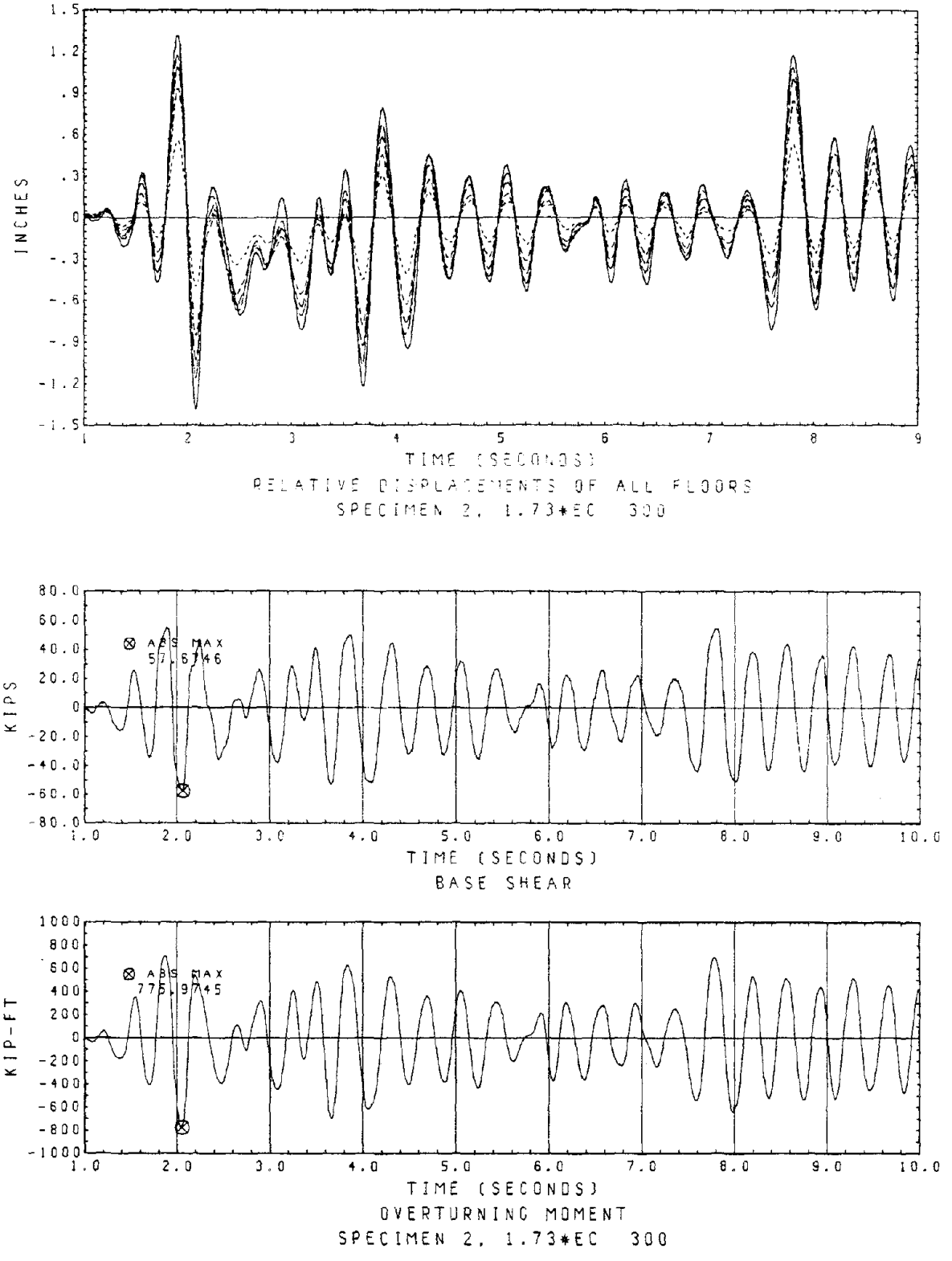

Fig. 86 Floor Displacements, Base Shear and Overturning Moment

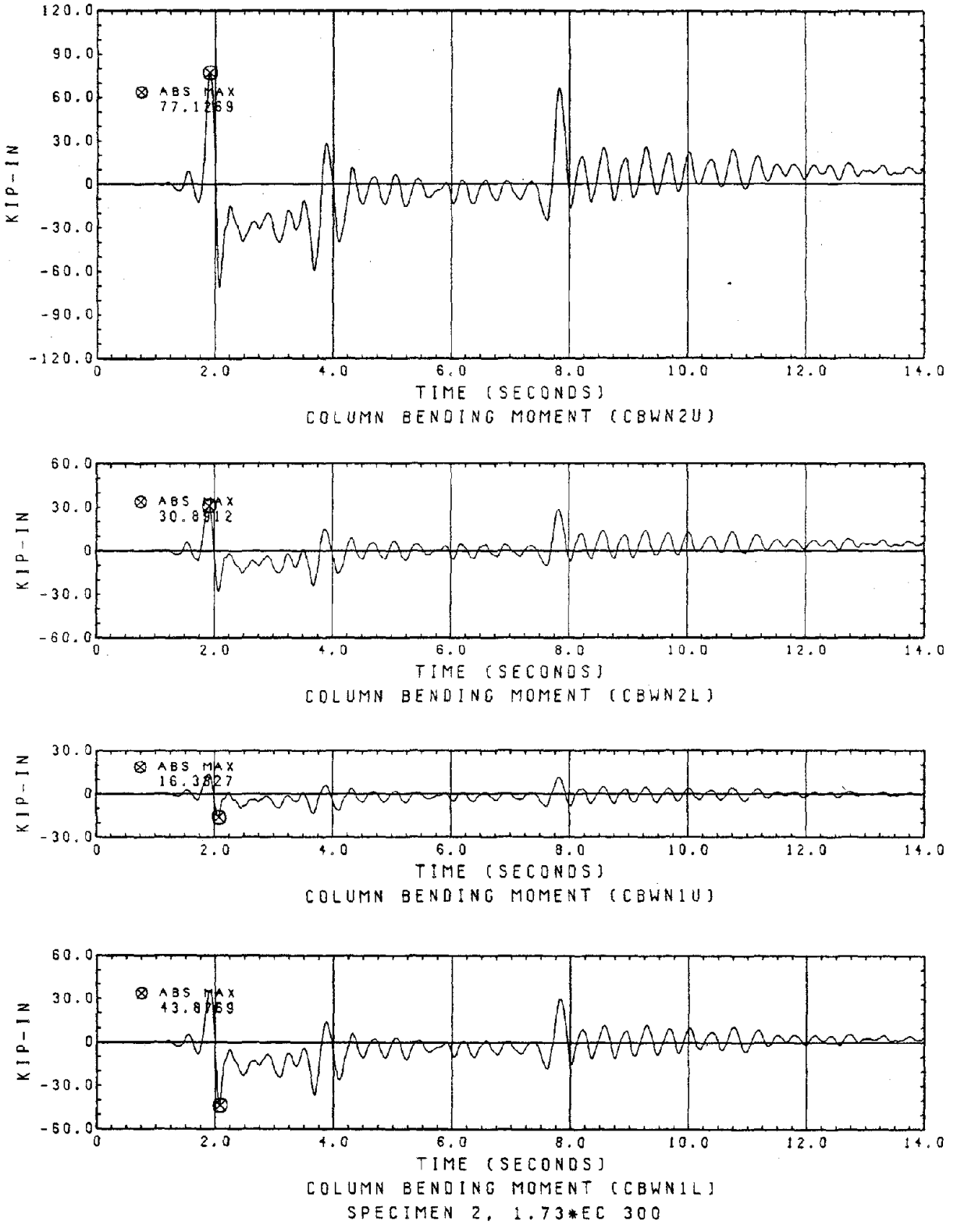

Fig. 87 Column Bending Moments

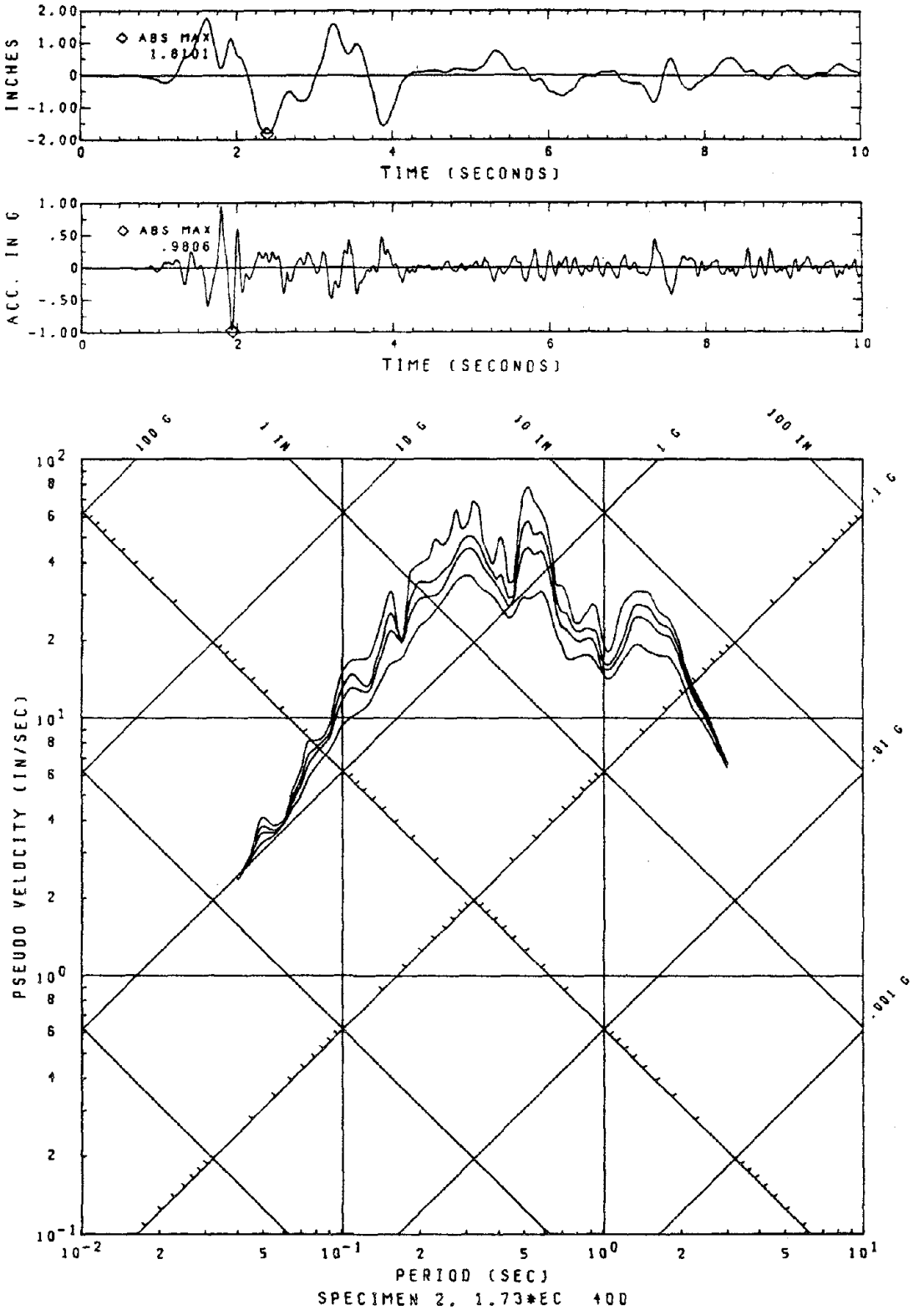

Fig. 88 Displacement, Acceleration of Table Motion 1.73*EC 400 and Its Response Spectra (Damping Ratios = 0.01, 0.03, 0.05, 0.10)

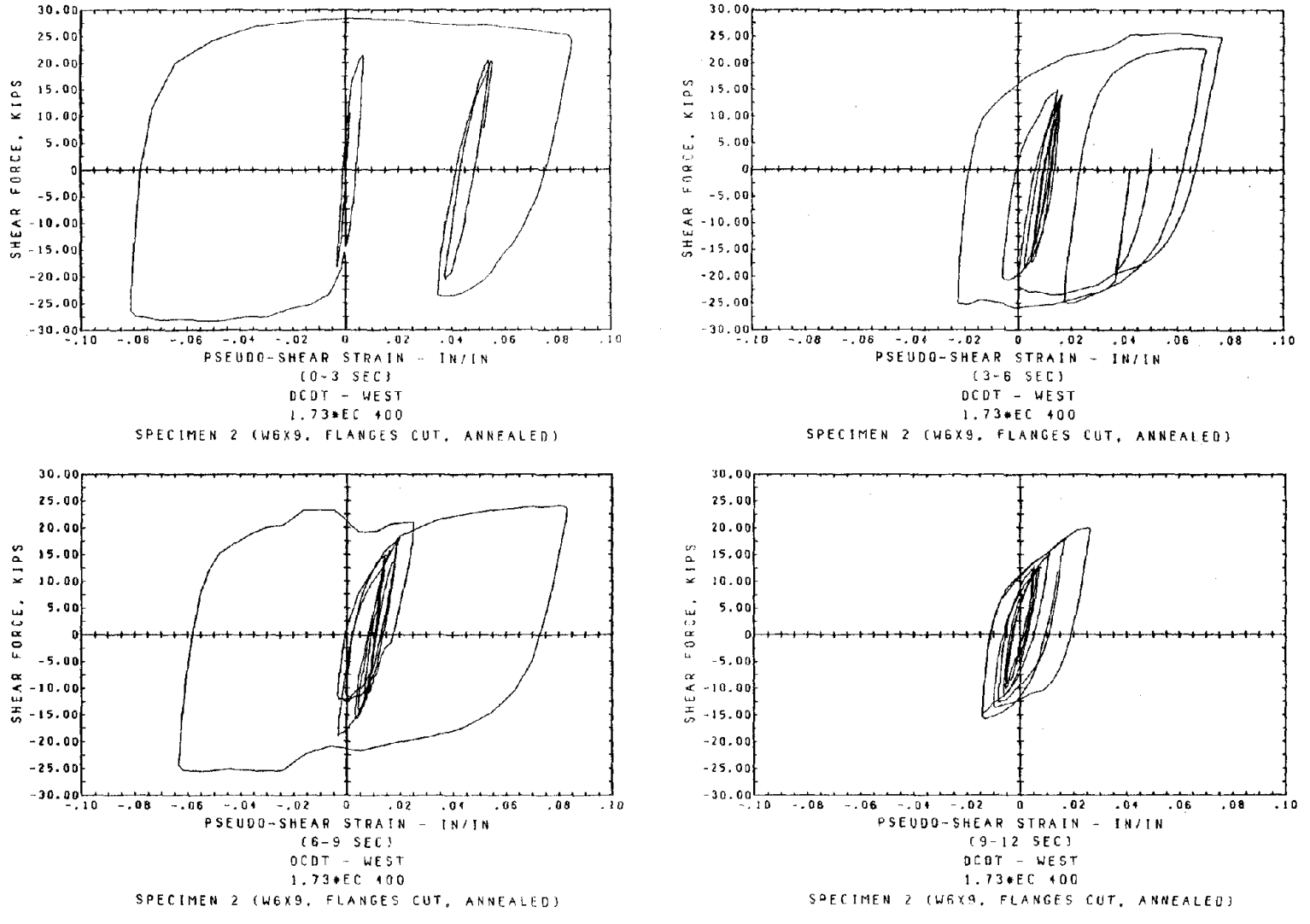

Fig. 89 Shear Link Hysteresis: Link Shear Force vs. Pseudo-Shear Strain

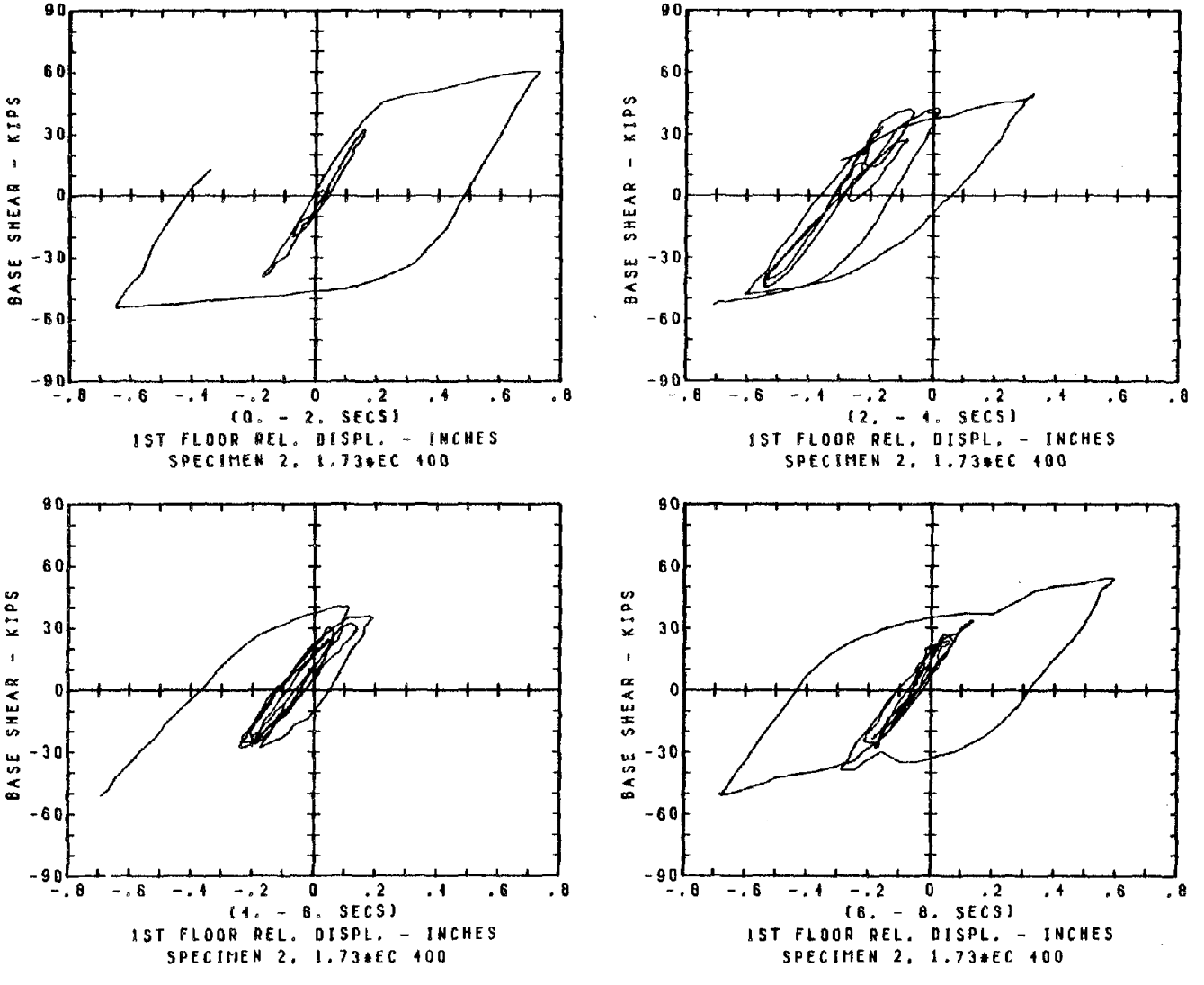

Fig. 90 Structural Hysteresis: Base Shear vs. First Story Drift

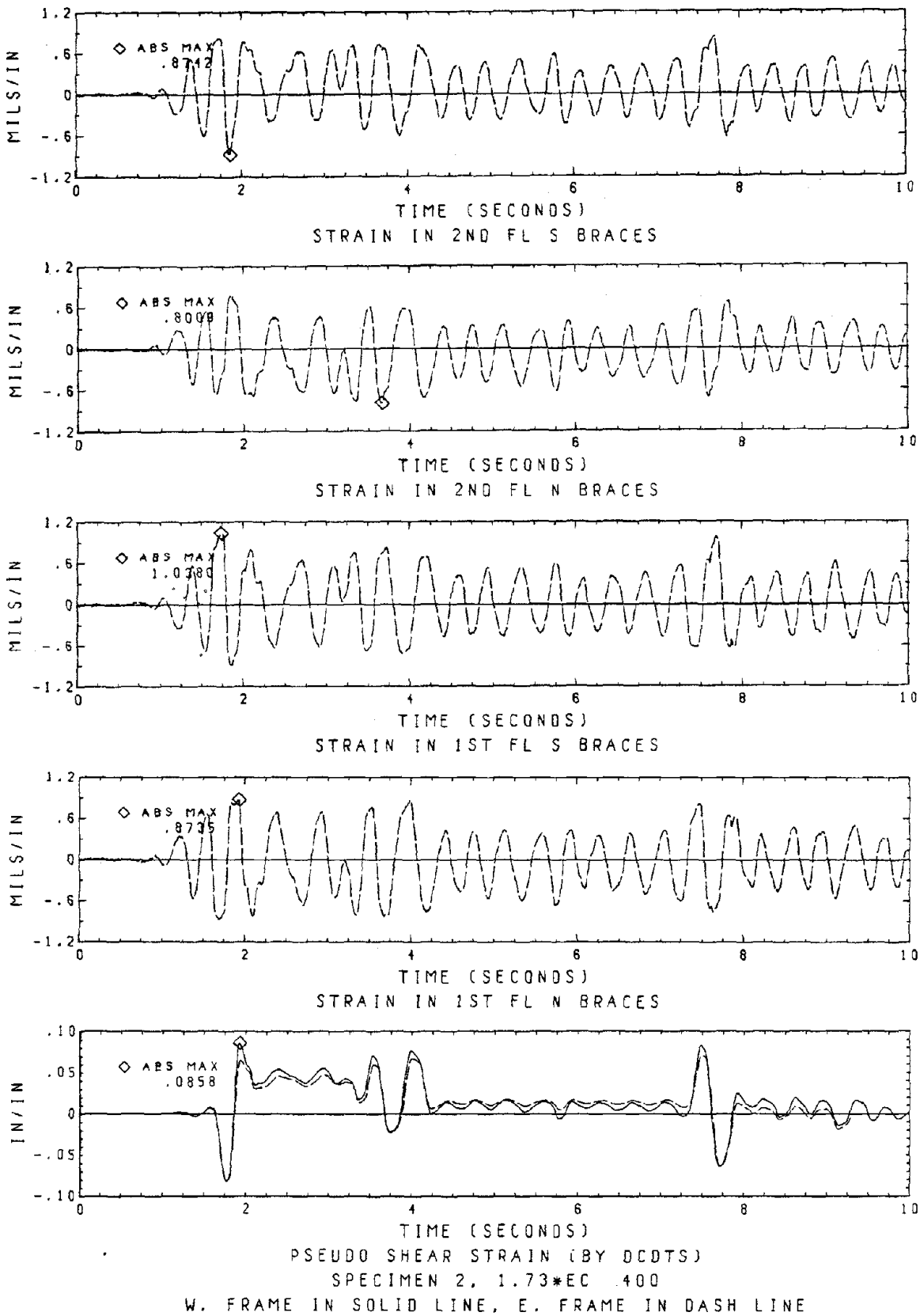

Fig. 91 Brace Strains and Pseudo Shear Strain

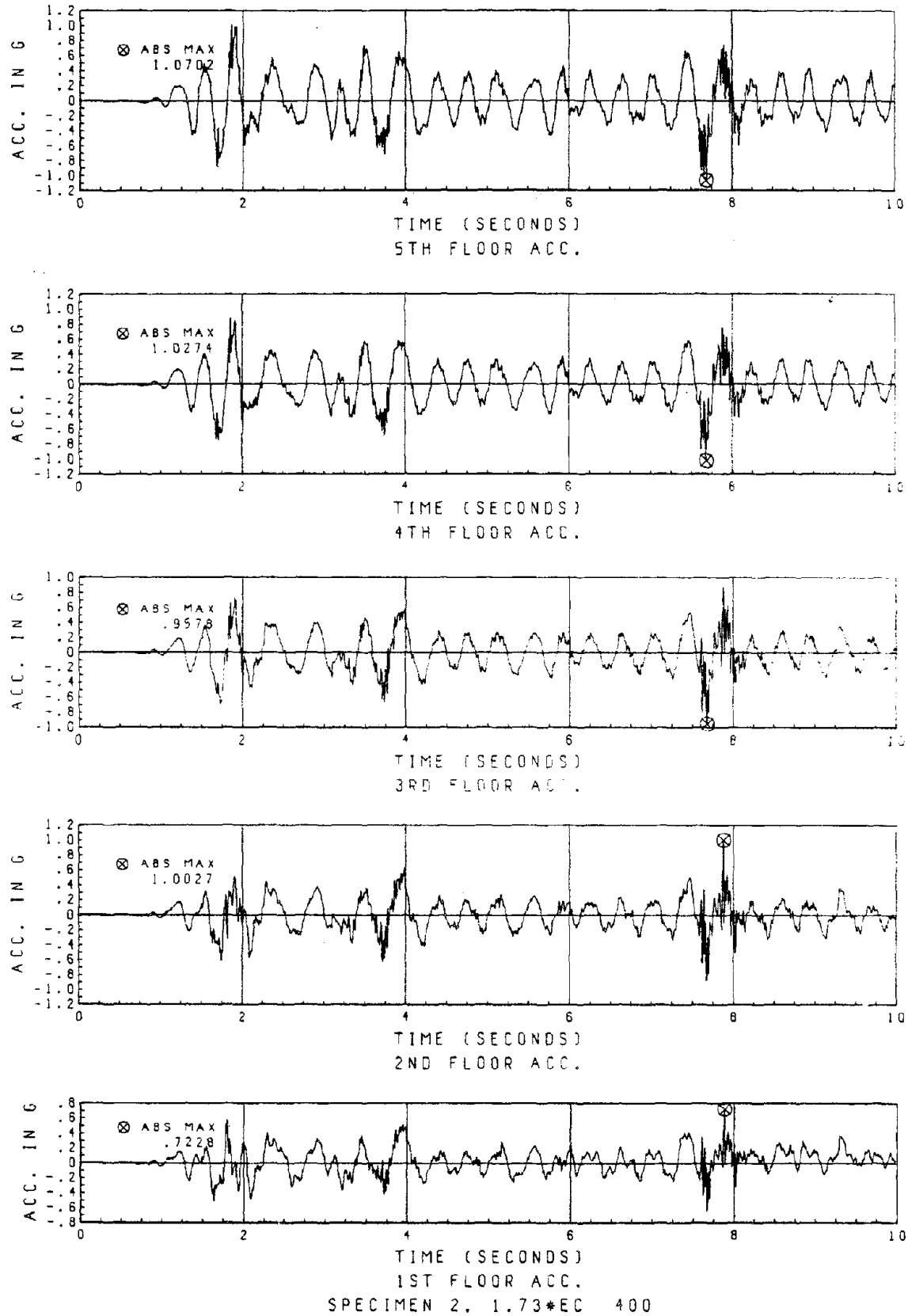

Fig. 92 Floor Accelerations

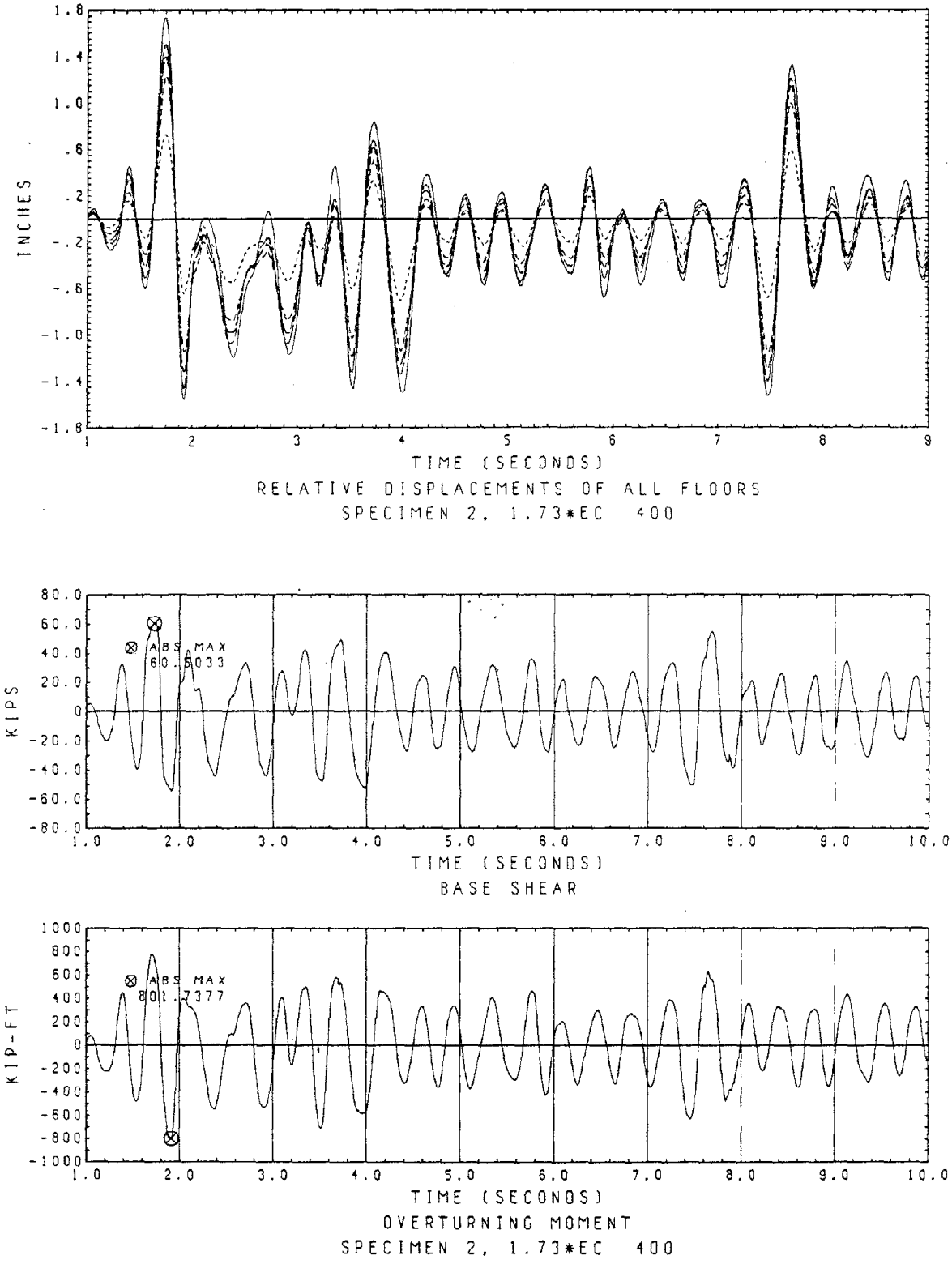

Fig. 93 Floor Displacements, Base Shear and Overturning Moment

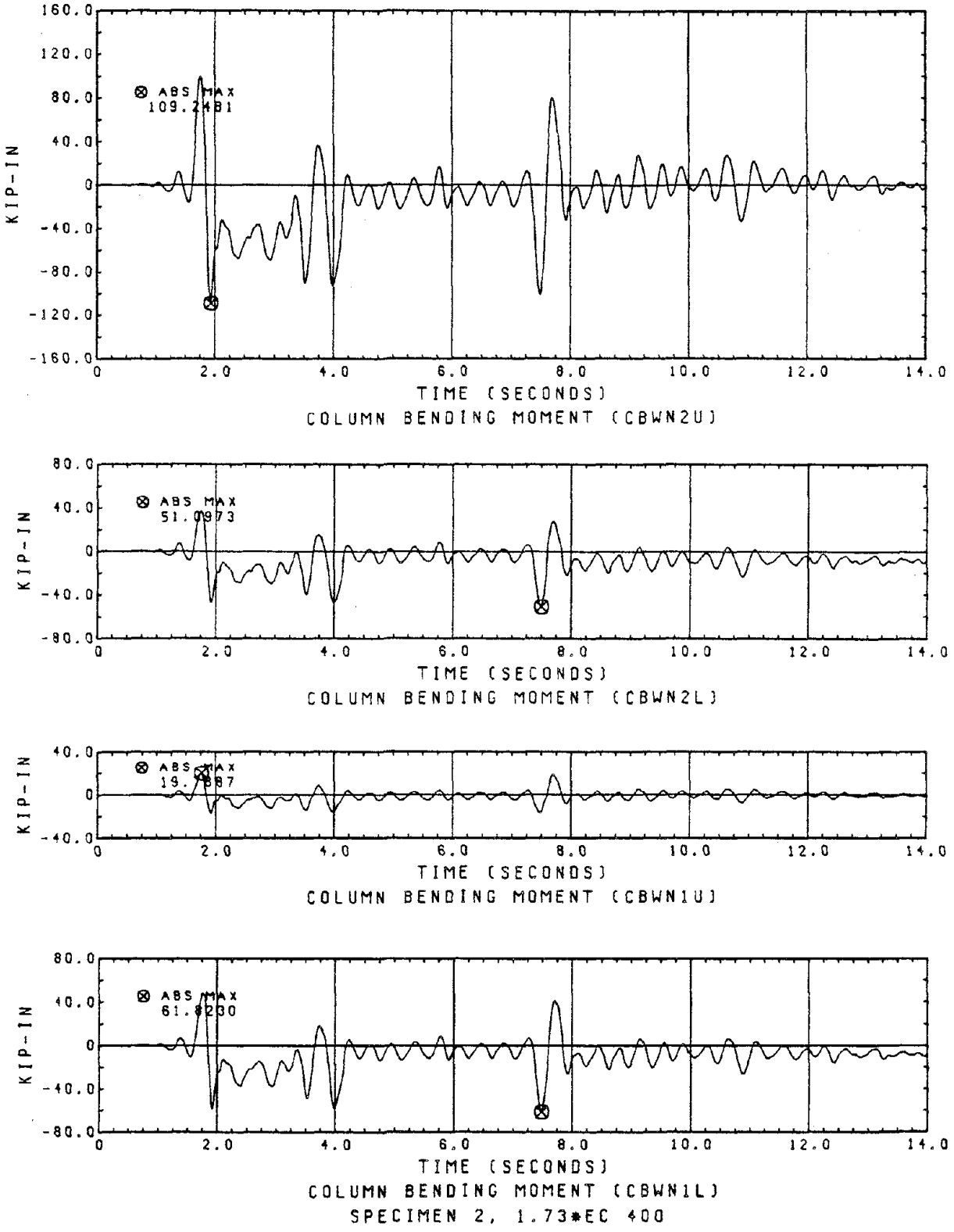

Fig. 94 Column Bending Moments

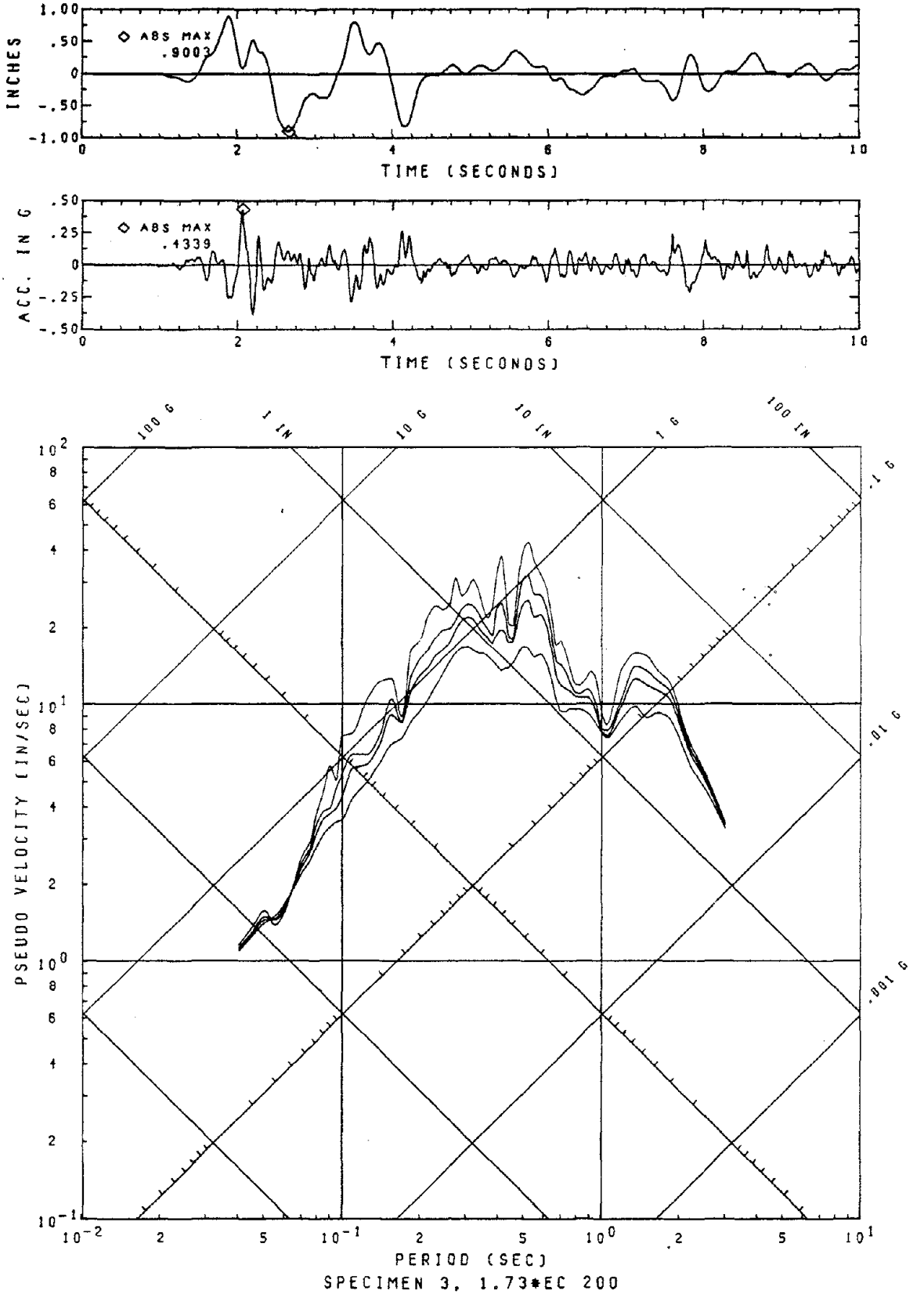

Fig. 95 Displacement, Acceleration of Table Motion 1.73*EC 200 and Its Response Spectra (Damping Ratios = 0.01, 0.03, 0.05, 0.10)

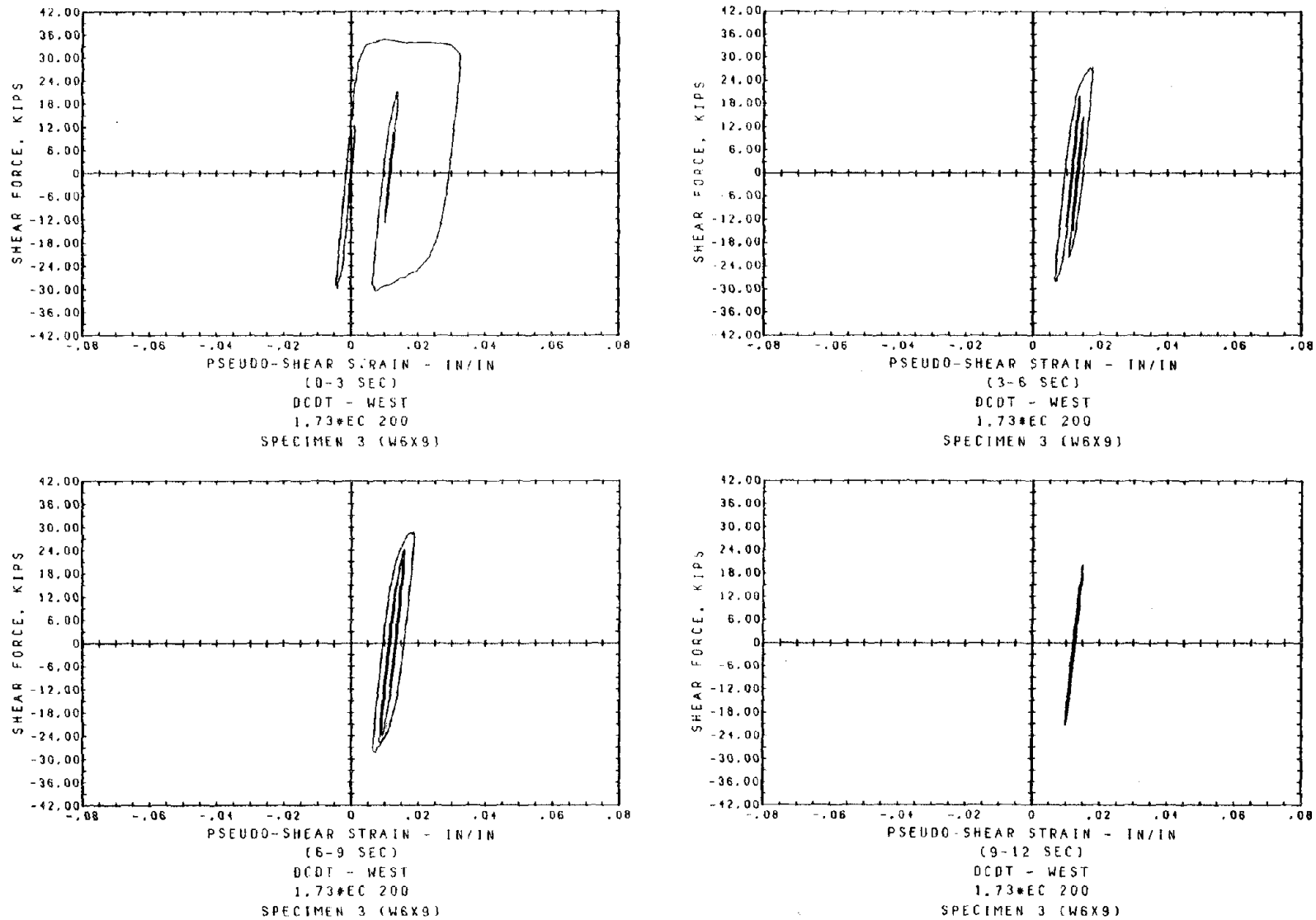

Fig. 96 Shear Link Hysteresis: Link Shear Force vs. Pseudo-Shear Strain

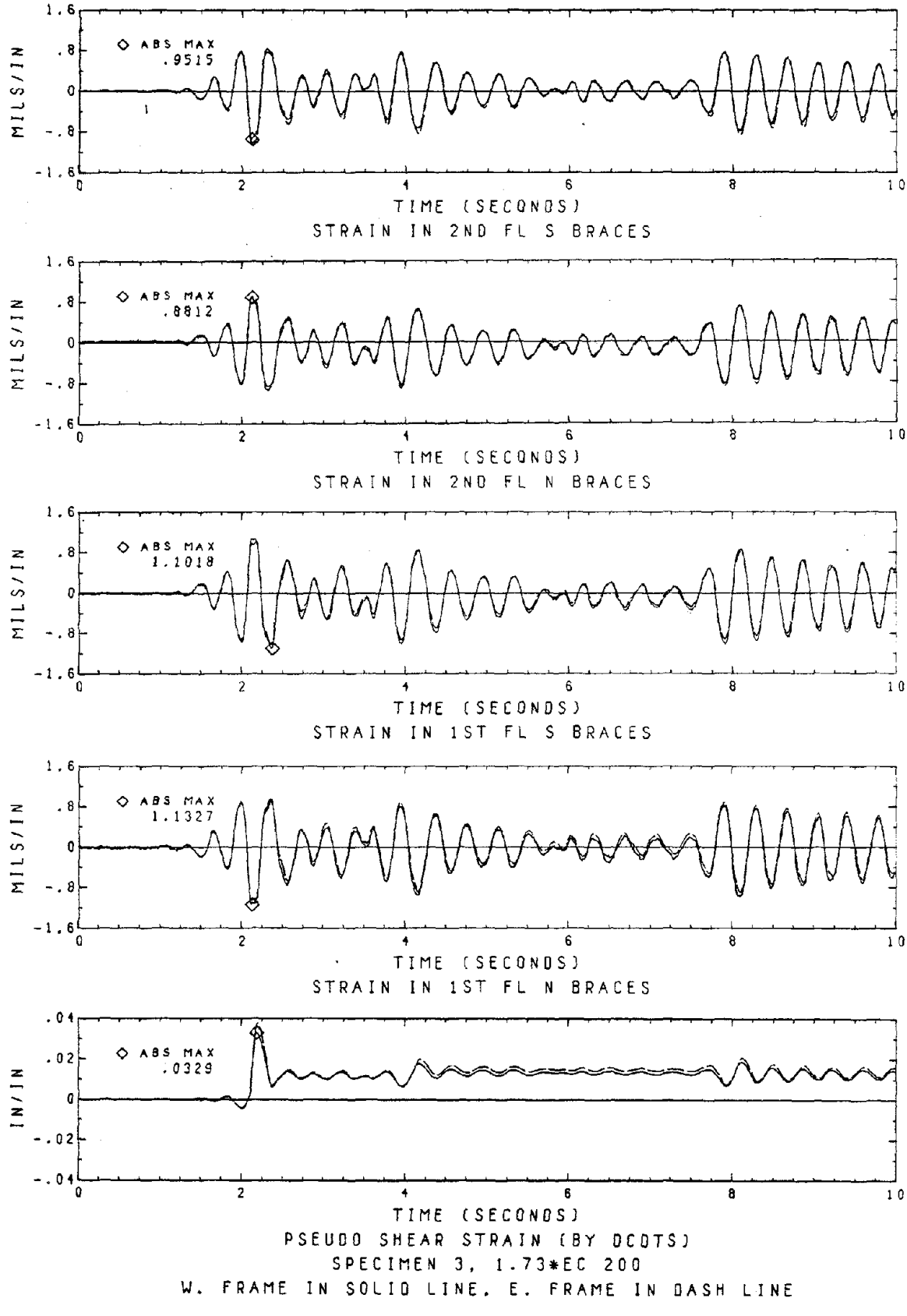

Fig. 97 Brace Strains and Pseudo Shear Strain

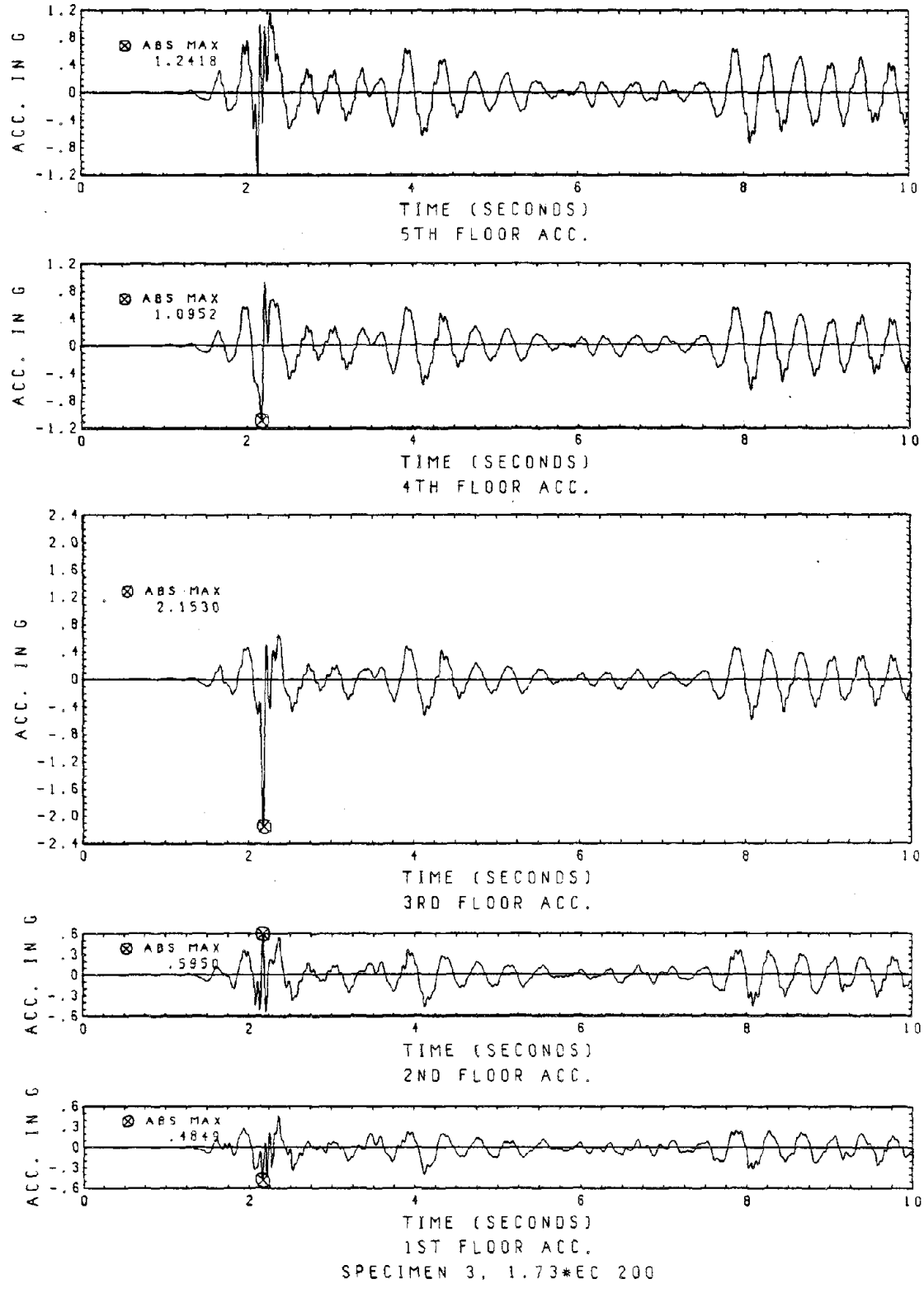

Fig. 98 Floor Accelerations

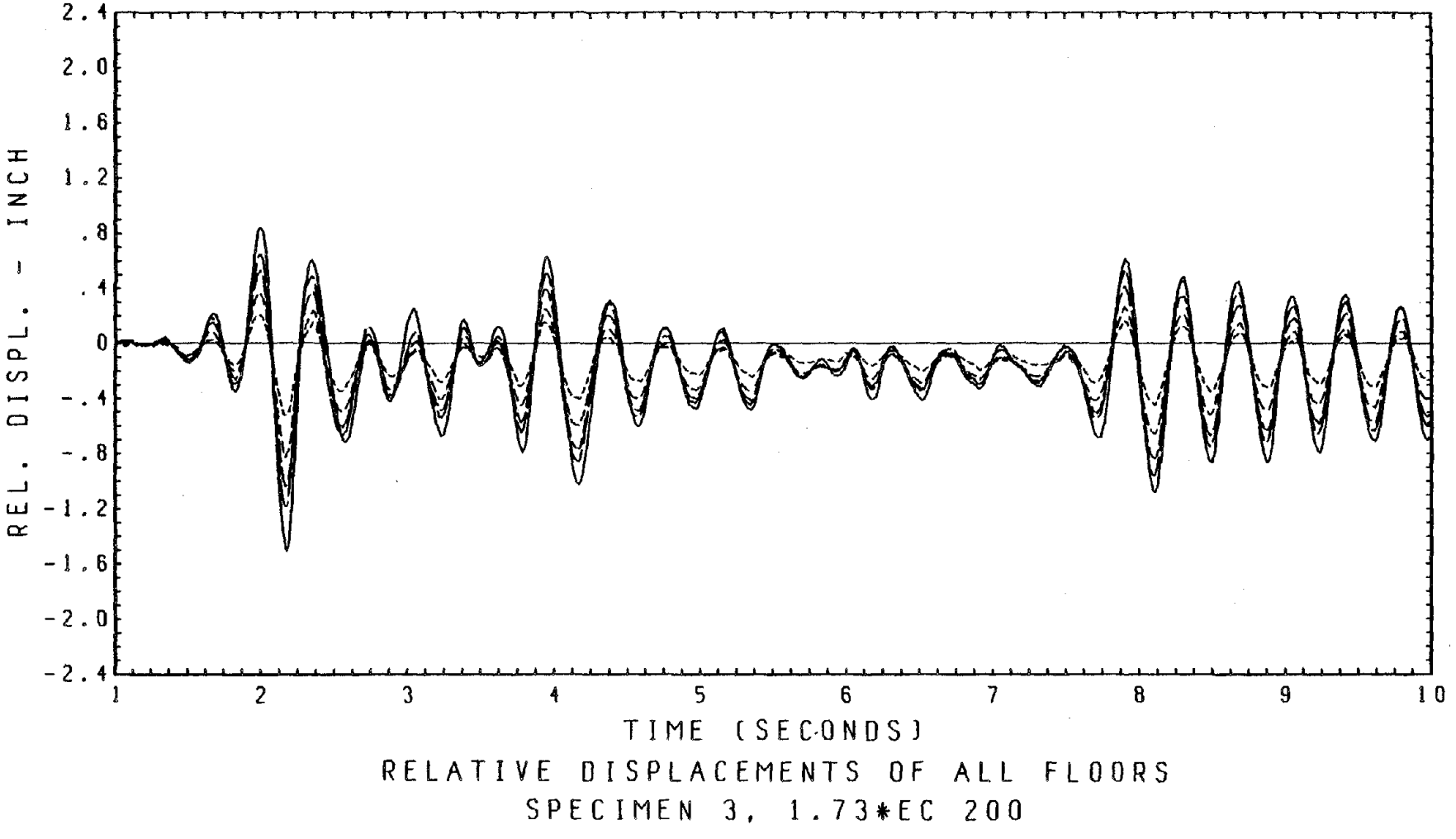

Fig. 99 Floor Displacements

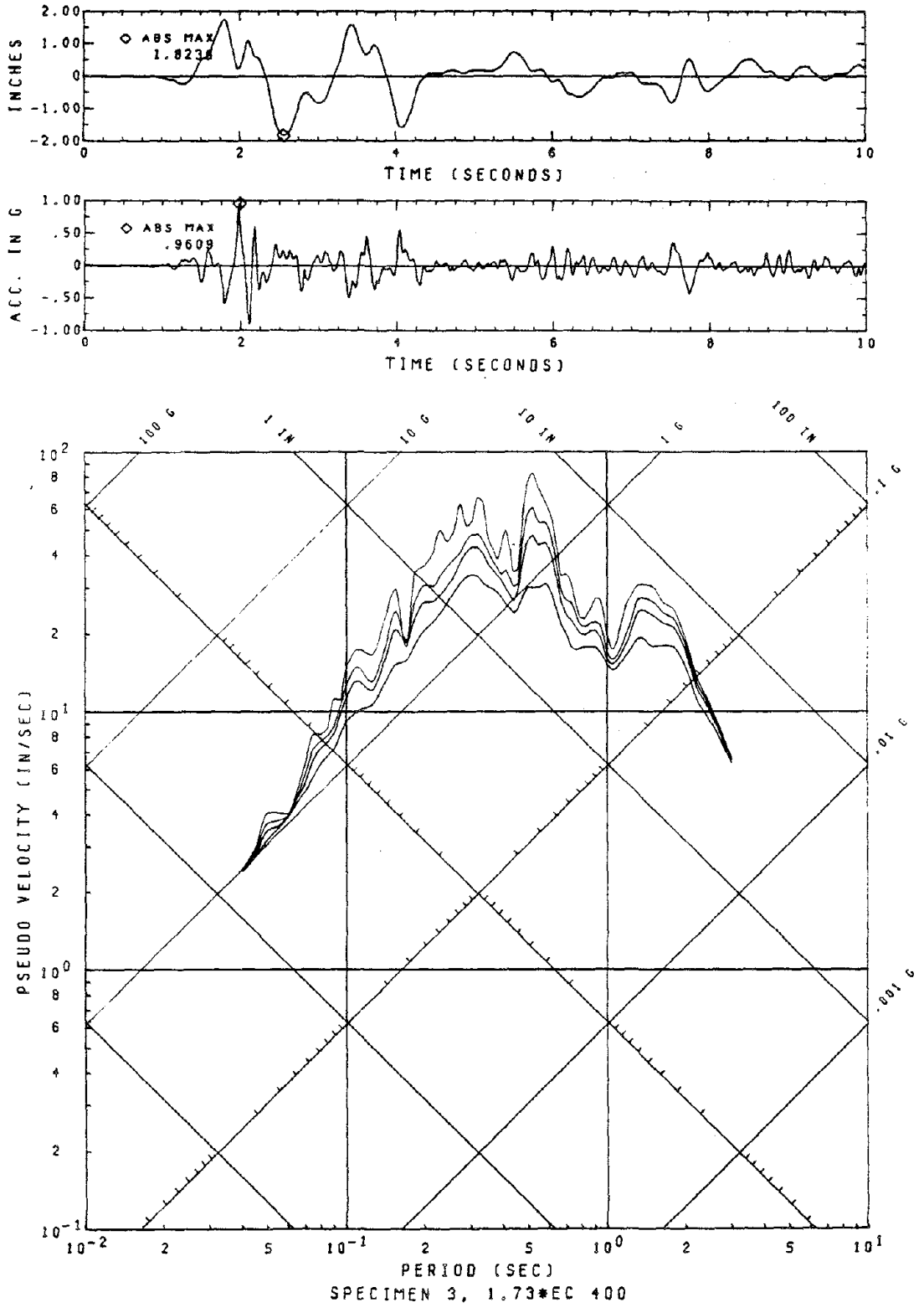

Fig. 100 Displacement, Acceleration of Table Motion 1.73*EC 400 and Its Response Spectra (Damping Ratios = 0.01, 0.03, 0.05, 0.10)

Reproduced from
best available copy.

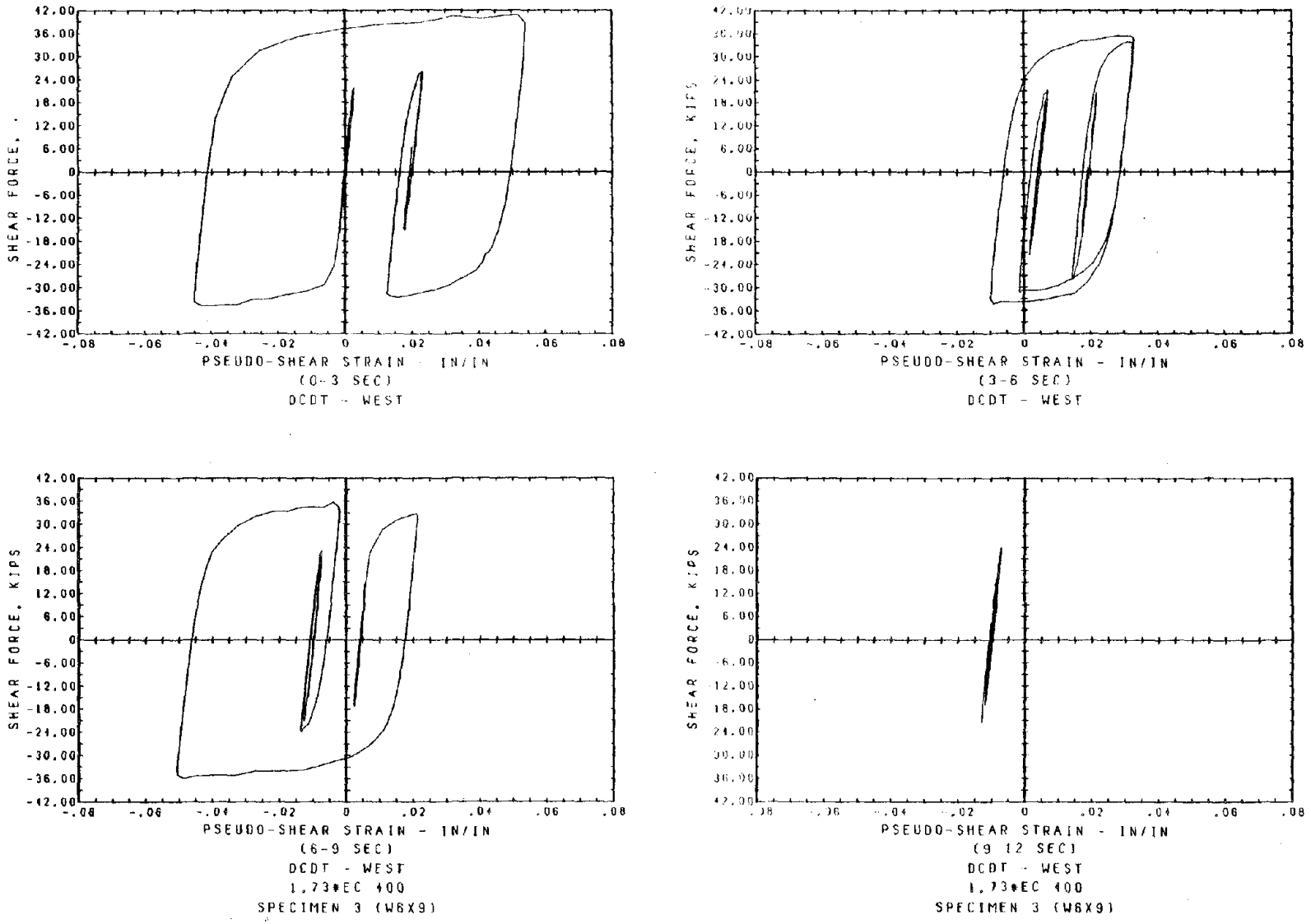

Fig. 101 Shear Link Hysteresis: Link Shear Force vs. Pseudo-Shear Strain

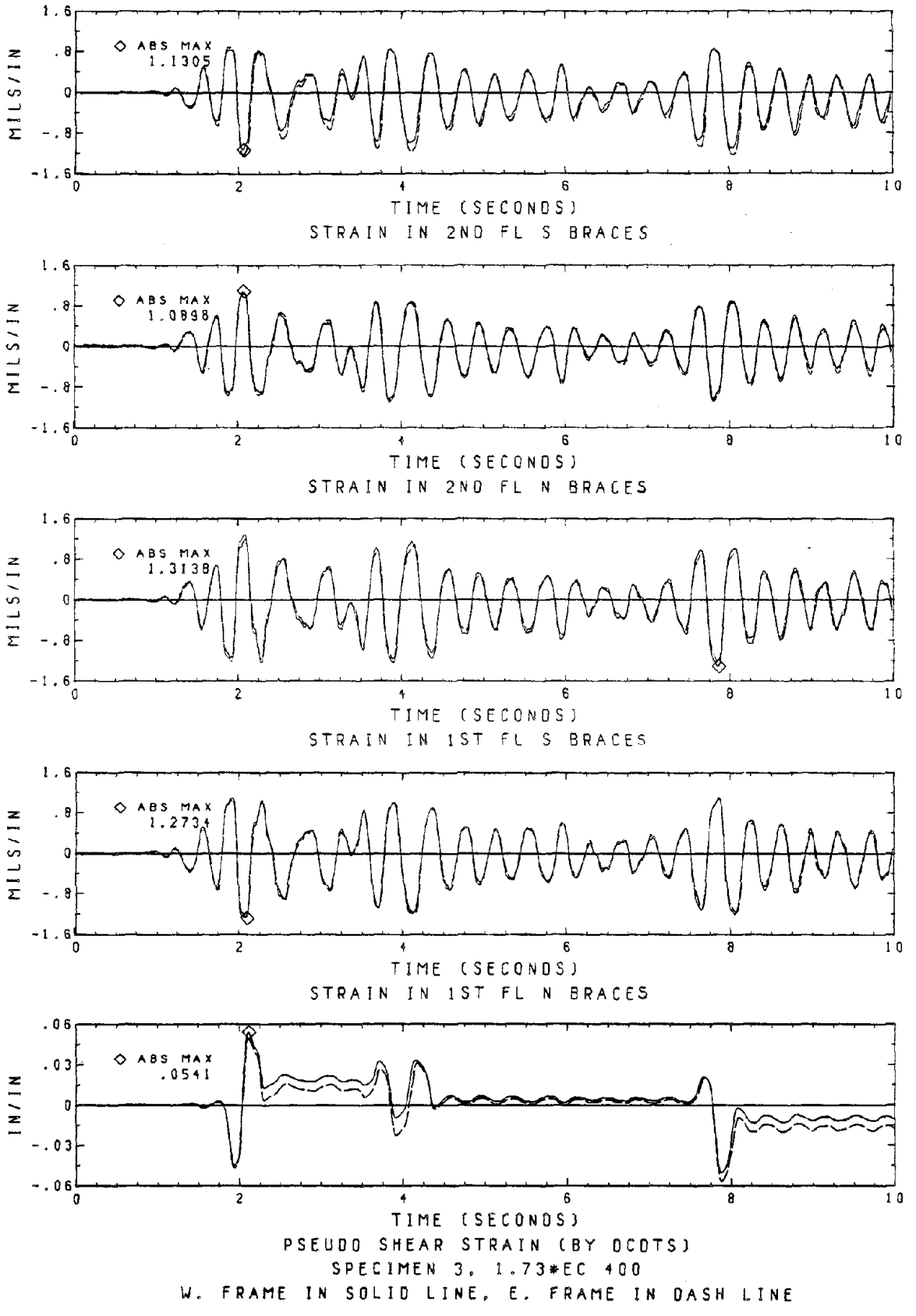

Fig. 102 Brace Strains and Pseudo Shear Strain

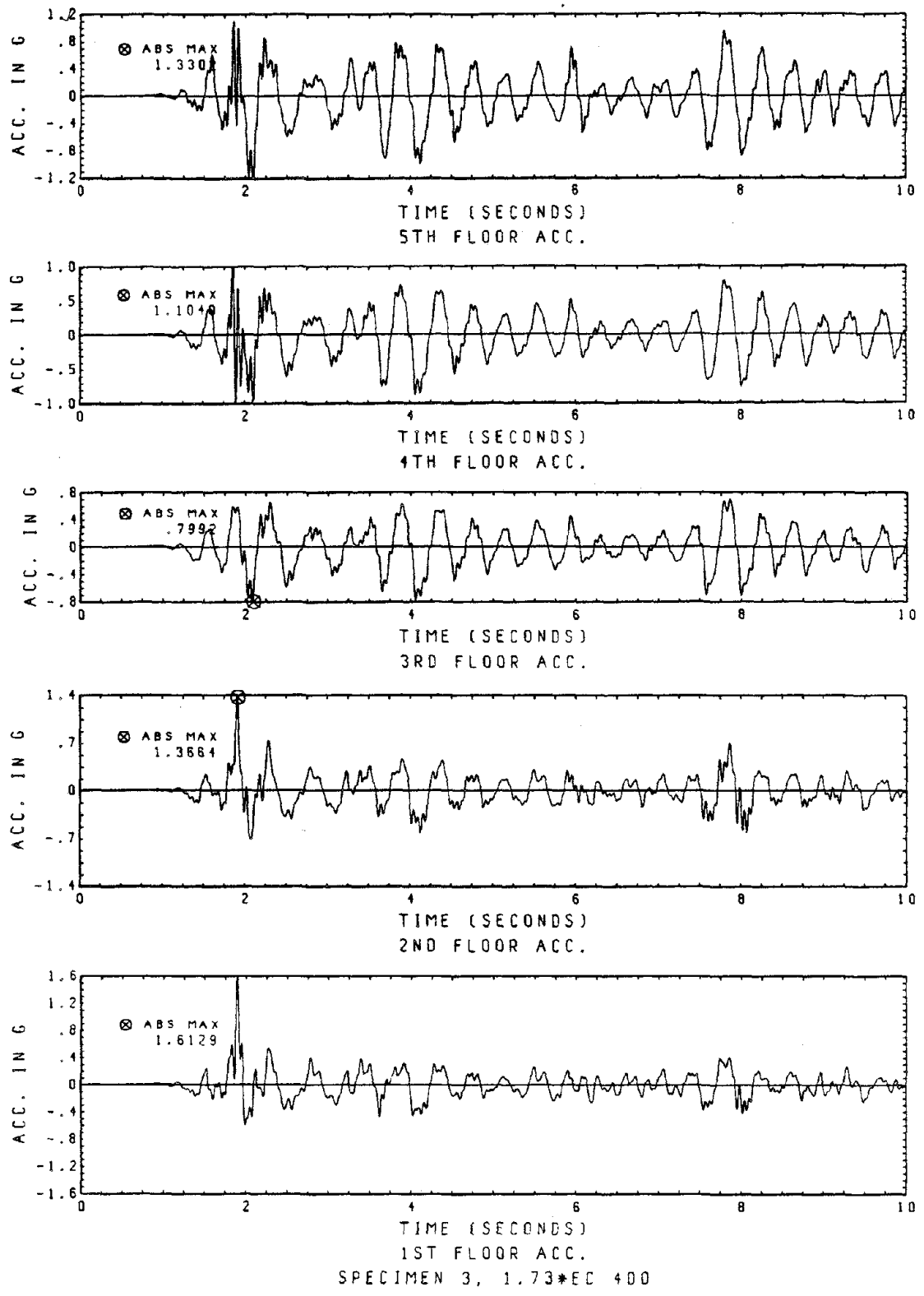

Fig. 103 Floor Accelerations

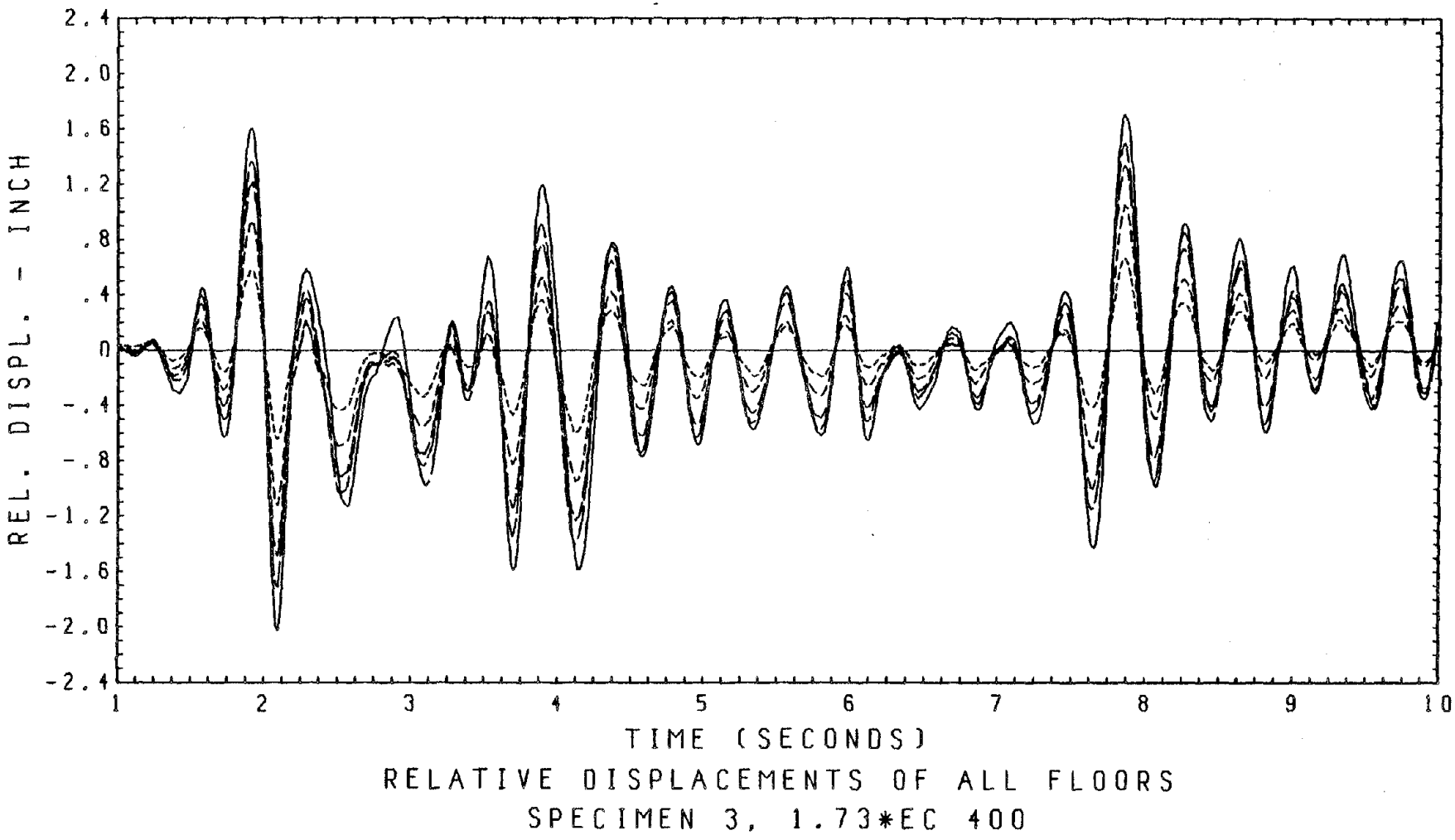

Fig. 104 Floor Displacements

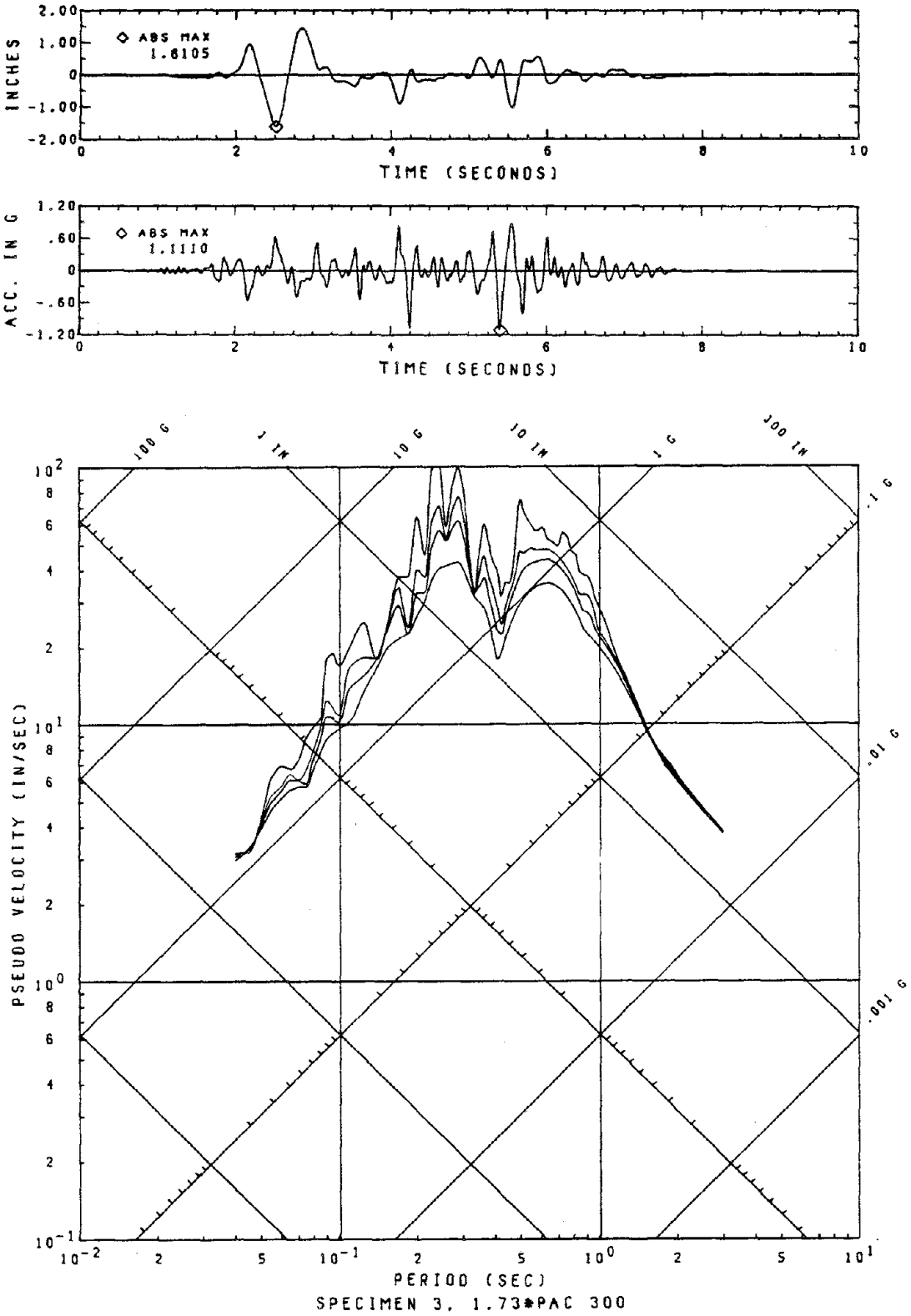

Fig. 105 Displacement, Acceleration of Table Motion 1.73*PAC300 and Its Response Spectra (Damping Ratios = 0.01, 0.03, 0.05, 0.10)

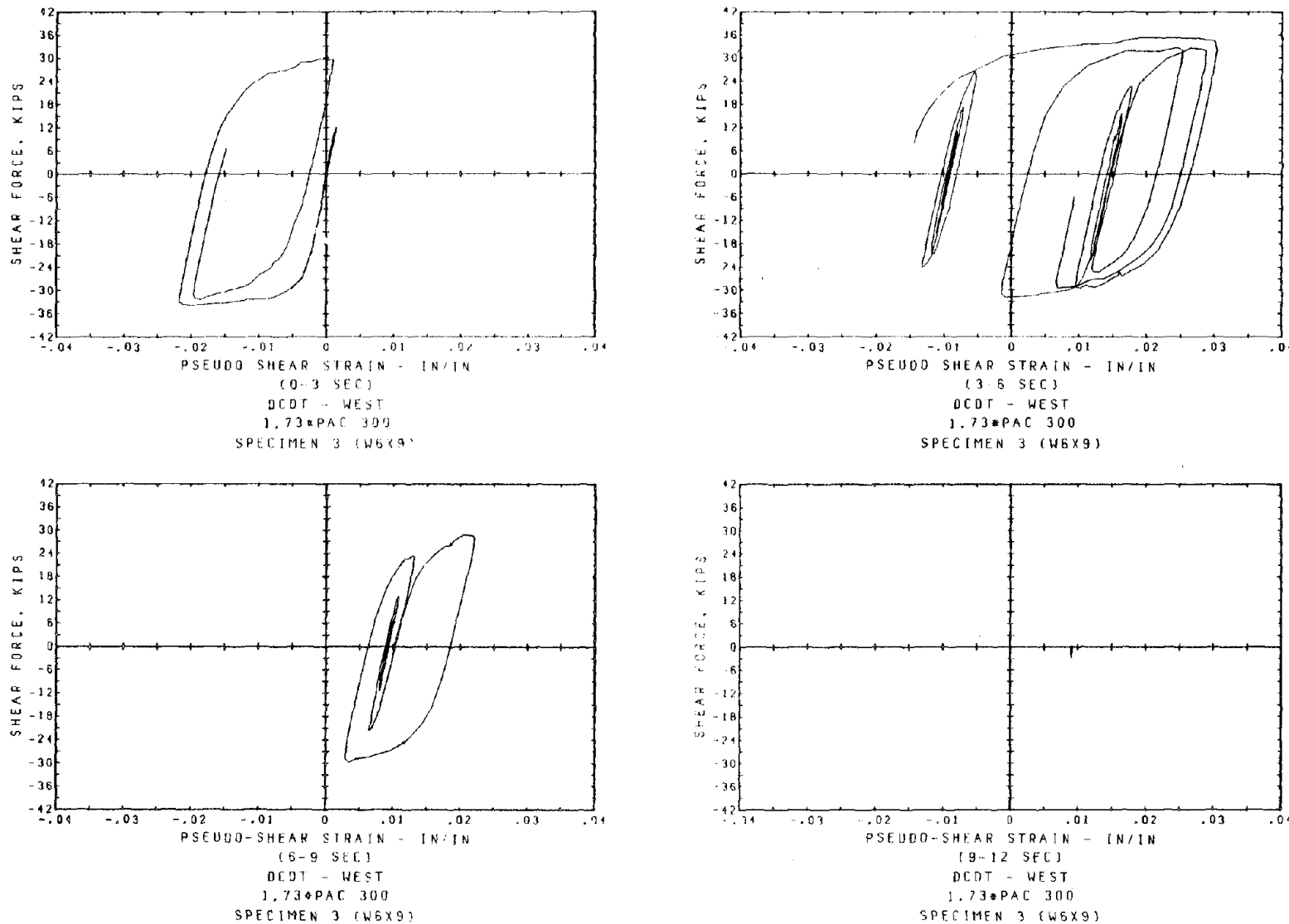

Fig. 106 Shear Link Hysteresis: Link Shear Force vs. Pseudo-Shear Strain

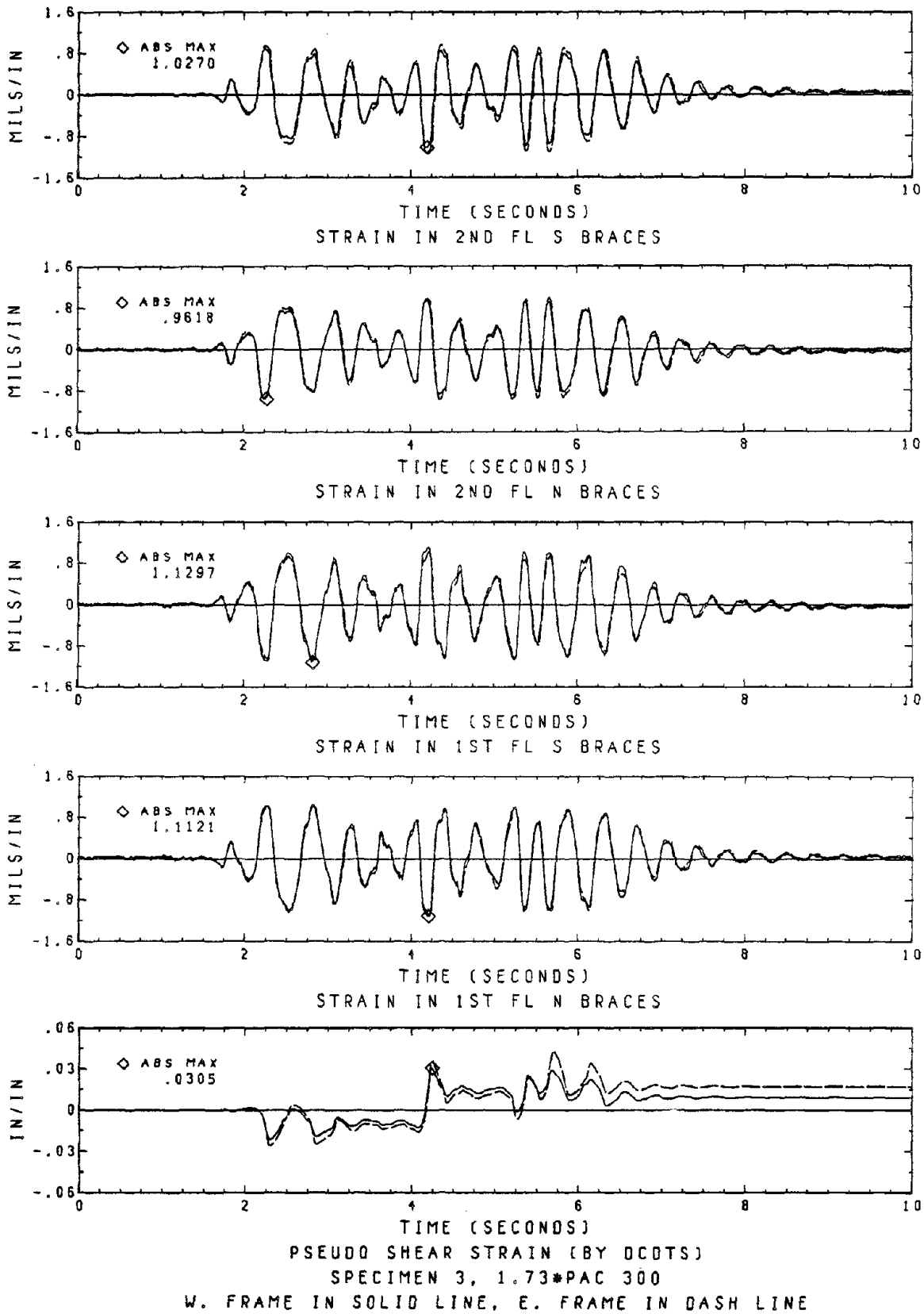

Fig. 107 Brace Strains and Pseudo Shear Strain

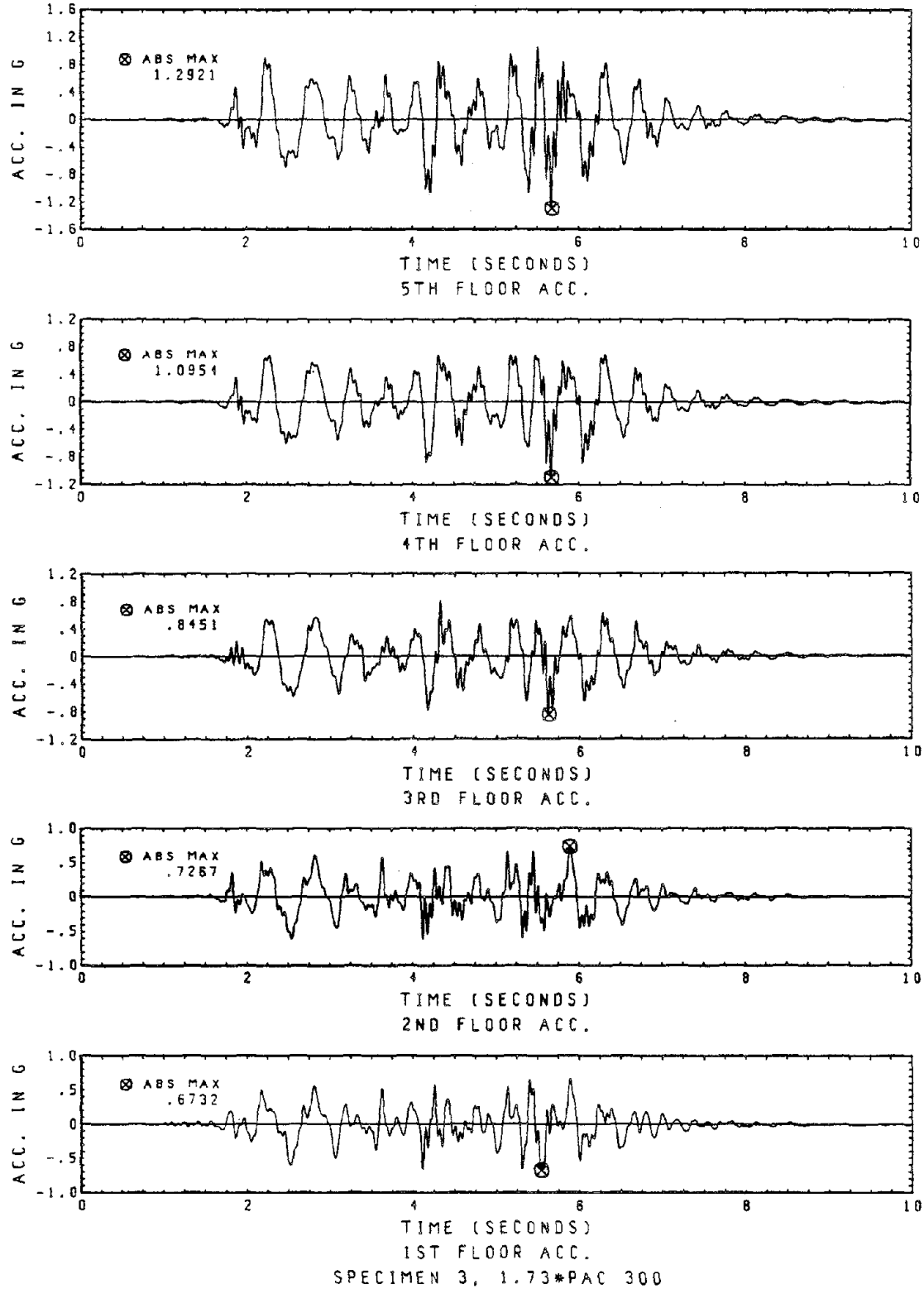

Fig. 108 Floor Accelerations

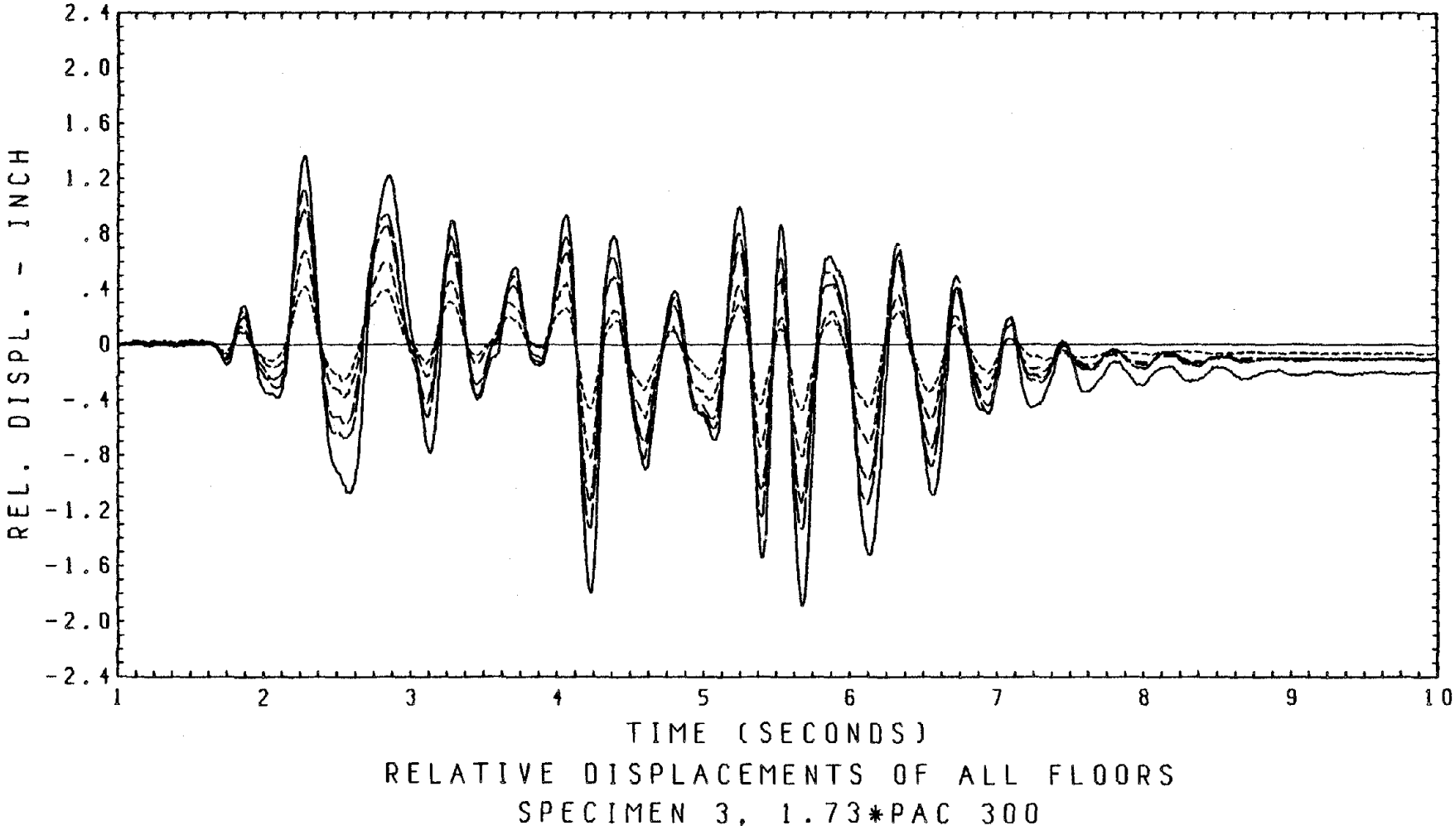

Fig. 109 Floor Displacements

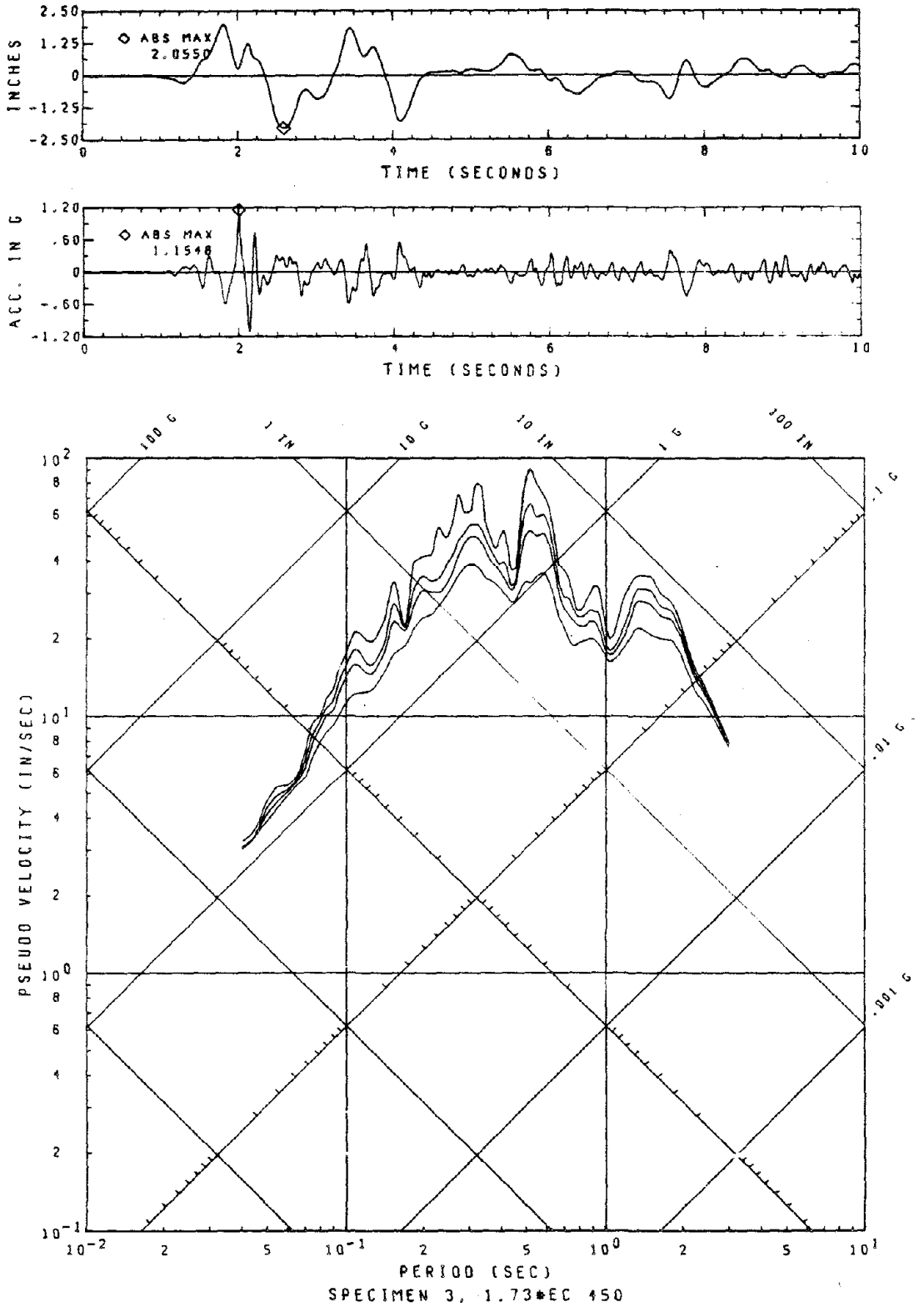

Fig. 110 Displacement, Acceleration of Table Motion 1.73*EC 450 and Its Response Spectra (Damping Ratios = 0.01, 0.03, 0.05, 0.10)

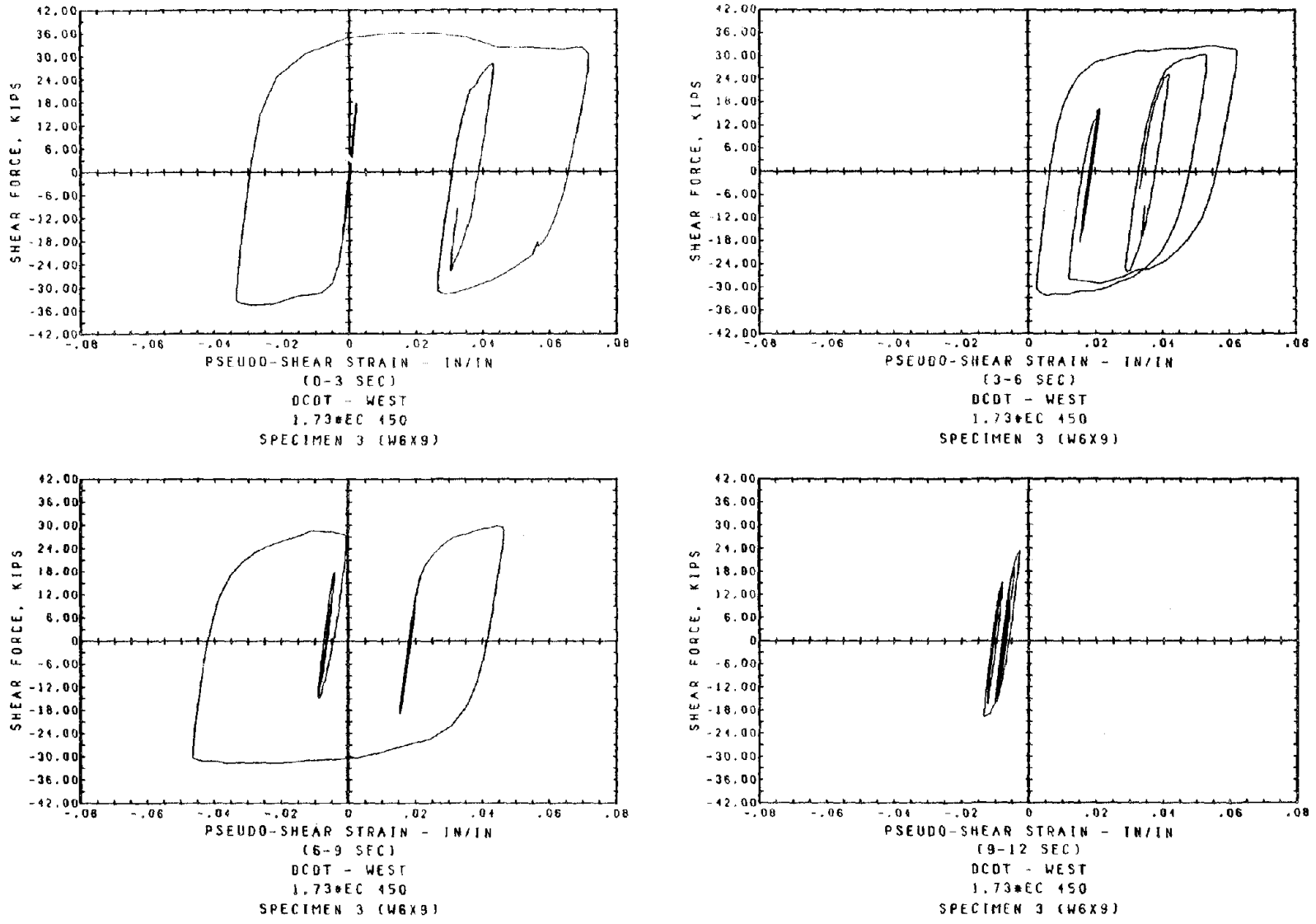

Fig. 111 Shear Link Hysteresis: Link Shear Force vs. Pseudo-Shear Strain

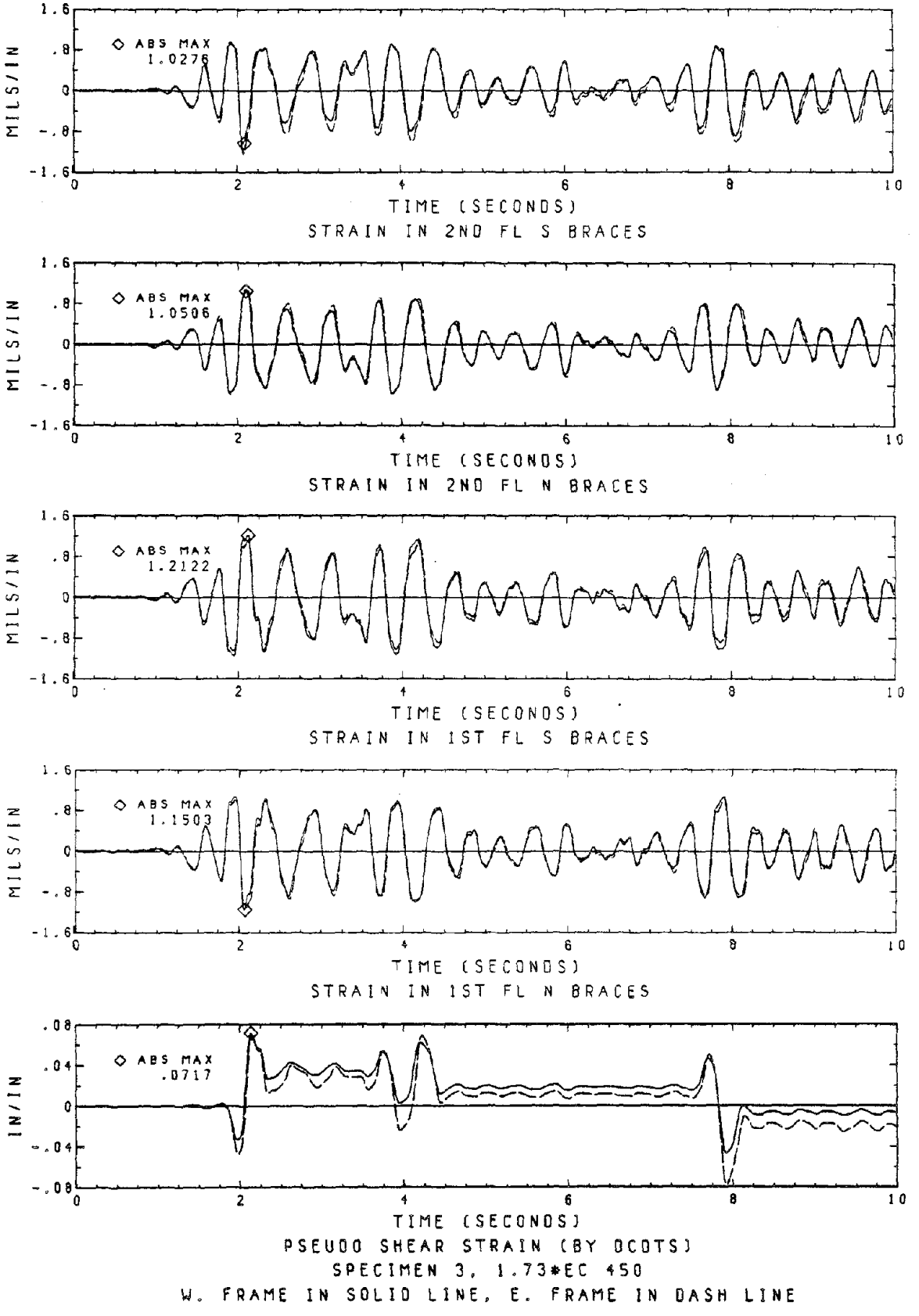

Fig. 112 Brace Strains and Pseudo Shear Strain

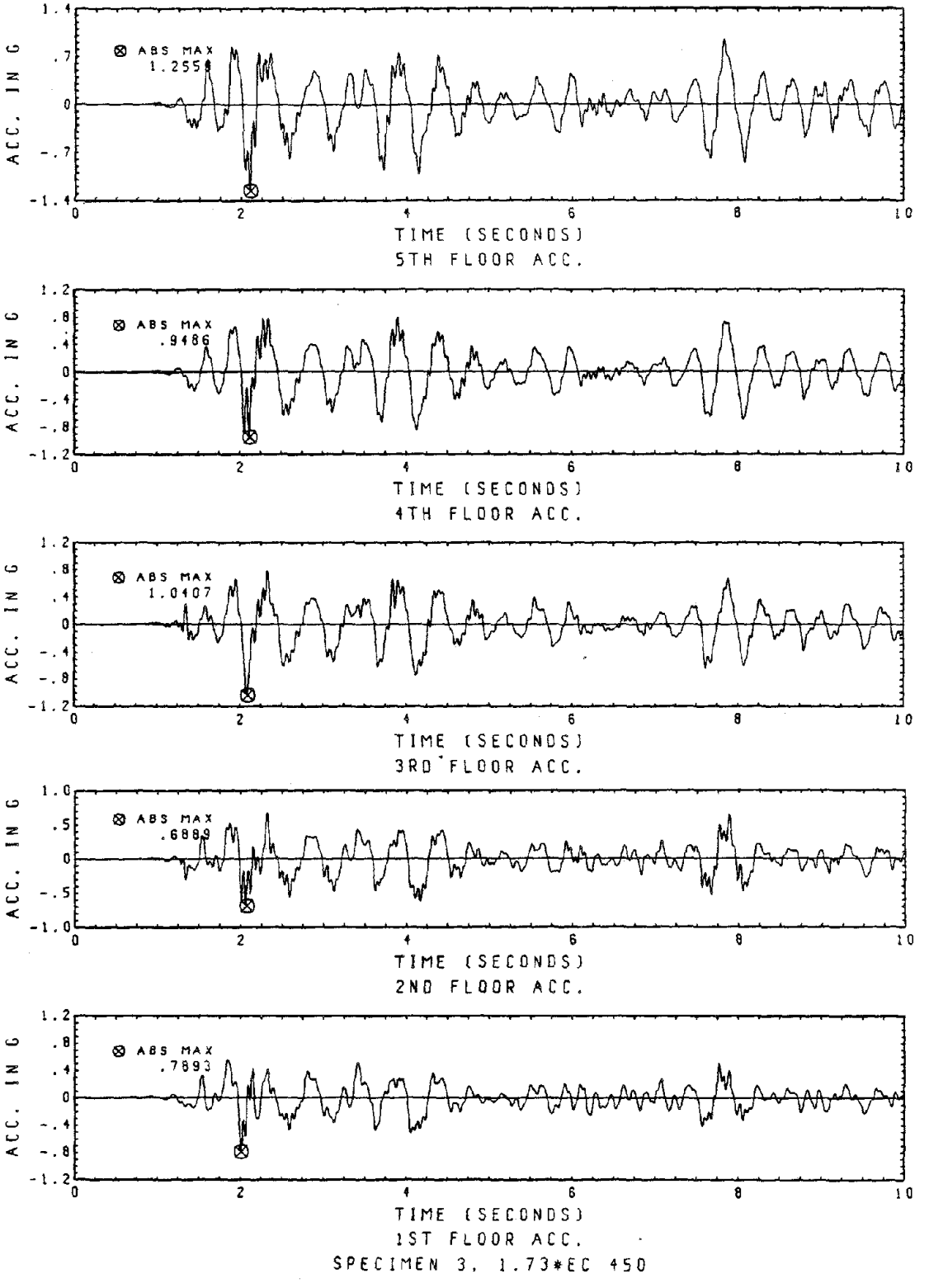

Fig. 113 Floor Accelerations

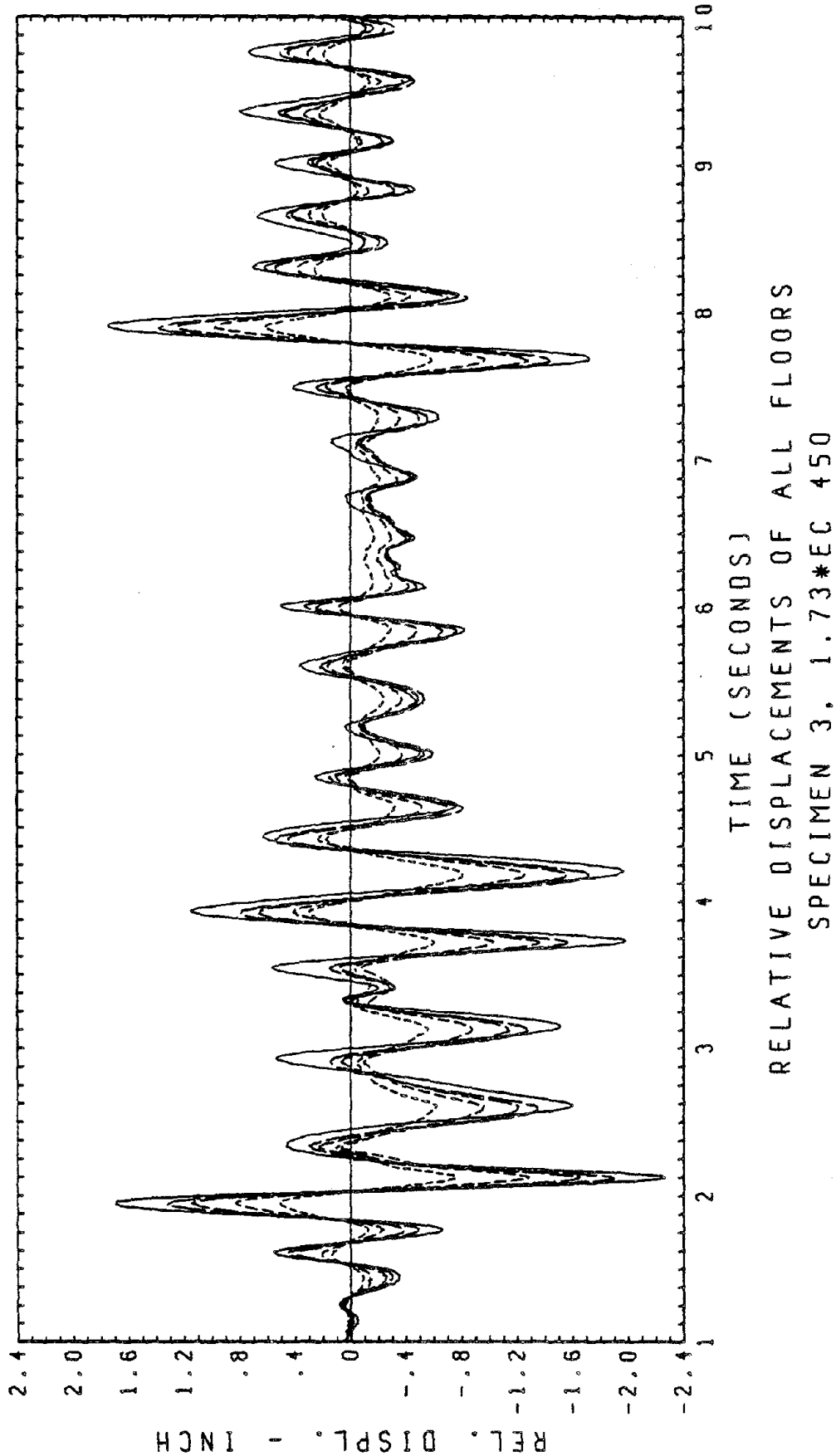

Fig. 114 Floor Displacements

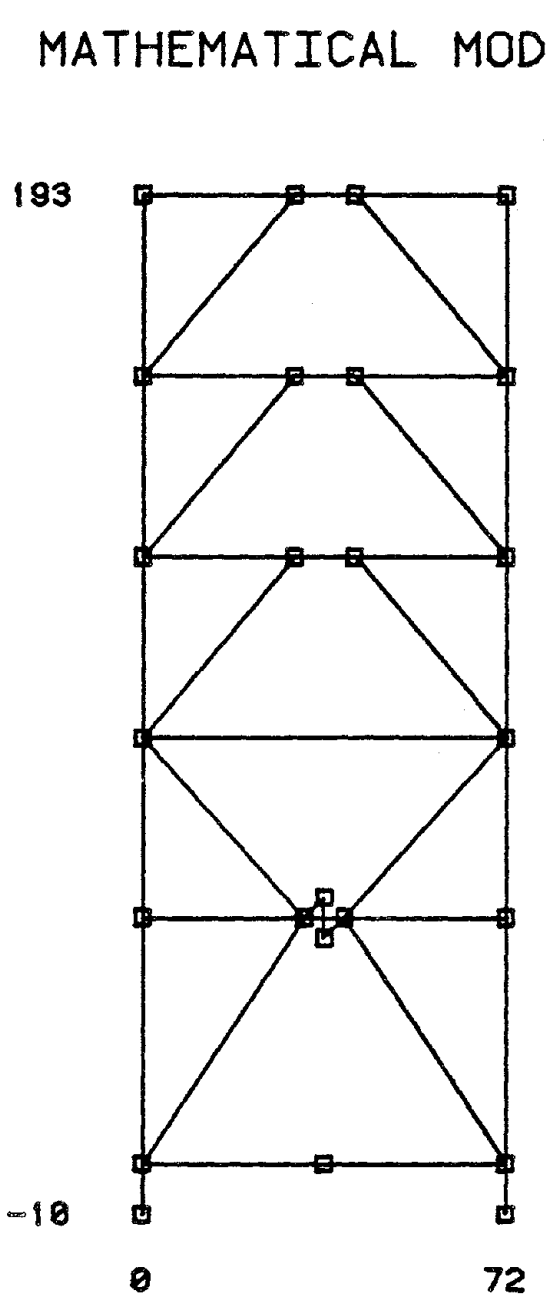

Fig. 115 A Mathematical Model

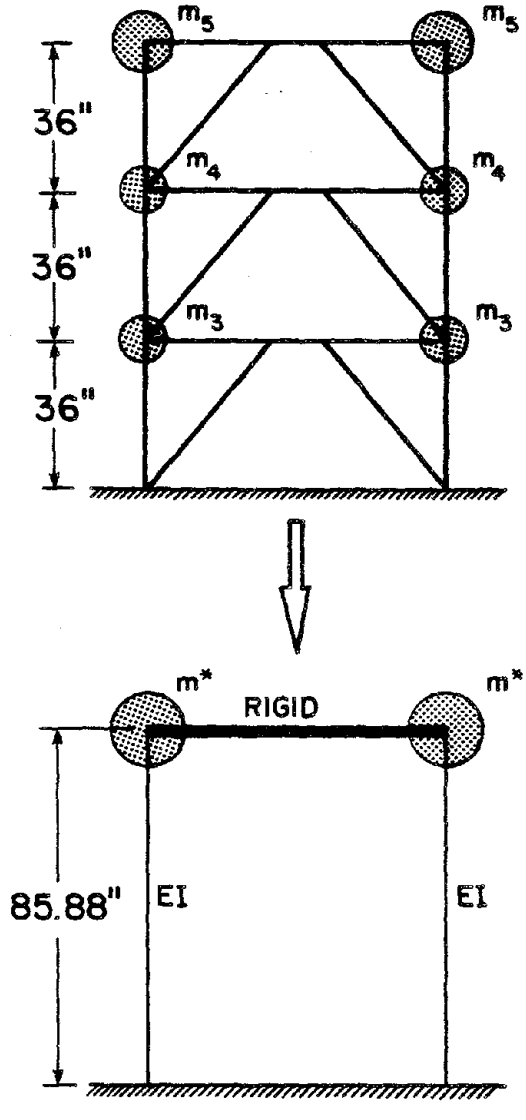

$f_1 = 7.050$ cps

$m_5 = 16.19$ lb·sec^2/in

$m_4 = 12.31$ lb·sec^2/in

$m_3 = 12.31$ lb·sec^2/in

$f = 7.050$ cps

$m^* = 36.32$ lb·sec^2/in

$EI = 3,761,180,740$ lb·in^2

Fig. 116 Dynamic Simplification of the Upper Three Braced Stories
(The First Mode Base Shear and Overturning Moment are Preserved)

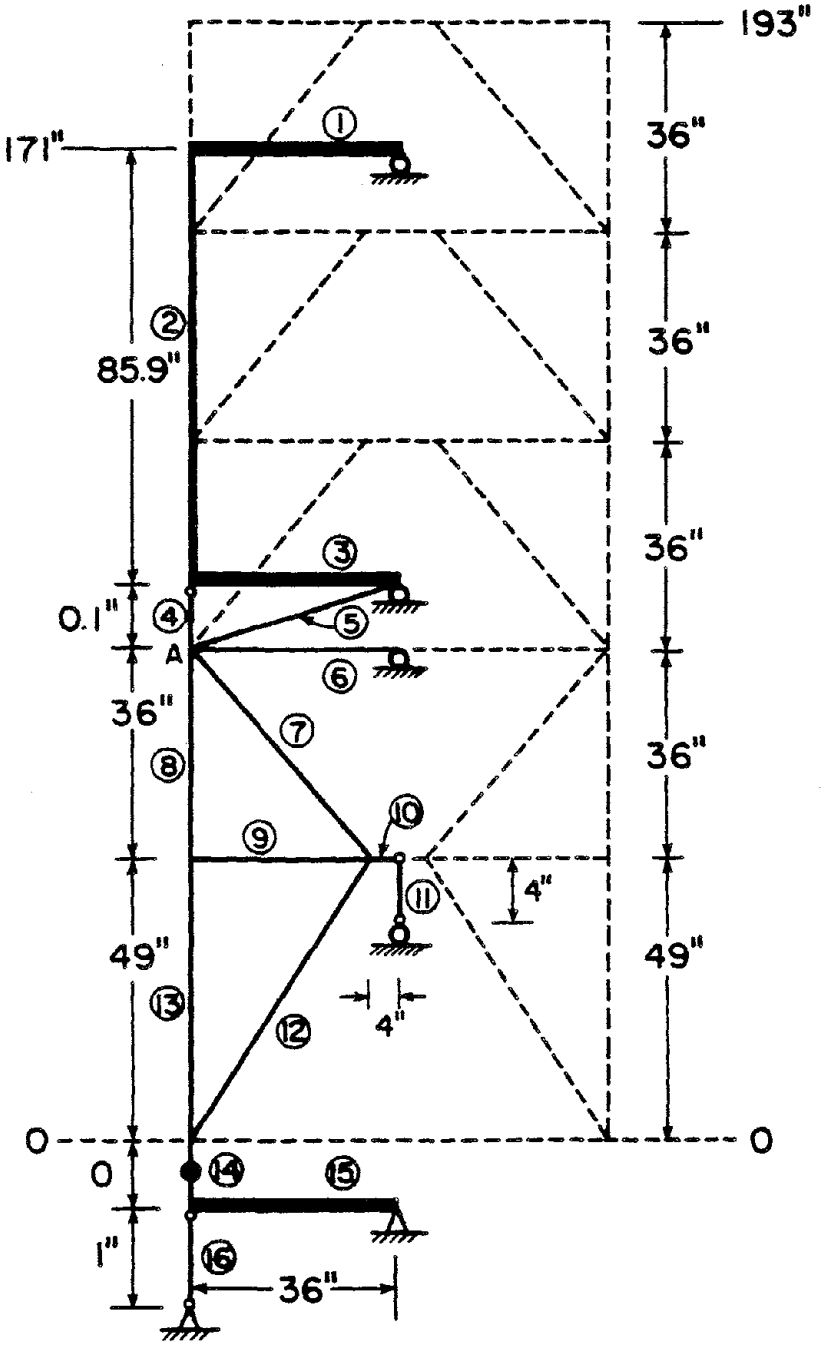

Fig. 117 The Mathematical Model for the Correlation Study

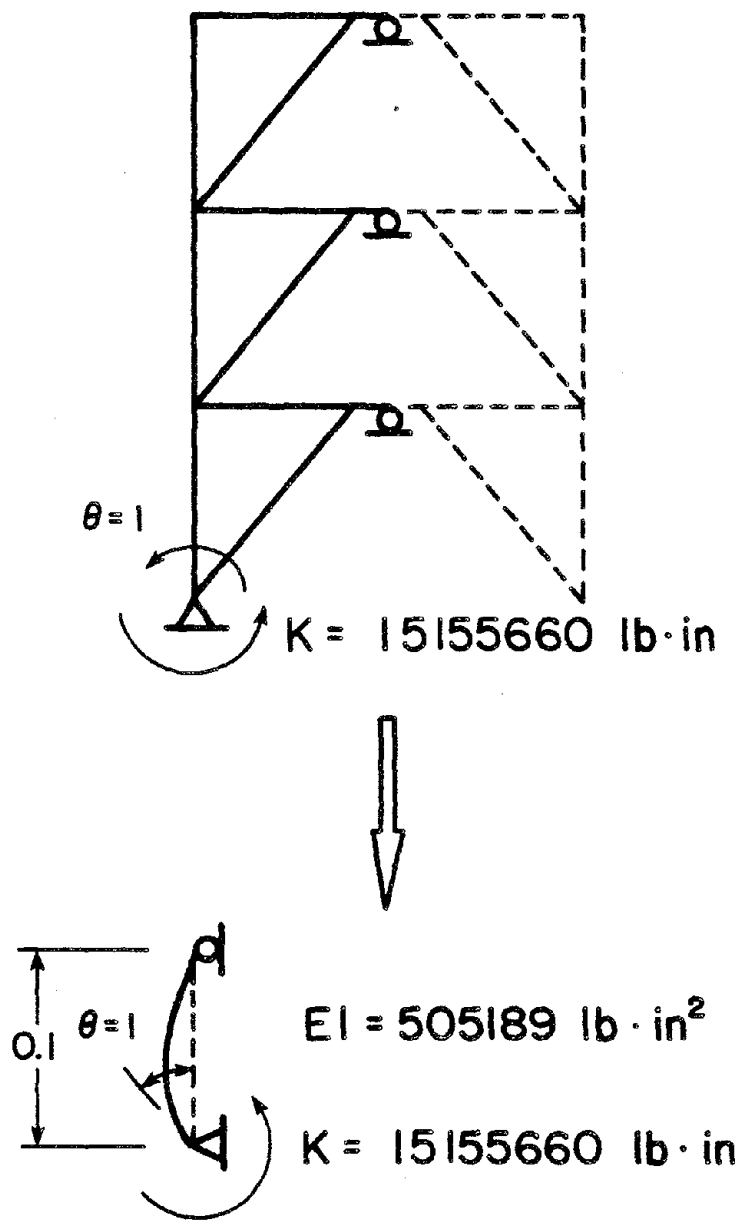

Fig. 118 Equivalent Column to Simulate the Rotatioal Stiffness of the Upper Three Stories

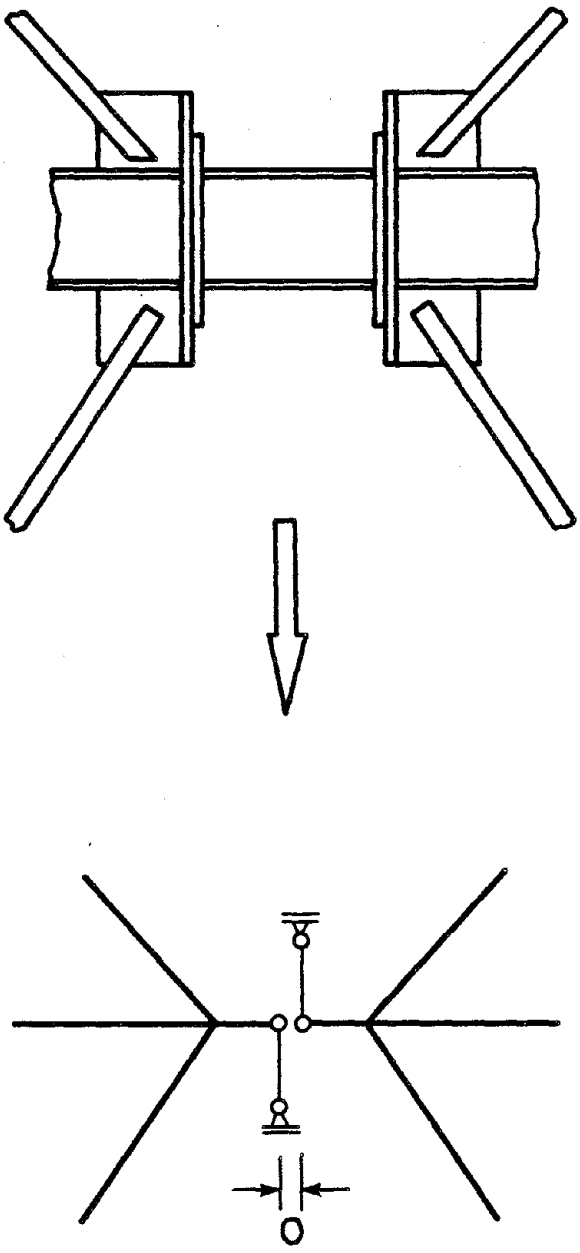

Fig. 119 Mathematical Model for Link Shear Yielding

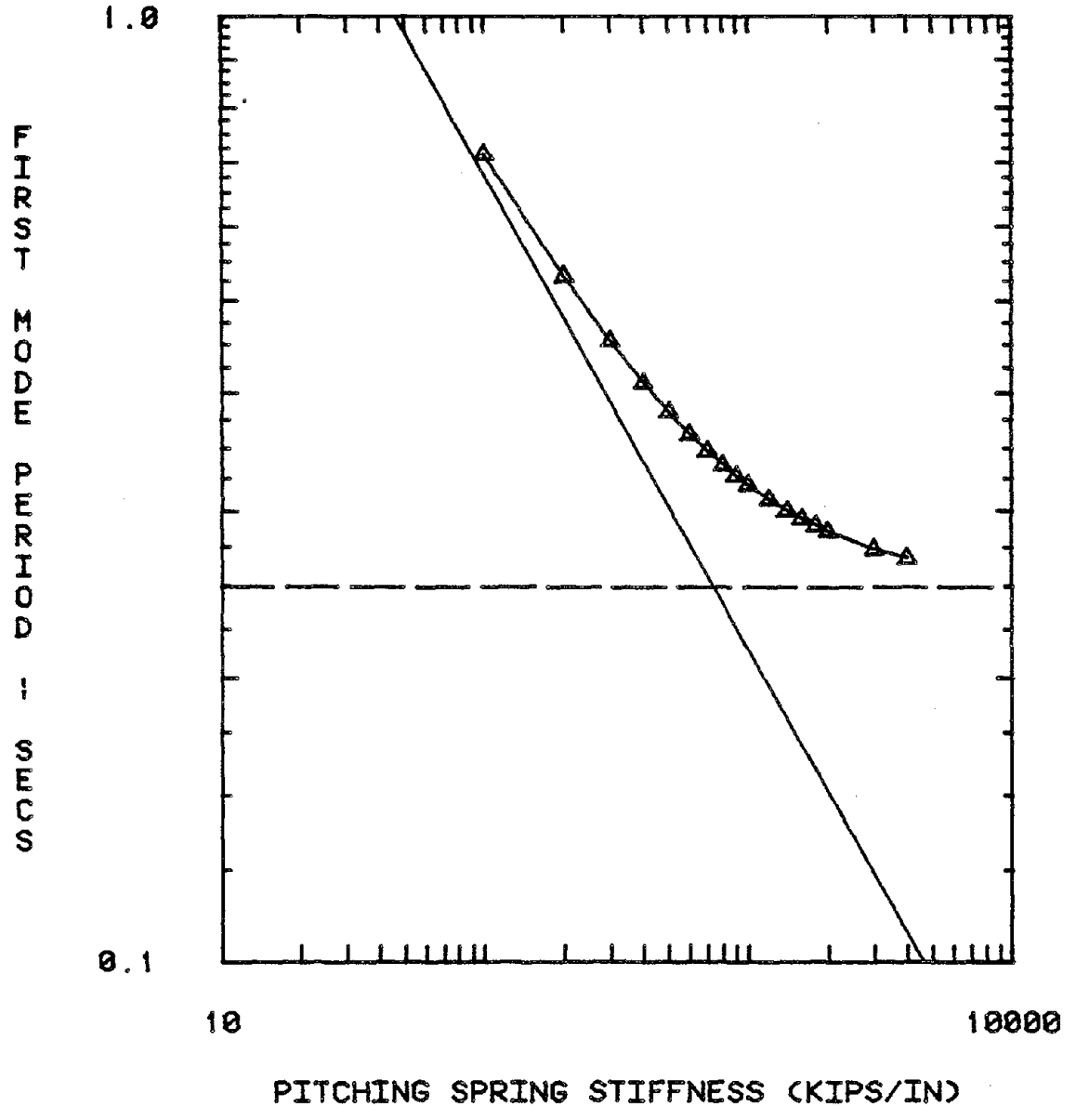

Fig. 120 Dependence of First Mode Periods of the Test Structure on the Pitching (Spring) Stiffnesses

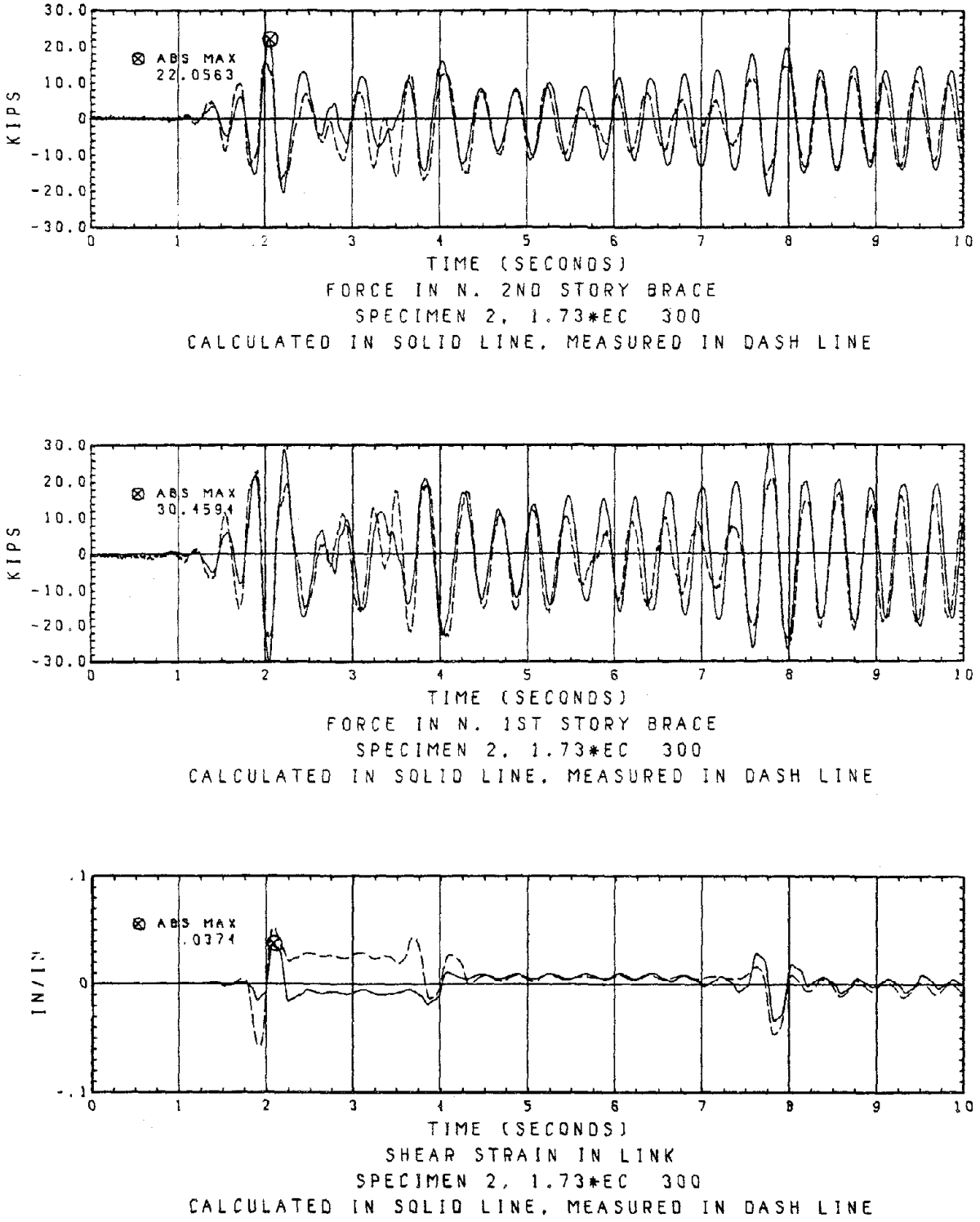

Fig. 121 First Correlation of Brace Strains and Pseudo Shear Strain

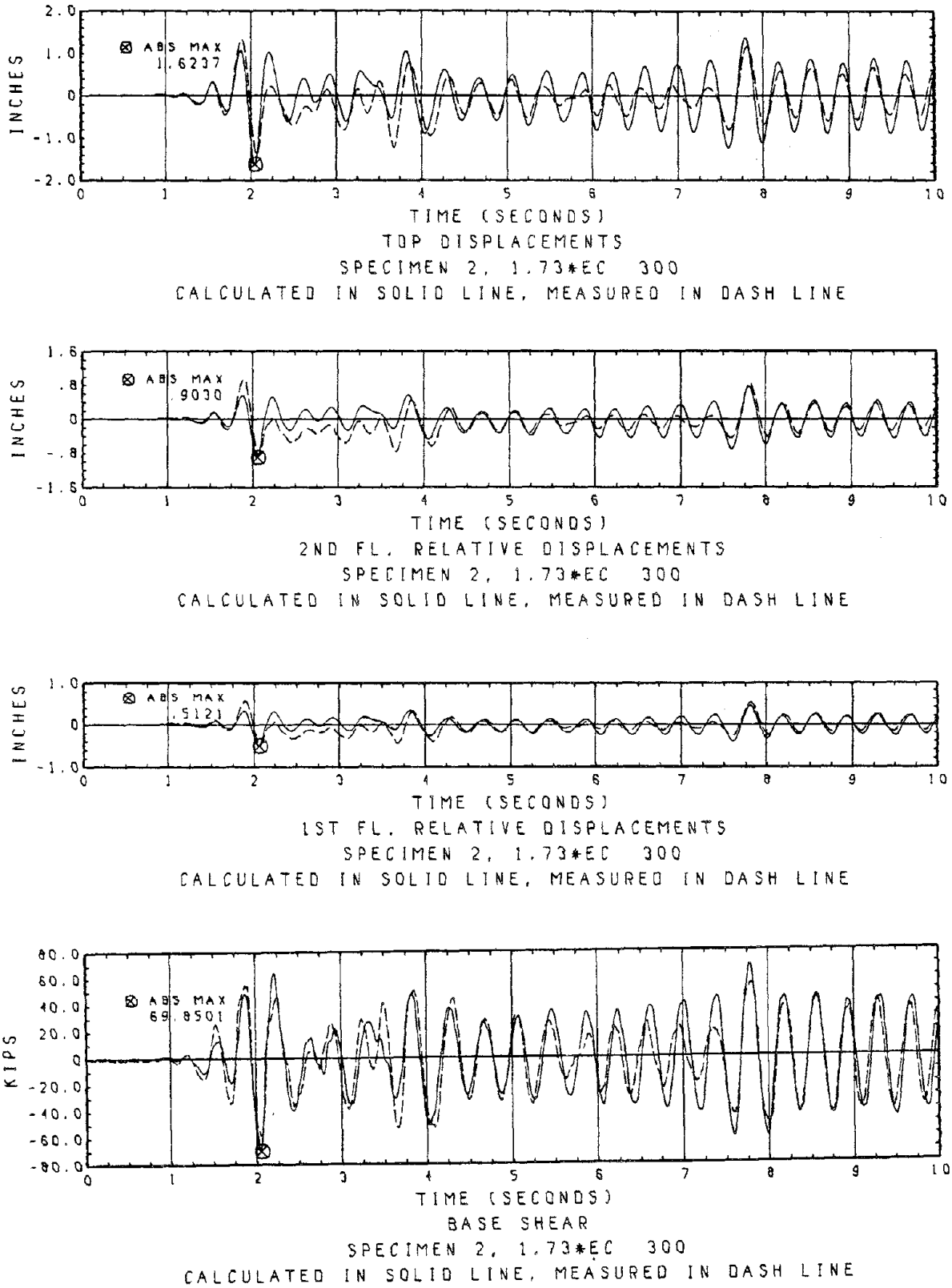

Fig. 122 First Correlation of Reladisplacements and Base Shear

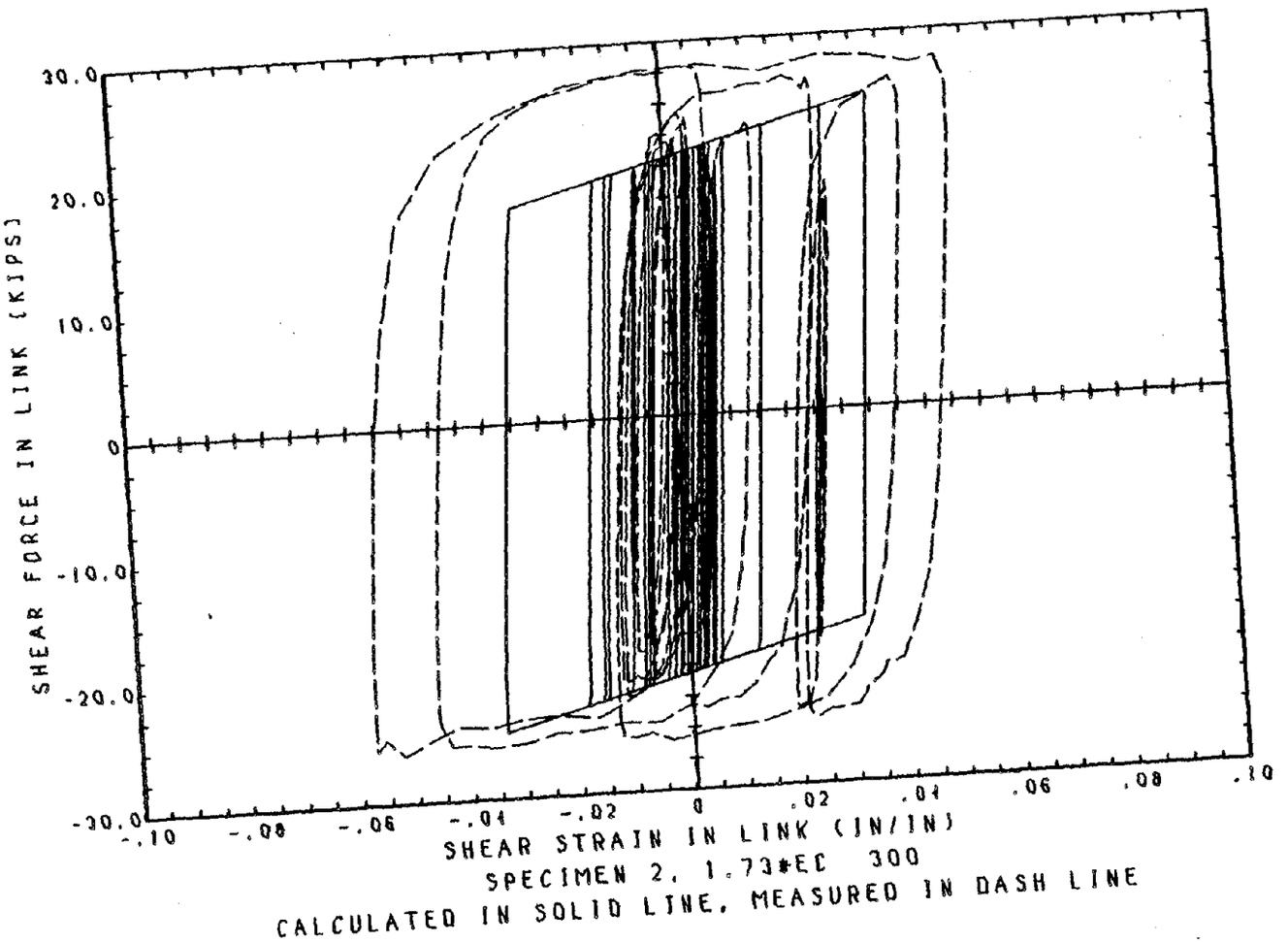

Fig. 123 First Correlation of Hysteresis Behavior

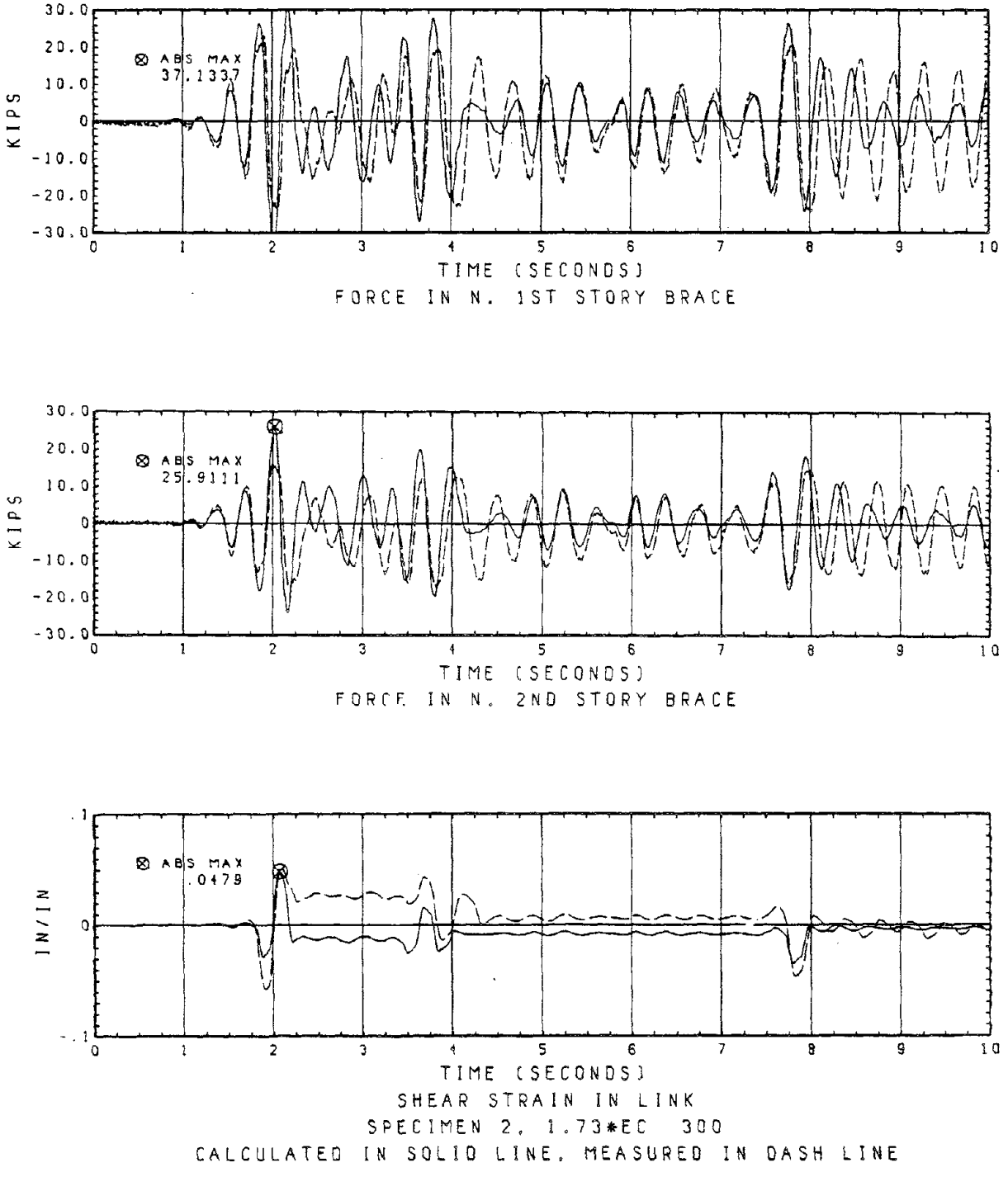

Fig. 124 Second Correlation of Brace Strains and Pseudo Shear Strain

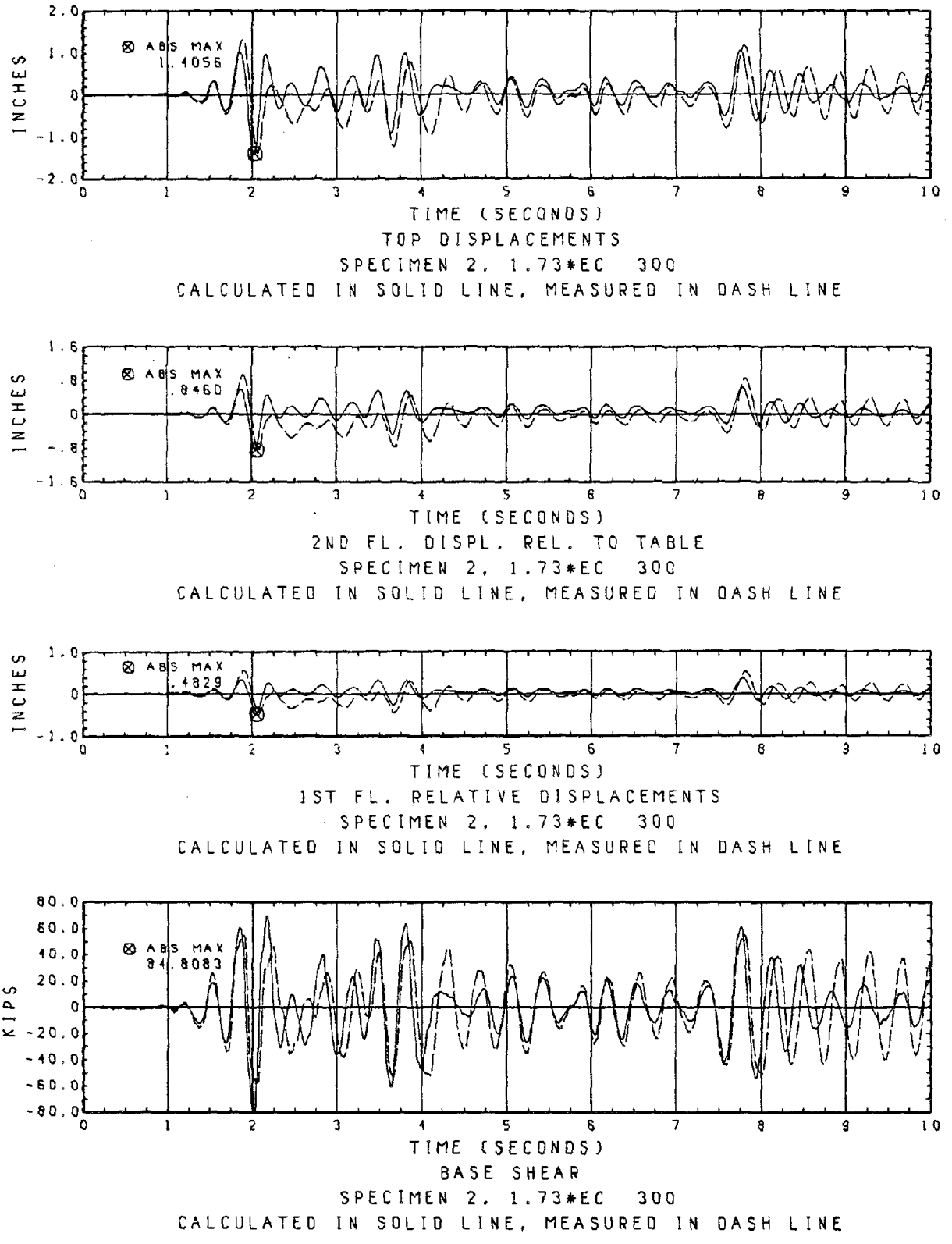

Fig. 125 Second Correlation of Reladisplacements and Base Shear

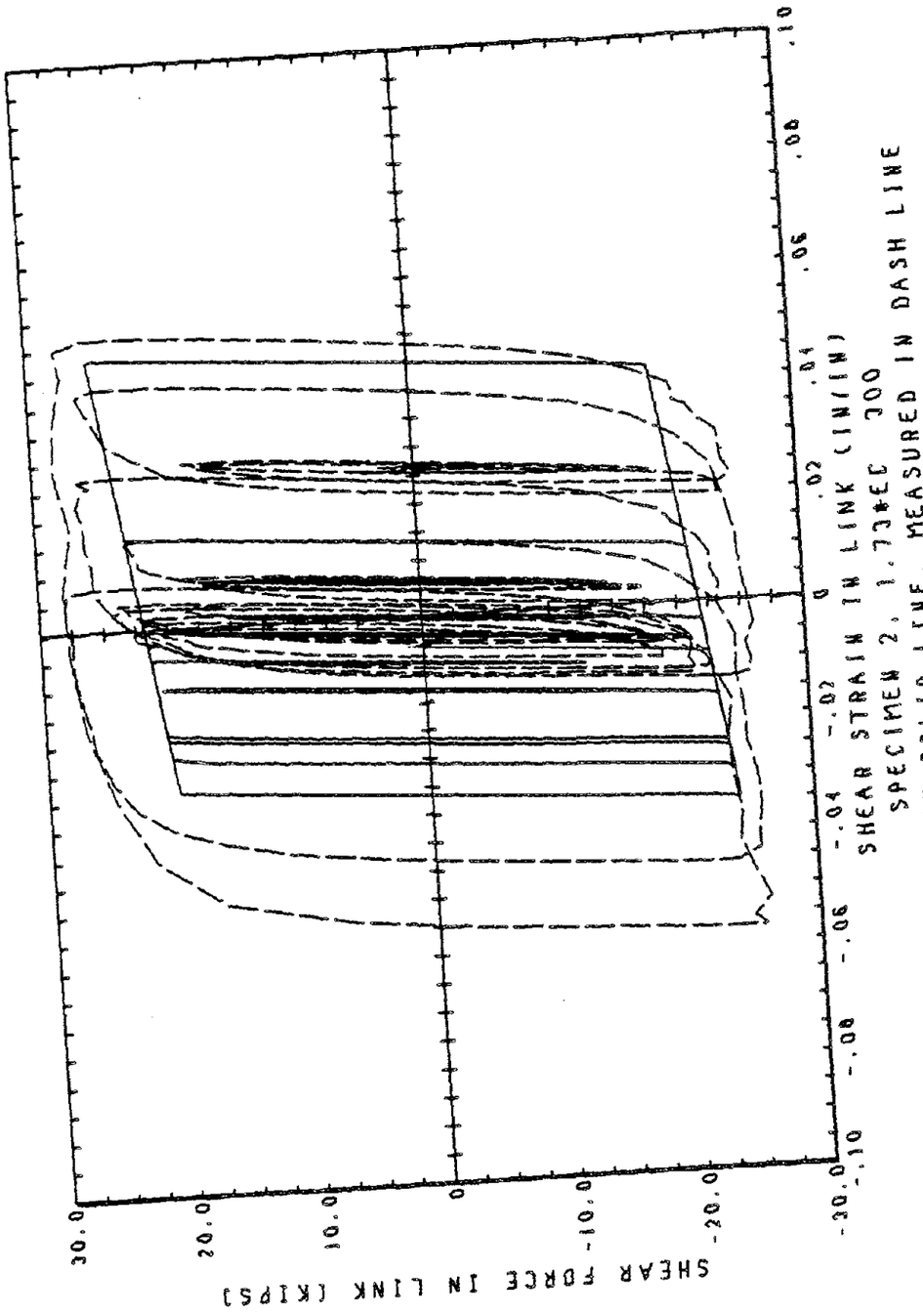

Fig. 126 Second Correlation of Hysteresis Behavior

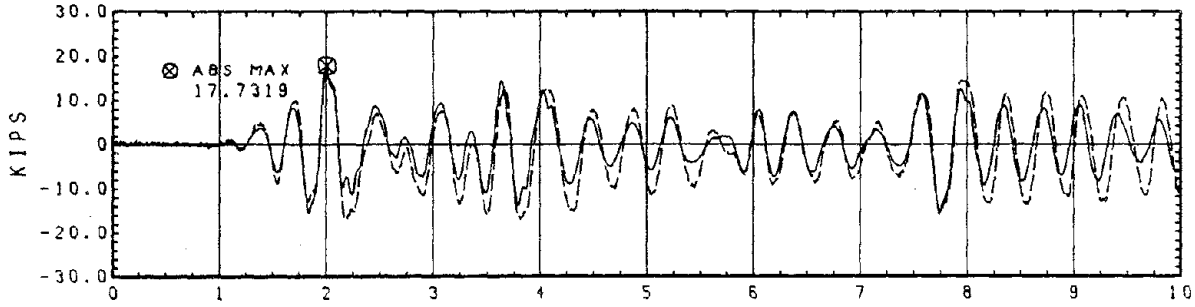

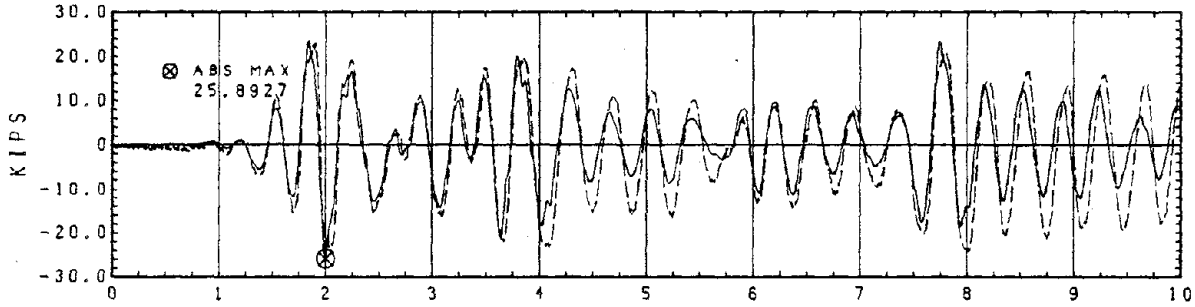

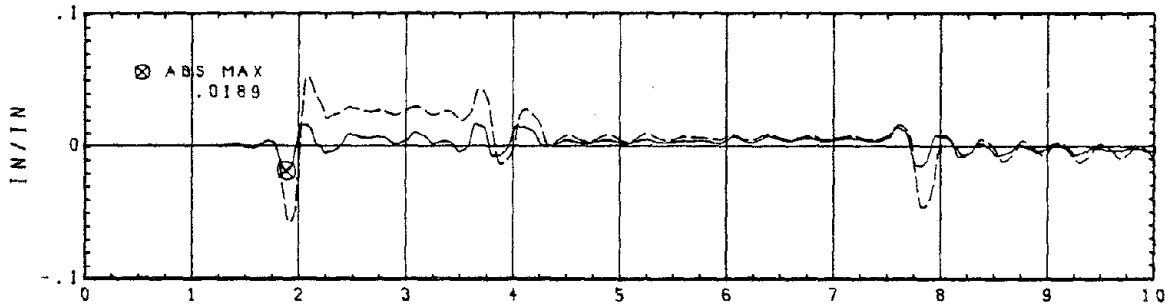

Fig. 127 Third Correlation of Brace Strains and Pseudo Shear Strain

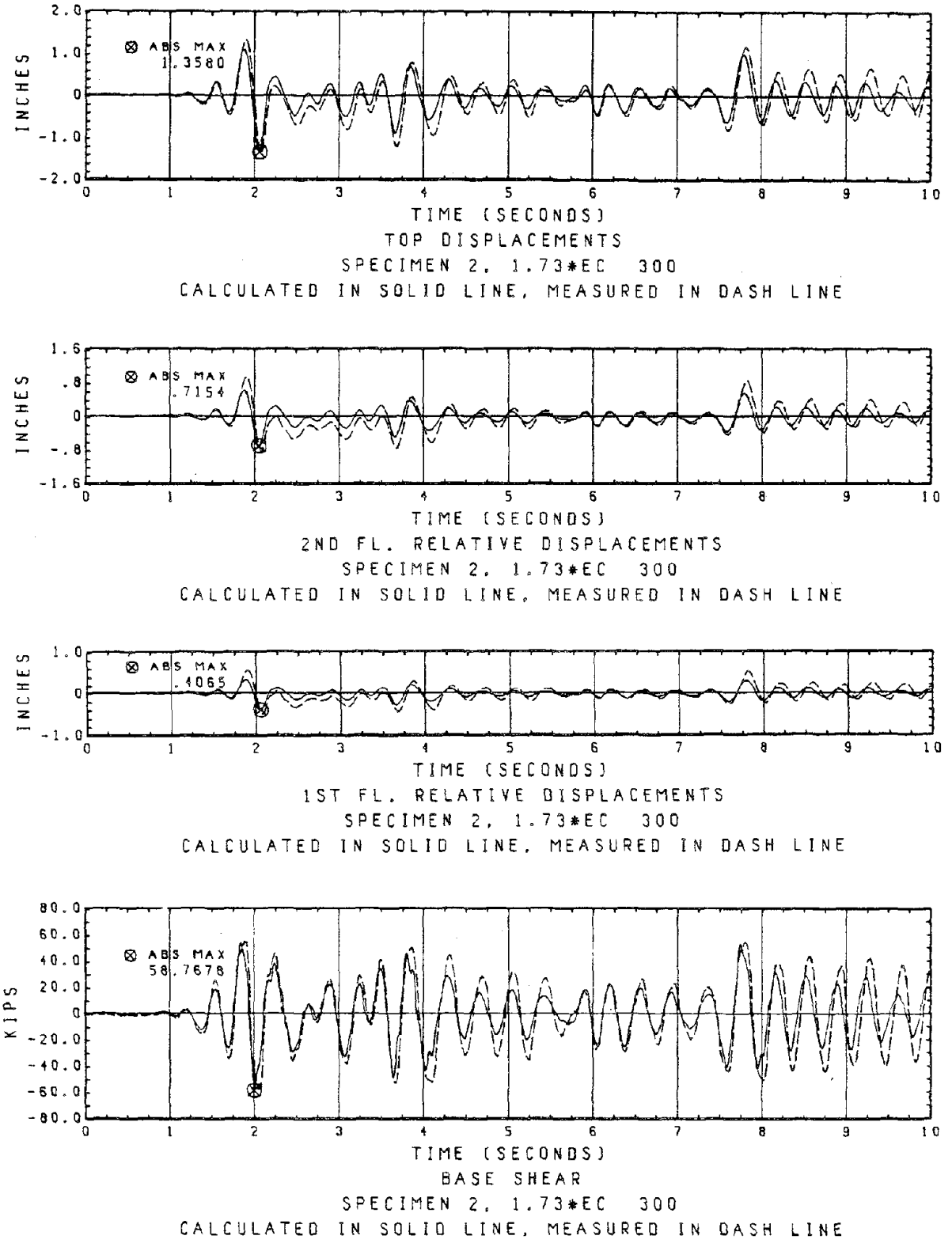

Fig. 128 Third Correlation of Reladisplacements and Base Shear

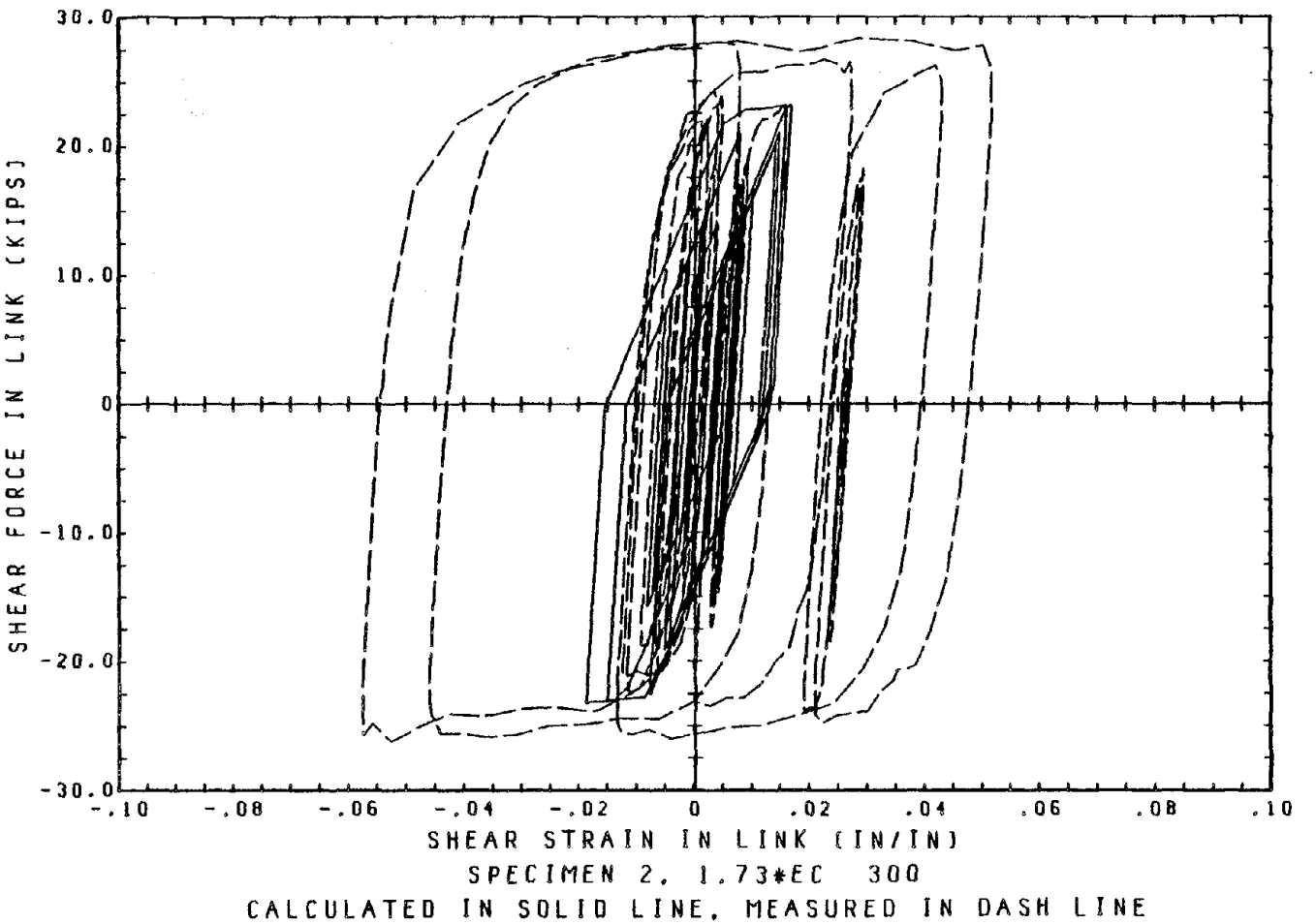

Fig. 129 Third Correlation of Hysteresis Behavior

APPENDIX A

LIST OF DATA CHANNELS

MNEMONIC NOTATION FOR
CHANNEL NAMES DESCRIPTIONS

AV	average	flr	floor
ACC	acceleration	frme	frame
DISP	displacement	W	west
STR	strain	E	east
INT	interior frame	N	north
A	axial	S	south
B	bending	bend	bending strain
C	column	col	column
D	diagonal	mid	middle
E	east frame	horiz	horizontal
F	rosette	diag	diagonal
G	girder	vert	vertical
H	horizontal	comp	component
I	interior frame	post.y	postyield
L	lower	axial	axial strain
M	middle		
N	north		
P	post-yield		
S	south		
T	shaking table		
U	upper		
V	vertical		
W	west frame		
X	brace		
Z	shear link		
1	first story		
2	second story		

LIST* OF DATA CHANNELS OF SPECIMEN 1		
No.	**Name**	**Description**
0	AV H T DISP	average horiz table displacement
1	AV V T DISP	average vert table displacement
2	AV H T ACC	average horiz table acceleration
3	AV V T ACC	average vert table acceleration
4	PITCH ACC	angular pitching acceleration
5	ROLL ACC	angular rolling acceleration
6	TWIST ACC	angular twisting acceleration
7	blank	
11	ACC-1	1st floor acceleration
12	ACC-2	2nd floor aceleration
13	ACC-3	3rd floor acceleration
14	ACC-4	4th floor acceleration
15	ACC-5	5th floor acceleration
16	DISP-1W	1st flr displ of W frme
17	DISP-2W	2nd flr displ of W frme
18	DISP-3W	3rd flr displ of W frme
19	DISP-4W	4th flr displ of W frme
20	DISP-5W	5th flr displ of W frme
21	DISP-5W INT	5th flr displ of W interior frme
22	DISP-5E INT	5th flr displ of E interior frme
23	DISP-5E	5th flr displ of E frme
24	DISP-4W INT	4th flr displ of W interior frme
25	DISP-4E INT	4th flr displ of E interior frme
26	blank	
27	blank	
28	STR-CBWN2UP	N col bend, 2nd story, upper end, postyield
29	STR-CBWS2UP	S col bend, 2nd story, upper end, postyield
30	STR-CBWN1UP	N col bend, 1st story, upper end, postyield
31	STR-CBWS1UP	S col bend, 1st story, upper end, postyield
32	STR-CBWN1LP	N col bend, 1st story, lower end, postyield
33	STR-CBWS1LP	S col bend, 1st story, lower end, postyield
34	STR-CBWN2U	W frme, N col bend, 2nd story, upper end
35	STR-CBWN2L	W frme, N col bend, 2nd story, lower end
36	STR-CBWS2U	W frme, S col bend, 2nd story, upper end
37	STR-CBWS2L	W frme, S col bend, 2nd story, lower end
38	STR-CBWN1U	W frme, N col bend, 1st story, upper end
39	STR-CBWN1L	W frme, N col bend, 1st story, lower end
40	STR-CBWS1U	W frme, S col bend, 1st story, upper end
41	STR-CBWS1L	W frme, S col bend, 1st story, lower end
42	STR-GBWNN	girder bend, W frme, N half girder, N end
43	STR-GBWNS	girder bend, W frme, N half girder, S end
44	STR-GBWSN	girder bend, W frme, S half girder, N end
45	STR-GBWSS	girder bend, W frme, S half girder, S end
46	STR-ZBWNP	link bend, W link, N end, post-yield
47	STR-ZBWSP	link bend, W link, S end, post-yield
48	STR-ZBWN	link bend, W link, N end
49	STR-ZBWS	link bend, W link, S end
50	STR-CAWN	col axial, W frme, N col

LIST* OF DATA CHANNELS OF SPECIMEN 1 (Cont'd)		
No.	**Name**	**Description**
51	STR-CAWS	col axial, W frme, S col
52	STR-XAWNU	brace axial, W frme, N 2nd story brace
54	STR-XAWNL	brace axial, W frme, N 1st story brace
55	STR-XAWSL	brace axial, W frme, S 1st story brace
56	STR-FWNH	W link, N rosette, horiz comp, postyield
57	STR-FWND	W link, N rosette, diag comp, postyield
58	STR-FWNV	W link, N rosette, vert comp, postyield
59	STR-FWMH	W link, mid rosette, horiz comp, postyield
60	STR-FWMD	W link, mid rosette, diag comp, postyield
61	STR-FWMV	W link, mid rosette, vert comp, postyield
62	STR-FWSH	W link, S rosette, horiz comp, postyield
63	STR-FWSD	W link, S rosette, diag comp, postyield
64	STR-FWSV	W link, S rosette, vert comp, postyield
65	STR-XAESU	brace axial, E frme, S 2nd story brace
66	STR-XAENU	brace axial, E frme, N 2nd story brace
67	STR-XAESL	brace axial, E frme, S 1st story brace
68	STR-XAENL	brace axial, E frme, N 1st story brace
69	STR-FEMH	E link, mid rosette, horiz comp, postyield
70	STR-FEMD	E link, mid rosette, diag comp, postyield
71	STR-FEMV	E link, mid rosette, vert comp, postyield
72	STR-CBINU	col bend, W interior N col, upper end
73	STR-CBINL	col bend, W interior N col, lower end
74	STR-CBISU	col bend, W interior S col, upper end
75	STR-CBISL	col bend, W interior S col, lower end
76	STR-CAIN	col axial, W interior frme, N col
77	STR-CAIS	col axial, W interior frme, S col
78	STR-HORIZ	W link, 2nd mid rosette, horiz comp, post.y
79	STR-DIAG	W link, 2nd mid rosette, diag comp, post.y
80	STR-VERT	W link, 2nd mid rosette, vert comp, post.y
81	STR-XAWSU	brace axial, W frme, S 2nd story brace
84	DISP-A W	DCDT, W link, negative slope diagonal
85	DISP-B W	DCDT, W link, positive slope diagonal
86	DISP-C W	DCDT, axial elong, W frme, 1st story N brace
87	DISP-D W	DCDT, axial elong, W frme, 1st story S brace
88	DISP-A E	DCDT, E link, negative slope diagonal
89	DISP-B E	DCDT, E link, positive slope diagonal
90	DISP-C E	DCDT, axial elong, E frme, 1st story N brace
91	DISP-D E	DCDT, axial elong, E frme, 1st story S brace
92	DISP-X DCDT	lateral displ, W frme, 1st story N brace
93	DISP-X DCDT2	Lateral displ, W frme, 1st story S brace

* Data were picked in such a sequence as listed in the table.
Those channels that are not listed were not used.

LIST* OF DATA CHANNELS OF SPECIMEN 2		
No.	**Name**	**Description**
0	AV H T DISP	average horiz table displacement
1	AV V T DISP	average vert table displacement
2	AV H T ACC	average horiz table acceleration
3	AV V T ACC	average vert table acceleration
4	PITCH ACC	angular pitching acceleration
5	ROLL ACC	angular rolling acceleration
6	TWIST ACC	angular twisting acceleration
7	blank	
11	ACC-1	1st floor acceleration
12	ACC-2	2nd floor aceleration
13	ACC-3	3rd floor acceleration
14	ACC-4	4th floor acceleration
15	ACC-5	5th floor acceleration
16	DISP-1W	1st flr displ of W frme
17	DISP-2W	2nd flr displ of W frme
18	DISP-3W	3rd flr displ of W frme
19	DISP-4W	4th flr displ of W frme
20	DISP-5W	5th flr displ of W frme
21	DISP-5W INT	5th flr displ of W interior frme
22	DISP-5E INT	5th flr displ of E interior frme
23	DISP-5E	5th flr displ of E frme
24	DISP-4W INT	4th flr displ of W interior frme
25	DISP-4E INT	4th flr displ of E interior frme
26	blank	
27	blank	
28	STR-CBWN2UP	N col bend, 2nd story, upper end, postyield
29	STR-CBWS2UP	S col bend, 2nd story, upper end, postyield
30	STR-CBWN1UP	N col bend, 1st story, upper end, postyield
31	STR-CBWS1UP	S col bend, 1st story, upper end, postyield
32	STR-CBWN1LP	N col bend, 1st story, lower end, postyield
33	STR-CBWS1LP	S col bend, 1st story, lower end, postyield
34	STR-CBWN2U	W frme N col bend, 2nd story, upper end
35	STR-CBWN2L	W frme N col bend, 2nd story, lower end
36	STR-CBWS2U	W frme S col bend, 2nd story, upper end
37	STR-CBWS2L	W frme S col bend, 2nd story, lower end
38	STR-CBWN1U	W frme N col bend, 1st story, upper end
39	STR-CBWN1L	W frme N col bend, 1st story, lower end
40	STR-CBWS1U	W frme S col bend, 1st story, upper end
41	STR-CBWS1L	W frme S col bend, 1st story, lower end
42	STR-GBWNN	girder bend, W frme, N half girder, N end
43	STR-GBWNS	girder bend, W frme, N half girder, S end
44	STR-GBWSN	girder bend, W frme, S half girder, N end
45	STR-GBWSS	girder bend, W frme, S half girder, S end
46	STR-ZBWNP	link bend, W link, N end, post-yield
47	STR-ZBWSP	link bend, W link, S end, post-yield
49	STR-ZBWS	link bend, W link, S end
50	STR-CAWN	col axial, W frme, N col

LIST* OF DATA CHANNELS OF SPECIMEN 2 (Cont'd)		
No.	**Name**	**Description**
51	STR-CAWS	col axial, W frme, S col
52	STR-XAWNU	brace axial, W frme, N 2nd story brace
54	STR-XAWNL	brace axial, W frme, N 1st story brace
55	STR-XAWSL	brace axial, W frme, S 1st story brace
56	STR-FWNH	W link, N rosette, horiz comp, postyield
57	STR-FWND	W link, N rosette, diag comp, postyield
58	STR-FWNV	W link, N rosette, vert comp, postyield
59	STR-FWMH	W link, mid rosette, horiz comp, postyield
60	STR-FWMD	W link, mid rosette, diag comp, postyield
61	STR-FWMV	W link, mid rosette, vert comp, postyield
62	STR-FWSH	W link, S rosette, horiz comp, postyield
63	STR-FWSD	W link, S rosette, diag comp, postyield
64	STR-FWSV	W link, S rosette, vert comp, postyield
65	STR-XAESU	brace axial, E frme, S 2nd story brace
66	STR-XAENU	brace axial, E frme, N 2nd story brace
67	STR-XAESL	brace axial, E frme, S 1st story brace
68	STR-XAENL	brace axial, E frme, N 1st story brace
69	STR-FEMH	E link, mid rosette, horiz comp, postyield
70	STR-FEMD	E link, mid rosette, diag comp, postyield
71	STR-FEMV	E link, mid rosette, vert comp, postyield
72	STR-CBINU	col bend, W interior N col, upper end
73	STR-CBINL	col bend, W interior N col, lower end
74	STR-CBISU	col bend, W interior S col, upper end
75	STR-CBISL	col bend, W interior S col, lower end
76	STR-CAIN	col axial, W interior frme, N col
77	STR-CAIS	col axial, W interior frme, S col
78	STR-HORIZ	W link, 2nd mid rosette, horiz comp, post.y
79	STR-DIAG	W link, 2nd mid rosette, diag comp, post.y
80	STR-VERT	W link, 2nd mid rosette, vert comp, post.y
81	STR-XAWSU	brace axial, W frme, S 2nd story brace
84	DISP-A W	DCDT, W link, negative slope diagonal
85	DISP-B W	DCDT, W link, positive slope diagonal
86	DISP-C W	DCDT, axial elong, W frme, 1st story N brace
87	DISP-D W	DCDT, axial elong, W frme, 1st story S brace
88	DISP-A E	DCDT, E link, negative slope diagonal
89	DISP-B E	DCDT, E link, positive slope diagonal
90	DISP-C E	DCDT, axial elong, E frme, 1st story N brace
91	DISP-D E	DCDT, axial elong, E frme, 1st story S brace
92	DISP-X DCDT	lateral displ, W frme, 1st story N brace
93	DISP-X DCDT2	Lateral displ, W frme, 1st story S brace
82	STR-ZBWN	link bend, W link, N end

* Data were picked in such a sequence as listed in the table.
Those channels that are not listed were not used.

LIST* OF DATA CHANNELS OF SPECIMEN 3		
No.	**Name**	**Description**
0	AV H T DISP	average horiz table displacement
1	AV V T DISP	average vert table displacement
2	AV H T ACC	average horiz table acceleration
3	AV V T ACC	average vert table acceleration
4	PITCH ACC	angular pitching acceleration
5	ROLL ACC	angular rolling acceleration
6	TWIST ACC	angular twisting acceleration
7	blank	
83	ACC-1	1st floor acceleration
12	ACC-2	2nd floor aceleration
13	ACC-3	3rd floor acceleration
14	ACC-4	4th floor acceleration
15	ACC-5	5th floor acceleration
16	DISP-1W	1st flr displ of W frme
17	DISP-2W	2nd flr displ of W frme
18	DISP-3W	3rd flr displ of W frme
19	DISP-4W	4th flr displ of W frme
20	DISP-5W	5th flr displ of W frme
21	DISP-5W INT	5th flr displ of W interior frme
22	DISP-5E INT	5th flr displ of E interior frme
23	DISP-5E	5th flr displ of E frme
24	DISP-4W INT	4th flr displ of W interior frme
25	DISP-4E INT	4th flr displ of E interior frme
26	blank	
27	blank	
28	STR-CBWN2UP	N col bend, 2nd story, upper end, postyield
29	STR-CBWS2UP	S col bend, 2nd story, upper end, postyield
30	STR-CBWN1UP	N col bend, 1st story, upper end, postyield
31	STR-CBWS1UP	S col bend, 1st story, upper end, postyield
32	STR-CBWN1LP	N col bend, 1st story, lower end, postyield
33	STR-CBWS1LP	S col bend, 1st story, lower end, postyield
34	STR-CBWN2U	W frme N col bend, 2nd story, upper end
35	STR-CBWN2L	W frme N col bend, 2nd story, lower end
36	STR-CBWS2U	W frme S col bend, 2nd story, upper end
37	STR-CBWS2L	W frme S col bend, 2nd story, lower end
38	STR-CBWN1U	W frme N col bend, 1st story, upper end
39	STR-CBWN1L	W frme N col bend, 1st story, lower end
40	STR-CBWS1U	W frme S col bend, 1st story, upper end
41	STR-CBWS1L	W frme S col bend, 1st story, lower end
42	STR-GBWNN	girder bend, W frme, N half girder, N end
43	STR-GBWNS	girder bend, W frme, N half girder, S end
44	STR-GBWSN	girder bend, W frme, S half girder, N end
45	STR-GBWSS	girder bend, W frme, S half girder, S end
46	STR-ZAW	link axial, W frme
49	STR-ZBWS	link bend, W link, S end
50	STR-CAWN	col axial, W frme, N col

LIST* OF DATA CHANNELS OF SPECIMEN 3 (Cont'd)		
No.	**Name**	**Description**
51	STR-CAWS	col axial, W frme, S col
8	STR-XAWNU	brace axial, W frme, N 2nd story brace
10	STR-XAWNL	brace axial, W frme, N 1st story brace
9	STR-XAWSL	brace axial, W frme, S 1st story brace
56	STR-FWNH	W link, N rosette, horiz comp, postyield
57	STR-FWND	W link, N rosette, diag comp, postyield
58	STR-FWNV	W link, N rosette, vert comp, postyield
59	STR-FWMH	W link, mid rosette, horiz comp, postyield
60	STR-FWMD	W link, mid rosette, diag comp, postyield
61	STR-FWMV	W link, mid rosette, vert comp, postyield
62	STR-FWSH	W link, S rosette, horiz comp, postyield
63	STR-FWSD	W link, S rosette, diag comp, postyield
64	STR-FWSV	W link, S rosette, vert comp, postyield
65	STR-XAESU	brace axial, E frme, S 2nd story brace
66	STR-XAENU	brace axial, E frme, N 2nd story brace
67	STR-XAESL	brace axial, E frme, S 1st story brace
68	STR-XAENL	brace axial, E frme, N 1st story brace
69	STR-FEMH	E link, mid rosette, horiz comp, postyield
70	STR-FEMD	E link, mid rosette, diag comp, postyield
71	STR-FEMV	E link, mid rosette, vert comp, postyield
72	STR-CBINU	col bend, W interior N col, upper end
73	STR-CBINL	col bend, W interior N col, lower end
74	STR-CBISU	col bend, W interior S col, upper end
75	STR-CBISL	col bend, W interior S col, lower end
76	STR-CAIN	col axial, W interior frme, N col
77	STR-CAIS	col axial, W interior frme, S col
78	STR-HORIZ	W link, 2nd mid rosette, horiz comp, post.y
79	STR-DIAG	W link, 2nd mid rosette, diag comp, post.y
80	STR-VERT	W link, 2nd mid rosette, vert comp, post.y
81	STR-XAWSU	brace axial, W frme, S 2nd story brace
84	DISP-A W	DCDT, W link, negative slope diagonal
85	DISP-B W	DCDT, W link, positive slope diagonal
86	DISP-C W	DCDT, axial elong, W frme, 1st story N brace
87	DISP-D W	DCDT, axial elong, W frme, 1st story S brace
88	DISP-A E	DCDT, E link, negative slope diagonal
89	DISP-B E	DCDT, E link, positive slope diagonal
90	DISP-C E	DCDT, axial elong, E frme, 1st story N brace
91	DISP-D E	DCDT, axial elong, E frme, 1st story S brace
92	DISP-X DCDT	lateral displ, W frme, 1st story N brace
93	DISP-X DCDT2	Lateral displ, W frme, 1st story S brace
82	STR-ZBWN	link bend, W link, N end

* Data were picked in such a sequence as listed in the table.
Those channels that are not listed were not used.

APPENDIX B

COUPON TEST RESULTS

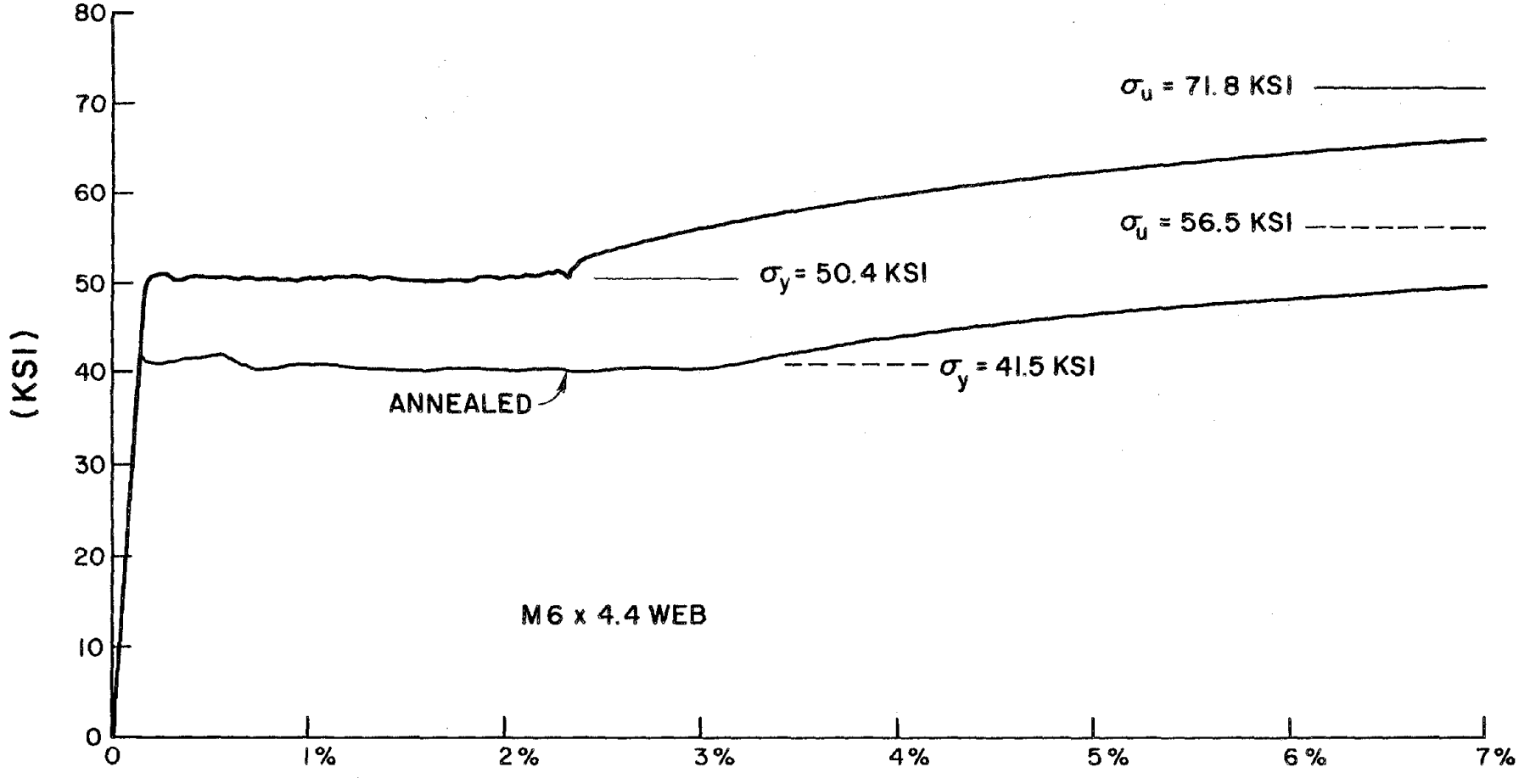

Fig. B.1 Coupon Results (M6×4.4 Web)

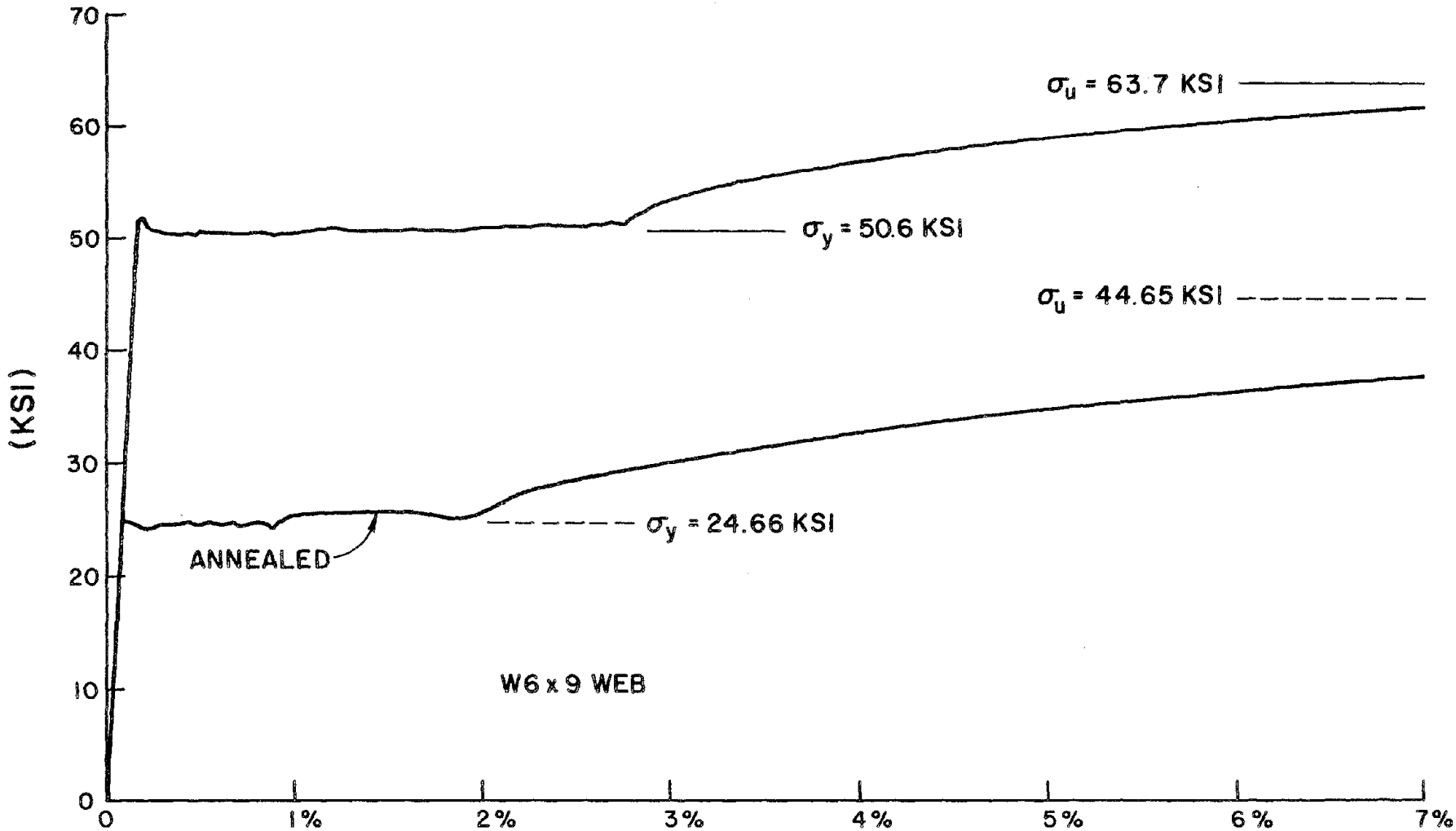

Fig. B.2 Coupon Results (W6×9 Web)

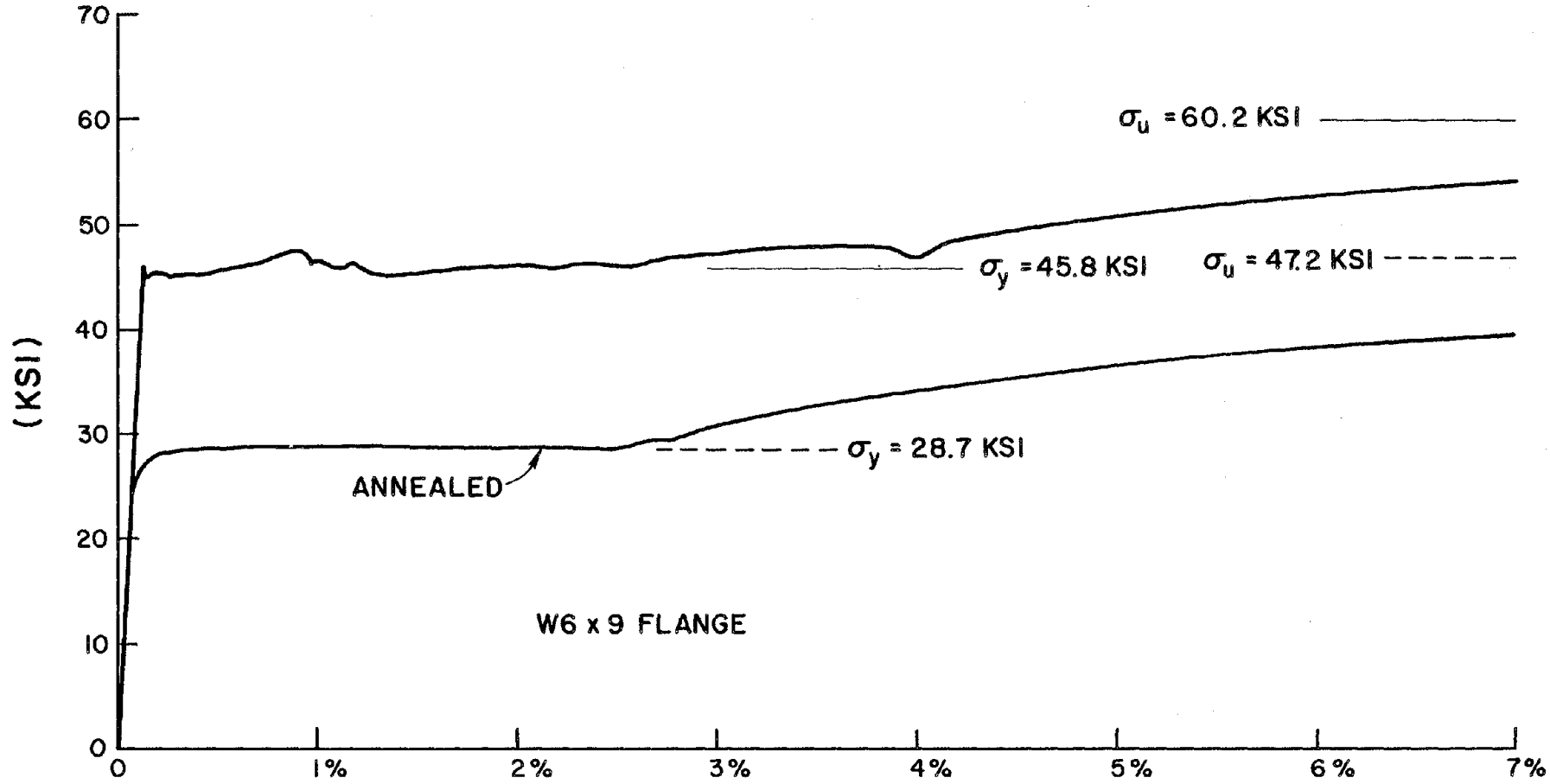

Fig. B.3 Coupon Results (W6×9 Flange)

EARTHQUAKE ENGINEERING RESEARCH CENTER REPORTS

Numbers in parentheses are Accession Numbers assigned by the National Technical Information Service; these are followed by a price code. Copies of the reports may be ordered from the National Technical Information Service, 5285 Port Royal Road, Springfield, Virginia, 22161. Accession Numbers should be quoted on orders for reports (PB --- ---) and a remittance must accompany each order. Reports without this information were not available at time of printing. A complete list of EERC reports (from EERC 67-1) is available upon request from the Earthquake Engineering Research Center, University of California, Berkeley, 47th Street and Hoffman Boulevard, Richmond, California 94804.

UCB/EERC-77/01 "PLUSH - A Computer Program for Probabilistic Finite Element Analysis of Seismic Soil-Structure Interaction," by M.P. Romo Organista, J. Lysmer and H.B. Seed - 1977 (PB81 177 651)A05

UCB/EERC-77/02 "Soil-Structure Interaction Effects at the Humboldt Bay Power Plant in the Ferndale Earthquake of June 7, 1975," by J.E. Valera, H.B. Seed, C.F. Tsai and J. Lysmer - 1977 (PB 265 795)A04

UCB/EERC-77/03 "Influence of Sample Disturbance on Sand Response to Cyclic Loading," by K. Mori, H.B. Seed and C.K. Chan - 1977 (PB 267 352)A04

UCB/EERC-77/04 "Seismological Studies of Strong Motion Records," by J. Shoja-Taheri - 1977 (PB 269 655)A10

UCB/EERC-77/05 Unassigned

UCB/EERC-77/06 "Developing Methodologies for Evaluating the Earthquake Safety of Existing Buildings," by No. 1 - B. Bresler; No. 2 - B. Bresler, T. Okada and D. Zisling; No. 3 - T. Okada and B. Bresler; No. 4 - V.V. Bertero and B. Bresler - 1977 (PB 267 354)A08

UCB/EERC-77/07 "A Literature Survey - Transverse Strength of Masonry Walls," by Y. Omote, R.L. Mayes, S.W. Chen and R.W. Clough - 1977 (PB 277 933)A07

UCB/EERC-77/08 "DRAIN-TABS: A Computer Program for Inelastic Earthquake Response of Three Dimensional Buildings," by R. Guendelman-Israel and G.H. Powell - 1977 (PB 270 693)A07

UCB/EERC-77/09 "SUBWALL: A Special Purpose Finite Element Computer Program for Practical Elastic Analysis and Design of Structural Walls with Substructure Option," by D.Q. Le, H. Peterson and E.P. Popov - 1977 (PB 270 567)A05

UCB/EERC-77/10 "Experimental Evaluation of Seismic Design Methods for Broad Cylindrical Tanks," by D.P. Clough (PB 272 280)A13

UCB/EERC-77/11 "Earthquake Engineering Research at Berkeley - 1976," - 1977 (PB 273 507)A09

UCB/EERC-77/12 "Automated Design of Earthquake Resistant Multistory Steel Building Frames," by N.D. Walker, Jr. - 1977 (PB 276 526)A09

UCB/EERC-77/13 "Concrete Confined by Rectangular Hoops Subjected to Axial Loads," by J. Vallenas, V.V. Bertero and E.P. Popov - 1977 (PB 275 165)A06

UCB/EERC-77/14 "Seismic Strain Induced in the Ground During Earthquakes," by Y. Sugimura - 1977 (PB 284 201)A04

UCB/EERC-77/15 Unassigned

UCB/EERC-77/16 "Computer Aided Optimum Design of Ductile Reinforced Concrete Moment Resisting Frames," by S.W. Zagajeski and V.V. Bertero - 1977 (PB 280 137)A07

UCB/EERC-77/17 "Earthquake Simulation Testing of a Stepping Frame with Energy-Absorbing Devices," by J.M. Kelly and D.F. Tsztoo - 1977 (PB 273 506)A04

UCB/EERC-77/18 "Inelastic Behavior of Eccentrically Braced Steel Frames under Cyclic Loadings," by C.W. Roeder and E.P. Popov - 1977 (PB 275 526)A15

UCB/EERC-77/19 "A Simplified Procedure for Estimating Earthquake-Induced Deformations in Dams and Embankments," by F.I. Makdisi and H.B. Seed - 1977 (PB 276 820)A04

UCB/EERC-77/20 "The Performance of Earth Dams during Earthquakes," by H.B. Seed, F.I. Makdisi and P. de Alba - 1977 (PB 276 821)A04

UCB/EERC-77/21 "Dynamic Plastic Analysis Using Stress Resultant Finite Element Formulation," by P. Lukkunapvasit and J.M. Kelly - 1977 (PB 275 453)A04

UCB/EERC-77/22 "Preliminary Experimental Study of Seismic Uplift of a Steel Frame," by R.W. Clough and A.A. Huckelbridge 1977 (PB 278 769)A08

UCB/EERC-77/23 "Earthquake Simulator Tests of a Nine-Story Steel Frame with Columns Allowed to Uplift," by A.A. Huckelbridge - 1977 (PB 277 944)A09

UCB/EERC-77/24 "Nonlinear Soil-Structure Interaction of Skew Highway Bridges," by M.-C. Chen and J. Penzien - 1977 (PB 276 176)A07

UCB/EERC-77/25 "Seismic Analysis of an Offshore Structure Supported on Pile Foundations," by D.D.-N. Liou and J. Penzien 1977 (PB 283 180)A06

UCB/EERC-77/26 "Dynamic Stiffness Matrices for Homogeneous Viscoelastic Half-Planes," by G. Dasgupta and A.K. Chopra - 1977 (PB 279 654)A06

UCB/EERC-77/27 "A Practical Soft Story Earthquake Isolation System," by J.M. Kelly, J.M. Eidinger and C.J. Derham - 1977 (PB 276 814)A07

UCB/EERC-77/28 "Seismic Safety of Existing Buildings and Incentives for Hazard Mitigation in San Francisco: An Exploratory Study," by A.J. Meltsner - 1977 (PB 281 970)A05

UCB/EERC-77/29 "Dynamic Analysis of Electrohydraulic Shaking Tables," by D. Rea, S. Abedi-Hayati and Y. Takahashi 1977 (PB 282 569)A04

UCB/EERC-77/30 "An Approach for Improving Seismic - Resistant Behavior of Reinforced Concrete Interior Joints," by B. Galunic, V.V. Bertero and E.P. Popov - 1977 (PB 290 870)A06

UCB/EERC-78/01 "The Development of Energy-Absorbing Devices for Aseismic Base Isolation Systems," by J.M. Kelly and D.F. Tsztoo - 1978 (PB 284 978)A04

UCB/EERC-78/02 "Effect of Tensile Prestrain on the Cyclic Response of Structural Steel Connections, by J.G. Bouwkamp and A. Mukhopadhyay - 1978

UCB/EERC-78/03 "Experimental Results of an Earthquake Isolation System using Natural Rubber Bearings," by J.M. Eidinger and J.M. Kelly - 1978 (PB 281 686)A04

UCB/EERC-78/04 "Seismic Behavior of Tall Liquid Storage Tanks," by A. Niwa - 1978 (PB 284 017)A14

UCB/EERC-78/05 "Hysteretic Behavior of Reinforced Concrete Columns Subjected to High Axial and Cyclic Shear Forces," by S.W. Zagajeski, V.V. Bertero and J.G. Bouwkamp - 1978 (PB 283 858)A13

UCB/EERC-78/06 "Three Dimensional Inelastic Frame Elements for the ANSR-I Program," by A. Riahi, D.G. Row and G.H. Powell - 1978 (PB 295 755)A04

UCB/EERC-78/07 "Studies of Structural Response to Earthquake Ground Motion," by O.A. Lopez and A.K. Chopra - 1978 (PB 282 790)A05

UCB/EERC-78/08 "A Laboratory Study of the Fluid-Structure Interaction of Submerged Tanks and Caissons in Earthquakes," by R.C. Byrd - 1978 (PB 284 957)A08

UCB/EERC-78/09 Unassigned

UCB/EERC-78/10 "Seismic Performance of Nonstructural and Secondary Structural Elements," by I. Sakamoto - 1978 (PB81 154 593)A05

UCB/EERC-78/11 "Mathematical Modelling of Hysteresis Loops for Reinforced Concrete Columns," by S. Nakata, T. Sproul and J. Penzien - 1978 (PB 298 274)A05

UCB/EERC-78/12 "Damageability in Existing Buildings," by T. Blejwas and B. Bresler - 1978 (PB 80 166 978)A05

UCB/EERC-78/13 "Dynamic Behavior of a Pedestal Base Multistory Building," by R.M. Stephen, E.L. Wilson, J.G. Bouwkamp and M. Button - 1978 (PB 286 650)A08

UCB/EERC-78/14 "Seismic Response of Bridges - Case Studies," by R.A. Imbsen, V. Nutt and J. Penzien - 1978 (PB 286 503)A10

UCB/EERC-78/15 "A Substructure Technique for Nonlinear Static and Dynamic Analysis," by D.G. Row and G.H. Powell - 1978 (PB 288 077)A10

UCB/EERC-78/16 "Seismic Risk Studies for San Francisco and for the Greater San Francisco Bay Area," by C.S. Oliveira - 1978 (PB 81 120 115)A07

UCB/EERC-78/17 "Strength of Timber Roof Connections Subjected to Cyclic Loads," by P. Gülkan, R.L. Mayes and R.W. Clough - 1978 (HUD-000 1491)A07

UCB/EERC-78/18 "Response of K-Braced Steel Frame Models to Lateral Loads," by J.G. Bouwkamp, R.M. Stephen and E.P. Popov - 1978

UCB/EERC-78/19 "Rational Design Methods for Light Equipment in Structures Subjected to Ground Motion," by J.L. Sackman and J.M. Kelly - 1978 (PB 292 357)A04

UCB/EERC-78/20 "Testing of a Wind Restraint for Aseismic Base Isolation," by J.M. Kelly and D.E. Chitty - 1978 (PB 292 833)A03

UCB/EERC-78/21 "APOLLO - A Computer Program for the Analysis of Pore Pressure Generation and Dissipation in Horizontal Sand Layers During Cyclic or Earthquake Loading," by P.P. Martin and H.B. Seed - 1978 (PB 292 835)A04

UCB/EERC-78/22 "Optimal Design of an Earthquake Isolation System," by M.A. Bhatti, K.S. Pister and E. Polak - 1978 (PB 294 735)A06

UCB/EERC-78/23 "MASH - A Computer Program for the Non-Linear Analysis of Vertically Propagating Shear Waves in Horizontally Layered Deposits," by P.P. Martin and H.B. Seed - 1978 (PB 293 101)A05

UCB/EERC-78/24 "Investigation of the Elastic Characteristics of a Three Story Steel Frame Using System Identification," by I. Kaya and H.D. McNiven - 1978 (PB 296 225)A06

UCB/EERC-78/25 "Investigation of the Nonlinear Characteristics of a Three-Story Steel Frame Using System Identification," by I. Kaya and H.D. McNiven - 1978 (PB 301 363)A05

UCB/EERC-78/26 "Studies of Strong Ground Motion in Taiwan," by Y.M. Hsiung, B.A. Bolt and J. Penzien - 1978 (PB 298 436)A06

UCB/EERC-78/27 "Cyclic Loading Tests of Masonry Single Piers: Volume 1 - Height to Width Ratio of 2," by P.A. Hidalgo, R.L. Mayes, H.D. McNiven and R.W. Clough - 1978 (PB 296 211)A07

UCB/EERC-78/28 "Cyclic Loading Tests of Masonry Single Piers: Volume 2 - Height to Width Ratio of 1," by S.-W.J. Chen, P.A. Hidalgo, R.L. Mayes, R.W. Clough and H.D. McNiven - 1978 (PB 296 212)A09

UCB/EERC-78/29 "Analytical Procedures in Soil Dynamics," by J. Lysmer - 1978 (PB 298 445)A06

UCB/EERC-79/01 "Hysteretic Behavior of Lightweight Reinforced Concrete Beam-Column Subassemblages," by B. Forzani, E.P. Popov and V.V. Bertero - April 1979(PB 298 267)A06

UCB/EERC-79/02 "The Development of a Mathematical Model to Predict the Flexural Response of Reinforced Concrete Beams to Cyclic Loads, Using System Identification," by J. Stanton & H. McNiven - Jan. 1979(PB 295 875)A10

UCB/EERC-79/03 "Linear and Nonlinear Earthquake Response of Simple Torsionally Coupled Systems," by C.L. Kan and A.K. Chopra - Feb. 1979(PB 298 262)A06

UCB/EERC-79/04 "A Mathematical Model of Masonry for Predicting its Linear Seismic Response Characteristics," by Y. Mengi and H.D. McNiven - Feb. 1979(PB 298 266)A06

UCB/EERC-79/05 "Mechanical Behavior of Lightweight Concrete Confined by Different Types of Lateral Reinforcement," by M.A. Manrique, V.V. Bertero and E.P. Popov - May 1979(PB 301 114)A06

UCB/EERC-79/06 "Static Tilt Tests of a Tall Cylindrical Liquid Storage Tank," by R.W. Clough and A. Niwa - Feb. 1979 (PB 301 167)A06

UCB/EERC-79/07 "The Design of Steel Energy Absorbing Restrainers and Their Incorporation into Nuclear Power Plants for Enhanced Safety: Volume 1 - Summary Report," by P.N. Spencer, V.F. Zackay, and E.R. Parker - Feb. 1979(UCB/EERC-79/07)A09

UCB/EERC-79/08 "The Design of Steel Energy Absorbing Restrainers and Their Incorporation into Nuclear Power Plants for Enhanced Safety: Volume 2 - The Development of Analyses for Reactor System Piping,""Simple Systems" by M.C. Lee, J. Penzien, A.K. Chopra and K, Suzuki "Complex Systems" by G.H. Powell, E.L. Wilson, R.W. Clough and D.G. Row - Feb. 1979(UCB/EERC-79/08)A10

UCB/EERC-79/09 "The Design of Steel Energy Absorbing Restrainers and Their Incorporation into Nuclear Power Plants for Enhanced Safety: Volume 3 - Evaluation of Commercial Steels," by W.S. Owen, R.M.N. Pelloux, R.O. Ritchie, M. Faral, T. Ohhashi, J. Toplosky, S.J. Hartman, V.F. Zackay and E.R. Parker - Feb. 1979(UCB/EERC-79/09)A04

UCB/EERC-79/10 "The Design of Steel Energy Absorbing Restrainers and Their Incorporation into Nuclear Power Plants for Enhanced Safety: Volume 4 - A Review of Energy-Absorbing Devices," by J.M. Kelly and M.S. Skinner - Feb. 1979(UCB/EERC-79/10)A04

UCB/EERC-79/11 "Conservatism In Summation Rules for Closely Spaced Modes," by J.M. Kelly and J.L. Sackman - May 1979(PB 301 328)A03

UCB/EERC-79/12 "Cyclic Loading Tests of Masonry Single Piers; Volume 3 - Height to Width Ratio of 0.5," by P.A. Hidalgo, R.L. Mayes, H.D. McNiven and R.W. Clough - May 1979(PB 301 321)A08

UCB/EERC-79/13 "Cyclic Behavior of Dense Course-Grained Materials in Relation to the Seismic Stability of Dams," by N.G. Banerjee, H.B. Seed and C.K. Chan - June 1979(PB 301 373)A13

UCB/EERC-79/14 "Seismic Behavior of Reinforced Concrete Interior Beam-Column Subassemblages," by S. Viwathanatepa, E.P. Popov and V.V. Bertero - June 1979(PB 301 326)A10

UCB/EERC-79/15 "Optimal Design of Localized Nonlinear Systems with Dual Performance Criteria Under Earthquake Excitations," by M.A. Bhatti - July 1979(PB 80 167 109)A06

UCB/EERC-79/16 "OPTDYN - A General Purpose Optimization Program for Problems with or without Dynamic Constraints," by M.A. Bhatti, E. Polak and K.S. Pister - July 1979(PB 80 167 091)A05

UCB/EERC-79/17 "ANSR-II, Analysis of Nonlinear Structural Response, Users Manual," by D.P. Mondkar and G.H. Powell July 1979(PB 80 113 301)A05

UCB/EERC-79/18 "Soil Structure Interaction in Different Seismic Environments," A. Gomez-Masso, J. Lysmer, J.-C. Chen and H.B. Seed - August 1979(PB 80 101 520)A04

UCB/EERC-79/19 "ARMA Models for Earthquake Ground Motions," by M.K. Chang, J.W. Kwiatkowski, R.F. Nau, R.M. Oliver and K.S. Pister - July 1979(PB 301 166)A05

UCB/EERC-79/20 "Hysteretic Behavior of Reinforced Concrete Structural Walls," by J.M. Vallenas, V.V. Bertero and E.P. Popov - August 1979(PB 80 165 905)A12

UCB/EERC-79/21 "Studies on High-Frequency Vibrations of Buildings - 1: The Column Effect," by J. Lubliner - August 1979 (PB 80 158 553)A03

UCB/EERC-79/22 "Effects of Generalized Loadings on Bond Reinforcing Bars Embedded in Confined Concrete Blocks," by S. Viwathanatepa, E.P. Popov and V.V. Bertero - August 1979(PB 81 124 018)A14

UCB/EERC-79/23 "Shaking Table Study of Single-Story Masonry Houses, Volume 1: Test Structures 1 and 2," by P. Gülkan, R.L. Mayes and R.W. Clough - Sept. 1979 (HUD-000 1763)A12

UCB/EERC-79/24 "Shaking Table Study of Single-Story Masonry Houses, Volume 2: Test Structures 3 and 4," by P. Gülkan, R.L. Mayes and R.W. Clough - Sept. 1979 (HUD-000 1836)A12

UCB/EERC-79/25 "Shaking Table Study of Single-Story Masonry Houses, Volume 3: Summary, Conclusions and Recommendations," by R.W. Clough, R.L. Mayes and P. Gülkan - Sept. 1979 (HUD-000 1837)A06

UCB/EERC-79/26 "Recommendations for a U.S.-Japan Cooperative Research Program Utilizing Large-Scale Testing Facilities," by U.S.-Japan Planning Group - Sept. 1979(PB 301 407)A06

UCB/EERC-79/27 "Earthquake-Induced Liquefaction Near Lake Amatitlan, Guatemala," by H.B. Seed, I. Arango, C.K. Chan, A. Gomez-Masso and R. Grant de Ascoli - Sept. 1979(NUREG-CR1341)A03

UCB/EERC-79/28 "Infill Panels: Their Influence on Seismic Response of Buildings," by J.W. Axley and V.V. Bertero Sept. 1979(PB 80 163 371)A10

UCB/EERC-79/29 "3D Truss Bar Element (Type 1) for the ANSR-II Program," by D.P. Mondkar and G.H. Powell - Nov. 1979 (PB 80 169 709)A02

UCB/EERC-79/30 "2D Beam-Column Element (Type 5 - Parallel Element Theory) for the ANSR-II Program," by D.G. Row, G.H. Powell and D.P. Mondkar - Dec. 1979(PB 80 167 224)A03

UCB/EERC-79/31 "3D Beam-Column Element (Type 2 - Parallel Element Theory) for the ANSR-II Program," by A. Riahi, G.H. Powell and D.P. Mondkar - Dec. 1979(PB 80 167 216)A03

UCB/EERC-79/32 "On Response of Structures to Stationary Excitation," by A. Der Kiureghian - Dec. 1979(PB 80166 929)A03

UCB/EERC-79/33 "Undisturbed Sampling and Cyclic Load Testing of Sands," by S. Singh, H.B. Seed and C.K. Chan Dec. 1979(ADA 087 298)A07

UCB/EERC-79/34 "Interaction Effects of Simultaneous Torsional and Compressional Cyclic Loading of Sand," by P.M. Griffin and W.N. Houston - Dec. 1979(ADA 092 352)A15

UCB/EERC-80/01 "Earthquake Response of Concrete Gravity Dams Including Hydrodynamic and Foundation Interaction Effects," by A.K. Chopra, P. Chakrabarti and S. Gupta - Jan. 1980(AD-A087297)A10

UCB/EERC-80/02 "Rocking Response of Rigid Blocks to Earthquakes," by C.S. Yim, A.K. Chopra and J. Penzien - Jan. 1980 (PB80 166 002)A04

UCB/EERC-80/03 "Optimum Inelastic Design of Seismic-Resistant Reinforced Concrete Frame Structures," by S.W. Zagajeski and V.V. Bertero - Jan. 1980(PB80 164 635)A06

UCB/EERC-80/04 "Effects of Amount and Arrangement of Wall-Panel Reinforcement on Hysteretic Behavior of Reinforced Concrete Walls," by R. Iliya and V.V. Bertero - Feb. 1980(PB81 122 525)A09

UCB/EERC-80/05 "Shaking Table Research on Concrete Dam Models," by A. Niwa and R.W. Clough - Sept. 1980(PB81 122 368)A06

UCB/EERC-80/06 "The Design of Steel Energy-Absorbing Restrainers and their Incorporation into Nuclear Power Plants for Enhanced Safety (Vol 1A): Piping with Energy Absorbing Restrainers: Parameter Study on Small Systems," by G.H. Powell, C. Oughourlian and J. Simons - June 1980

UCB/EERC-80/07 "Inelastic Torsional Response of Structures Subjected to Earthquake Ground Motions," by Y. Yamazaki April 1980(PB81 122 327)A08

UCB/EERC-80/08 "Study of X-Braced Steel Frame Structures Under Earthquake Simulation," by Y. Ghanaat - April 1980 (PB81 122 335)A11

UCB/EERC-80/09 "Hybrid Modelling of Soil-Structure Interaction," by S. Gupta, T.W. Lin, J. Penzien and C.S. Yeh May 1980(PB81 122 319)A07

UCB/EERC-80/10 "General Applicability of a Nonlinear Model of a One Story Steel Frame," by B.I. Sveinsson and H.D. McNiven - May 1980(PB81 124 877)A06

UCB/EERC-80/11 "A Green-Function Method for Wave Interaction with a Submerged Body," by W. Kioka - April 1980 (PB81 122 269)A07

UCB/EERC-80/12 "Hydrodynamic Pressure and Added Mass for Axisymmetric Bodies," by F. Nilrat - May 1980(PB81 122 343)A08

UCB/EERC-80/13 "Treatment of Non-Linear Drag Forces Acting on Offshore Platforms," by B.V. Dao and J. Penzien May 1980(PB81 153 413)A07

UCB/EERC-80/14 "2D Plane/Axisymmetric Solid Element (Type 3 - Elastic or Elastic-Perfectly Plastic) for the ANSR-II Program," by D.P. Mondkar and G.H. Powell - July 1980(PB81 122 350)A03

UCB/EERC-80/15 "A Response Spectrum Method for Random Vibrations," by A. Der Kiureghian - June 1980(PB81122 301)A03

UCB/EERC-80/16 "Cyclic Inelastic Buckling of Tubular Steel Braces," by V.A. Zayas, E.P. Popov and S.A. Mahin June 1980(PB81 124 885)A10

UCB/EERC-80/17 "Dynamic Response of Simple Arch Dams Including Hydrodynamic Interaction," by C.S. Porter and A.K. Chopra - July 1980(PB81 124 000)A13

UCB/EERC-80/18 "Experimental Testing of a Friction Damped Aseismic Base Isolation System with Fail-Safe Characteristics," by J.M. Kelly, K.E. Beucke and M.S. Skinner - July 1980(PB81 148 595)A04

UCB/EERC-80/19 "The Design of Steel Energy-Absorbing Restrainers and their Incorporation into Nuclear Power Plants for Enhanced Safety (Vol 1B): Stochastic Seismic Analyses of Nuclear Power Plant Structures and Piping Systems Subjected to Multiple Support Excitations," by M.C. Lee and J. Penzien - June 1980

UCB/EERC-80/20 "The Design of Steel Energy-Absorbing Restrainers and their Incorporation into Nuclear Power Plants for Enhanced Safety (Vol 1C): Numerical Method for Dynamic Substructure Analysis," by J.M. Dickens and E.L. Wilson - June 1980

UCB/EERC-80/21 "The Design of Steel Energy-Absorbing Restrainers and their Incorporation into Nuclear Power Plants for Enhanced Safety (Vol 2): Development and Testing of Restraints for Nuclear Piping Systems," by J.M. Kelly and M.S. Skinner - June 1980

UCB/EERC-80/22 "3D Solid Element (Type 4-Elastic or Elastic-Perfectly-Plastic) for the ANSR-II Program," by D.P. Mondkar and G.H. Powell - July 1980(PB81 123 242)A03

UCB/EERC-80/23 "Gap-Friction Element (Type 5) for the ANSR-II Program," by D.P. Mondkar and G.H. Powell - July 1980 (PB81 122 285)A03

UCB/EERC-80/24 "U-Bar Restraint Element (Type 11) for the ANSR-II Program," by C. Oughourlian and G.H. Powell July 1980(PB81 122 293)A03

UCB/EERC-80/25 "Testing of a Natural Rubber Base Isolation System by an Explosively Simulated Earthquake," by J.M. Kelly - August 1980(PB81 201 360)A04

UCB/EERC-80/26 "Input Identification from Structural Vibrational Response," by Y. Hu - August 1980(PB81 152 308)A05

UCB/EERC-80/27 "Cyclic Inelastic Behavior of Steel Offshore Structures," by V.A. Zayas, S.A. Mahin and E.P. Popov August 1980(PB81 196 180)A15

UCB/EERC-80/28 "Shaking Table Testing of a Reinforced Concrete Frame with Biaxial Response," by M.G. Oliva October 1980(PB81 154 304)A10

UCB/EERC-80/29 "Dynamic Properties of a Twelve-Story Prefabricated Panel Building," by J.G. Bouwkamp, J.P. Kollegger and R.M. Stephen - October 1980(PB82 117 128)A06

UCB/EERC-80/30 "Dynamic Properties of an Eight-Story Prefabricated Panel Building," by J.G. Bouwkamp, J.P. Kollegger and R.M. Stephen - October 1980(PB81 200 313)A05

UCB/EERC-80/31 "Predictive Dynamic Response of Panel Type Structures Under Earthquakes," by J.P. Kollegger and J.G. Bouwkamp - October 1980(PB81 152 316)A04

UCB/EERC-80/32 "The Design of Steel Energy-Absorbing Restrainers and their Incorporation into Nuclear Power Plants for Enhanced Safety (Vol 3): Testing of Commercial Steels in Low-Cycle Torsional Fatigue," by P. Spencer, E.R. Parker, E. Jongewaard and M. Drory

UCB/EERC-80/33 "The Design of Steel Energy-Absorbing Restrainers and their Incorporation into Nuclear Power Plants for Enhanced Safety (Vol 4): Shaking Table Tests of Piping Systems with Energy-Absorbing Restrainers," by S.F. Stiemer and W.G. Godden - Sept. 1980

UCB/EERC-80/34 "The Design of Steel Energy-Absorbing Restrainers and their Incorporation into Nuclear Power Plants for Enhanced Safety (Vol 5): Summary Report," by P. Spencer

UCB/EERC-80/35 "Experimental Testing of an Energy-Absorbing Base Isolation System," by J.M. Kelly, M.S. Skinner and K.E. Beucke - October 1980(PB81 154 072)A04

UCB/EERC-80/36 "Simulating and Analyzing Artificial Non-Stationary Earthquake Ground Motions," by R.F. Nau, R.M. Oliver and K.S. Pister - October 1980(PB81 153 397)A04

UCB/EERC-80/37 "Earthquake Engineering at Berkeley - 1980," - Sept. 1980(PB81 205 874)A09

UCB/EERC-80/38 "Inelastic Seismic Analysis of Large Panel Buildings," by V. Schricker and G.H. Powell - Sept. 1980 (PB81 154 338)A13

UCB/EERC-80/39 "Dynamic Response of Embankment, Concrete-Gravity and Arch Dams Including Hydrodynamic Interaction," by J.F. Hall and A.K. Chopra - October 1980(PB81 152 324)A11

UCB/EERC-80/40 "Inelastic Buckling of Steel Struts Under Cyclic Load Reversal," by R.G. Black, W.A. Wenger and E.P. Popov - October 1980(PB81 154 312)A08

UCB/EERC-80/41 "Influence of Site Characteristics on Building Damage During the October 3, 1974 Lima Earthquake," by P. Repetto, I. Arango and H.B. Seed - Sept. 1980(PB81 161 739)A05

UCB/EERC-80/42 "Evaluation of a Shaking Table Test Program on Response Behavior of a Two Story Reinforced Concrete Frame," by J.M. Blondet, R.W. Clough and S.A. Mahin

UCB/EERC-80/43 "Modelling of Soil-Structure Interaction by Finite and Infinite Elements," by F. Medina - December 1980(PB81 229 270)A04

UCB/EERC-81/01 "Control of Seismic Response of Piping Systems and Other Structures by Base Isolation," edited by J.M. Kelly - January 1981 (PB81 200 735)A05

UCB/EERC-81/02 "OPTNSR - An Interactive Software System for Optimal Design of Statically and Dynamically Loaded Structures with Nonlinear Response," by M.A. Bhatti, V. Ciampi and K.S. Pister - January 1981 (PB81 218 851)A09

UCB/EERC-81/03 "Analysis of Local Variations in Free Field Seismic Ground Motions," by J.-C. Chen, J. Lysmer and H.B. Seed - January 1981 (AD-A099508)A13

UCB/EERC-81/04 "Inelastic Structural Modeling of Braced Offshore Platforms for Seismic Loading," by V.A. Zayas, P.-S.B. Shing, S.A. Mahin and E.P. Popov - January 1981(PB82 138 777)A07

UCB/EERC-81/05 "Dynamic Response of Light Equipment in Structures," by A. Der Kiureghian, J.L. Sackman and B. Nour-Omid - April 1981 (PB81 218 497)A04

UCB/EERC-81/06 "Preliminary Experimental Investigation of a Broad Base Liquid Storage Tank," by J.G. Bouwkamp, J.P. Kollegger and R.M. Stephen - May 1981(PB82 140 385)A03

UCB/EERC-81/07 "The Seismic Resistant Design of Reinforced Concrete Coupled Structural Walls," by A.E. Aktan and V.V. Bertero - June 1981(PB82 113 358)A11

UCB/EERC-81/08 "The Undrained Shearing Resistance of Cohesive Soils at Large Deformations," by M.R. Pyles and H.B. Seed - August 1981

UCB/EERC-81/09 "Experimental Behavior of a Spatial Piping System with Steel Energy Absorbers Subjected to a Simulated Differential Seismic Input," by S.F. Stiemer, W.G. Godden and J.M. Kelly - July 1981

UCB/EERC-81/10 "Evaluation of Seismic Design Provisions for Masonry in the United States," by B.I. Sveinsson, R.L. Mayes and H.D. McNiven - August 1981 (PB82 166 075)A08

UCB/EERC-81/11 "Two-Dimensional Hybrid Modelling of Soil-Structure Interaction," by T.-J. Tzong, S. Gupta and J. Penzien - August 1981(PB82 142 118)A04

UCB/EERC-81/12 "Studies on Effects of Infills in Seismic Resistant R/C Construction," by S. Brokken and V.V. Bertero - September 1981 (PB82 166 190)A09

UCB/EERC-81/13 "Linear Models to Predict the Nonlinear Seismic Behavior of a One-Story Steel Frame," by H. Valdimarsson, A.H. Shah and H.D. McNiven - September 1981(PB82 138 793)A07

UCB/EERC-81/14 "TLUSH: A Computer Program for the Three-Dimensional Dynamic Analysis of Earth Dams," by T. Kagawa, L.H. Mejia, H.B. Seed and J. Lysmer - September 1981(PB82 139 940)A06

UCB/EERC-81/15 "Three Dimensional Dynamic Response Analysis of Earth Dams," by L.H. Mejia and H.B. Seed - September 1981 (PB82 137 274)A12

UCB/EERC-81/16 "Experimental Study of Lead and Elastomeric Dampers for Base Isolation Systems," by J.M. Kelly and S.B. Hodder - October 1981 (PB82 166 182)A05

UCB/EERC-81/17 "The Influence of Base Isolation on the Seismic Response of Light Secondary Equipment," by J.M. Kelly - April 1981 (PB82 255 266)A04

UCB/EERC-81/18 "Studies on Evaluation of Shaking Table Response Analysis Procedures," by J. Marcial Blondet - November 1981 (PB82 197 278)A10

UCB/EERC-81/19 "DELIGHT.STRUCT: A Computer-Aided Design Environment for Structural Engineering," by R.J. Balling, K.S. Pister and E. Polak - December 1981 (PB82 218 496)A07

UCB/EERC-81/20 "Optimal Design of Seismic-Resistant Planar Steel Frames," by R.J. Balling, V. Ciampi, K.S. Pister and E. Polak - December 1981 (PB82 220 179)A07

UCB/EERC-82/01 "Dynamic Behavior of Ground for Seismic Analysis of Lifeline Systems," by T. Sato and A. Der Kiureghian - January 1982 (PB82 218 926)A05

UCB/EERC-82/02 "Shaking Table Tests of a Tubular Steel Frame Model," by Y. Ghanaat and R. W. Clough - January 1982 (PB82 220 161)A07

UCB/EERC-82/03 "Behavior of a Piping System under Seismic Excitation: Experimental Investigations of a Spatial Piping System supported by Mechanical Shock Arrestors and Steel Energy Absorbing Devices under Seismic Excitation," by S. Schneider, H.-M. Lee and W. G. Godden - May 1982 (PB83 172 544)A09

UCB/EERC-82/04 "New Approaches for the Dynamic Analysis of Large Structural Systems," by E. L. Wilson - June 1982 (PB83 148 080)A05

UCB/EERC-82/05 "Model Study of Effects of Damage on the Vibration Properties of Steel Offshore Platforms," by F. Shahrivar and J. G. Bouwkamp - June 1982 (PB83 148 742)A10

UCB/EERC-82/06 "States of the Art and Practice in the Optimum Seismic Design and Analytical Response Prediction of R/C Frame-Wall Structures," by A. E. Aktan and V. V. Bertero - July 1982 (PB83 147 736)A05

UCB/EERC-82/07 "Further Study of the Earthquake Response of a Broad Cylindrical Liquid-Storage Tank Model," by G. C. Manos and R. W. Clough - July 1982 (PB83 147 744)A11

UCB/EERC-82/08 "An Evaluation of the Design and Analytical Seismic Response of a Seven Story Reinforced Concrete Frame - Wall Structure," by F. A. Charney and V. V. Bertero - July 1982(PB83 157 628)A09

UCB/EERC-82/09 "Fluid-Structure Interactions: Added Mass Computations for Incompressible Fluid," by J. S.-H. Kuo - August 1982 (PB83 156 281)A07

UCB/EERC-82/10 "Joint-Opening Nonlinear Mechanism: Interface Smeared Crack Model," by J. S.-H. Kuo - August 1982 (PB83 149 195)A05

UCB/EERC-82/11 "Dynamic Response Analysis of Techi Dam," by R. W. Clough, R. M. Stephen and J. S.-H. Kuo - August 1982 (PB83 147 496)A06

UCB/EERC-82/12 "Prediction of the Seismic Responses of R/C Frame-Coupled Wall Structures," by A. E. Aktan, V. V. Bertero and M. Piazza - August 1982 (PB83 149 203)A09

UCB/EERC-82/13 "Preliminary Report on the SMART 1 Strong Motion Array in Taiwan," by B. A. Bolt, C. H. Loh, J. Penzien, Y. B. Tsai and Y. T. Yeh - August 1982 (PB83 159 400)A10

UCB/EERC-82/14 "Shaking-Table Studies of an Eccentrically X-Braced Steel Structure," by M. S. Yang - September 1982